ENGINEERING THE ELECTROCHROMISM AND ION CONDUCTION OF LAYER-BY-LAYER ASSEMBLED FILMS

by

Dean M. DeLongchamp

B.S. Chemical Engineering
Georgia Institute of Technology, 1998

M.S.C.E.P Chemical Engineering
Massachusetts Institute of Technology, 2000

Submitted to the Department of Chemical Engineering
in partial fulfillment of the requirements for the degree of

Doctor of Philosophy
at the
Massachusetts Institute of Technology
[September 2003]
May 2003

Signature of author:_____
Department of Chemical Engineering
May 28, 2003

Certified by:_____
Paula T. Hammond
Thesis Supervisor

Accepted by:_____
Daniel Blankschtein
Chairman, Committee for Graduate Students

ENGINEERING THE ELECTROCHROMISM AND ION CONDUCTION OF LAYER-BY-LAYER ASSEMBLED FILMS

by

Dean M. DeLongchamp

Submitted to the Department of Chemical Engineering on May 28, 2003 in partial fulfillment of the requirements for the degree of Doctor of Philosophy in Chemical Engineering

Abstract

This work applies the processing technique of layer-by-layer (LBL) assembly to the creation and development of new electrochemically active materials. Elements of the thin-film electrochromic cell were chosen as a particular focus for LBL fabrication. Layer-by-layer assembly is the ideal processing tool to tailor the electrochemical systems within electrochromic cells because modulating processing conditions can greatly impact the nanoscale composition and morphology of the resultant films. For the first time, this control was used to:

1) intelligently design electrochromic LBL assembled composite films that facilitated ion motion for faster switching and exhibited enhanced or shifted coloration,
2) combine multiple electrochromic materials into novel LBL assembled composites with even higher contrast, faster switching, and multiple colored states, and finally
3) develop and optimize several LBL assembled polymer electrolyte films that display high ionic conductivity and sound mechanical integrity.

Electrochromic cell elements were chosen not only for their undeveloped commercial potential, but also because they incorporate multifunctional material systems with alternative applications. Studies of LBL fabrication and the operation of electrochromic cells provide insight into intermolecular interactions, internal and external film interfaces, thin film electrochemistry, and charged species mobility in polymer solids.

First investigated was the capability of LBL assembly to alter the properties of electrochromic films by varying molecular blending. The electrochromophores for this investigation were appropriated from all corners of the materials spectrum, including discrete electrochromic polymers, conjugated polymers, soft colloidal suspensions, and inorganic particle dispersions. In each system, the influence of assembly conditions and film composition was elucidated; in particular systems the hydrophobicity, acidity, and morphology of the films were found to impact the electrochemistry and optical character of the films, providing a means to modulate these properties by directing LBL assembly design choices. Because of the high uniformity and thickness control allowed by LBL assembly, the contrast and switching performance of all LBL assembled electrochromic films were in general superior to those of films containing the same electrochromophores fabricated by other methods. One particularly promising system involved novel LBL assembled films containing electrochromic metal hexacyanoferrate nanocrystals of the Prussian blue family. These films displayed fast and deep coloration; synthetic nanocrystal variation extended absorbance over a broad spectral range so that these inorganic/polymer composite films could potentially be considered as elements in a full-color switchable CMYK display. The power of the LBL assembly technique was leveraged further with the successful fabrication of "dual electrochrome" electrodes. The concept of combining two electrochromophores into a single film led to two strategies: enhanced contrast

and multihued coloration. The LBL combination of polyviologen and the PEDOT colloid resulted in a film with electrochromic contrast superior to all but one polymer electrochrome reported in literature to date. The LBL combination of polyaniline and Prussian blue into the same electrode resulted in highly tunable multihued coloration, switching reversibly between clear, green, and blue.

The ionic conductivity of LBL assembled films can exceed the requirements of electrochromic devices and sensors with the appropriate choice of component polymers and assembly conditions. Electrostatically assembled films based on linear poly(ethylene imine) combined with various polyacids can achieve levels exceeding 10^{-5} S/cm while hydrogen-bonded LBL assembled films based on poly(ethylene oxide) and poly(acrylic acid) can attain levels close to 10^{-4} S/cm. To achieve these conductivity levels required plasticization with water. These high-performance LBL assembled polymer electrolyte systems thus resemble crosslinked gels; they maintain shape and do not flow or dissolve regardless of hydration level. The ionic conductivity of electrostatic LBL assembled films can be greatly influenced by polycation and polyanion choice, and design selections in this work resulted in an increase of LBL assembled film ionic conductivity of approximately two orders of magnitude over previous reports. Strong influences of LBL deposition conditions such as ionic strength and pH were elucidated, and several systems were optimized. For both electrostatically LBL assembled and hydrogen bond LBL assembled films, ionic conductivity could be enhanced by post-assembly salt exposure. This thesis is amongst the first published works to study the hydrogen-bonded poly(ethylene oxide) /poly(acrylic acid) system. During the course of study, it was discovered that the change in polymer solution morphology of poly(ethylene oxide) with salt addition by dehydrating Lewis acid/base interactions that cause it to assume a more globular shape can also influence both the final thickness and morphology of the LBL assembled film. This result reveals that the processing of hydrogen-bonded LBL assembled films can be modulated using the same flexible set of variables commonly associated with electrostatic LBL assembly.

This work has explored the great breadth of electrochemical behavior that can be achieved in LBL assembled films. The subject of LBL assembled electrochemical materials has proven to be both fruitful and rich, with a diverse range of phenomena to be observed and a host of variables that can be manipulated to create an ever-expanding library of electroactive materials. Using this fine control, applications could be extended to the creation of polymer batteries, biosensors, or photovoltaic devices, to name but a few possibilities. Chemical engineers considering electrochemical experimentation or devices should consider the LBL assembly process as a powerful and flexible alternative to traditional fabrication methods.

TABLE OF CONTENTS

Chapter 1. Introduction and background

Contents

Figures

1.1 Introduction

Engineering is distinct from pure science in that it emphasizes not only understanding phenomena of the universe, but also how to harness those phenomena for the betterment of humankind. Engineers use the discoveries of pure science as tools to create. In the process of creation, new scientific principles are often discovered, and thus engineers contribute to scientific understanding. Greater understanding adds to the body of pure science, and thus more can be created, completing a cycle in which both engineering and pure science are required to bring about positive change in the world.

This thesis is based on an engineering application pursued with the intent of also contributing to the body of pure science. The application arena is the recent strong commercial interest in developing low-cost elements with multiple reflective or transmissive colors suitable for flexible or wearable displays and smart windows. Electrochromic materials may be ideally suited to meet the needs of these emerging applications: they are cheap and simple to produce, and they can provide reasonable contrast in multiple colors. Electrochromic devices are particularly well adapted to large area displays due to low power consumption and forgiving manufacturing tolerances. Though electrochromic film research has been ongoing for many decades, there has been a recent resurgence of interest as industries search for an "electronic paper" technology that is a cheap alternative to liquid crystal and light emitting diode displays. This revitalized electrochromic film research increasingly looks to polymer and polymer / inorganic thin films for advancement. As is typical for most electroactive polymers, these electrochromic polymer films are customarily deposited on substrates by spin coating, electropolymerization, or surface polymerization by chemical means. A few challenges remain before the capabilities of these materials can be fully commercialized, in particular somewhat poor contrast and slow switching speed. Once these obstacles are overcome, full commercial exploitation of this promising technology will be possible.

This work has applied the relatively new processing technique of layer-by-layer (LBL) assembly to solve the remaining challenges of electrochromic film performance optimization. LBL assembly is a recently developed type of assisted self-assembly that creates macromolecular composites in ultra thin films with a fine degree of control. Composites of practically any material system including polymers, inorganic nanoparticles, and biological materials can be assembled on any charged substrate by alternating exposure to aqueous solutions or dispersions with opposite attractive functionalities. LBL assembly is the ideal tool to optimize the capabilities of electrochromic films. This tool can be used to tailor the composition and morphology of electrochromic films on the nanoscale, combining existing electrochromic materials into new,

high-performance composites with higher contrast and faster switching. Two materials that would aggregate or separate in a bulk mixture can easily be stably combined using this technique. This ability to create fine-grained composite films with extraordinary smoothness and practically unlimited thickness makes LBL assembly potentially far more powerful than traditional electrochromic film fabrication techniques such as electropolymerization or spin-coating.

Moreover, the work led beyond electrochromic film formation to a secondary intricate and potentially rewarding proposition: to fabricate *solid polymer electrolytes* using LBL assembly. All thin film electrochemical cells have three functional elements: anodes and cathodes that are electrochemically oxidized and reduced, respectively, and a solid electrolyte between, which provides electronic resistance and fast ion transport. The properties of this solid electrolyte are critical to the performance of electrochemical cells such as batteries, fuel cells, and electrochemical sensors.

The work in this thesis thus explores two complementary aspects of electroactive properties in LBL assembled films. This chapter provides the modern and historical context for this work in the greater realms of LBL assembly, electrochromic films, and polymer electrolytes. A general review of the assembly mechanism and properties of LBL assembled films is provided, followed by a review of electrochromism concepts and common materials. This chapter concludes with a description of common strategies and materials systems employed in the frontier field of polymer electrolyte engineering. Some background on less common measurement techniques is also provided. Together this information should provide a context for critical examination of the results of this thesis work, and also promote understanding of the role that this approach can play in the general fabrication of polymer films to suit the needs of many electrochemical devices.

1.2 Layer-by-layer assembly

Layer-by-layer processing is the core technique used to create the wide variety of materials investigated in this thesis. The technique forms thin films that are inherently two-component composites. Attractive forces between molecules are required to bring about the fabrication; for this reason LBL assembled films are sometimes described as "self assembled." However, the technique requires periodic intervention – the changing of exposure solutions – to create the films, so the technique may be better described as a type of "assisted self assembly" or "molecular assembly," removing the onus that the film must spring into existence from a single solution. There are in truth many examples of hybrid assembly approaches where the hand of man is assisted by molecular structures and rearrangements at the molecular level. Obvious examples are Langmuir-Blodgett film formation or the orientation of polymer chains along the axis of a fiber spinneret, but all materials derive some physical properties from their own self-arrangement (or lack of it). In fact, as most environments in which "true self assembly" occurs require a great deal of contrivance to achieve, we must regard this distinction as largely artificial, and instead consider materials processing to be a spectrum of possibilities where the interplay between natural and human forces always exists, bringing about a transformation from raw material to useful product.

1.2.1 The classical layer-by-layer technique

The layer-by layer (LBL) assembly technique was first described by Iler in 1966.[1] This early work focused on harnessing Coulombic interactions between water-dispersed polyvalent entities and a charged substrate to build thin films with nanometer-scale dimensions. Iler's work concentrated primarily on macroscopic species such as charged colloidal oxides, polymer beads, and some proteins. Unfortunately for Iler, his work appeared just at the point when interest in colloidal polyelectrolyte complexes was declining after peaking immediately post-war, and important contemporary figures in polyelectrolyte complex research such as A.S. Michaels (strong polyelectrolyte colloidal complexes)[2] and H.G.B. de Jong (weak, biologically derived polyelectrolyte colloidal complexes)[3] were moving on to other pursuits.

The advent of the modern incarnation of the technique is credited to Decher, who first published on the LBL assembly of water-soluble polyelectrolytes in 1991.[4-6] The technique was (re)developed almost by happenstance during the course of a particularly problematic Langmuir-Blodgett film fabrication involving the assembly of rodlike bipolar amphiphiles. Since that

report, the technique has gained growing acclaim and now over a decade later it is rare for polymer and organic thin film journals to publish a single issue without at least one LBL assembly report included.

The classical polyelectrolyte LBL assembly technique as described by Decher and as practiced by most researchers requires a charged substrate and dilute aqueous solutions of polycation and polyanion (see Figure 1.1). The substrate is first immersed into the solution in which the polyelectrolyte of opposite charge to the substrate is dissolved. Exposure time is variable – from 1 to 30 minutes depending upon investigator preferences and the system under investigation. After exposure, the substrate is removed from polyelectrolyte solution, rinsed, and then immersed in a polyelectrolyte solution of opposite charge to the first polyelectrolyte. With each step, sufficient polyelectrolyte adsorbs from solution onto the substrate so that surface charge reversal is achieved, and film growth can be maintained indefinitely by continuing alternating exposure. The initial adsorption of polymer chains in every step is entropically favored due to the liberation of counterions from both polyions into the solution,[7] while the surface charge reversal that results provides an electrostatic barrier to uncontrolled adsorption, ensuring that a typically reproducible amount of each polyion is deposited each exposure step.

This apparently unlimited ionization charge reversal is not predicted from adsorption models of single polyelectrolytes onto hard surfaces that would suggest surface neutralization.[8] Overcompensation and charge reversal in LBL systems stems from three factors: 1) entanglement and interpenetration of the depositing polyion with previously deposited layers, 2) multiple adhesion points between the depositing polyion and substrate in 3 rather than 2 dimensions, and 3) the irreversibility of multiple electrostatic interactions on the time scale of polymer chain relaxation during deposition.[8] This last factor is the most important; the electrostatic interactions have enthalpy similar to that of a covalent bond, and the time scale required for the polymer to re-dissociate from those bonds, reorient, and re-associate into a more equilibrated structure with greater charge neutrality is simply experimentally unachievable, especially considering that this rearrangement would have to be concerted with already-bonded neighboring chains. Thus the polycation/polyanion arrangement within LBL assembled films must be regarded as kinetically "frozen" and not representative of a thermodynamically equilibrated structure.

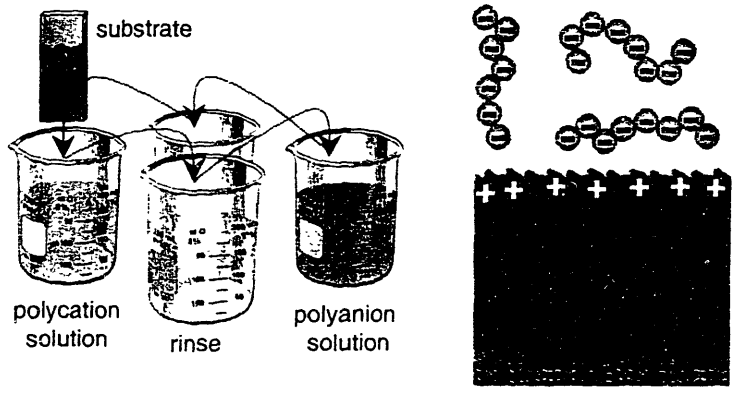

Figure 1.1 - The layer-by-layer assembly process.

1.2.2 Layer-by-layer processing controls

Even from this simple description of LBL assembly, it is clear that the technique is very flexible because adjusting the layer pair number can control film thickness and manipulating the identity of polycation and polyanion can control film composition. However, there exist other more subtle methods to influence the properties of LBL assembled films. The electrostatic LBL assembly process is inherently dependent upon the solution conformation and the ionization charge density of the system components. The solution conformation of polyelectrolytes is often manipulated by the addition of small dissociable ions to the deposition solution. This addition results in a change of polyelectrolyte solution morphology from the typical extended coil that is adopted in the absence of salt, to a more globular conformation as a result of a lessening of coulombic repulsion along the polyelectrolyte backbone due to ionic screening. This change in solution morphology leads to different deposition behavior. Nomenclature and general arguments for this phenomenon are well described for the deposition of strong polyelectrolytes onto hard substrates in a rigorous mean-field modeling investigation by Van deSteeg et. al.[9] The change to this more globular conformation results first in an increase in the thickness of an adsorbed polyelectrolyte layer, termed *screening enhanced adsorption.*[10,11] The layer thickness continues to increase up to 0.2-1 M added salt concentration before polyelectrolyte deposition is inhibited due to shielding of Coulombic attractions. This decrease is termed *screening reduced adsorption.*[12] The regulation of the properties of LBL-assembled polymer films by manipulating ionic strength of the deposition environment was first described by Lvov and Decher[13] and has since been exploited by many researchers.[14-16] The combination of adsorption enhancement and reduction leads to a rise–peak–fall type of layer pair thickness profile with increasing deposition solution ionic strength.

A second means to influence polyelectrolyte conformation in solution is to directly manipulate the charge density on the polyelectrolyte backbone. This manipulation is typically achieved by modulation of deposition solution pH for polyelectrolytes that have pH-sensitive ionizable groups (termed weak polyelectrolytes). The most common of these groups are carboxylic acids and amines. Carboxylic acids are fully charged at higher pH and less charged at low pH. In contrast, amines become fully charged under acidic conditions and uncharged under very basic conditions. The monolayer thickness adsorption maximum for polyacids has been predicted to occur at a pH 1-1.5 units below the polyacid solution pK_a;[17] this prediction has been confirmed by several studies.[18-21] The maximum appears at a point where the ability of the polyacid to redistribute surface-compensating ionization becomes limited. Decreasing pH beyond this maximum point results in a decrease of the adsorbed thickness.[17] The use of pH to modulate the ionization of weak polyelectrolytes and therefore influence the properties of weak polyelectrolyte colloidal complexes was first employed by de Jong.[3] The regulation of the properties of LBL assembled films formed from weak polyelectrolytes by adjusting assembly pH was first described in detail by Rubner and Shiratori,[22-24] and has since been employed by those researchers and many others to create films of widely varying composition, morphology, and physical properties from the same component polyions.[25-33]

1.2.3 Expansions on the classical technique

With tunable controls of polyelectrolyte selection, layer pair number, ionic strength, and pH to modulate film properties, it can be said without hyperbole that LBL assembly is one of the most powerful thin film processing techniques that has ever been developed. Therefore, it is not surprising that the technique has experienced an exponential growth in popularity and publication. Even a few years ago it was possible to describe the key LBL assembly research efforts and the general direction of research, but now the spread of applications has become too diverse for any one person to follow. Thankfully, there are several valuable reviews that cover most of the key advancements in the area; the reader is referred to the most recent by Decher[34] and Hammond,[35] as well as a recent volume with manuscripts prepared by many of the key contributors to the science and engineering of modern LBL assembly.[36]

Some of the most critical expansions upon the classical technique must be mentioned. One of these expansions most relevant to the work in this thesis was the incorporation of important families of functional materials into LBL assembled films. One of the first examples of this was the work of Rubner and co-workers in 1994 that resulted in LBL assembled films containing electronically conductive conjugated polymer systems.[37-42] This advancement was

quickly followed within the same laboratory with the announcement of LED fabrication employing LBL assembled films that contained the poly(phenylene vinelene) emitter[43-45] and subsequently a light-emitting LBL-assembled electrochemical cell based on the electrochemiluminescence of a tris-chelated ruthenium complex.[46,47] These early reports form the foundation for the great number of articles that have been published concerning electroactive thin films created by LBL assembly.[48-69]

Another of these expansions has been the application of the technique to nonplanar substrates. Application of LBL assembly to dispersed colloids has primarily been covered by Caruso et. al., and includes a wide variety of colloidal materials that are either encapsulated or dissolved to crease empty spheres, core shell structures, and an ever-increasing range of other particulate architectures.[30,70-74] A different extension of the technique to nonplanar substrates has resulted in the first commercial application of LBL assembly – the hydrophilizing of contact lens surfaces employing a sprayed LBL-style coating of weak polyelectrolyte complex.[75] The use of this technique in a large-scale commercial application is promising as it suggests that LBL assembly will remain a vital processing method for years to come, as opposed to the fast-disappearing Langmuir-Blodgett film formation that LBL assembly has largely displaced.

A critical advancement that has been made for planar LBL assembled films has been the discovery that patterning surface charge can direct the deposition of polyelectrolyte LBL assembled films. The first description of this work employed the novel technique of microcontact printing. Alternating regions of different chemical functionality were achieved by using a poly(dimethylsiloxane) (PDMS) stamp cast from a photolithographed silicon master to deliver a self-assembled monolayer (SAM) in predetermined pattern, and then backfilling the unstamped surface with a different SAM.[76] Polyelectrolyte LBL deposition was then controllably directed to areas of specific functionality by modulating the depositing system and assembly conditions. The effects of molecular weight,[77] ion type,[77] ionic strength,[78] and pH[79] have been studied for this selective deposition of micron-scale LBL architectures. High deposition selectivity occurs for low molecular weight polymers at intermediate salt concentrations. Recent investigations have added to the flexibility of this patterning technique with the introduction of polymer-on-polymer stamping (POPS). In the POPS paradigm, a polyion or block copolymer is directly stamped onto a continuous LBL platform to chemically pattern the surface.[80,81] The resultant chemical pattern, which can be reproduced from the PDMS master down to the nanometer scale,[81] can then be used to direct colloidal adhesion,[82,83] electroless metal plating,[84] or cell attachment, to name but a few of the diverse applications for this powerful nanofabrication concept.

A final variation of the classical LBL technique takes the form of altering the interaction between the adsorbing species. This concept was first proposed by Rubner, who demonstrated that hydrogen bonding interactions between polyaniline and various nonionic polymers were suitable for constructing LBL assembled films.[41] This work was advanced by Wang and co-workers in a series of reports of the hydrogen bonding of pyridine-containing polymers with a wide variety of nonionic materials.[85-88] Very recently, hydrogen bonding forces have been used by Sukhishvili and Granick to assemble extremely delicate, pH-sensitive structures from poly(ethers) and poly(acryl amides) that can be induced to dissolve under certain pH conditions.[89,90] Controlled solubility of these systems has since been exploited by Rubner and Yang to attain patterned films by inkjet printing water of controlled pH.[91] Knowledge of these hydrogen bonded structures is still in its infancy. Considering that the most richly complex nanoengineered materials - biological tissues - are composed of proteins and lipids that maintain integrity and structure almost entirely by virtue of weak forces such as hydrophobic interactions and hydrogen bonding, it is clear that LBL assembly based on these forces may eventually provide a wealth of useful composites with startling new properties just as its electrostatically-driven cousin has done over the past decade.

1.3 Electrochromism

1.3.1 On color

Correlation between color and molecular structure in organic compounds has been studied since the late 19th century. Early explanations were entirely empirical, stressing the importance of a conjugated system of double bonds and the need for electron donor and acceptor moieties as part of the molecule. Current explanations of color-structure relationships are comprised of several qualitative chemical explanations and more holistic (and more computationally demanding) quantum theory models.[92]

Very simply put, in order for a material to appear colored, it must absorb a part of the visible spectrum. The reflected color corresponds to the incident wavelengths minus the absorbed wavelengths. Hence a molecule that absorbs higher energy visible light will appear red, while lower energy absorbance will appear blue. To absorb visible light, a molecule must channel the absorbed energy into some intramolecular or intermolecular process. Color in many organic molecules comes about as the energy of visible light is absorbed to effect electron transitions between the highest occupied molecular orbital (HOMO) and the lowest unoccupied molecular orbital (LUMO). This transition is responsible for the color of azo-based dyes, for example. The absorbance bands may be rather broad because simultaneous changes in rotation and vibration states can subtly increase or decrease the photonic energy absorbed. Additionally, more than one type of electronic transition may take place, as for the color green, which is caused by two separate absorbance maxima at 400-450 nm and 580-700 nm.[92] Although any electrons in a molecule can be excited, bonding electrons in π orbitals and unbound electrons (i.e. lone pairs) are particularly susceptible due to the lack of strong nuclear association.

A compound is more likely to be colored if it contains conjugated double bonds.[93] In a system with several conjugated double bonds, s and p atomic orbitals become sp^2 hybridized while the remaining p orbitals form bonding π orbitals, which are delocalized over conjugated molecular structures. With the formation of π orbitals, π^* (antibonding) orbitals of higher energy are also formed. A greater extent of conjugation reduces the band gap between the HOMO and the LUMO, which in turn lowers the energy required for the electronic transition to longer wavelengths of visible light. Electrons in the π orbital can then absorb visible photonic radiation to travel to the higher energy π^* orbital in a $\pi \rightarrow \pi^*$ transition. Lone pair electrons can also be excited to the π^* orbital in a $n \rightarrow \pi^*$ transition. The latter type of excitation is particularly common in colored heterocyclic ring structures.[93]

A more complex form of color in organic systems is termed "donor-acceptor" chromicity. Molecules that display this type of coloration have an electron donor group (e.g. -NH2) linked directly to a conjugated double bond structure. Absorbed radiation again causes electron excitation to a higher energy orbital and this transfer shifts electron density from the electron donor moiety to the rest of the system. The electronic excitation is often of the $n \rightarrow \pi^*$ type as donor groups typically carry lone pair electrons. The excited electron density can be distributed over several locations within the system or to one simple "acceptor" structure (e.g. -NO2). Donor-acceptor chromicity can be generalized to intermolecular charge transfer complexes as well, where electron density is exchanged between electron-rich and electron-poor species that are not covalently bonded. This type of coloration is apparent in viologens, where excited electrons are exchanged between the dipyridyl moiety and counterions, and also in hexacyanoferrate complexes, where electrons are exchanged between adjacent iron (II) and iron (III) ions through a cyano bridge.

The molecular environment of a chromogen can have a pronounced effect on the position and intensity of optical absorbance bands. This is often due to polarity differences between the excited state and the ground state of the chromogen. If the excited state is more polar than the ground state, then a polar environment such as an aqueous solution should enhance color intensity. Shifts to different absorbance bands are also possible. Intermolecular hydrogen bonding can reduce the color intensity of $n \rightarrow \pi^*$ transitions by sequestering lone pair electrons. These environmental effects on chromic activity are even more pronounced on solid substrates than in liquid solutions.[93]

Color can also be explained quantitatively and in some cases predicted by quantum mechanical theories. These methods are too mathematically complex to be useful to be applied to large molecules and have little utility for describing polymers.[93] Fortuitously, the electrochromic materials employed within this thesis possess well-understood coloration mechanisms, which will be reviewed individually as required.

1.3.2 Electrochemical color change

An *electrochromic* material exhibits a change in optical absorbance upon an electron transfer oxidation or reduction (hereafter redox) reaction. This change can stem from an alteration in any of the electronic configurations described above for UV-Vis energy electron excitation. The phenomenon is no different than expecting a completely chemically derived synthetic product to display a color different than those of its reactants; the only complexity is that added by electrochemical factors.

Although almost any material might be considered electrochromic, there are far fewer materials that are reversibly so. For example, the color change brought about by the electronic oxidation of cellulose fibers in a tree struck by lightning is an example of irreversible electrochromism. Reversibly electrochromic materials must be able to undergo reversible electrochemistry; the color change might be considered a byproduct of that electrochemistry. The most sought-after electrochromic materials undergo a transition from a deeply colored state to an essentially colorless or bleached state. These materials are prized because they form the highest contrast displays and the most useful light-modulating solar windows. Another sought-after property of electrochromic materials is that they be bistable – that is, in the switching environment, both the colored and bleached forms should be inert and should not undergo chemically based reversal of the switching electrochemistry or (even worse) chemical degradation.

Color change upon the advent of oxidation or reduction usually does not involve the instantaneous instantiation of an excitable electron system. More typically, the electron system already exists, and oxidation or reduction acts to shift the excitation energy of that system. For materials that feature both a bleached state and a colored state, this transition can occur as an increase in the energy of absorbance from the infrared region to the visible region, or a decrease in the energy of absorbance from the ultraviolet to the visible range. This change in absorbance energy is achieved during oxidation or reduction by: 1) increasing or decreasing the electron density of an acceptor or donor moiety, or 2) introducing, removing, or shifting a stable electron orbital within an existing HOMO LUMO bandgap.

Materials that display reversible electrochromism are typically fabricated into thin films on transparent conductive substrates for evaluation as electrochromic windows, though alternative cells employ strategies such as dissolving the electrochrome in the electrolyte. There exist a variety of performance metrics employed to compare the quality of electrochromic films. The most important of these is that they must exhibit *high contrast.* Contrast is typically defined as the change in the transmittance at a specific wavelength during electrochromic switching, which is linearly related to the change in the absolute number of photons absorbed by the film and thus is closely correlated to contrast perception in the human eye. For obvious reasons, high contrast is critical for image clarity in displays and significant solar radiation modulation in windows.

The second most important performance metric is *switching speed.* The speed of color change is the speed of the electrochemical reaction. In most reversibly electrochromic materials, reaction kinetics are not limited by electron transfer but rather are limited by the exchange of

ions with the electrolyte. In standard chemical engineering terminology, this is to say that the reactions are not rate-limited but rather are transport-limited. The ionic exchange is necessary to compensate for the inevitable change in valence that occurs during electrochemical oxidation or reduction. Thus the switching speed is dependent on the ion migration environment in the film and the length scale of migration – the full film thickness.

A final important property that is desired but rarely discovered in electrochromic materials is *multi-hued* coloration. Materials of this type would display multiple colored states in addition to a colorless bleached state. The possession of multiple stable redox states requires either multiple, different redox sites that can be accessed at different potentials or a single redox site that has multiple stable oxidation states. Very few materials have been synthesized that fit these criteria. Some materials that partially fit the former criterion are the viologens, which feature two sequential reductions that result in the formation of two differently colored reduced states in addition to the colorless, fully oxidized state. The second, more cathodic reduction of viologens is not stable in protic environments and inevitably results in film degradation over long term switching. Materials that may fit the latter criterion are the pthalocyanine compounds of transition metals, lanthanides, and actinides, most notably the "double decker" lutetium bis(phthalocyanine),[94-97] which apparently exhibits over five stable, differently colored oxidation states. Films of electrochromic phthalocyanines have so far primarily been fabricated using vacuum sublimation in a painstaking and costly process, though Langmuir-Blodgett film formation has also been considered.

1.3.3 Common electrochromes

1.3.3.1 Viologens

Viologens are the most extensively studied organic cathodic electrochromes. Viologens can be prepared by one-step quaternization of 4,4'-dipyridyl with organic halides a synthesis termed the Anderson reaction (for heterocyclic amines)[98] and analogous to the more general Menshutkin reaction of alkyl amines.[99] The resulting molecule is quite stable but can be degraded to an organic alcohol and 4,4'-dipyridyl by strong bases.[100] The fully oxidized dication is typically a pale yellow solid, the bleached state of the dipyridyl species. Reduction of the dication results in a deeply colored radical cation. Delocalization of the radical electron and positive charge over the conjugated structure greatly enhances the radical cation stability (18 canonical forms can be drawn).[101] However, the radical reacts readily with molecular oxygen to form peroxides and reverts to the dication.[102] The radical cation can manifest several colors ranging from deep blue or red (the compound's namesake) to a dark green, depending on the extent of double bond

conjugation on the nitrogen substituent.[103] Color is produced by charge transfer between the radical cation and its counter-anion. The radical cation color is often quite intense, with an extinction coefficient of 8400-9200 M^{-1} cm^{-1} attained for alkyl viologens covalently grafted as pendant groups onto polymer films[104] and electrostatically bound to Nafion polymer films;[105] the extinction can approach 14,000 M^{-1} cm^{-1} for methyl viologen in solution.[106] The striking contrast between the bleached and colored states of dipyridyl species is the primary reason that these materials have been studied so heavily for display applications.[100]

Viologens possess one of the most cathodic formal reduction potentials of any organic system showing a significant degree of reversibility.[100] This indicates that singly-reduced viologen is itself an excellent reducing agent (the motivation for its reduction of molecular oxygen). Formal reduction potentials for the single reduction of small molecule viologens vary from –0.8 to –1.1 V vs. SCE depending on nitrogen substituent. The second reduction proceeds at a slightly more negative potential. The narrow proximity window between reduction potentials has been a subject of some concern because the less stable, doubly reduced species may be inadvertently generated near defects in devices.[107]

In order to combat diffusion of colored viologen away from an electrode surface, many applications of viologen electrochemistry have involved the sequestering of small molecule viologens on a cathode using anionic polyelectrolytes such as poly(2-acrylamido 2-methyl propane sulfonic acid) (PAMPS) or Nafion.[108,109] However, viologens can also be incorporated into polymers that retain many of the same chemical and electrochemical properties of small-molecule viologens.[100] Viologen polymers can sterically inhibit dimer formation of the colored radical cation[107,110] that in small molecules can lead to a stacking crystallization and electrochemical deactivation.[111] It has also been shown that incorporating viologens as pendant groups onto polystyrene may reduce the potential required for the first reduction and widen the potential gap between the first and second reduction of the dication, curtailing inadvertent reduction to the less reversible uncharged state.[107] The most commonly studied poly(viologens) are main-chain with small alkyl spacers (C_2-C_{10}), typically manifesting a strong blue color upon reduction. As polyelectrolytes, these polymers are readily water soluble, though stable poly(viologen) films have been electrodeposited from poorer polar solvents.[112]

1.3.3.2 Conducting polymers

Conducting polymers feature extended conjugation – alternating single and double bonds that create an extended π orbital structure along the direction of the polymer chain. As extended double bond conjugation contributes to color, all electronically conducting polymers are

potentially electrochromic.[110] In order to achieve extended conjugation, only a few simple molecular design motifs have emerged. The first motif is that of pure conjugated hydrocarbons, which include poly(acetylene), ladder-type polymers, and hybrids such as poly(phenylene vinylene) (PPV). Other conjugated polymer motifs include heteroatoms such as nitrogen or sulfur to stabilize the conjugated structure. The most common heteroatom motifs are the poly(anilines), poly(thiophenes), and poly(pyrroles). New conducting polymers are overwhelmingly derived from one of these four general types. The most common and profound method of changing the coloration (or emitting or fluorescing) properties of a conducting polymer is to alter its primary molecular structure. Covalent modifications are typically made to the monomer, which is then typically electropolymerized[113-128] or more rarely polymerized by chemical oxidation.[45,69,129-131] Substituent addition to one of the four key motifs is the most common method of covalently altering conducting polymer character.[132]

Electrochemical reactions of conducting polymers involve the creation of oxidized or reduced sites on the conjugated chain, a process termed doping. Upon oxidation, an electron is removed from one orbital in the HOMO band, resulting in an increase in energy of that orbital and a decrease in energy of its corresponding antibonding orbital within the LUMO band. Upon reduction, an electron is added to an orbital in the LUMO band, resulting in a decrease in energy for that orbital and an increase in the energy of its corresponding bonding orbital in the HOMO band. Thus introduction of oxidized or reduced states on the polymer backbone causes the formation of stable electron orbitals within the bandgap. Electrons can be excited to the intermediate band from the HOMO or excited from this band to the LUMO, depending on the nature of doping. The oxidized or reduced sites cause structural distortion; these sites are paired charged radicals termed polarons that are stable by virtue of resonance with extensive delocalization over several conjugated repeats. Polarons and the associated bipolarons are essentially mobile distortion states that can shuttle electronic charge along the length of a conjugated polymer. The presence of these defect states is required to achieve high electronic conductivity. Oxidatively modified conducting polymers are described as p-doped while reductively modified conducting polymers are described as n-doped; this nomenclature was appropriated from the inorganic semiconductor field, although the import of these definitions as applied to conducting polymers is very different and often cause for confusion.[133] The p-doped (oxidized) radical cations forms of conjugated polymers are typically much more stable and thus more commonly studied, although n-doped types have also been synthesized.

Most conjugated polymers have a native HOMO-LUMO transition with absorbance peaks in the ultraviolet, and when doping introduces an intermediate band, electrons require less

excitation energy than the original transition. Therefore the neutral forms of conjugated polymers are typically colorless while the doped forms are colored. These polymers are classified as "high band gap" and because they color on oxidative doping they are also anodically coloring. There also exist low band gap conjugated polymers that feature a native HOMO-LUMO band transition that is within the visible range. Doping of these polymers lowers the absorbance to the infrared, removing visible color. Because this doping is typically oxidative, these polymers are typically cathodically coloring, as color is re-established when the oxidative charge carriers are removed.

Polyaniline

Polyaniline (PANI) was synthesized as early as 1862 and is the most widely recognized conducting polymer.[132] The polymer is highly conjugated and exists in a variety of forms depending on the oxidation state and extent of protonation of the nitrogen groups. Colors cross a broad range from transparent yellow for the fully oxidized leucoemeradine form, through yellow/green for the partially oxidized emeraldine salt, and finally to dark blue/black for the fully reduced pernigraniline.[110]

Polyaniline films are generally formed by potentiostatic or galvanostatic electro-oxidation polymerization of aniline monomer onto a working electrode.[134] The compound is deposited in this manner from aqueous acid resulting in a powder or film of p-doped PANI.[135] Initial cyclic voltammetric studies of PANI electrochromism suggested the existence of distinct redox reactions accompanied by color change to yellow at -0.2 V, green at 0.5 V, dark blue at 0.8 V, and black at 1.0 V (vs. SCE). However, the material could be cycled through this voltage range no more than ~300 times before the film became completely black and was no longer electrochromic. Yoneyama determined that the cyclic voltammetry peak at 0.5 V increased with cycles and concluded that this peak was the result of buildup of polyaniline decomposition products. The redox reaction at 0.8 V was found to correspond to polymer decomposition from hydrolysis of the imine nitrogens that are more abundant at higher oxidation states.[136] Thus many earlier studies reporting PANI spectroelectrochemical properties are actually based on superimposed spectra from polyaniline and polyaniline decomposition products (often created during the electrochemical synthesis). Practical electrochromism from PANI stems primarily from visible yellow-blue/green cycling between -0.2V and 0.6 V with an upper limit of 0.7 V (again vs. SCE). The oxidized (blue/green) form is very stable while the reduced (yellow) form is less stable, reacting readily with molecular oxygen to a partially oxidized intermediate form.[136]

As might be expected, pH has a strong effect on the electrochemistry of polyaniline. The potential of the first reduction shifts to lower potentials with pH for pH less than 1, while there is no potential change for pH 1-4. The potential of the second reduction shifts to lower potentials almost linearly with pH for pH less than 4. Polyaniline exhibits no electroactivity at pH greater than 4.[137]

Polyaniline is not soluble in many polar solvents, including water. However, PANI derivatives have been prepared which are soluble in water and exhibit electrochromism.[138] Additionally, PANI can be dissolved in aqueous medium using a co-solvent where PANI is first dissolved in dimethylacetamide (DMAC) which is then added to water in a 90:10 water to DMAC ratio. This method has been used to prepare LBL assembled thin films of PANI and SPS which displayed electrical conductivity of up to 1 S/cm.[2,38,42] LBL assembled films based on hydrogen bonding interactions were cosntructed from PANI and poly(ethylene oxide) PEO which demonstrated similar conductivity.[41] The electrochemistry of polyaniline Langmuir-Blodgett (LB) films has also been explored. The LB films were found to be poorly electrochromic (slow redox switching) due to poor ion transport in the closely-packed polymer matrix.[139]

Though pH effects complicate the electrochemistry of polyaniline, strong color switching makes this material suitable for an anode electrochrome. Polyaniline in its doped state is ionic, which allows the construction of LBL assembled films. Possible challenges involve preventing oxygen bleaching and avoiding electrochemical decomposition to electronically inert by-products.

Polythiophenes

Polythiophenes form a second important group of conducting polymer electrochromes. Polythiophenes are easy to synthesize and process and are very chemically stable. Unlike PANI electrochemistry, polythiophene electrochemistry is not complicated by pH and generally involves simple switching between a doped and a neutral state. Neutral polythiophene becomes oxidized (p-doped) at 1.1 V and reduced (n-doped) at -1.4 V vs. Ag^+/Ag.[135] Unmodified polythiophene films are blue when oxidized and red when neutral. Color can be tailored depending on the type of thiophene monomer chosen.[110]

Polythiophenes can be covalently modified by changing β-substituents or incorporating a second conjugated structure between adjacent thiophene monomers.[113,114,140] The addition of β-position substituents has resulted in poly(3,4-ethylenedioxythiophene) (PEDOT) as well as the commonly investigated poly(3-methylthiophene) and many other 3-substituted poly(thiophene) types. In fact, thiophene monomers have been prepared using these strategies that result in

conjugated polymers possessing red, orange, yellow, green, and blue coloration, spanning almost the entire visible spectrum.[118]

1.3.3.3 Inorganics

A review of electrochromic materials would be incomplete without describing some of the properties of inorganic electrochromes. Inorganic electrochromic films have been studied far longer than organic electrochromes, which are comparative newcomers to the field. The two primary classes of inorganic electrochromes are based on the transition metal oxides and the transition metal hexacyanometallates. For both of these classes, electrochemical transitions are facilitated by the availability of multiple stable oxidation states for the transition metal chromophores.

Tungsten oxide (WO_3) is quite possibly the most-studied electrochromic material ever discovered, and even today is believed to be one of the most promising candidates for the eventual development of commercial devices. WO_3 films are typically applied to electrode surfaces by electrochemical deposition, chemical vapor deposition, or RF sputtering. The coloration of WO_3 occurs cathodically and is accompanied by intercalation –the insertion of protons or alkali metal cations from the electrolyte into the metal oxide film. The intercalation mechanism has been shown to be accompanied by a change in tungsten valence from W^{+6} to mixed $W^{+5/+6}$; this change is accompanied by structural rearrangement and a dramatic increase in the coloration of the normally transparent oxide to a deep blue color. Because WO_3 has been so extensively studied, numerous reviews are available; the reader is referred in particular to those by Granqvist,[141,142] which together contain well over 1000 citations and exhaustively describe all aspects of this transition metal oxide.

Other transition metal oxides display intercalation coloration mechanisms analogous to that of tungsten oxide. Some that have shown particular promise are MoO_3, V_2O_5, and Nb_2O_5.[141] The coloration in these materials is clear to blue upon reduction, exactly the same as that of WO_3, but none can match the high extinction of tungsten oxide coloration. Some of these oxides, most notably V_2O_5, have been employed as transparent counterelectrodes in electrochromic devices because the color change upon reduction is so faint. There also exist transition metal complexes that color upon oxidation – these materials include $Ir(OH)_3$ and $Ni(OH)_2$. The coloration mechanism in these materials is uncertain, with both proton extraction and anion insertion routes being proposed.[143]

A final important class of inorganic electrochromic materials is the transition metal hexacyanometallates.[143-153] The prototype compound of this class is iron(III) hexacyanoferrate(II),

more commonly known as Prussian Blue (PB). Unlike the transition metal oxides, the electrochemistry of PB and analogues is based on direct oxidation or reduction of one of the two metal ion centers, which changes the energy of an intervalence charge transfer complex and causes a concomitant color change. This change in valence is of course accompanied by ion exchange, typically by potassium cations, though other electrolytes can be employed. PB and its analogues display a rich variety of coloration and electrochemical variation that is described in detail in the Chapter 2 of this thesis.

1.3.4 Assembly concepts applied to electrochromic films

Self-assembly concepts have only rarely been applied to the design of electrochromic materials. One of the more persistent assembly concepts is Langmuir-Blodgett (LB) formation of electrochromic electrodes. This LB fabrication almost exclusively concerns the formation of mono- or multilayers of transition metal, lanthanide, and actinide phthalocyanines and derivatives.[154-165] Though electrochromic applications for these LB films were often proposed, the low extinction of the very thin, flat layers was never sufficient to support serious consideration for actual electrochromic devices. Therefore, the LB study of phthalocyanine layers for the most part remained concerned with quantifying charge transfer effects in the highly oriented systems that resulted. Currently the prevalence of new publications in this research area is waning.

Another assembly concept that has been very successfully applied to the fabrication of electrochromic films is sol-gel processing.[166-171] Sol gel concepts have been used to apply all of the known electrochromic (and non-electrochromic) transition metal oxides onto a variety of electrode substrates as thin films. Unlike LB fabrication, these sol gel efforts remain strongly published and in fact seem to be experiencing increased interest as the commercial possibilities of electrochromic displays are once again being considered. Compared to these older and specialized assembly techniques, LBL assembly is a relative newcomer, and the few published examples of LBL assembled electrochromic electrodes will be reviewed in detail in the introduction to Chapter 2 of this thesis.

1.3.5 Analysis techniques

Electrochemical processes are an important area of physical chemistry. Controlled electrochemical experiments have been performed ever since the creation of the galvanic cell provided a reliable power source. This long history of experimentation has resulted in a great preponderance of diverse and complex electrochemical techniques. Many of these techniques are now a part of history, and modern analytical electrochemistry focuses only on a few key procedures. Because these techniques are designed to be sensitive to small amounts of analytes,

they are overwhelmingly voltammetric (imposed potential) rather than amperometric (imposed current). As the potential of the working electrode is modulated, the measured current response of the cell can be used to describe and in some cases quantify the electrochemical processes that are taking place on the working electrode surface. Purposeful variation of the potential is required to attain useful information. Two of the most common potential waveforms that are employed are 1) a linear potential sweep, often cycled multiple times in a "sawtooth" waveform termed cyclic voltammetry, and 2) a square wave potential step waveform, termed either double potential step chronocoulometry or chronoamperometry. This section will briefly review these two general techniques as applied to electrochromic thin films. Several texts are available providing more detailed background concerning electrochemistry.[172-174]

1.3.5.1 Electrochemistry – cyclic voltammetry

Cyclic voltammetry (CV) is the most commonly employed analytical electrochemical technique. New materials are typically subjected to CV in order to determine potentials for redox reactions and the general nature of electrochemical processes. Simply put, CV is an experiment in which the potential of a working electrode is linearly cycled between an upper and lower limit. During potential cycling, the current entering or exiting the electrode is continuously monitored. The resultant data are presented as a current vs. potential plot. Typically the plot exhibits current peaks at the location of greatest oxidation or reduction. Much of the quantitative interpretation of classical solution CV requires an explanation of the mode of kinetic control of the electrode reaction. There are two possibilities: control by *activation* or the rate of the charge transfer process, and control by *diffusion* or the rate of mass transfer of the reacting species to the electrode surface.

If an electrochemical reaction is controlled by the rate of charge transfer at the electrode surface, then the resultant current density will be described by the Butler-Volmer equation which gives the relationship between the measurable current, the exchange current (rate of back-and-forth transfer between oxidized and reduced forms when the electrode is at equilibrium at a given potential), the anodic and cathodic transfer coefficients (which may be asymmetric), and the overpotential of the electrode, all of which control the rate of the chemical reaction and the shape of the cyclic voltammogram. For example, if there is a very low exchange current (very slow establishment of equilibrium), then the cyclic voltammogram will exhibit greater hysteresis between oxidation and reduction peaks with increasing scan rate as the current response progressively lags the applied potential. If there is asymmetry in the anodic and cathodic transfer coefficients, then there will exist corresponding asymmetry in the oxidation and reduction peak

character. Together, this collection of influences renders the electrochemical reaction "electrochemically irreversible," nomenclature that essentially indicates that the electrode reaction is too slow to instantaneously establish equilibrium at a given potential. If there exists a chemical side-reaction of either the oxidized or reduced form, the resultant asymmetry is also sufficient to render the system electrochemically irreversible.

If an electrode reaction is limited by mass transport, then the current is controlled directly by the character of that mass transport. Typically Fickian diffusion is assumed to give a current flow at the electrode that is proportional to the diffusion constant of the electrolyte and the concentration of the active species in the bulk and inversely proportional to the diffusion layer thickness. Mass-transport limited systems are termed "electrochemically reversible" as the electrode reaction features essentially instantaneous establishment of equilibrium between the oxidized and reduced forms of the reactant at the electrode at a given potential.

Although the terms "reversible" and "irreversible" are commonly used throughout electrochemical literature, it is more proper to describe electrochemically reversible reactions as possessing "fast" charge transfer steps and irreversible reactions as possessing "slow" charge transfer steps, because these terms do *not* address the actual chemical reversibility of the oxidation or reduction. A slow, electrochemically irreversible electrode reaction may be completely reversible in the *chemical* sense in that it might be alternately oxidized and reduced indefinitely without loss of material due to degradation. Importantly, the classification of slow and fast electrochemical reactions can change depending on testing conditions; if the electrode potential changes fast enough, the composition of *any* system eventually fails to keep pace, and all reactions are eventually electrochemically irreversible at some limiting potential scan rate. By a similar argument, the structure of electrodes can influence the speed of reaction – porous or coated electrodes can substantially slow the rate of an electrode reaction, rendering it electrochemically irreversible.

For electrochemically reversible reactions, the thermodynamic relation between equilibrium and the electrode potential is given by the Nernst equation:

$$E = E^{\circ\prime} + \frac{RT}{zF} \ln\left[\frac{a_{OX}}{a_{RED}}\right] \qquad \textit{Equation 1}$$

Where $E^{\circ\prime}$ is the formal standard reduction potential of the reactant, z is the number of electrons transferred, a_{OX} and a_{RED} are the chemical activities of the oxidized and reduced species respectively, R is the gas constant, T is the absolute temperature, and F is Faraday's constant. The Nernst equation is often employed to analyze the shape of voltammograms provided that the

reaction is electrochemically reversible over the entire scan. For example, from simultaneous solution of the Nernst equation and diffusion equations for oxidized and reduced species, the Randles-Sevcik equation indicates that the CV current peak height for dissolved redox species should increase linearly with the square root of the scan rate, whereas a similar solution indicates that the peak height for a sequestered monolayer of redox material should increase linearly with the scan rate. Reversible CVs also possess equivalent current density peak heights for oxidation and reduction, and the potential locations of these peaks are independent of scan rate and separated by ~59 mV. Furthermore, the average potential of the reduction and oxidation peaks $E_{1/2}$ is equivalent to the formal potential of a redox couple $E^{o'}$.

Much of the elegance of CV interpretation is lost when considering the electrochemistry of polymer films thicker than a monolayer, because such systems almost invariably manifest electrochemically irreversible behavior. The primary factor that causes non-ideal behavior is the variable separation between the electrode surface and the reaction zone. As the reaction proceeds through the bulk of a film, the location of the redox "front" must move (presumably) outward away from the electrode surface. This displacement forces electrons through already-reacted material to travel between the electrode surface and reaction front. The electronic conductivity of the electrode film thus plays a key role in the speed of thick electrode film reactions because the voltage drop that is the product of the passed current and the resistance of the current path limits the potential at the reaction front, which can then be significantly different than the nominal applied potential reported by the potentiostat. This resistance can be considerable for many systems because reacting electrons must essentially make a long series of tunneling jumps rather than one single jump at a clean planar electrode (as for solution electrochemistry). Reactions that might be electrochemically reversible in a monolayer or in free solution will inevitably appear irreversible in a thicker film due to this "variable iR drop." This description is even more complicated in that the electrochemical conversion of real films most likely does not proceed in a linear front but more likely proceeds in a branching and highly distributed manner throughout the electrode film depending on the connectivity of the redox material and local tunneling barriers. Because the speed and local availability of mass transport can influence the speed and nature of this redox propagation (and thus the nature of charge transfer steps), contributions between mass transport and charge transfer are highly interacting in thicker films. Furthermore, diffusion processes in solid films are often activated processes rather than pure Fickian diffusion, so that reactions can appear limited by charge transfer (an activated process) but in reality might be limited by activated mass transport.

Electrochemical irreversibility such as that described above is indicated in CV scans by an increasing hysteresis in the oxidation and reduction peaks with increasing scan rates. This hysteresis increases with increasing resistance in the electrodes, and thus it is possible to distinguish different degrees of irreversibility by considering the extent of this hysteresis. Some of the mathematics of reversible solution electrochemistry can be applied to electrochemistry of irreversible films. Most importantly, scan-rate dependencies derived from Randles-Sevcik can still be applied, albeit in a more qualitative fashion. Electrochemical reactions in polymer films that are slowed by ionic diffusion will show a more linear dependence between peak height and the square root of scan rate, whereas a linear dependence between height and rate suggests faster ion diffusion as compared to electron transfer.

Because the monitored current for reductive and oxidative sweeps in CV is primarily Faradaic – relating to reacting electrons rather than capacitative charge storage – this current is often integrated in order to determine the Faradaic charge capacity of the electrode. Faradaic charge capacity is the total number of Coulombs of charge that are consumed or produced by the electrochemical reaction, and can be related directly to molar amounts of electrons using Faraday's constant. Due to resistive contributions to the CV from thick polymer films, the establishment of a proper baseline for integrating the CV current response is often problematic.

Deeper mathematical analysis of electrochemically irreversible reactions in thin polymer films is considerably more complicated that that of reversible, solution-phase redox species in solution. Any calculation would require intrinsic knowledge of the complete system architecture, local density variations, orientation and connectivity of redox material in the film, resistances to intermolecular charge transfer, diffusion coefficients in every region, and complete quantification of mechanisms of charge and ion transfer within the film. Such a calculation would almost certainly involve a finite element approach and numerical solution of simultaneous electric field and ionic flux equations. As such, the quantitative derivation of fundamental physical parameters from CVs of polymer films, aside from redox potential determination and qualitative judgments of electrochemical behavior, is beyond the scope of this thesis work.

1.3.5.2 Electrochemistry – square wave switching

Square wave switching provides an alternative to CV that can more simply be used to determine the Faradaic charge capacity of films, which can then be stoichiometrically related to the absolute number of redox centers in the film, leading to important compositional information. In this method, the potential of the electrode is instantaneously switched between a potential where the electrode film is entirely reduced to a potential of complete oxidation.

Stepping is typically performed multiple times. The current is monitored during this square wave switching, and integration of this current can give a Faradaic charge capacity. The speed at which the film approaches reaction completion can be observed directly by the speed of current decay, which is also the speed that the Coulombic integration approaches a limiting value.

Some factors must be taken into account for this type of coulometry to assure that the current is entirely Faradaic. Contributions to the current response from capacitative charging and parasitic resistances must be subtracted or otherwise eliminated. Capacitative charging can be determined by performing preliminary switching experiments on bare electrodes. The charging current can then be subtracted from the response of a film-coated electrode. Typically the capacitative contribution is an order of magnitude smaller than Faradaic contributions. Persistent parasitic resistances can be evaluated at by holding the electrode at a single potential until equilibrium is achieved. The parasitic current that is recorded, again usually much smaller than the Faradaic contribution, can then be removed from the switching response.

1.3.5.3 Spectroelectrochemistry

By the intention of their design, electrochromic films must eventually be evaluated using some sort of visible spectroscopy. This measurement is typically performed by depositing the electrochromic film on a transparent electrode and then immersing that electrode in an electrochemical cell, through which is passed a collimated UV-Vis light beam. The film absorbs the light beam, and the variation in light absorbance can be measured as a function of potential. If the measurement speed of the spectrograph is sufficiently fast, then the kinetics of color change can also be measured by evaluation of the change in absorbance at a particular wavelength during the application of a square potential wave.

Different representations of optical absorbance data are employed depending on the intention of the investigator and the envisioned application. The absorbance of ultraviolet-visible (UV-Vis) light by colored species is typically quantified by either percent transmittance (%T) or absorbance units as a function of light wavelength or energy. The former gives an absolute account of the percentage of light energy allowed through the film, and is often used to quantify the performance of light-blocking devices such as liquid-crystal displays or electrochromic thin films. The %T is an extrinsic quantity as it is completely dependent on the path length of the beam through the absorbing species and the quantity or concentration of absorbing species.

Absorption units are related directly to the Beer-Lambert law (Equation 2), which is often used to quantify visible absorbance from soluble species.

$$\varepsilon cl = Log\left[\frac{I_O}{I}\right] \qquad \textit{Equation 2}$$

In the Beer-Lambert law, the product of ε the extinction coefficient, c the colored species concentration, and l the beam path length, is equal to the base-10 logarithm of the ratio of incident intensity divided by the transmitted intensity. This logarithm is the commonly used "absorbance unit." The extinction coefficient ε is an intrinsic quantity related directly to the species being evaluated. As ε is independent of path length and concentration, it is perhaps the best indicator of relative performance when comparing the optical absorbance of different species. In particular, the difference between ε in the bleached vs. the colored state should be an important performance indication for an electrochromic species.

The *Beer-Lambert* law can also be applied to electrochromic thin films. In thin films, the path length l is the film thickness, while the concentration c is now the solid chromophore concentration. Film thickness can be easily determined by a number of methods, and chromophore concentration can be determined from the Faradaic charge density attained by square wave switching or integration of CV scans. These data together allow a complete calculation of the intrinsic coloration capabilities of an electrochromic material as the extinction coefficient can be fully described. Chromophore concentration and extinction coefficient information are more useful than thickness-dependent metrics that are commonly used such as the optical density, coloration efficiency, and colorimetric luminance because they allow the calculation of optimum film thickness to reach a desired performance goal expressed by any of these extrinsic metrics.

1.3.6 The Electrochromic Device

Commercial electrochromic devices (ECDs) have been envisioned for over 30 years, yet ECD performance is only now becoming commercially viable. Early research indicated that the switching speed of ECDs was too slow for dynamic display applications. Furthermore, many devices had a short working cycle life, with performance gradually deteriorating over time. Liquid crystal displays and the cathode ray tube did not suffer from these faults and absorbed the lion's share of research funds. As a result of these early weaknesses, ECDs have thus far received little attention, except for applications where LCD and CRT technology are less appropriate, such as "smart windows." ECD development has focused on enhancing switching speed and device lifetime, as well as providing a greater spectral range to devices. To improve performance in this fashion, ECD architecture and material systems must be addressed. An ECD is a simple one-dimensional construction of three different material systems described below.

The *anode* and *cathode electrochromes* provide color for the ECD. Important issues with these electrochromic electrodes have already been described above, including contrast, speed, and color range. An additional factor that must be considered when these electrodes are operating in a device is the cycle life, or the number of times that the electrodes can be reversibly switched between the colored and bleached states before coloration is degraded. Ideally, an electrochromic cell would feature a complementary configuration with electrochromes that are simultaneously transparent and color together. Additionally, the redox reaction should be infinitely reversible, and the speed of coloration should be limited only by the natural reaction kinetics and not ion transport through the electrochrome film. Although these ideals are not truly achievable, candidate material systems can be selected based on these criteria.

The *electrolyte* provides ions for charge transport between the cathode and anode. Typically, the electrolyte presents the greatest resistance to coloration due to poor ion transport. Ideally, an electrolyte would not severely limit the speed of a device. However in most devices, both the electrochrome and electrolyte films are solids, and transport is naturally inhibited. A detailed description of the properties of polymer electrolytes is provided in the following section of this background chapter.

Despite these stringent materials requirements, there exist many examples of successful organic ECDs. One of the earliest was a solution-phase hexylviologen device developed in the early 70's by Schoot.[175] This device featured coloration times of 10-100 ms and erasure times of 10-50 ms, both limited by chromophore diffusion. Perhaps the most sophisticated device ever constructed so far was developed by IBM in the mid 1980s, which features an array of 96,000 micron-scale devices similar to Schoot's, with write times of 2 ms and 32 levels of gray scale, integrated as the dynamic flat-panel display shown in Figure 1.2.[176]

Figure 1.2 - IBM heptylviologen ECD display[176]

Other displays developed by the IBM group have been based on light scattering of viologen radical cations (rather than chromic properties).[177] More recent displays have not strayed profoundly from the original devices, as seen in a recent characterization of a 3X3 matrix array of heptylviologen in solution.[178] With the increase in development of conjugated electronically conducting polymers, the use of these materials in ECDs has risen to a level approximately equal to that of the viologen family. An example is the recent interest in hybrid organic/inorganic PANI/PAMPS/WO_3 devices.[179-181] These were designed for electrochromic windows, with coloration and bleaching times of 10-30 seconds.[179] EDOT-derived PEDOT/PMAA+Li^+/PBEDOT devices developed by Reynolds featured switching times more on the order of 100 ms, while demonstrating about 40% optical response deterioration over 10^4 cycles.[118]

An important new electrochemical cell concept has recently appeared from development efforts at NTera Ltd, an organic/inorganic electronics research concern based in Ireland and Switzerland that has developed both electrochromic devices[182] and more recently photovoltaic devices[183-185] exploiting the incorporation of semiconducting nanoparticles onto electrode surfaces. The electrochromic devices fabricated by NTera possess porous / particulate electrodes of n-type semiconducting material such as anatase TiO_2, with pore and crystallite sizes ranging over 5-20 nm. The surfaces of these pores and particles are modified by chemisorbing a monolayer of specially synthesized viologen that behaves as a phosphonic-type SAM and binds irreversibly to the oxide. Electrochemical switching of this monolayer is very fast because the switching material is in intimate contact with both the nanostructured electrode and liquid electrolyte; there is essentially no charge transfer or ion transport limitation and the switching of these devices is limited only by the intrinsic reaction rate with the result of full switching in as fast as 20 milliseconds. Coloration is greatly exaggerated by the large modified surface area and internal reflections within the modified electrode, enhancing the contrast of the viologen monolayer 100-1000 times as compared to a flat monolayer that would not exhibit contrast visible to the human eye. This cell concept is thus far the only electrochromic cell that has displayed such promising characteristics, evincing performance that is competitive with LCD displays.

1.4 Solid polymer electrolytes

1.4.1 Introduction to polymer electrolytes

Solid polymer electrolytes are becoming increasingly important in the design of lithium batteries, fuel cells, sensors, and electrochromic devices. Solid electrolytes are superior to liquid electrolytes in that they do not flow and generally are more chemically compatible with electrode materials. Polymer-type solid electrolytes have been the most-studied because they can be easily applied as a flexible and conformal film, are generally of low cost, and conduct well at room temperature.[186] In fact, the conductivity of some polymer-based electrolytes can approach that of liquid solutions at ambient temperature.

The development of solid polymer electrolytes focuses on the key goal of increasing ionic conductivity in the electrolyte matrix. Increasing the ionic conductivity leads to higher battery power density because there is less power lost to heat generated by electrolyte resistance during charging and discharging. Higher ionic conductivity can also lead to faster electrochromic film switching speeds and the faster response of electrochemically-based sensors. It remains vital that the mechanical properties of solid electrolytes also be improved. In particular, improved mechanical integrity of the electrolyte can lead to a decrease in the thickness of the electrolyte layer that is required to avoid shorting defects. Also, the chemical compatibility of the electrolyte layer is important; side reactions with either the cathode or the anode typically inflict detrimental effects on device performance, be it a decrease in the recharge depth of batteries with the formation of a resistive plaque on the graphite/lithium anode or a reduction in the color contrast of electrochromic films with the formation of colored byproducts within the electrolyte.

1.4.2 Common types of polymer electrolytes

1.4.2.1 Salt hosts

Ionically conductive polymers can be derived from several key types. The most commonly employed anhydrous polymer electrolyte is composed of a polar matrix or "host" polymer such as poly(ethylene oxide) (PEO), poly(acrylonitrile) or some other highly polar polymer. This host is then used as a "solid solvent" to dissolve an alkali metal salt – in lithium batteries most often a low lattice energy salt such as lithium triflate. Strong associations between lithium cations and the host polymer cause dissociation and coordination within the lattice to be enthalpically favored. This process is especially favored in PEO, where the atomic spacing is optimized for lithium dissolution and geometry results in a 5-membered ring arrangement of the dissolved lithium cation and PEO chain. Ionic conduction is then facilitated in this matrix by an

activated process whereby the lithium cations "hop" from coordination cradle to coordination cradle within the PEO host matrix. This hopping mechanism is directly coupled to short-range segmental motion of PEO chains. In fact, it might be said that the PEO actually "moves" the lithium cation by the rearrangement of PEO polymer chains that brings a lithium cation into unimpeded close proximity to another coordination site. Solid electrolytes based on PEO/lithium salt complexes exhibit conductivities up to 10^{-4} S/cm at temperatures above the 65°C melting point of PEO. At temperatures lower than its melting point, PEO becomes highly crystalline, and lithium transport is greatly hindered due to the general absence of facilitating segmental motions. Room temperature conductivity is typically 10^{-8} S/cm or lower, impractical for most commercial applications. The potential of polymer electrolytes of this type was first described by Armand in 1973,[187] who is considered the grandfather of the polymer electrolyte field and has written several reviews.[188-194]

Because of the lowered ionic conductivity at room temperature, the strategy of adding plasticizer or solvent to the host polymer to improve ion mobility has been successfully employed for years and remains the primary paradigm for fabricating polymer electrolytes for use in lithium battery applications. Typical plasticizers include propylene carbonate, ethylene carbonate, N, N-dimethyl formamide, and γ-butyrolactone.[186] However, any type of solvent swelling (e.g. water) will increase ionic conductivity by increasing plasticity and thus reducing hindrance to ionic mobility, which is now widely recognized as the key factor controlling ionic conductivity.[195] It is important to note that plasticized ion conductors sometimes employ other polar polymers rather than PEO to achieve different mechanical properties because the conductivity mechanism is no longer dependent on the special ion-solvation properties of PEO due to the plasticizer acting as a solvent for the salt.[186] Plasticized polymer electrolytes, while not completely solid, display room-temperature conductivities approaching 10^{-3} S/cm, which are suitable for applications such as lithium-ion batteries.

1.4.2.2 Polyelectrolytes

A second class of polymer electrolytes are the *polyelectrolytes*. Polyelectrolytes are almost always employed while hydrated to encourage the dissociation of counterions to act as mobile species. Without this dissociation (and in some cases even with dissociation), polyelectrolytes typically self-organize into hydrophobic matrices with dry ionic clusters that display poor ion conductivity and poor mechanical flexibility.[186] A polyelectrolyte that is a current favorite of the electrochromic community is poly(2-acrylamido 2-methyl propane sulfonic acid) (PAMPS).[179-181] The most popular electrochromic application for PAMPS involves WO_3|PAMPS|PANI hybrid

organic/inorganic electrochromic cells.[179,196,197] Apparently the PAMPS acts to chemically dope the PANI, providing some electrical conduction even when the PANI is primarily neutral. However, just as for plasticized PEO, hydrated PAMPS gels are not truly solid polymer electrolytes in the sense that they are customarily hydrated and pH-adjusted depending on application.

Some very specialized polyelectrolytes form a subclass of perfluorinated ionomers. This group of materials are composed of random copolymers containing (typically) a poly(tetrafluoroethylene) (PTFE) backbone with the random inclusion of monomer units possessing perfluoroether side chains tipped with acid groups. The most well-known perfluorinated ionomer is DuPont's Nafion, which is a poly(sulfonic acid). Because of the proximity of highly electronegative fluorine groups, sulfonic acid groups of Nafion are exceptionally acidic and in fact Nafion is considered a solid superacid in ion exchange applications. The perfluorinated ionomers are insoluble in most solvents. When properly processed, these materials can form membranes that possess the mechanical strength of the PTFE backbone with the added benefit of acid-lined pores of 5-10 nm diameter that connect through the thickness of the film and facilitate fast ionic conduction when fully wetted by proton hopping between sulfonic acid groups. The flexible perfluoroether side chains assist in this motion, which takes place in an essentially fully liquid phase. Polyelectrolytes such as Nafion that possess this specialized secondary structure exhibit ionic conductivity close to that of liquid solutions; values near 10^{-2} S/cm are not unusual. Levels of this magnitude are required for the proper operation of fuel cell membrane electrode assemblies. Higher resistance levels increase waste heat, which can vaporize the water in the membrane, which in turn lowers conductivity further in a runaway failure mode than can result in cell destruction. The structure of perfluorinated ionomers is critical to their performance, in particular pore size and connectivity.

1.4.3 Assembly concepts for polymer electrolytes

The most common assembly concept to be applied to the design of polymer electrolytes is the phase segregation and rearrangement of block copolymers. This perhaps comes as no surprise considering the high conductivity of the Nafion system that has been known since the early 1970s. Nafion features essentially random poration, whereas the highly controlled cylindrical architectures of block copolymers are regarded as a more ideal structure for polymer electrolytes. Typically the major phase of the block copolymer would be a structurally sound and chemically stable polymer, whereas the minor phase would be a polyether of some sort. The first full realization of this strategy was published in the mid-1980s by Gray and MacCallum for the

grafting of PEO side chains to a poly(styrene-b-isoprene-b-sytrene).[198] The technique has since been advanced by other researchers, to include many types of diblock, comb, and triblock systems.[199-206] The concept has been extended to the creation of nanostructured battery electrodes as well.[207]

A second assembly mechanism that has been applied to the formation of polymer electrolytes has been the dispersion of inorganic oxide particles in the solid polymer matrix. While this may not be considered a truly assembly-based technique, it bears some hallmarks of nanoengineering in the sense that the inorganic nanoparticles directly affect the phase behavior of the polymer. In general, the addition of either ion-conducting or inert ceramic nanoparticles has been shown to increase the room-temperature conductivity of unplasticized polymer electrolytes. Interestingly, this enhancement appeared in the literature at about the same time as the block copolymer solid electrolytes were first investigated.[208] Upon initial consideration, the conductivity increase is unlooked-for because ceramic addition should increase the polymer T_g and decrease conductivity in the bulk. The generally accepted explanation for the conductivity increase is that the ion transport takes place at amorphous polymer-ceramic grain boundaries, which are increased in area and number for smaller particles and larger particle loadings. Reviews of this phenomenon and important advances in the work have been written by Kumar and Scanlon.[209,210]

Because of the amorphous and presumably homogenous films that LBL assembly can create, it would be expected that any benefits derived from LBL assembled polymer electrolytes would be due to amorphicity-enhancing properties more similar to those provided by the inorganic/polymer nanocomposites rather than the phase-segregation benefits of block copolymers. Thus far there has been only one investigation into the ion conduction properties of LBL assembled films[211] that will be discussed in detail in Chapter 5 of this thesis.

1.4.4 Impedance analysis

Impedance analysis is the primary test used to evaluate the performance of polymer electrolytes. Like the other electrochemical techniques employed in this work, impedance analysis in its most common form is a voltammetric technique. Importantly, however, impedance analysis as employed in this thesis is not a Faradaic technique because the potentials employed are carefully chosen to be far below those required for any electrochemical reactions. Instead impedance analysis can be used to determine the non-Faradaic contributions to the current response of solid electrolytes, most notably ionic motion.

Theoretically, these non-Faradaic contributions could be probed using the same set of tools used to probe Faradaic processes, but at smaller potential levels. For example, the capacitative response of a material might be probed by applying a potential square wave and monitoring the rate of current decay. However, these DC techniques cannot discriminate between the multiple contributions that influence such a response; a lumped response is attained, and deconvolution is an intractable problem. To overcome these difficulties, the technique of AC impedance was introduced to the solid electrolyte field in 1969,[212] though it had been used in solution electrochemistry for some time previously.[213] In small-amplitude AC impedance analysis, a sinusoidal AC perturbation is introduced across a polymer electrolyte film. Unlike a high amplitude DC signal, a small AC perturbation introduces no changes to the film composition or morphology and does not cause sustained polarization. Instead the AC signal is responsible for small-scale movements of ions and dipole orientation and relaxation effects in the film; the scale of ion motion and relaxation processes is limited by the fast application duration and bulk polarization does not occur (except at very low frequencies). Typically the AC signal is scanned over a large frequency range in order to separate responses that may take place within the film at different time scales. If the AC signal does activate certain processes, these processes will interact with the AC potential signal either by altering the magnitude of the current response (resistive effects such as ion motion) or changing the phase of the current response (reactive effects such as dipole relaxations). All materials display both resistive and reactive behavior at some time scale.

Impedance analysis thus measures a current response that is correlated to a certain voltage perturbation as a function of frequency. There are many possible ways to represent such data, but the most common is based on an electrical engineering abstraction termed the complex impedance. The complex impedance completely describes the relationship between the magnitude and phase of the applied voltage and current response at a given frequency. Various mathematical descriptions of a complex quantity such as the impedance Z are shown in Equation 3.

$$Z = Z' + jZ'' = |Z|e^{j\theta} = |Z|(\cos\theta + j\sin\theta) \qquad \textit{Equation 3}$$

The complex representation of applied AC potential can be divided by impedance to return the current response, which will have a magnitude $|V||Z|^{-1}$ and be phase-shifted from the potential by θ. An AC impedance analysis derives the complex impedance Z from the measured current response, and that complex impedance can be further analyzed to derive information concerning

important physical processes in the film, separated based on the time scale (or frequency) of the response. The impedance can be directly transformed into admittance, dielectric modulus, and dielectric permittivity using only physical parameters of the system in the calculation and no further data collection. For analysis of ionic conducting polymer electrolytes, however, the complex impedance is typically the immitance of most interest because *resistance* contributions can be directly examined. In highly ion conducting systems, the strong contribution of ion motion to all of the immitances typically obviates detailed investigations into dielectric phenomena in the same materials.[214] The presence of any plasticizer further decreases the probability of observing dielectric phenomona directly related to the polymer host.

The complex impedance is typically represented on a plot of $-Z''$ vs. Z' on the complex plane with implicit frequency. On this plane, purely resistive contributions will appear as positive translations in the real component while reactive contributions will cause positive (capacitative) or negative (inductive) translations on the complex axis with ever-increasing or ever-decreasing magnitude. While at first blush the derivation of physical parameters from this representation may seem straightforward, such derivation becomes complicated with the realization that in real samples multiple reactive and resistive effects can occur simultaneously, and interactions between these effects are complicated by sample layout, geometry, and the type of physical process (parallel vs. series arrangement of elements). The simultaneous activation of one resistive and one reactive component (arranged in parallel) results in a semicircle on the complex plane with a diameter equal to the resistance and a maximum imaginary component "peak" exactly at the characteristic time scale of the reactive component. Thus the impedance analysis of real samples on the complex plane typically appears as some intricate combination of positive real translations, semicircles, and reactive imaginary spikes.

Given the preponderance of electrical engineering analogy used thus far in the analysis of impedance, it is perhaps no surprise that the primary method for extracting physical parameters from the complex impedance is to design an "equivalent circuit" built from ideal electrical engineering components such as resistors and capacitors and representing the investigator's best understanding of the physical arrangement of processes within the material. A material that is primarily conducting such as a metal could be represented as a single resistor while a material that is extremely resistive yet polarizable such as a ceramic might be represented as a single capacitor. More complex materials exhibiting polarization processes *and* conductivity might be represented as a capacitor and resistor in parallel. Typically, contributions from the cell design and measurement apparatus must be taken into account as well, further complicating the equivalent circuit.

Often the real response of a system does not easily fit into an idealized electrical engineering combination of capacitors, resistors, or inductors. The most common solution to this problem has been to develop nonstandard elements for the equivalent circuit to achieve a better match between the model and reality. One example of a nonstandard element is the so-called Warburg impedance, which models the Faradaic charge exchange at an electrode where the charge transfer is diffusion controlled. Being representative of a Faradaic process, the Warburg impedance does not appear in equivalent circuit models developed within this thesis. Another example of a nonstandard circuit element is the constant phase element (CPE). The CPE is a reactance element similar to a capacitor that is very commonly used to model systems that show some sort of distribution or dispersion in the characteristic reactance time of the system. Distributed systems are often modeled more rigorously using a construct of interconnected resistors and capacitors termed a "transmission line." The transmission line also shows constant phase behavior, and mathematically a CPE and transmission line are identical,[215] except that the CPE is a lumped response with far fewer fit parameters that is more appropriate for situations in which the individual elements of a transmission line cannot be discriminated and accurately fit. One example of this behavior is the appearance of a low-frequency CPE typically attributed to microscopic fractality (roughness) at electrode surfaces that gives rise to a distribution in the interaction of the double layer with the electrode surface that should not appear if the electrode were atomically flat. High-frequency CPE behavior characteristic of the bulk sample is often attributed to a distribution of bulk dipole relaxation times due to heterogeneity in sample composition. The impedance of a CPE is given by the following equation.

$$Z_{CPE} = \frac{1}{Q(j\omega)^{\alpha}} \qquad \textit{Equation 4}$$

It is important to note that the quantities Q and α *do not* have associated physical meanings as do most equivalent circuit elements, although α might be regarded as indicating the extent of dispersion in the system reactance. As α approaches 1, the CPE becomes a capacitor with capacitance Q. One fingerprint of CPE-like behavior is the existence of depressed semicircles on the imaginary plane. The depression of the semicircles is generally attributed to a distributed property of the system, and the substitution of a CPE for the capacitative element enhances the fit. MacDonald observes that the CPE often fits real systems so surprisingly well that few investigators are dissuaded from using it even though its basis is almost completely empirical.[216] The CPE is described in detail here because it fits the reactance behavior of bulk LBL assembled films quite well, allowing the extraction of ionic resistance from the equivalent circuit with less

error. Given that these films are complex mixtures of multiple components, possibly containing multiple domains, some dispersion in the reactance of the films might be expected and the use of the CPE appears appropriate in this context.

Once an equivalent circuit is designed from both standard and nonstandard elements, it is straightforward to use mathematical techniques to vary the values of the individual components and fit the response of the circuit to that of the real impedance cell. The values attained from this fitting can often be directly related to physical processes; typically, the ionic resistance component of the sample is represented by one of the resistors in the equivalent circuit. With an ionic resistance and knowledge of the physical measurements of the cell (the cell constant), the conductivity can be directly calculated. Deeper discussion of impedance analysis as applied to the evaluation of ionically conductive LBL assembled films engineered in this thesis is provided in Chapter 5. The reader is also referred to several reviews and texts on the subject.[214,216-218]

1.5 Cited Literature

(1) Iler, R. K. *J. Colloid Interface Sci.* **1966**, 569.
(2) Michaels, A. S. *Ind. Eng. Chem.* **1965**, *57*, 32-40.
(3) deJong, H. G. B. In *Colloid Science*; Kruyt, H. R., Ed.; Elsevier Pub. Co.: New York, 1949; Vol. 2, pp 335-480.
(4) Decher, G.; Hong, J. D. *Makromol. Chem., Macromol. Symp.* **1991**, *46*, 321-327.
(5) Decher, G.; Hong, J. D. *Ber. Bunsen-Ges. Phys. Chem. Chem. Phys.* **1991**, *95*, 1430-1434.
(6) Decher, G.; Hong, J. D.; Schmitt, J. *Thin Solid Films* **1992**, *210*, 831-835.
(7) Stuart, M. A. C. In *Proceeding of the XXXth Rencontres de Moriond*; Daillant, J., Guenoun, P., Marques, C., Muller, P., Vân, J. T. T., Eds.; Gif-sur-Yvette: Paris, 1996, pp 1-12.
(8) Lowack, K.; Helm, C. A. *Macromolecules* **1998**, *31*, 823-833.
(9) van de Steeg, H. G. M.; Cohen Stuart, M. A.; de Keizer, A.; Bijsterbosch, B. H. *Langmuir* **1992**, *8*, 2538.
(10) Bonekamp, B. C.; Vanderschee, H. A.; Lyklema, J. *Croat. Chem. Acta* **1983**, *56*, 695-704.
(11) Stuart, M. A. C.; Tamai, H. *Langmuir* **1988**, *4*, 1184-1188.
(12) Durand, G.; Lafuma, F.; Audebert, R. *Prog. Colloid Polym. Sci.* **1988**, *76*, 278-282.
(13) Lvov, Y.; Decher, G.; Mohwald, H. *Langmuir* **1993**, *9*, 481-486.
(14) Krozer, A.; Nordin, S. A.; Kasemo, B. *J. Colloid Interface Sci.* **1995**, *176*, 479-484.
(15) Glinel, K.; Moussa, A.; Jonas, A. M.; Laschewsky, A. *Langmuir* **2002**, *18*, 1408-1412.
(16) Xie, A. F.; Granick, S. *Macromolecules* **2002**, *35*, 1805-1813.
(17) Bohmer, M. R.; Evers, O. A.; Scheutjens, J. *Macromolecules* **1990**, *23*, 2288-2301.
(18) Tanaka, H.; Tachiki, K.; Sumimoto, M. *Tappi* **1979**, *62*, 41-44.
(19) Blaakmeer, J.; Bohmer, M. R.; Stuart, M. A. C.; Fleer, G. J. *Macromolecules* **1990**, *23*, 2301-2309.
(20) Bohmer, M. R.; Sofi, Y. E.; Foissy, A. *J. Colloid Interface Sci.* **1994**, *164*, 126-135.
(21) Dupont, L.; Foissy, A. *Colloid Surf. A-Physicochem. Eng. Asp.* **1996**, *110*, 235-248.
(22) Yoo, D.; Shiratori, S. S.; Rubner, M. F. *Macromolecules* **1998**, *31*, 4309-4318.
(23) Shiratori, S. S.; Rubner, M. F. *Macromolecules* **2000**, *33*, 4213-4219.
(24) Dubas, S. T.; Schlenoff, J. B. *Macromolecules* **2001**, *34*, 3736-3740.
(25) Linse, P. *Macromolecules* **1996**, *29*, 326-336.
(26) Mendelsohn, J. D.; Barrett, C. J.; Chan, V. V.; Pal, A. J.; Mayes, A. M.; Rubner, M. F. *Langmuir* **2000**, *16*, 5017-5023.
(27) Amirpour, M. L.; Ghosh, P.; Lackowski, W. M.; Crooks, R. M.; Pishko, M. V. *Analytical Chemistry.* **2001**, *73*, 1560-1566.
(28) Chen, B.; Rubner, M.; Cohen, R. 2001.
(29) Choi, J. Y.; Rubner, M. E. *J. Macromol. Sci.-Pure Appl. Chem.* **2001**, *38*, 1191-1206.
(30) Fery, A.; Scholer, B.; Cassagneau, T.; Caruso, F. *Langmuir* **2001**, *17*, 3779-3783.
(31) Chung, A. J.; Rubner, M. F. *Langmuir* **2002**, *18*, 1176-1183.
(32) Finkenstadt, D.; Johnson, D. D. *Langmuir* **2002**, *18*, 1433-1436.
(33) Kato, N.; Schuetz, P.; Fery, A.; Caruso, F. *Macromolecules* **2002**, *35*, 9780-9787.
(34) Decher, G. *Science* **1997**, *277*, 1232.
(35) Hammond, P. T. *Curr. Opin. Colloid Interface Sci.* **2000**, *4*, 430-442.
(36) Decher, G.; Schlenoff, J. B., Eds. *Multilayer thin films*; Wiley: Weinheim, 2003.
(37) Ferreira, M.; Cheung, J. H.; Rubner, M. F. *Thin Solid Films* **1994**, *244*, 806-809.
(38) Cheung, J. H.; Fou, A. F.; Rubner, M. F. *Thin Solid Films* **1994**, *244*, 985-989.
(39) Fou, A. C.; Rubner, M. F. *Macromolecules* **1995**, *28*, 7115-7120.
(40) Ferreira, M.; Rubner, M. F. *Macromolecules* **1995**, *28*, 7107-7114.
(41) Stockton, W. B.; Rubner, M. F. *Macromolecules* **1997**, *30*, 2717-2725.
(42) Cheung, J. H.; Stockton, W. B.; Rubner, M. F. *Macromolecules* **1997**, *30*, 2712-2716.

(43) Ferreira, M. S.; Rubner, M. F.; Hsieh, B. R. In *MRS Symposium Proceedings, 1995*, 1995; Vol. 328, pp 119-124.
(44) Fou, A. C.; Onitsuka, O.; Ferreira, M.; Rubner, M. F.; Hsieh, B. R. *J. Appl. Phys.* **1996**, *79*, 7501-7509.
(45) Baur, J. W.; Kim, S.; Balanda, P. B.; Reynolds, J. R.; Rubner, M. F. *Adv. Mater.* **1998**, *10*, 1452-1455.
(46) Wu, A.; Yoo, D.; Lee, J. K.; Rubner, M. F. *J. Am. Chem. Soc.* **1999**, *121*, 4883-4891.
(47) Clark, S. L.; Handy, E. S.; Rubner, M. F.; Hammond, P. T. *ACS Polym. Prepr.* **1998**, *39*, 1079-1080.
(48) Kim, T. S.; Crooks, R. M.; Tsen, M.; Sun, L. *J. Am. Chem. Soc.* **1995**, *117*, 3963-3967.
(49) Pigoislandureau, E.; Nicolau, Y. F.; Delamar, M. *Synth. Met.* **1995**, *72*, 111-119.
(50) Tian, J.; Wu, C. C.; Thompson, M. E.; Sturm, J. C.; Register, R. A. *Chem. Mater.* **1995**, *7*, 2190-2198.
(51) Kim, D. S.; Char, C.; Hong, J. D.; Yu, S. H.; Jin, J. I. *Polym.-Korea* **1996**, *20*, 915-924.
(52) Zhou, P. G.; Samuelson, L.; Alva, K. S.; Chen, C. C.; Blumstein, R. B.; Blumstein, A. *Macromolecules* **1997**, *30*, 1577-1581.
(53) Cassagneau, T.; Mallouk, T. E.; Fendler, J. H. *J. Am. Chem. Soc.* **1998**, *120*, 7848-7859.
(54) Neumann, R.; Davidov, D. *Acta Polym.* **1998**, *49*, 642-651.
(55) Tarabia, M.; Hong, H.; Davidov, D.; Kirstein, S.; Steitz, R.; Neumann, R.; Avny, Y. *J. Appl. Phys.* **1998**, *83*, 725-732.
(56) Ram, M. K.; Salerno, M.; Adami, M.; Faraci, P.; Nicolini, C. *Langmuir* **1999**, *15*, 1252-1259.
(57) Ho, P. K. H.; Kim, J. S.; Burroughes, J. H.; Becker, H.; Li, S. F. Y.; Brown, T. M.; Cacialli, F.; Friend, R. H. *Nature* **2000**, *404*, 481-484.
(58) Kovtyukhova, N. I.; Gorchinskiy, A. D.; Waraksa, C. *Mater. Sci. Eng. B-Solid State Mater. Adv. Technol.* **2000**, *69*, 424-430.
(59) Raposo, M.; Oliveira, O. N. *Langmuir* **2000**, *16*, 2839-2844.
(60) Sarkar, N.; Ram, M. K.; Sarkar, A.; Narizzano, R.; Paddeu, S.; Nicolini, C. *Nanotechnology* **2000**, *11*, 30-36.
(61) Li, D.; Lutt, M.; Shi, X.; Fitzsimmons, M. R. *Mater. Res. Soc. Symp. Proc.* **1998**, *488*, 401-406.
(62) Lukkari, J.; Salomaki, M.; Viinikanoja, A.; Aaritalo, T.; Paukkunen, J.; Kocharova, N.; Kankare, J. *J. Am. Chem. Soc.* **2001**, *123*, 6083-6091.
(63) Zotti, G.; Schiavon, G.; Zecchin, S.; Berlin, A.; Giro, G. *Synth. Met.* **2001**, *121*, 1381-1382.
(64) Zotti, G.; Zecchin, S.; Berlin, A.; Schiavon, G.; Giro, G. *Chem. Mater.* **2001**, *13*, 43-52.
(65) Baba, A.; Park, M. K.; Advincula, R. C.; Knoll, W. *Langmuir* **2002**, *18*, 4648-4652.
(66) Ferreira, M.; Zucolotto, V.; Huguenin, F.; Torresi, R. M.; Oliveira, O. N. *J. Nanosci. Nanotechnol.* **2002**, *2*, 29-32.
(67) Xin, H.; Li, F. Y.; Huang, Y. Y.; Huang, C. H. *J. Rare Earths* **2002**, *20*, 333-338.
(68) Zhai, L.; McCullough, R. D. *Adv. Mater.* **2002**, *14*, 901-905.
(69) Cutler, C. A.; Bouguettaya, M.; Reynolds, J. R. *Adv. Mater.* **2002**, *14*, 684-688.
(70) Caruso, F.; Caruso, R. A.; Mohwald, H. *Science* **1998**, *282*, 1111-1114.
(71) Caruso, F.; Lichtenfeld, H.; Giersig, M.; Mohwald, H. *J. Am. Chem. Soc.* **1998**, *120*, 8523-8524.
(72) Caruso, F.; Mohwald, H. *J. Am. Chem. Soc.* **1999**, *121*, 6039-6046.
(73) Caruso, F. *Adv. Mater.* **2001**, *13*, 11-+.
(74) Khopade, A. J.; Caruso, F. *Nano Lett.* **2002**, *2*, 415-418.
(75) Winterton, L. C.; Lally, J. M.; Rubner, M. F.; Qiu, Y. In *PCT Int. Appl.*; (Novartis A.-G., Switz.; Novartis-Erfindungen Verwaltungsgesellschaft m.b.H.). WO, 2001, p 30 pp.
(76) Kumar, A.; Biebuyck, H. A.; Whitesides, G. M. *Langmuir* **1994**, *10*, 1498-1511.

(77) Clark, S. L.; Montague, M.; Hammond, P. T. *Supramol. Sci.* **1997**, *4*, 141-146.
(78) Clark, S. L.; Montague, M.; Hammond, P. T. *Polym. Mater. Sci. Eng.* **1997**, *77*, 620-621.
(79) Clark, S. L. In *Chemical Engineering*; Massachusetts Institute of Technology: Cambridge, 1999, p 187.
(80) Jiang, X. P.; Hammond, P. T. *Langmuir* **2000**, *16*, 8501-8509.
(81) Jiang, X. P.; Zheng, H. P.; Gourdin, S.; Hammond, P. T. *Langmuir* **2002**, *18*, 2607-2615.
(82) Chen, K. M.; Jiang, X. P.; Kimerling, L. C.; Hammond, P. T. *Langmuir* **2000**, *16*, 7825-7834.
(83) Zheng, H. P.; Rubner, M. F.; Hammond, P. T. *Langmuir* **2002**, *18*, 4505-4510.
(84) Lee, I.; Zheng, H.; Rubner, M.; Kimerling, L. C.; Hammond, P. T. *Abstracts of Papers, 222nd ACS National Meeting, Chicago, IL, United States, August 26-30, 2001* **2001**, POLY-344.
(85) Wang, L. Y.; Wang, Z. Q.; Zhang, X.; Shen, J. C.; Chi, L. F.; Fuchs, H. *Macromol. Rapid Commun.* **1997**, *18*, 509-514.
(86) Wang, L. Y.; Fu, Y.; Wang, Z. Q.; Wang, Y.; Sun, C. Q.; Fan, Y. G.; Zhang, X. *Macromol. Chem. Phys.* **1999**, *200*, 1523-1527.
(87) Wang, L. Y.; Fu, Y.; Wang, Z. Q.; Fan, Y. G.; Zhang, X. *Langmuir* **1999**, *15*, 1360-1363.
(88) Wang, L. Y.; Cui, S. X.; Wang, Z. Q.; Zhang, X.; Jiang, M.; Chi, L. F.; Fuchs, H. *Langmuir* **2000**, *16*, 10490-10494.
(89) Sukhishvili, S. A.; Granick, S. *J. Am. Chem. Soc.* **2000**, *122*, 9550-9551.
(90) Sukhishvili, S. A.; Granick, S. *Macromolecules* **2002**, *35*, 301-310.
(91) Yang, S. Y.; Rubner, M. F. *J. Am. Chem. Soc.* **2002**, *124*, 2100-2101.
(92) Zollinger, H. *Color Chemistry*; 2nd ed.; Weinheim: New York, 1991.
(93) Griffiths, J. *Colour and Constitution of Organic Molecules*; Academic Press: London, 1976.
(94) Moskalev, P. N.; Kirin, I. S. *Opt. Spektrosk.* **1970**, *29*, 414.
(95) Moskalev, P. N.; Shapkin, G. N. *Soviet Electrochemistry* **1978**, *14*, 486-488.
(96) Sidorov, A. N.; Moskalev, P. N. *Zh. Fiz. Khim.* **1988**, *62*, 3015-3019.
(97) Moskalev, P. N.; Shapkin, G. N.; Darovskikh, A. N. *Zh. Neorg. Khim.* **1979**, *24*, 340-346.
(98) Anderson, T. *Leibig's Ann. Chem.* **1855**, *94*, 358.
(99) Menshutkin, N. *Z. Phys. Chem.* **1890**, *5*, 589.
(100) Bird, C. L.; Kuhn, A. T. *Chem. Soc. Rev.* **1981**, *10*, 49-82.
(101) Bard, A. J.; Ledwith, A.; Shine, H. J. *Adv. Phys. Org. Chem.* **1976**, *13*, 155-278.
(102) Sawyer, D. T.; Nanni, E. J.; Angelis, C. T.; Dickson, J. *J. Am. Chem. Soc.* **1981**, *103*, 4268-4270.
(103) Monk, P. M. S.; Mortimer, R. J.; Rosseinsky, D. R. *Electrochromism: Fundamentals and Applications*; Weinheim: New York, 1995.
(104) Oyama, N.; Ohsaka, T.; Yamamoto, H.; Kaneko, M. *Journal of Physical Chemistry* **1986**, *90*, 3850-3856.
(105) Johansen, O.; Loder, J. W.; Mau, A. W. H.; Rabani, J.; Sasse, W. H. F. *Langmuir* **1992**, *8*, 2577-2581.
(106) Thornley, R. N. F. *Biochemica et Biophysical Acta* **1974**, *333*, 487-496.
(107) Sato, H.; Tamamura, T. *J. Appl. Polym. Sci.* **1979**, *24*, 2075-2085.
(108) Monk, P. M. S.; Fairweather, R. D.; Ingram, M. D.; Duffy, J. A. *J. Electroanal. Chem.* **1993**, *359*, 301-306.
(109) Sammells, A. F.; Pujare, N. U. *J. Electrochem. Soc.* **1986**, *133*, 1270-1271.
(110) Mortimer, R. J. *Electrochim. Acta* **1999**, *44*, 2971-2981.
(111) Monk, P. M. S. *The Viologens*; John Wiley & Sons Ltd.: West Sussex, England, 1998.
(112) Kawata, T.; Yamano, M. *Nihon Kagaku Kaishi* **1977**, *7*, 941-946.
(113) Reynolds, J. R.; Rajeshwar, K.; Ruiz, J. P.; Basak, S.; Tsai, E. W. *J. Electrochem. Soc.* **1989**, *136*, 3683-3689.

(114) Kumar, A.; Reynolds, J. R. *Macromolecules* **1996**, *29*, 7629-7630.
(115) Reynolds, J. R.; Sapp, S. A.; Sotzing, G. A.; Reddinger, J. L. *Polym. Mater. Sci. Eng.* **1996**, *75*, 414-415.
(116) Sapp, S. A.; Sotzing, G. A.; Reddinger, J. L.; Reynolds, J. R. *Adv. Mater.* **1996**, *8*, 808-811.
(117) Kumar, A.; Welsh, D. M.; Morvant, M. C.; Piroux, F.; Abboud, K. A.; Reynolds, J. R. *Chem. Mater.* **1998**, *10*, 896-902.
(118) Sapp, S. A.; Sotzing, G. A.; Reynolds, J. R. *Chem. Mater.* **1998**, *10*, 2101-2108.
(119) Welsh, D. M.; Kumar, A.; Meijer, E. W.; Reynolds, J. R. *Adv. Mater.* **1999**, *11*, 1379-1382.
(120) Byrd, H.; Holloway, C. E.; Pogue, J.; Kircus, S.; Advincula, R. C.; Knoll, W. *Langmuir* **2000**, *16*, 10322-10328.
(121) Thompson, B. C.; Schottland, P.; Zong, K.; Reynolds, J. R. *Chem. Mater.* **2000**, *12*, 1563-1571.
(122) Rauh, R. D.; Wang, F.; Reynolds, J. R.; Meeker, D. L. *Electrochim. Acta* **2001**, *46*, 2023-2029.
(123) Schwendeman, I.; Hwang, J.; Welsh, D. M.; Tanner, D. B.; Reynolds, J. R. *Adv. Mater.* **2001**, *13*, 634-637.
(124) Thompson, B. C.; Schottland, P.; Sonmez, G.; Reynolds, J. R. *Synth. Met.* **2001**, *119*, 333-334.
(125) Rudge, A.; Raistrick, I.; Gottesfeld, S.; Ferraris, J. P. *Electrochim. Acta* **1994**, *39*, 273-287.
(126) Ferraris, J. P.; Eissa, M. M.; Brotherston, I. D.; Loveday, D. C. *Chem. Mater.* **1998**, *10*, 3528-3535.
(127) Mudigonda, D. S. K.; Meeker, D. L.; Loveday, D. C.; Osborn, J. M.; Ferraris, J. P. *Polymer* **1999**, *40*, 3407-3412.
(128) Mudigonda, D. S. K.; Boehme, J. L.; Brotherston, I. D.; Meeker, D. L.; Ferraris, J. P. *Chem. Mater.* **2000**, *12*, 1508-1509.
(129) Balanda, P. B.; Ramey, M. B.; Reynolds, J. R. *Macromolecules* **1999**, *32*, 3970-3978.
(130) Boehme, J. L.; Mudigonda, D. S. K.; Ferraris, J. P. *Chem. Mater.* **2001**, *13*, 4469-4472.
(131) Brotherston, I. D.; Mudigonda, D. S. K.; Osborn, J. M.; Belk, J.; Chen, J.; Loveday, D. C.; Boehme, J. L.; Ferraris, J. P.; Meeker, D. L. *Electrochim. Acta* **1999**, *44*, 2993-3004.
(132) Stenger-Smith, J. D. *Progress in Polymer Science* **1998**, *23*, 57-79.
(133) Hydo, K. *Electrochim. Acta* **1993**, *39*, 265-272.
(134) Diaz, A. F.; Logan, J. A. *J. Electroanal. Chem.* **1980**, *111*, 111-114.
(135) Evans, G. P. In *Advances in Electrochemical Science and Engineering*; Gerischer, H., Tobias, C. W., Eds.; VCH Verlagsgesellschaft mbH: Weinheim, Germany, 1990; Vol. 1, pp 1-74.
(136) Kobayashi, T.; Yoneyama, H.; Tamura, H. *J. Electroanal. Chem.* **1984**, *161*, 419-423.
(137) MacDiarmid, A. G.; Humphrey, B. D.; Huang, W.-S. *J. Chem. Soc., Faraday Trans. 1* **1986**, *82*, 2385-2400.
(138) Dong, S.; Jiang, R. *Synth. Met.* **1988**, *24*, 255-265.
(139) Contractor, A. Q.; Dabke, R. B.; Dhanabalan, A.; Major, S.; Talwar, S. S.; Lal, R. *Thin Solid Films* **1998**, *335*, 203-208.
(140) Elsenbaumer, R. L.; Miller, G. G.; Jen, K.-Y. *Jounral of the Chemical Society, Chemical Communications* **1986**, 1346-1347.
(141) Granqvist, C. G. *Handbook of Inorganic Electrochromic Materials*; Elsevier: Amsterdam, 1995.
(142) Granqvist, C. G. *Sol. Energy Mater.* **2000**, *60*, 201-262.
(143) Mortimer, R. J. *Chem. Soc. Rev.* **1997**, *26*, 147-156.
(144) Buser, H. J.; Schwarzenbach, D.; Petter, W.; Ludi, A. *Inorg. Chem.* **1977**, *16*, 2704-2710.
(145) Neff, V. D. *J. Electrochem. Soc.* **1978**, *125*, 886-887.
(146) Ellis, D.; Eckhoff, M.; Neff, V. D. *Journal of Physical Chemistry* **1981**, *85*, 1225-1231.
(147) Leventis, N.; Chung, Y. C. *J. Electrochem. Soc.* **1990**, *137*, 3321-3322.

(148) Jelle, B. P.; Hagen, G. *J. Electrochem. Soc.* **1993**, *140*, 3560-3564.
(149) Millward, R. C.; Madden, C. E.; Sutherland, I.; Mortimer, R. J.; Fletcher, S.; Marken, F. *Chem. Commun.* **2001**, 1994-1995.
(150) Monk, P. M. S.; Delage, F.; Vieira, S. M. C. *Electrochim. Acta* **2001**, *46*, 2195-2202.
(151) Pyrasch, M.; Tieke, B. *Langmuir* **2001**, *17*, 7706-7709.
(152) Moriguchi, I.; Kamogawa, H.; Hagiwara, K.; Teraoka, Y. *Chem. Lett.* **2002**, 310-311.
(153) Pyrasch, M.; Toutianoush, A.; Jin, W. Q.; Schnepf, J.; Tieke, B. *Chem. Mater.* **2003**, *15*, 245-254.
(154) Yamamoto, H.; Sugiyama, T.; Tanaka, M. *Jpn. J. Appl. Phys. Part 2 - Lett.* **1985**, *24*, L305-L307.
(155) Liu, Y. Q.; Shigehara, K.; Yamada, A. *Thin Solid Films* **1989**, *179*, 303-308.
(156) Katz, H. E.; Scheller, G.; Putvinski, T. M.; Schilling, M. L.; Wilson, W. L.; Chidsey, C. E. D. *Science* **1991**, *254*, 1485-1487.
(157) Lukas, B.; Lovett, D. R.; Silver, J. *Thin Solid Films* **1992**, *210*, 213-215.
(158) Souto, J.; Tomilova, L.; Aroca, R.; Desaja, J. A. *Langmuir* **1992**, *8*, 942-946.
(159) Rodriguezmendez, M. L.; Aroca, R.; Desaja, J. A. *Chem. Mater.* **1993**, *5*, 933-937.
(160) Goldenberg, L. M. *J. Electroanal. Chem.* **1994**, *379*, 3-19.
(161) Lukas, B.; Silver, J.; Lovett, D. R.; Cook, M. J. *Chem. Phys. Lett.* **1995**, *241*, 351-354.
(162) Dabke, R. B.; Dhanabalan, A.; Major, S.; Talwar, S. S.; Lal, R.; Contractor, A. Q. *Thin Solid Films* **1998**, *335*, 203-208.
(163) Ravaine, S.; Lafuente, C.; Mingotaud, C. *Langmuir* **1998**, *14*, 6347-6349.
(164) Qian, D. J.; Liu, H. G.; Jiang, J. Z. *Colloid Surf. A-Physicochem. Eng. Asp.* **2000**, *163*, 191-197.
(165) Xiang, H. Q.; Tanaka, K.; Takahara, A.; Kajiyama, T. *Langmuir* **2002**, *18*, 2223-2228.
(166) Chemseddine, A.; Henry, M.; Livage, J. *Revue De Chimie Minerale* **1984**, *21*, 487-495.
(167) Nabavi, M.; Doeuff, S.; Sanchez, C.; Livage, J. *Mater. Sci. Eng. B-Solid State Mater. Adv. Technol.* **1989**, *3*, 203-207.
(168) Lee, G. R.; Crayston, J. A. *J. Mater. Chem.* **1991**, *1*, 381-386.
(169) Livage, J. *Chem. Mater.* **1991**, *3*, 578-593.
(170) Agrawal, A.; Cronin, J. P.; Zhang, R. *Sol. Energy Mater.* **1993**, *31*, 9-21.
(171) Aliev, A. E.; Shin, H. W. *Solid State Ion.* **2002**, *154*, 425-431.
(172) Bard, A. J.; Faulkner, L. R. *Electrochemical methods : fundamentals and applications*; 2 ed.; John Wiley: New York, 2001.
(173) Crow, D. R. *Principles and applications of electrochemistry*; Blackie: London ; New York, 1994.
(174) Hibbert, D. B.; James, A. M. *Dictionary of Electrochemistry*; 2 ed.; Wiley Interscience: New York, 1984.
(175) Schoot, C. J.; Ponjee, J. J.; van Dam, H. T.; van Doorn, R. A.; Bolwijn, P. T. *Appl. Phys. Lett.* **1973**, *23*, 64-65.
(176) Barclay, D. J.; Martin, D. H. In *Technology of Chemicals and Materials for Electronics*; Howells, E. R., Ed.; John Wiley and Sons: New York, 1984, pp 266-276.
(177) Barclay, D. J.; Dowden, B. F.; Lowe, A. C.; Wood, J. C. *Appl. Phys. Lett.* **1983**, *42*, 911-913.
(178) Leventis, N.; Chen, M.; Liapis, A. I.; Johnson, J. W.; Jain, A. *J. Electrochem. Soc.* **1998**, *145*, L55-L58.
(179) Goff, A. H.-L.; Bernard, M.-C.; Zang, W. *Electrochim. Acta* **1998**, *44*, 781-796.
(180) Goff, A. H.-L.; Bernard, M. C. *Synth. Met.* **1999**, *102*, 1342-1345.
(181) Jelle, B. P.; Hagen, G. *J. Appl. Electrochem.* **1998**, *28*, 1061-1065.
(182) Bach, U.; Corr, D.; Lupo, D.; Pichot, F.; Ryan, M. *Adv. Mater.* **2002**, *14*, 845-848.
(183) Plass, R.; Pelet, S.; Krueger, J.; Gratzel, M.; Bach, U. *J. Phys. Chem. B* **2002**, *106*, 7578-7580.

(184) Wang, P.; Zakeeruddin, S. M.; Exnar, I.; Gratzel, M. *Chem. Commun.* **2002**, 2972-2973.
(185) Wang, P.; Zakeeruddin, S. M.; Comte, P.; Exnar, I.; Gratzel, M. *J. Am. Chem. Soc.* **2003**, *125*, 1166-1167.
(186) Gray, F. M. *Polymer Electrolytes*; The Royal Society of Chemistry: Cambridge, UK, 1997.
(187) Armand, M. B. In *Fast Ion Transport in Solids*; VanGool, W., Ed.; North Holland: Amsterdam, 1973, p 665.
(188) Armand, M. *Solid State Ion.* **1983**, *9-10*, 745-754.
(189) Armand, M.; Kapfer, B.; Belanger, A.; Robitaille, M. *J. Electrochem. Soc.* **1983**, *130*, C107-C107.
(190) Berthier, C.; Gorecki, W.; Minier, M.; Armand, M. B.; Chabagno, J. M.; Rigaud, P. *Solid State Ion.* **1983**, *11*, 91-95.
(191) Armand, M. *Adv. Mater.* **1990**, *2*, 278-286.
(192) Armand, M. *Solid State Ion.* **1994**, *69*, 309-319.
(193) Armand, M. *Phys. World* **1995**, *8*, 28-29.
(194) Tarascon, J. M.; Armand, M. *Nature* **2001**, *414*, 359-367.
(195) Song, J. Y.; Wang, Y. Y.; Wang, C. C. *J. Power Sources* **1999**, *77*, 183-197.
(196) Jelle, B. P.; Hagen, G.; Sunde, S.; Odegard, R. *Synth. Met.* **1993**, *54*, 315-320.
(197) Moon, H. S.; Park, J. K. *Synth. Met.* **1998**, *92*, 223-228.
(198) Gray, F. M.; Maccallum, J. R.; Vincent, C. A.; Giles, J. R. M. *Macromolecules* **1988**, *21*, 392-397.
(199) Khan, I. M.; Yuan, Y. X.; Fish, D.; Wu, E.; Smid, J. *Macromolecules* **1988**, *21*, 2684-2689.
(200) Xie, H. Q.; Dong, X.; Jin, L. *Polym.-Plast. Technol. Eng.* **1989**, *28*, 355-369.
(201) Alloin, F.; Sanchez, J. Y.; Armand, M. B. *Electrochim. Acta* **1992**, *37*, 1729-1731.
(202) Ishizu, K. *Polym.-Plast. Technol. Eng.* **1994**, *33*, 575-603.
(203) Sadoway, D. R.; Huang, B. Y.; Trapa, P. E.; Soo, P. P.; Bannerjee, P.; Mayes, A. M. *J. Power Sources* **2001**, *97-8*, 621-623.
(204) Epps, T. H.; Bailey, T. S.; Pham, H. D.; Bates, F. S. *Chem. Mater.* **2002**, *14*, 1706-1714.
(205) Jannasch, P. *Polymer* **2002**, *43*, 6449-6453.
(206) Jannasch, P. *Chem. Mater.* **2002**, *14*, 2718-2724.
(207) Mui, S. C.; Trapa, P. E.; Huang, B.; Soo, P. P.; Lozow, M. I.; Wang, T. C.; Cohen, R. E.; Mansour, A. N.; Mukerjee, S.; Mayes, A. M.; Sadoway, D. R. *J. Electrochem. Soc.* **2002**, *149*, A1610-A1615.
(208) Skaarup, S.; West, K.; Zachauchristiansen, B. *Solid State Ion.* **1988**, *28*, 975-978.
(209) Kumar, B.; Scanlon, L. G. *J. Power Sources* **1994**, *52*, 261-268.
(210) Kumar, B.; Scanlon, L. G.; Spry, R. J. *J. Power Sources* **2001**, *96*, 337-342.
(211) Durstock, M. F.; Rubner, M. F. *Langmuir* **2001**, *17*, 7865-7872.
(212) Bauerle, J. E. *J. Phys. Chem. Solid* **1969**, *30*, 2657.
(213) Sluyters-Rehbach, M.; Sluyters, J. H. In *Electroanalytical Chemistry*; Bard, A. J., Ed.; Marcel Dekker: New York, 1970; Vol. 4, pp 1-127.
(214) Mellander, B. E.; Albinsson, I. *Solid State Ionics, [Proc. Asian Conf.], 5th* **1996**, 83-95.
(215) Raistrick, I. D. *Solid State Ion.* **1986**, *18-9*, 40-49.
(216) MacDonald, J. R.; Johnson, W. B. In *Impedance Spectroscopy*; MacDonald, J. R., Ed.; John Wiley & Sons: New York, 1987, pp 1-20.
(217) Jiang, S. P.; Love, J. G.; Badwal, S. P. S. *Key Eng. Mater.* **1997**, *125-126*, 81-132.
(218) Mount, A. R.; Robertson, M. T. *Compr. Chem. Kinet.* **1999**, 439-459.

Chapter 2. Layer-by-layer assembled single-electrochrome electrodes

Contents

Figures

Tables

2.1 Introduction to single-electrochrome LBL assembled films

Given the many advantages of LBL assembly, it is apparent this powerful technique could be applied to tailor the composition and morphology of electrochromic films on the nanoscale, combining existing electrochromic materials into high-performance electrochromic composites. The ability to create fine-grained composite films with extraordinary smoothness and controllable thickness on practically any substrate makes LBL assembly more powerful and flexible than traditional electrochromic film fabrication techniques such as electropolymerization or spin-coating. In fact, layer-by-layer (LBL) assembly may be the ideal processing platform with which to create electrochromic electrodes because the technique enables engineers to easily adjust not only film thickness, but also composition and to some extent morphology.

To enable electrochromic effects in LBL assembled films requires the incorporation of at least one suitable electrochromic species. The simplest strategy for the creation of LBL assembled electrochromic electrodes is to fabricate a film by pairing a single electrochromic species with a redox-inert polyion. This strategy should result in a film with unambiguous redox and electrochromic properties stemming from the color-changing active species only. In this chapter we explore a wide breadth of the single electrochrome composites that can be obtained with the LBL assembly of common, readily available electrochromic materials.

The LBL process requires that the assembled species be soluble or dispersable in an aqueous medium and also possess the potential for multiple intermolecular or interparticle interactions with a suitable partner material. The fabrication of LBL single electrochromes is to some extent confined by the low availability of electrochromic materials that meet these criteria. In particular, *water-soluble* species capable of reversible electrochromism are quite rare. Of electrochromic polymers, poly(alkyl viologens) are perhaps the most promising possibility because their inherent ionization as easily dissociable polysalts renders them fully water-soluble.[1-9] However, a full treatment of electrochromism in LBL assembled films would be remiss if it did not include a study of conjugated polymers as they represent by far the most strongly investigated and published family of electrochromic polymers. Electrochromic conjugated systems are often conducting, semiconducting, or light-emitting and the colored electrochromic states of these materials have been shown to absorb light over the entire range of the visible spectrum through systematic synthetic variation.[10-16] However, the utilization of conjugated polymers in LBL assembled films requires some finesse as they are rarely soluble in water.[17-23] Finally, a wide variety of inorganic materials also display reversible electrochromism,[24-29] though attaining suitable aqueous solutions or suspensions of ionized inorganic moieties that could potentially be assembled using the LBL technique is often a challenge.[30-32]

Thus far, there have been few previous LBL assembly investigations into electrochromic effects. These investigations have exclusively concerned films that contained single electrochromes. The first formal demonstration of electrochromic effects in LBL assembled films was performed by Schlenoff and co-workers, who fabricated LBL assembled films based on a poly(viologen) / poly(styrene sulfonate) pair and fully characterized the electrochromic properties of this system in a series of publications.[5,6,8] The electrochromic aspects of the work were later used in demonstrations to characterize the internal architecture and extent of layer delocalization in certain LBL assembled films.[33] Schlenoff and co-workers did not extend their study of electrochromic films to examine commercial-level performance, and no research efforts have since revisited the electrochromism of poly(viologen) LBL assembled films in more detail despite the promise hinted at by these early studies.

Even before Schlenoff's electrochromism demonstration, the first LBL-assembled systems that were *potentially* electrochromic were films containing conjugated poly(pyrrole), poly(aniline) (PANI), and poly(3-hexylthiophene), first LBL assembled by Rubner and co-workers.[17-23] The PANI system in particular provided a demonstration of a novel alternative strategy to incorporate conjugated polymer; dissolution was accomplished owing to the high polarity and intrinsic charge at low pH that PANI possesses as well as the employment of a water/organic solvent pair. The intrinsic amine/imine sites on PANI at low pH allowed LBL assembly with both polyanions and hydrogen bonding polymers. This work included a thorough investigation of the PANI LBL assembled film properties, in particular the very high electronic conductivity that was the focus of the work. However, no investigation into the redox or electrochromic properties of the films was performed. Based on this early seminal work, many other LBL assembled films containing conjugated polymers have since been studied.[34-55] Despite the great diversity of the conjugated LBL assembled films that have been produced, and the excellent conducting, sensing, and luminescing properties of many, there have been *no* investigations into the electrochromic properties of these conjugated films aside from the very recent design of a LBL assembled electrochromic film from the assembly of a specially synthesized, self-doping polyanionic form of PEDOT[55] that appeared subsequent to the publication of PEDOT work within this thesis.

Inorganic electrochromic materials are very rarely incorporated into LBL assembled films. There are few existing examples, most of which involve the assembly of inorganic, tungstate-containing macroions such as sodium dodecatungstate[32] or other polyoxometallates.[31,56-62] There have also been some recent efforts to make hexacyanoferrate complex films using a covalent variant of the LBL assembly process that synthesizes the complexes *in situ* by alternating exposure

to step-growth reactants resulting in completely inorganic, zeolitic thin films.[63-67] Even for the few LBL assembled films that have contained inorganic electrochromes are infrequently tested for electrochromism except in some rare cases that provide a simple demonstration.[31]

From this review, it is apparent that very little knowledge exists concerning LBL assembled electrochromic composites. Although there have been a small handful of demonstrations, the electrochromism phenomenon has never actually been studied in any detail. One of the focal points of this thesis work is to fill this gap with the first comprehensive investigation into LBL assembled electrochromic composites. This thesis then proposes a second step: the leveraging of this new knowledge to engineer *enhanced* electrochromic performance from LBL assembled electrochromic films. To examine the full range of possibilities necessitates the consideration of a wide variety of electrochromic species assembled with a wide variety of counterpolyions. Furthermore the performance of these materials must be investigated with an eye to application as well as the establishment of this novel functionality in LBL assembled films. This process could be considered the "intelligent design" of LBL assembled electrochromic electrodes with the ultimate goal creating high-performance electrochromic films for eventual use in devices.

An intelligent design approach requires some forethought regarding of the key elements that LBL assembly could introduce into electrochromic thin films. These influences can be best addressed by first considering the three factors that control the electrochromic properties of any film (in their order of importance):

1) The primary chemical structure of the electrochromic material.
2) The morphology and composition of the film – in particular the film thickness and roughness, the connectivity and density of the electrochromic species, and the ion conduction capability of the entire film.
3) The chemical environment, which to some extent can provide secondary chemical interactions to shift absorbance properties or redox properties of the polymer.

These factors are quite general, and might be considered applicable to any functional polymer film.

Optimization of the first factor necessitates the chemical synthesis of new materials. To avoid extensive synthetic efforts, variation in electrochromic materials can come from considering those available commercially, available by simple syntheses, or available through collaboration. Often, this limited selection can be sufficient for the design of a wide variety of materials given the combinatorial advantages of LBL assembly that will be emphasized in the next

two chapters of this thesis. The strongest influence the engineer has over this factor is the careful selection of an electrochromic material at the outset of a targeted project.

The second factor is the influence of morphology and composition. Differences of this nature are often observed between electropolymerized and spin-coated films of the same conjugated polymer. In this case, the influence of morphology is due to changes in the conformation of the extended conjugated chain. Perfect extended conjugation requires π orbital overlap between adjacent conjugated monomer units. Overlap requires proper *trans* orientation of each monomer unit and complete linearity of the chain. Color change is sometimes observed when the linearity of the extended π orbital is interrupted, because the polymer bandgap blue-shifts to higher energies due to a lowered degeneracy of states. Similar effects have been noted for electron conduction in polymer films; PANI in particular has been subjected to various types of processing in order to encourage linearity and achieve higher electronic conductivity. Ion permeability has also been explored in electrochromic thin films; blends of conjugated electrochromic polymers with highly polar polymers typically switch far faster than pure conjugated films due to the enhancement of ion conduction in the electrode film. Of the three factors influencing electrochromic properties, this factor is most relevant to the performance of LBL assembled electrochromic electrodes. Facilitation of ion motion could be introduced by choosing an appropriate counterpolyion for assembly, faster switching could be enabled by adjusting deposition to allow for a greater amount of the electrochromic species of interest, and even coloration might change depending on the morphological environment and connectivity of the electrochromic species within the LBL matrix.

The least influential factor that influences polymer electrochromism is the collective secondary interactions within the composite, which could produce an effect analogous to solvatochromism. By weak electronic interactions, the immediate environment of the electrochromic species could subtly influence redox potential or absorbance in polymer films. One particular example of this phenomenon is the curious influence of glycerol on the properties of the conducting polymer PEDOT (discussed in section 2.4),[68,69] though it is arguable that this influence is morphological in nature rather than solvatochromic.

Considering these factors, a wide span of experiments was designed to provide a complete performance assessment for single electrochrome LBL assembled films. These studies are separated in this chapter by the chosen electrochromic material. The first set of systems studied is based on the poly(viologens), the electroactive species of the first work on LBL assembled electrochromic films published by Schlenoff and co-workers. This study contributes to the small

existing body of knowledge pertaining to poly(viologen) LBL assembled films by elaborating the strong influence of counterpolyanion on the coloration and switching properties of a single poly(viologen) species. Earlier work by Schlenoff on layer stoichiometry is critically examined in the light of new insights gained from work in this thesis.

The second set of single electrochrome systems is based on the conducting polymer PANI, using the assembly technique described by Rubner and co-workers. This study includes a comparison of the electrochromic properties of a very wide variety of PANI electrochromic composites assembled both from electrostatic and hydrogen bonding interactions. The work is novel because electrochromism in PANI LBL assembled films has never before been studied. A particularly unique result is the revelation of a weak but consistent counterpolymer influence on the electrochromic character of the resultant PANI LBL assembled films.

The third set of systems is based on conjugated PEDOT incorporated into LBL assembled films in an approach developed wholly within this thesis work. PEDOT is extremely hydrophobic and insoluble in aqueous solution, yet can be attained in a soft colloidal suspension with a polyanion excess. It was discovered in this work that the PEDOT colloid acts as a polyanion in LBL assembly, providing a direct mechanism for LBL assembly with polycations. The PEDOT colloid was paired with several polycations to determine whether polycation character could affect the electrochromic properties of the resultant LBL assembled composites in a manner similar to that of glycerol. Although the effect of glycerol could not be emulated even by pairing PEDOT with strongly ethoxylated polycations, the resultant films did show differences in electrochromic behavior resulting from polycation character.

The final set of systems in this chapter involves electrochromic inorganic metal hexacyanoferrates. For this work, a synthesis for intrinsically ionizable nanoparticles of apparent dimensions less than 4 nm was developed. The particles possess an intrinsic negative ionization and could be LBL assembled with a polycation, resulting in rather ideal LBL growth of thin films. The electrochromic properties of these hexacyanoferrate LBL assembled films were completely explored, and the possibility of simple synthetic variation to result in LBL assembled films with different color states was fully realized.

Together, the four sections of this chapter represent work with almost every distinct type of electrochromic species: nonconducting discrete "molecular dyes" such as poly(viologens), conducting conjugated systems such as PANI and PEDOT, and inorganic nanoparticulate hexacyanoferrates. The results show conclusively that LBL assembly can directly influence the properties of electrochromic thin films, and moreover that LBL assembly is superior to many

traditional film formation techniques for the creation of high contrast, fast switching electrochromic films that promise broad functionality for many future applications.

2.2 Poly(viologen) LBL assembled films

2.2.1 Introduction to poly(viologens)

Poly(viologens) are intrinsically soluble, electrochromic polycations - an obvious first choice for incorporation into LBL assembled films. Small molecule viologens form the largest family of chemical compounds that have been investigated for electrochromic properties.[3,7,70,71] There are many reasons for this popularity: these molecules are very simple to synthesize, systematic synthetic variation is straightforward, and the resultant small molecule is often water soluble and therefore amenable to safe, cheap, and easily packaged aqueous electrolyte systems. Although poly(viologens) show to a great extent similar chemical and electrochemical properties as their small molecule counterparts,[1,2] they have not garnered nearly as much attention until very recently. This lack of poly(viologen) study is related to their perceived lack of utility; because the polymers are often soluble in the polar solvents typically used as electrolytes, they easily diffuse away from electrodes during or after switching, providing no real advantage in terms of switching time or electrochromic contrast as compared to the small molecule viologens. In fact, poly(viologen) diffusion and migration in aqueous solvents is most likely much slower than that of their small molecule counterparts, hampering the performance of solution-state electrochromic devices.

Like small molecule viologens, poly(viologens) are synthesized by quaternization of 4,4'-dipyridyl with alkyl halides, a synthesis termed the Anderson reaction (for heterocyclic amines)[72] and analogous to the more general Menshutkin reaction of alkyl amines.[73] Linear chain poly(viologens) are formed by employing an dihaloalkane with initial and terminal halogen.[1,2] The synthesis reaction for PXV follows a step-growth mechanism as shown in Figure 2.1. Polymer molecular weight and polydispersity are heavily influenced by stoichiometric parity between reactants. We expect a very large polydispersity and low molecular weight from this synthesis because the reaction products quickly become only sparingly soluble in most reaction solvents. This high polydispersity is not expected to strongly influence the electrochemical properties because of the isolation of redox centers –conjugation in most viologens is limited to bipyridilium units. By substitution of other alkyl or aromatic halides, the compositional range of poly(viologens) could be greatly expanded.

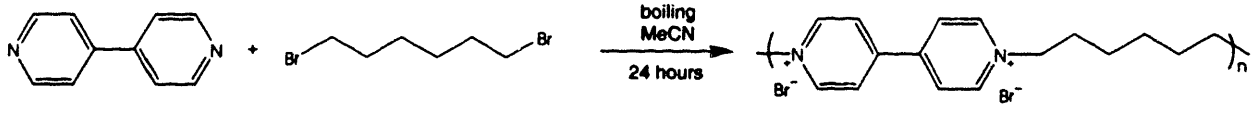

Figure 2.1 Synthesis of PXV by quaternization.

The LBL method provides an easy method to sequester poly(viologens) onto an electrochromic electrode, which could lead to faster (non-diffusion limited) switching and controllable, enhanced contrast. Although some the electrochemical and spectral description of these materials has been covered by Schlenoff and co-workers,[5,6,8] there remain many critical unanswered questions. The most provocative of these uncertainties is the unknown influence of counterpolyanion character on the assembly, electrochemical properties, and spectral properties of poly(viologen)-containing LBL assembled films. To explore this important issue and provide a definitive answer, a model poly(viologen) - poly(hexyl viologen) (PXV), was chosen as the workhorse electrochromic polyion for this study, and paired with several, very different polyanions. The first part of this section involves the assembly of PXV with sulfonated poly(styrene) (SPS). The polyanion selection was later extended to include a wider breadth of molecular character (see Figure 2.2). The assembly, electrochemical properties, and spectral properties of the resultant composites were fully analyzed, and the results provide firm conclusions regarding the influence of counterpolyanion character within poly(viologen) LBL assemblies.

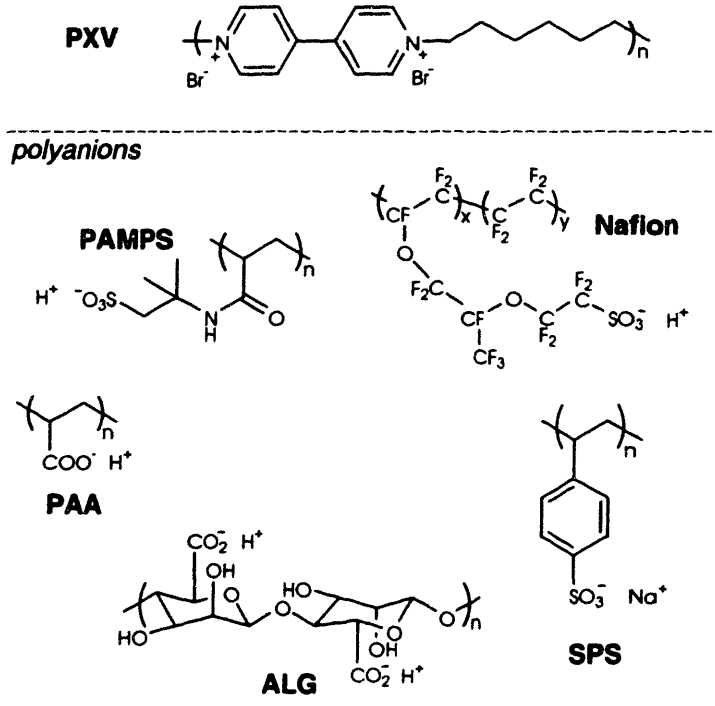

Figure 2.2 Molecular structures of the polyelectrolytes employed in PXV LBL studies.

2.2.2 Experimental details for poly(viologen) studies

2.2.2.1 Materials

Poly (hexyl viologen) (PXV) was synthesized by quaternization in dry, boiling acetonitrile from 1,6-bromohexane and 4,4'-dipyridyl (see Figure 2.1). Acetonitrile was dried before use using molecular sieves. 250 mL of stirred acetonitrile was brought to a boil with overhead cooling providing reflux. 4,4'-dipyridyl was added to the acetonitrile and allowed to dissolve. 1,6 bromohexane was then added dropwise to this solution. Reaction was apparent with the immediate evolution of a yellow color in the reaction mixture. Over several hours, a yellow/red precipitate formed, creating a stirred slurry. After 24 hours reaction time, the resultant slurry was filtered, and then the polymer was recrystallized from cold methanol. The overall yield by mass was approximately 50%.

Polyanions PAA (90,000 M_w, Polysciences), PAMPS (Aldrich), Nafion 117 (Fluka), and ALG (alginic acid, sodium salt, low viscosity, Sigma) were used a received. Polyelectrolytes were dissolved in MilliQ-filtered deionized water and then pH adjusted with dilute HCl or NaOH solutions. PXV solution was 0.010 M, PAMPS and ALG solutions were 0.002 M; PAA solutions were 0.020 M (polyelectrolyte concentrations are with respect to repeat unit). The Nafion 117 solution as received from Fluka was 5% polymer solution in light alcohols, (a mixture of isopropyl alcohol, 1-propanol, and methanol in an unspecified ratio. The as-received solution was diluted with MilliQ-filtered deionized water to 0.002 M Nafion for a final solvent alcohol composition of 4.4%. In general, the pH of all deposition baths was adjusted to pH 4 using aqueous NaOH and HCl solutions.

Thermally evaporated gold (100Å Cr, 1000Å Au) on <100> silicon (research grade, SiTech) was used for thickness monitoring. Before deposition, a carboxylic acid-functional self assembled monolayer was deposited onto the gold by exposing it for 20 minutes to a saturated solution of 16-mercaptohexadecanoic acid in ethanol. After exposure, the substrate was rinsed copiously with ethanol before use.

ITO-glass substrates with dimensions 0.7 cm × 5 cm (Delta Technologies, 6 Ω/square) were cleaned by ultrasonication in a series of solvents: dichloromethane, methanol, acetone, and Milli-Q water for 15 minutes each, followed by a 5-minute oxygen plasma etch (Harrick PCD 32G) to provide a clean, hydroxyl-rich surface.

2.2.2.2 Assembly

Assembly was performed by hand on gold-coated silicon substrates with 20-minute polyelectrolyte solution exposure times and a single rinse and drying step between exposures.

Film assembly was automated with a Carl Zeiss HMS DS-50 slide stainer. The substrates were exposed to polycation solution for 15 minutes, followed by copious water rinsing for 4 minutes in three consecutive Milli-Q water baths, and then exposed to polyanion solution for 15 minutes and again rinsed. This cycle was repeated for 40 layer pairs for each PXV-containing LBL system.

2.2.2.3 Measurement

Film thickness measurements on gold were performed using a Gaertner fixed-angle (70°) ellipsometer, typically by fixing film index at 1.45 and allowing fitting of the birefringence data to film thickness alone. Thickness measurements on ITO substrates were performed with a Tencor P10 profilometer by scoring the film and profiling the score. A tip force of 5 mg was used to avoid penetrating the polymer film.

Electrochemical analysis was performed using an EG&G 263A potentiostat/galvanostat. These measurements were performed in a flat cell of 30 mL volume and approximately 0.3 cm^2 working electrode area. The electrolyte used was aqueous 0.1 M NH_4Cl with a pH of approximately 5. The counterelectrode was 4 cm^2 platinum foil, and reference was a K-type saturated calomel electrode. CV was performed with potential limits of –0.9 V and 0.0 volts, at scan rates of 25, 50, 100, and 200 mV/s. Double potential step chronoamperomtery was performed by stepping between –0.9 V and 0.0 V vs. SCE, with 30 seconds per step and 60 seconds per cycle, with approximately 20 cycles performed sequentially before the measurement cycle. Spectral characterization was performed on a rail-mounted StellarNet EPP2000 concave grating UV-Vis-NIR spectrophotometer with combined incandescent and deuterium lamp sources. For spectroelectrochemistry, potential control was provided by EG&G 263A, with the polymer-coated ITO-glass substrate positioned in a quartz cell and immersed in electrolyte, along with a platinum wire counter electrode, and SCE reference.

2.2.3 Results and discussion for poly(viologen) LBL assembled films

2.2.3.1 Assembly of poly(viologen) LBL assembled films – initial studies

The electrochromic polycation PXV was the first electrochrome studied in this thesis work, and detailed assembly data was collected as part of an initial study into the feasibility of its LBL assembly. All of the assembly studies in this subsection were performed on carboxylic acid SAM-modified gold substrates. The first set of experiments pertained to the influence of ionic strength on the LBL deposition of the PXV/SPS system. For this study, NaCl was dissolved into both polyion deposition baths before assembly. The thickness of each film was measured after each polyion exposure by ellipsometry, and the entire process was performed by hand. The

thickness results for this study are shown in Figure 2.3. In all cases, after an initial period where the thickness appears to increase superlinearly with increasing layer pair number, the growth appears to become linear. Thickness increases with increasing ionic strength up to the maximum thickness and fastest growth achieved at 0.75 M NaCl. At higher ionic strengths, thickness decreases once again. The shape of this curve is due to the screening-enhanced and screening-reduced deposition mechanisms described in Chapter 1. The maximum thickness of 8.3 nm per layer pair at 0.75 M salt is significantly larger than the 4.7 nm per layer pair observed by Laurent et. al. for poly(butanyl viologen)(PBV)/SPS LBL assembled films at 0.5 M KBr,[5] a difference that may be explained by the presence of a drying step in this hand dipping procedure, which typically leads to an increase in deposited film thickness.[74-77]

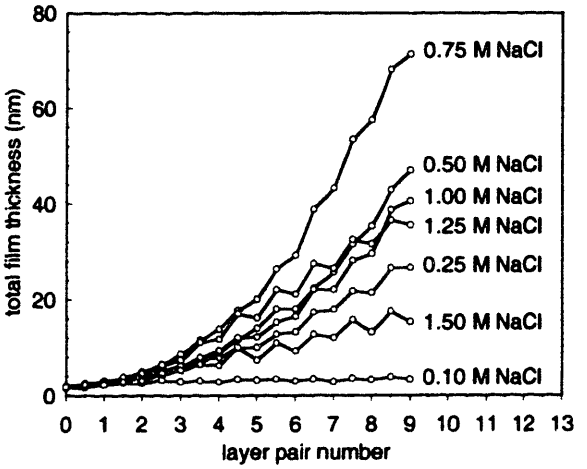

Figure 2.3 Growth of hand-dipped PXV/SPS LBL assembled films.

One notable phenomenon evinced in Figure 2.3 is the appearance of a "stepping" type of film growth where there appears to be (by thickness measurements) a much smaller amount of one polyion deposited and a much larger amount of the other. Indeed, at very high ionic strengths, the film thickness appears to oscillate thicker and thinner with each half layer pair that is deposited. There are several explanations for this type of behavior. The simplest explanation is that one polyion may be desorbing during the deposition or rinsing cycle of the opposite polyion. Although this simplistic explanation might explain such behavior, it should result in the pollution of one polyion deposition bath with visible insoluble polyion complexes, and no such complexes were observed. Such complexes could be soluble if very nonstoichiometrically paired, so this explanation may still be valid even with no observed precipitates. A second, more provocative explanation is that the film thickness could be oscillating due to fundamental changes in the film morphology or structure – that is, the film may be physically rearranging with

every polyion exposure, oscillating between polycation – rich and polyanion – rich forms that have different porosities or film densities.

The results shown in Figure 2.3 represent a great deal of experimental time investment as the films were assembled by manually exchanging assembly substrates between adsorption baths. Although this technique can provide detailed information on every layer, it is impractical for combinatorial studies involving multiple variables (such as ionic strength and polyanion identity). The thickness behavior of PXV/SPS was therefore re-examined by creating films using robotic automation. Films were assembled with 5 and 10 layer pairs. After assembly, the films were removed and dried and the final thickness was measured. Results of this automated study are shown in Figure 2.4.

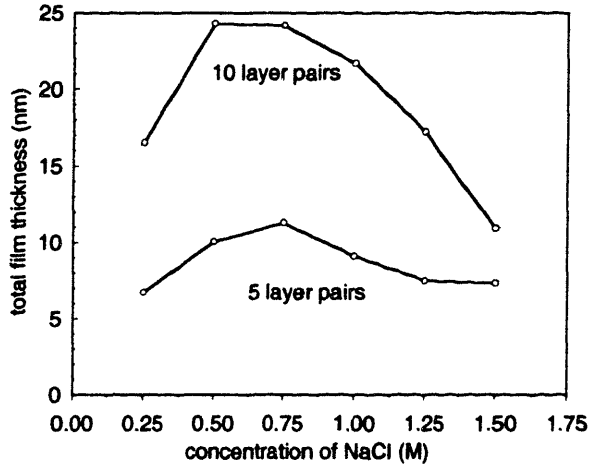

Figure 2.4 Final thickness of PXV/SPS LBL assembled films measured after automated assembly.

The results of the automated study are not fully consistent with those of the manually dipped study primarily due to the presence of a drying step in the manual study and the absence of one in the automated study. The presence of a drying step allows polyions with capability for hydrophobic interactions such as SPS to deposit more thickly onto a dried substrate than they might otherwise deposit onto a fully hydrated substrate. Thus, final thickness for LBL systems with such a drying step are typically greater than those without a drying step, which explains the disparity between the 9-layer pair final thicknesses shown in Figure 2.3 and the 10-layer pair thicknesses shown in Figure 2.4. In general, however, the *trends* are identical, and this system shows screening enhanced adsorption up to an ionic strength of 0.75 M, and then screening – reduced adsorption with an eventual decrease in assembly thickness and quality as ionic strength increases further.

The assembly of PXV was extended further by broadening the types of assembly polyanions. Figure 2.5 shows a growth study of PXV manually LBL assembled with the polyanions shown in Figure 2.2. The other polyanions were not adjusted with respect to ionic strength, and the pH of all solutions was controlled at pH 4.

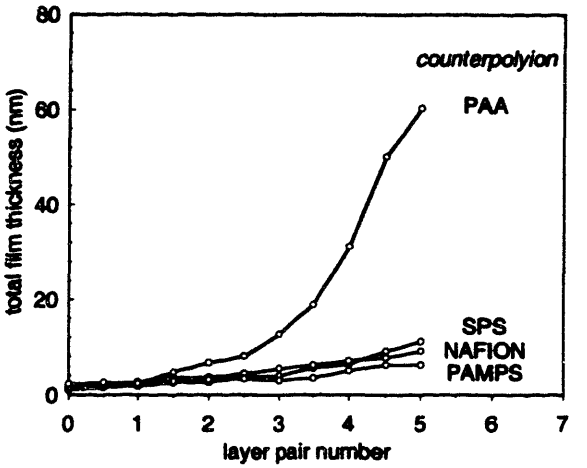

Figure 2.5 Growth of PXV hand-dipped LBL assembled films containing several counterpolyanions.

In general, thickness increases in a manner similar to that shown in Figure 2.3 for PXV/SPS. All of these systems are still within the exponential growth regime. Thickness is greatest for the pH-sensitive polyanion PAA, which is only partially charged at pH 4. The final thickness is least for the strong polyelectrolytes PAMPS and Nafion.

2.2.3.2 Assembly for electrochromism studies

Following the initial investigation into the assembly of PXV containing LBL assembled films, these films were revisited in order to fully characterize the electrochemical and optical properties of the assembled composites. For this work, the polycation PXV was LBL assembled with each of the polyanions shown in Figure 2.2 onto clean indium-doped tin oxide (ITO) substrates. The ITO substrates were first prepared by exposure to a 10 mM pH 4 linear (polyethylene imine) (LPEI) solution to encourage the initial adsorption of polymer onto the ITO surface. As the polyanions PAA and alginic acid (ALG, an anionic polysaccharide) contained pH-sensitive carboxylic acid groups, the pH of the assembly baths for all solutions in this study was kept constant at pH 4. The LBL assembled films were built to 40 layer pairs for each system.

The thickness and roughness of the resultant films are shown in Table 2-1. These results are completely consistent with the assembly trends shown in Figure 2.3 through Figure 2.5. The thickness of the films on ITO appear greater, most likely due to the different assembly substrate

(which in some cases can influence the entire film growth)[78,79] and enhancement of polyion adhesion due to the LPEI pretreatment.

Table 2-1. Thickness of several PXV LBL assembled films.

system	final thickness (per layer pair) (nm)		R_q rms roughness (nm)
$(PXV/SPS)_{40}$	171.9	(4.3)	4.1
$(PXV/Nafion)_{40}$	138.9	(3.5)	1.6
$(PXV/PAMPS)_{40}$	81.4	(2.0)	9.1
$(PXV/PAA)_{40}$	1831	(45.8)	69.3
$(PXV/ALG)_{40}$	5129	(128.2)	17.2

The weak polyanions PAA and ALG both deposit very thickly as compared to the strong polyanions SPS, Nafion, and PAMPS. This thick deposition results because the carboxyl groups on both are only weakly charged and highly protonated at pH 4. The weak charge allows the polyanion to assume a more globular conformation in solution; the polyanion then deposits in a thick, loopy layer. The lower charge density on the protonated chains also leads to a greater amount of polyanion deposition to satisfy PXV surface charge. ALG has an inherently smaller charge density than PAA and thus deposits even more thickly. The sulfonic acids, by contrast, deposit in thin, smooth layers between 2 and 4 nm per layer pair. This thickness is consistent with work examining the LBL assembly of poly(butyl viologen) performed by Schlenoff and co-workers, who found 5.1 nm per layer pair growth for assembly with SPS at an ionic strength of 0.5 M.[5] For all of the PXV films in this study, the roughness is small compared to the overall thickness – it is worth noting that the very thick $(PXV/ALG)_{40}$ film displays a roughness that is only 0.3% of its total thickness. This extreme uniformity is a hallmark of LBL assembly and one of its greatest advantages.

2.2.3.3 Electrochemistry – cyclic voltammetry

Following assembly, the PXV-containing LBL assembled films were subjected to cyclic voltammetry (CV) in order to elucidate the general electrochemical behavior of the films and determine potential ranges for reduction and oxidation. The potential range chosen for CV was between 0 and –0.9 V to capture the first reduction of the viologen moieties which is concomitant with a change in color from the optically clear fully oxidized PXV to the dark blue or violet singly-reduced color state, the namesake of all viologen species. Before testing the LBL-assembled films, the electrochemistry of neat PXV was evaluated by performing CV with a blank working electrode in a solution containing dilute PXV and electrolyte. The electrochemistry of PXV solution is shown below in Figure 2.6.

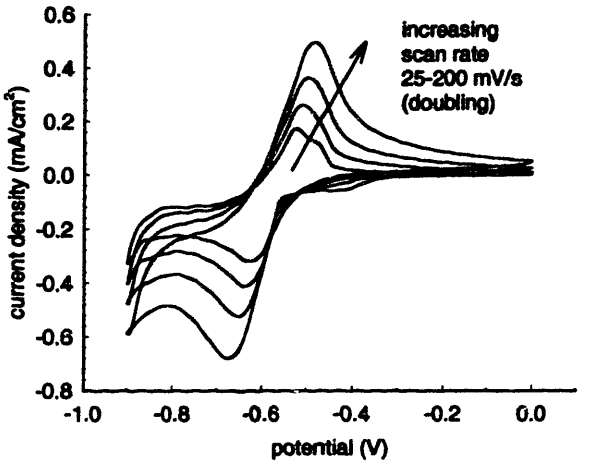

Figure 2.6 Cyclic voltammetry of PXV in solution.

The midpeak potential $E_{1/2}$ of the first reduction of PXV in free solution based on the centroid of oxidation and reduction peaks is consistently -0.58 V regardless of scan rate, well within the range that would be expected for alkyl viologens.[3,7] From the increasing peak spacing with increasing scan rate and the lack of symmetry in the anodic and cathodic waves, it is clear that even the electrochemistry of PXV in solution is not completely electrochemically reversible. This irreversibility is most likely due to the insolubility of singly-reduced PXV in the electrolyte solution; it cannot readily diffuse away from the electrode and a film accumulates that causes increasing resistance to charge transfer during oxidation and reduction. The onset of the second reduction of PXV is visible as a wave that begins at potentials less than –0.8 V; previous literature would suggest a potential of –0.7 to –0.9 V.[1-3] This second reduction is regarded as being somewhat chemically irreversible in aqueous solution due to protonation of the tertiary amines of doubly reduced PXV which encourages polymer chain scission.[7] From this initial solution electrochemistry it is clear that this potential range is suitable for evaluation of the first reduction of PXV within LBL assembled films, while avoiding for the most part the chemically degrading second reduction.

After testing the CV of PXV in solution, individual PXV-containing films were evaluated by CV. The results of these CVs are shown in Figure 2.7. The $(PXV/PAA)_{40}$ and $(PXV/ALG)_{40}$ films were too thick to perform electrochemistry upon – it was clear from some initial scans that redox centers within the films were only partially accessible and useful CVs could not be obtained. However, thinner films from strong polyanions could be tested.

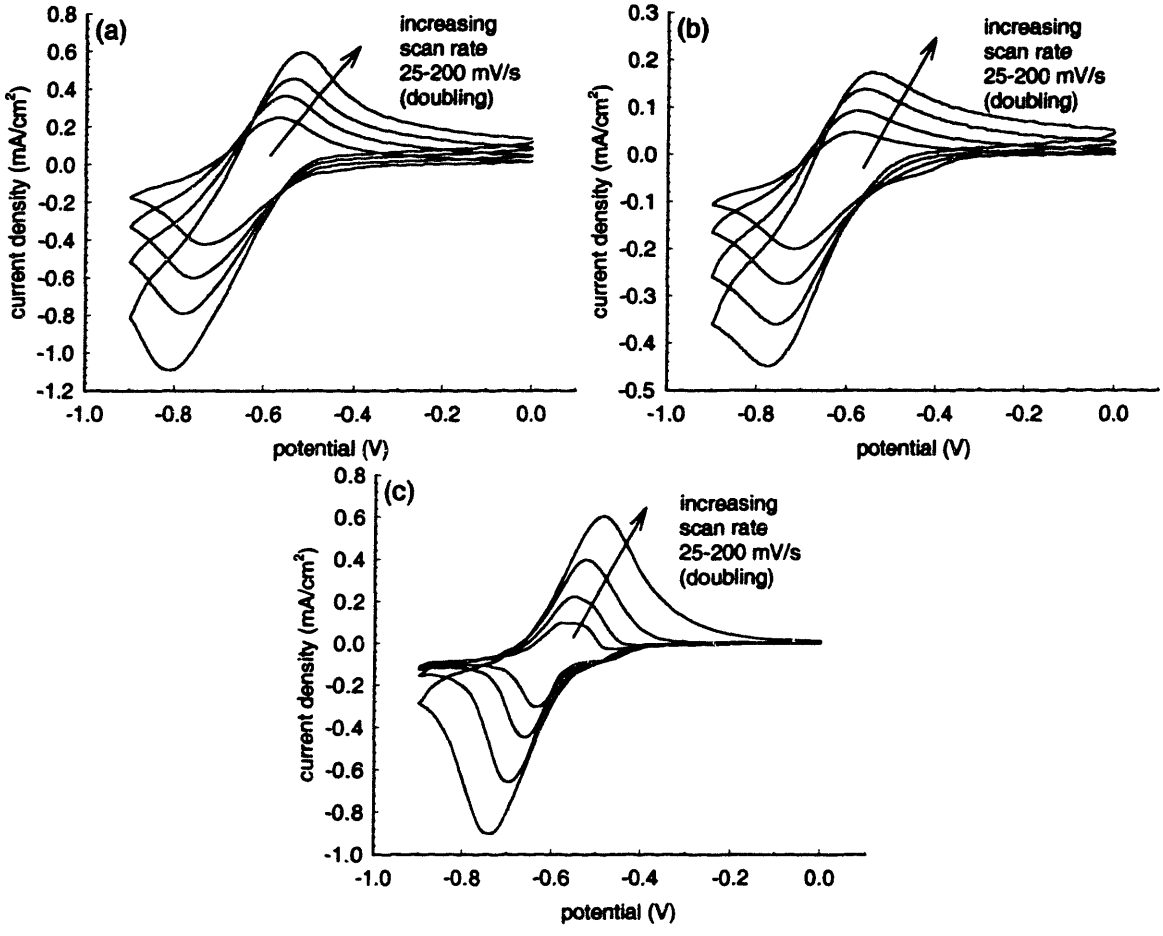

Figure 2.7 Cyclic voltammetry of PXV LBL assembled films (a) $(PXV/SPS)_{40}$ (b) $(PXV/Nafion)_{40}$ (c) $(PXV/PAMPS)_{40}$

The results shown in Figure 2.7 demonstrate the same general electrochemistry that was exhibited in Figure 2.6 by PXV solution, with a tendency toward more cathodic reaction potentials; the $E_{1/2}$ values for the SPS and Nafion LBL assembled composites were both -0.66 V, while the PAMPS composite displayed an $E_{1/2}$ of -0.61 V. This cathodic shift has been noted for other poly(viologen) / polyanion complexes, formed both in free solution[80] and in LBL assembled films[5] and must be attributed to the increased energy of Coulombic interactions between a *polyvalent* counteranion and the bipyridilium dication that adds stability to the fully oxidized state. As compared to the dissolved PXV, all of the LBL assembled films show greater hysteresis between the reduction and oxidation peaks, which indicates a greater amount of resistance to the redox reaction within the composites. As discussed in Chapter 1, this resistance stems from the tunneling barrier to charge transfer propagation that exists at any point within the film where viologen moieties are not immediately adjacent. The peaks are broadened and the reaction is further slowed by increasing inhibition of counterion migration into and out of the film. Ionic

resistance is lowered for highly hydrophilic, plastic, and high dielectric constant ion migration environments.

The relative speed of the electrochemical reactions can be determined by comparing the extent of hysteresis in each of the CVs. The greatest hysteresis is exhibited in the CV of PXV/SPS, followed by PXV/Nafion. PXV/PAMPS shows markedly less hysteresis and greater symmetry than the other two films, and its redox potential is closest to that of free solution PXV. In addition, the correlation of the PXV/PAMPS CV peak height to scan rate reveals the most linear trend out of all of the LBL assembled composites (the PXV/Nafion oxidation peak shows the least linear trend). Together, these factors indicate *highly enhanced* ion conduction that makes the PXV/PAMPS one of the electrochemically speediest PXV LBL assembled composites. Fast ion conduction from hydrated, PAMPS-containing LBL assembled films (and slow ion conduction from Nafion-containing LBL assembled films) is elucidated further for the design of LBL assembled polymer electrolytes in Chapter 5 of this thesis.

2.2.3.4 Electrochemistry – square wave switching

Following CV, the films were studied by double potential step chronocoulometry / chronoamperometry, in which the films were subjected to a potential square wave switching between 0.0 V and –0.9 V. At each step of the square potential wave, the current response initially spikes and then decays as the redox reaction progresses. Integration of the current wave results in the Faradaic charge wave for the step, which allows complete accounting of the molecular number and rate of charge uptake / withdrawal from the film (essentially "electron counting"). Results of square wave switching are shown in Figure 2.8 for the PXV films that were assembled with strong polyacids.

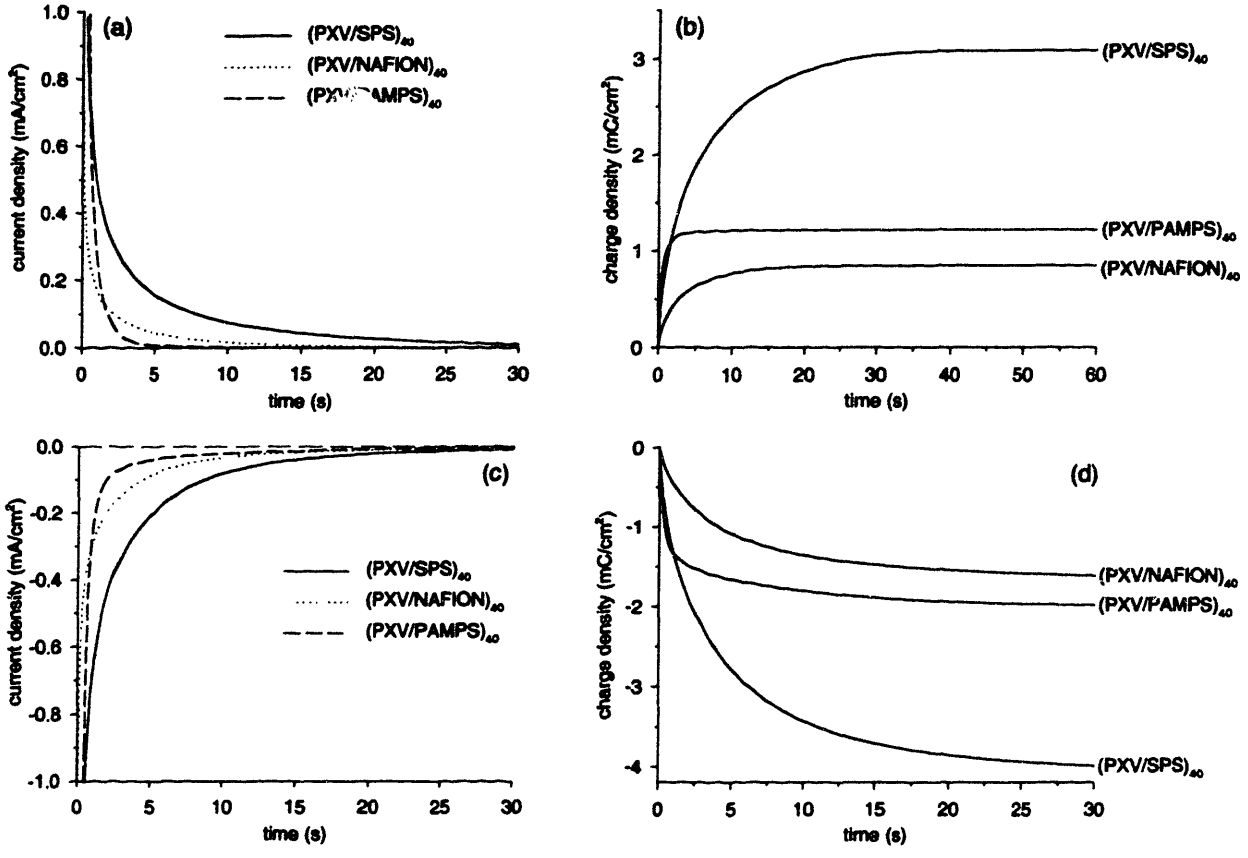

Figure 2.8 Square wave switching of PXV LBL assembled films: (a-b) oxidation (switch from -0.9 to 0.0 V at time 0); (c-d) reduction (switch from 0.0 V to -0.9 V at time 0).

From the current response, it is clear that the PXV/PAMPS composite switches most quickly because its current decay is most rapid. Even PXV/Nafion, which is thinner than PXV/PAMPS, switches slower than the PAMPS-containing composite. This is further confirmation that PAMPS fosters faster electrochemical behavior, most likely due to its facilitation of small ion permeation during redox switching because of its greater hydrophilicity and water plasticization.

One of the most striking features of Figure 2.8 is the disparity between reduction and oxidation in terms of the extent of oxidative and reductive Faradaic charge capacity. For all three films, there appear to be fewer electrons removed from the film during oxidation (25-50% less) as compared to the electrons injected into the film during reduction. The reason for this disparity is the facile oxidation of singly-reduced PXV by molecular oxygen.[3] When PXV is oxidized, chemical oxidation "works with" the electrochemical oxidation and fewer electrons are required to be removed electrochemically. Given that the chemical oxidation is more facile at an oxidizing potential (at which the fully oxidized PXV is the lowest free energy state), it can be assumed that the influence of chemical oxidation is primarily to decrease the Faradaic charge

uptake during oxidation, and charging during reduction can then be assumed to be representative of the full transformation of all redox centers within the film. It is important to note that this effect of viologens has been harnessed for application; facilitation of the reduction of molecular oxygen is industrially relevant, especially from the standpoint of fuel cell technology.[6,81,82]

By comparing charging during reduction, it is apparent that these films carry different amounts of PXV than otherwise might be expected based on the film thickness. In particular, the $(PXV/Nafion)_{40}$ film incorporates less PXV than $(PXV/PAMPS)_{40}$ incorporates, even though $(PXV/PAMPS)_{40}$ is a thicker film. A full tabulation of PXV concentration is provided below, assuming a single reduction of every viologen moiety on PXV. Conversion between charge coulombs and molar units is possible using Faraday's constant. From Table 2-2, the SPS- and PAMPS-containing films carry approximately the same concentration of PXV, even though film thicknesses are quite different. The Nafion-containing film carries half as much PXV. This effect is attributable to the larger equivalent weight of Nafion, which would increase the relative mass ratio of Nafion to PXV for 1:1 charge pairing within the film.

Table 2-2. Concentrations of redox centers within PXV LBL assembled films

system	thickness (nm)	charge (red.) (mC/cm^2)	vol. charge (C/cm^3)	PXV ($mmol/cm^3$)
$(PXV/SPS)_{40}$	171.9	4.1	236	2.44
$(PXV/Nafion)_{40}$	138.9	1.6	118	1.22
$(PXV/PAMPS)_{40}$	81.4	1.8	223	2.31

The analysis in Table 2-2 can be extended if assumptions are made concerning the extent of PXV dissociation. It cannot be immediately assumed that both PXV bromide counterions will completely dissociate in aqueous solution (see PXV molecular structure in Figure 2.2); the charge transfer interaction between the bipyridilium nitrogen and bromides could prohibit such full dissociation. If one assumes that both PXV bromides are dissociated (two charged sites available per PXV repeat) and fully paired with polyacid anionic sites, that all polysulfonic acids are completely paired, and that the LBL thin film density is 1.2 g/cm^3, as has been previously verified for similar polyelectrolyte LBL-assembled films,[83,84] (except for perfluorinated Nafion, with a dry density of 2 g/cm^3) the composition of each film can be estimated:

Table 2-3. PXV LBL assembled film composition based on complete PXV dissociation (false assumption).

system	PXV ($mmol/cm^3$)	PXV (g/cm^3)	polyanion (g/cm^3)	polyanion ($mmol/cm^3$)	PXV:polyanion (molar)
$(PXV/SPS)_{40}$	2.44	0.59	0.61	3.35	0.73 ✗
$(PXV/Nafion)_{40}$	1.22	0.29	0.91	1.42	0.89 ✗
$(PXV/PAMPS)_{40}$	2.31	0.56	0.64	3.11	0.74 ✗

Consideration of the compositional results shown in Table 2-3 reveals that the assumption of complete PXV dissociation is *false* because the resultant compositions would not be charge-balanced. The expected molar ratio of PXV:polyanion for full PXV dissociation must be 0.5 under this assumption due to the two charges per PXV molar repeat. Ratios in the range of 0.7-0.8 would necessitate a large amount of unpaired positive charge in the film that is not compensated for by any small molecule or polymer anions under this scenario.

If we then assume that exactly half of the bromide counterions dissociate from PXV (one charged site available per PXV repeat), then the results would appear as follows:

Table 2-4. PXV LBL assembled film composition based on 50% PXV dissociation (valid assumption).

system	PXV (mmol/cm^3)	PXV (g/cm^3)	polyanion (g/cm^3)	polyanion (mmol/cm^3)	PXV:polyanion (molar)
$(PXV/SPS)_{40}$	2.44	0.78	0.42	2.28	1.07 ✔
$(PXV/Nafion)_{40}$	1.22	0.39	0.81	1.26	1.00 ✔
$(PXV/PAMPS)_{40}$	2.31	0.74	0.46	2.22	1.04 ✔

From a glance at Table 2-4, it is clear that the assumption of 50% dissociation is *valid* because the expected molar ratio of PXV:polyanion for 50% PXV dissociation would be 1.0 for complete charge pairing due to the single charge per PXV molar repeat. In fact, 50% dissociation is the singular consistent solution to this composition profile analysis. These results prove that PXV is 50% dissociated when assembled in these LBL assembled films. The same conclusion was obtained for films of very different thickness, polyanion repeat unit molecular weight, and compositional character, and therefore cannot be easily dismissed as anomalous or system-dependent.

The most current work by Schlenoff and co-workers on poly(viologen) asserts that the molar ratio of poly(butanyl viologen) (PBV) to SPS *is* 0.5 in LBL assembled films,[5] indicating complete crosslinking between PBV and SPS, and precluding persistent pairing between viologen and bromide counterions. The evidence for this assertion lies in X-ray photoelectron spectroscopy (XPS), which fails to detect bromide or chloride ions on the film surface and indicates a N:S surface ratio of 1:1. However, data within the same publication refutes this conclusion. For a 10 layer pair, 48 nm thick PBV/SPS film assembled with 0.5 M KBr in the deposition bath, the authors describe a bulk PBV loading of 40 mg/m^2 based on both UV-Vis spectroscopy and electrochemical measurements. This loading corresponds to a PBV solid density of 0.82 g/cm^3 and therefore a SPS density of 0.38 g/cm^3 (as the authors themselves note in describing relative contributions to film thickness). It follows that the stoichiometric ratio of PBV:SPS, based on the repeat unit molecular weight of the fully dissociated forms, would be 1.8,

or roughly two PBV repeats per SPS repeat. This ratio is obviously inconsistent as it would result in an enormous overpopulation of unpaired positive charge within the PBV/SPS layers. Based on the authors' pairing assertions from XPS, this ratio should be exactly 0.5.

Re-analysis of the Schlenoff data indicates that the solid concentration of PBV repeats in the film would be 3.8 mmol/cm^3, which is much larger than the concentration found in the PXV-containing films assembled in this thesis and described in Table 2-4. This high concentration indicates that bromide-viologen pairing persists even more strongly with PBV system than in the PXV systems studied in this thesis. This lower PBV dissociation is because concentrated KBr was present in the PBV deposition solution (50 times more than the PBV concentration). In fact, analyzing the Schlenoff data further reveals that when the KBr in the deposition solution is reduced to 0.1 M, the concentration of PBV in the film is reduced to 3.1 mmol/m^3, a value more consistent with those described in Table 2-4, which correspond to films assembled with no added bromide salts. The effect of manipulating deposition KBr concentration to change PBV concentration in the film can only be attributed to dissociation equilibrium of PBV that is shifted toward less dissociation in the presence of more bromide counterions.

The inconsistencies of the paper referenced above emphasize that the surface character of LBL assembled thin films does not always accurately describe the character of the film bulk. XPS evidence of complete pairing on the surface of PBV/SPS films does not persist through the film interior and is contraindicated by a simple stoichiometric analysis.

2.2.3.5 Spectroelectrochemistry

The next step in the analysis of the PXV LBL assembled films was spectroelectrochemistry. The first step in the spectral analysis was to ascertain the coloration behavior of PXV without the influence of a polyanion. This test was made by immersing a blank ITO electrode into an electrochemical cell containing dissolved PXV and electrolyte. The film was polarized to –0.9 V vs. SCE and a colored film of insoluble singly-reduced PXV deposited onto the ITO. A UV-Vis spectrum of the film was measured at several steps during the coloration/deposition, which appeared to be self-limiting, as seen in Figure 2.9. Self-limitation is attributable to increasing resistance to charge transfer through the thickness of the growing film as well as growing electrostatic repulsion within the ionized PXV layer that is analogous to the self-limited growth forces present in LBL assembly.

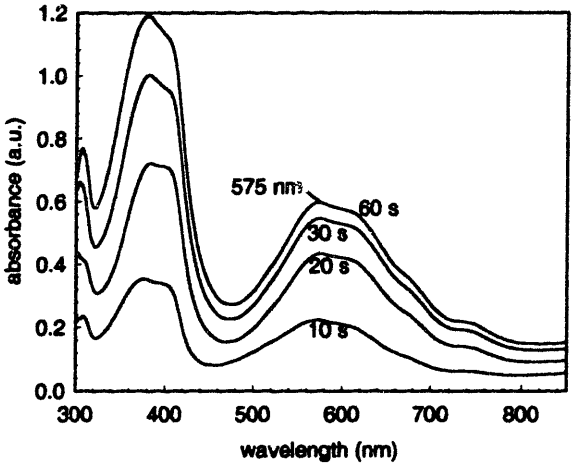

Figure 2.9 PXV coloration/deposition from electrolyte onto a bare transparent electrode.

Singly-reduced PXV shows a strong absorbance at 575 nm and a second weaker absorbance at 600nm, which are both typical for poly(viologen) species. The resultant color is a deep bluish purple. Film thickness was impossible to measure after working electrode polarization ceased due to chemical oxidation of the singly-reduced PXV (from molecular oxygen) and subsequent dissolution of fully oxidized PXV back into the electrolyte.

The existence of two peaks in the absorbance spectra of PXV is due to the presence of monomer (600 nm) and dimer (540-570 nm) forms of the polyviologen radical cation. This dimer is not related to covalent attachment, but rather is due to aromatic association of adjacent bipyridilium units, which shifts the electronic energy level scheme for the radical cation.[85] Dimer formation has been found to be overwhelmingly more prevalent in more solid environments,[86-88] whereas the monomer absorbance is often observed in liquid environments. The formation of dimer is also correlated to the hydrophobicity of the environment because the mechanism of dimer formation is entropically favored by the expulsion of waters of hydration about the bipyridilium units during π-π stacking. Presumably less water-friendly environments would support more facile dimer formation. According to the spectra in Figure 2.9, PXV shows approximately equal absorbance contributions from dimer and monomer; assuming that extinctions for the two are similar, this would indicate that about half of the bipyridilium radical cations are dimerized.

The spectra of the ephemeral electrodeposited PXV film can be compared with that of the stably solid LBL assembled PXV films. In this test, the LBL assembled film-coated ITO electrodes were immersed in an electrochemical cell that contained only electrolyte. A UV-Vis spectrum of the film was measured at several equilibrium potentials. Even though the PXV films containing weak polyacids were too thick for proper electrochemical evaluation using CV or switching

experiments, spectra of each could be taken, so they are included in this section. Spectroelectrochemistry results are shown in Figure 2.10.

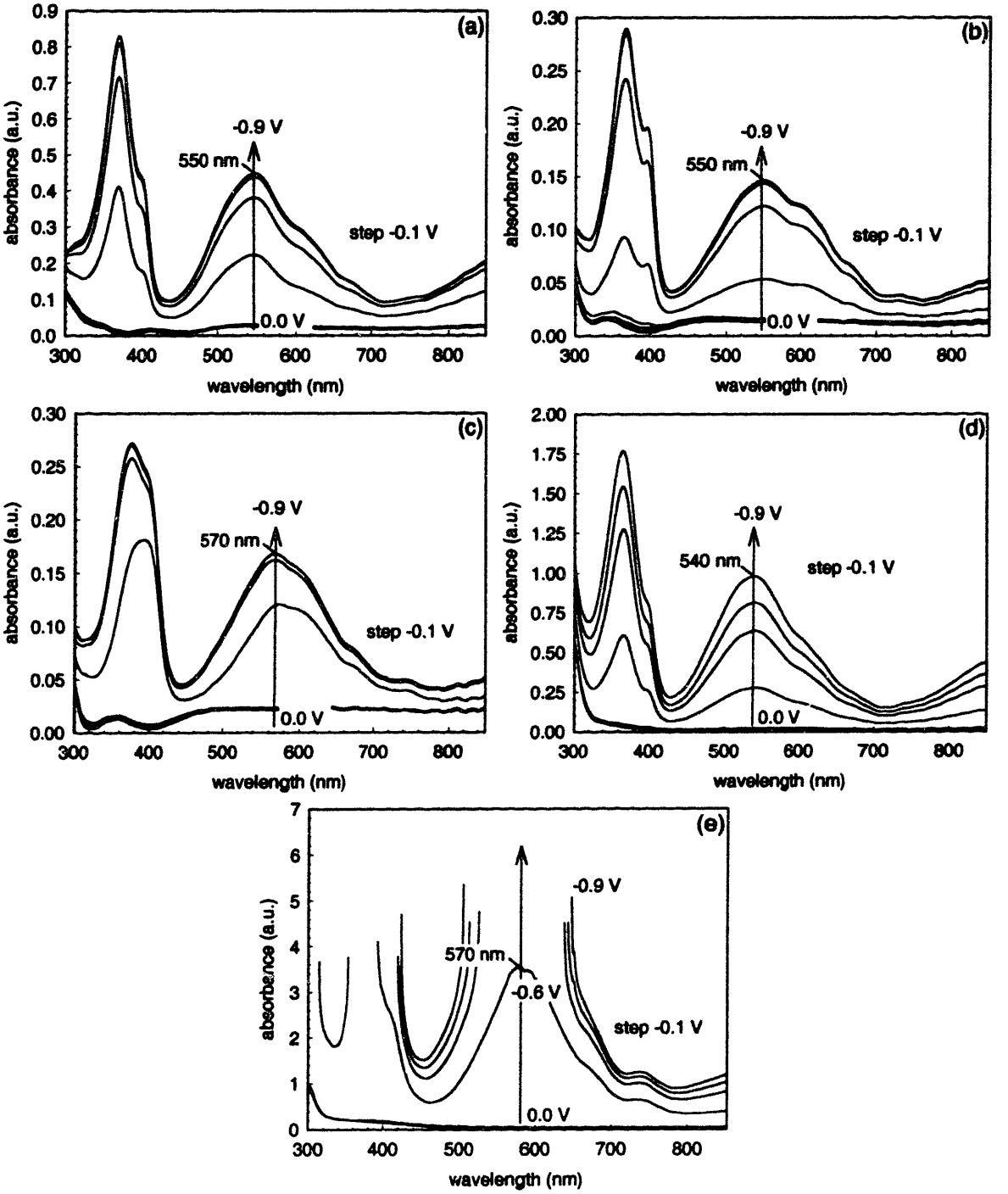

***Figure 2.10** Spectroelectrochemistry of PXV LBL films (a) $(PXV/SPS)_{40}$ (b) $(PXV/Nafion)_{40}$ (c) $(PXV/PAMPS)_{40}$ (d) $(PXV/PAA)_{40}$ (e) $(PXV/ALG)_{40}$. Sample (e) blinded the detector.*

The most marked difference between the various spectra shown in Figure 2.10 is the magnitude of the peak absorbance, which varies linearly with the charge uptake of the film (as described in Figure 2.8d and Table 2-2) for LBL assembled films assembled from polysulfonic acids. This linear variation of peak absorbance indicates that there is little observable influence of polyion character on the extinction coefficient of singly-reduced polyviologen – that is, each singly-reduced viologen center absorbs approximately the same amount of light regardless of counterpolyion environment. Molar extinction coefficients can be calculated based on the solid concentrations of PXV to be 9760 M^{-1} cm^{-1}, 8250 M^{-1} cm^{-1}, and 8500 M^{-1} cm^{-1} for the SPS-, Nafion- and PAMPS-containing PXV films, respectively. These extinction coefficients agree completely with literature values of 8400-9200 M^{-1} cm^{-1} attained for small-molecule alkyl viologens in both aqueous solution[89] and in Nafion polymer films.[90] Apparently there are few solvatochromic differences between the reductive coloration of viologens in water or in polyanion films with very different character.

While this result is initially disappointing from the standpoint of varying electrochromic respsonse by tailoring molecular environments using LBL assembly, upon further investigation it is clear that there is some type of counterpolyion influence – particularly upon the dimer peak absorbance energy and monomer / dimer split. Solution-phase PXV displays a peak dimer absorbance at 575 nm, while the peak absorbances of the LBL assembled films vary from 570 nm to 540 nm. This difference is sufficient to cause a color variation visible to the human eye; the PXV/PAA film (dimer peak 540 nm) appears purple while the PXV/ALG film (dimer peak 570 nm) appears vibrant blue. These peak values along with the monomer / dimer split are shown in Table 2-5. Comparison of the split by absorbance units is not the most rigorous evaluation, but the determination of an exact molar ratio or equilibrium constant would require knowledge of the individual extinction coefficients that cannot be determined for PXV in LBL assembled films because monomer and dimer always appear together.

Table 2-5. Dimer peak location and absorbance split.

system	dimer location (nm)	monomer:dimer (by abs)
PXV	575	0.94
$(PXV/SPS)_{40}$	550	0.67
$(PXV/Nafion)_{40}$	550	0.80
$(PXV/PAMPS)_{40}$	570	0.94
$(PXV/PAA)_{40}$	540	0.60
$(PXV/ALG)_{40}$	570	0.94

There are two possible causes for the shift in dimer peak absorbance. The shift could be due to a change in the energy of the charge transfer complex responsible for coloration. While this is possible, it is unclear whether the bromide counterion or the polyanion counterion remains

paired with the PXV after reduction – the strength of bromide counterion binding (exactly half do not dissociate) would seem to suggest that it may remain and all PXV-containing LBL assembled films may display a charge transfer pair based on bromide. In addition, a chloride anion from the NH_4Cl electrolyte used for spectroelectrochemistry could readily exchange with bromide, and the binding energy of chloride is stronger than that of bromide. Furthermore, the stability of the monomer coloration peak at 600 nm suggests that the counterion is indeed not changing. These considerations suggest that the change in radical cation coloration cannot be attributed to alternative charge-transfer pairs coordinated with bipyridilium even in LBL assembled films of very different compositions.

The shift in peak absorbance is more likely due to an alteration in the nature of the PXV dimerization, which for LBL assembled films will be complicated by interactions with the counterpolyion. Thus, systems that encourage dimerization due to low mobility and hydrophobicity may shift the location of the dimer absorbance peak to higher energies (indicating more complete dimerization), whereas systems that allow dimerization similar to that in free solution should present a dimer absorbance peak closer to the free solution value. It can be seen from Table 2-5 that the PAMPS and ALG composites show dimerization peak locations most similar to those of free solution PXV. Moreover, the ratio of monomer to dimer absorbance is highest in these systems as well, indicating that dimer formation is suppressed. It is thus possible that the fast-switching, highly ionically mobile, and hydrophilic PXV/PAMPS environment also allows greater mobility of individual PXV moieties, discouraging extensive dimerization, while the less mobile, more hydrophobic interiors of PXV/SPS and PXV/Nafion might encourage π-π stacking and immobilization, and thus show greater spectral evidence of dimerization. While switching times could not be properly collected from PXV/PAA and PXV/ALG due to the great thickness of the films, it stands to reason based on this logic that the hydrophilic and polysaccharidic PXV/ALG may provide a faster switching, more mobile environment while PXV/PAA may encourage singly-reduced PXV reorganization into dimers.

2.2.3.6 Optical switching

A final test of the electrochromic, PXV-containing LBL assembled films was made by observing spectral changes to the film during square-wave switching. The films were positioned as for spectroelectrochemistry, and the absorbance at the peak wavelength was evaluated over time. Results of this observation are shown in Figure 2.11. From the shape of the switching waves, it is again clear that PXV/PAMPS provides a very fast switching environment while PXV films containing other polyacids switch much slower.

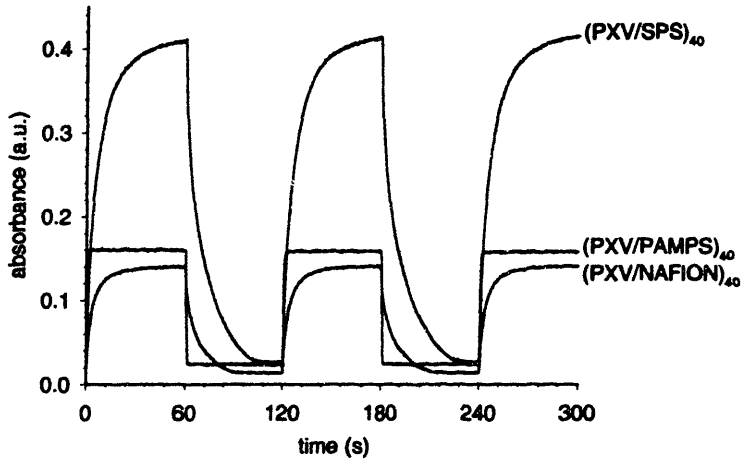

Figure 2.11 Optical switching of PXV LBL assembled films. Absorbance monitored at peak absorbance for each film.

The results shown in Figure 2.11 allow the quantification of switching times, with the selection of a suitable metric. If one defines the switching time as the time required to reach a 90% change in the absorbance of the film, then the switching times for bleaching and coloration would be as follows:

Table 2-6. Switching time and contrast of PXV LBL assembled films.

system	color time (s)	bleach time (s)	Δ%T
$(PXV/SPS)_{40}$	22.4	26.4	55.9% (550 nm)
$(PXV/Nafion)_{40}$	13.7	19.8	25.1% (550 nm)
$(PXV/PAMPS)_{40}$	1.3	1.1	26.3% (570 nm)

2.2.4 Conclusions from poly(viologen) studies

This work with PXV-containing LBL assembled films illustrates the potential the technique to create high-quality electrode films and also to modulate the electrochromism of those films in a purposeful and directed manner. Early observations of the LBL assembly of polyviologens indicated that counterpolyanion character can strongly influence the resultant film thickness and surface morphology. Electrochemical analyses revealed that the counterpolyion character also influences the speed of the redox reaction, in particular as the polyanion PAMPS was found to provide an exceptionally fast and electrochemically reversible reaction environment in the interior of the LBL assembled film, while the polyanions SPS and Nafion displayed a less propitious reaction environment. Electrochemical analysis proved to be a useful tool for describing LBL assembled films: based on coulombic uptake during reduction, an exact composition could be determined for several LBL assembled films, and the partial dissociation of PXV bromide counterions was elucidated and contrasted with earlier conclusions by other investigators.

Spectroelectrochemical analysis indicated that although singly-reduced PXV extinction coefficients do not vary significantly based on counterpolyion character, the energy of that absorbance does vary significantly. In particular, a trend in the location and prevalence of the radical cation dimer can be observed that directly relates to the hydrophobicity of the internal film environment and also correlates to the expected mobility of individual bipyridilium units. This variation is sufficient to create a change in the optical absorbance that is visible to the human eye, and represents the first time that LBL assembly has been shown to modulate the properties of a single electrochromic species in so fundamental a fashion. Finally, the spectral observation of switching confirms that these films could provide sufficient contrast and switching time to meet many practical applications. This work provides a foundation for the application of PXV in a wide variety of electrochromic electrodes, and opens the way for the development of more complex, double electrochrome electrodes that contain polyviologens as an active redox species.

2.3 Poly(aniline) LBL assembled films

2.3.1 Introduction to poly(aniline)

Poly(aniline) (PANI) is the most commonly utilized conjugated conducting polymer, and it has attracted much attention due to a simple and low cost preparation coupled with high electronic conductivity and good environmental stability.[91,92] Investigations of PANI and PANI derivatives have led to applications in corrosion protection,[93-95] hole transport in light emitting diodes,[96,97] and a wide variety of microelectronic device applications. Importantly, PANI exhibits electrochromic behavior upon oxidation and reduction as do most other conjugated polymers, though PANI electrochromism is exceptionally stable to repeated switching.[98] As an electrochromic polymer, PANI switches from a semi-transparent yellow, reduced state termed leucoemeraldine PANI to a darker, oxidized green emeraldine salt or blue emeraldine base (depending on pH).[99,100] Even greater optical absorbance is possible at higher oxidation states – for example the nigraniline base exhibits a blue-black color – but repeated cycling to the oxidative potentials required to attain these states inevitably causes degradation due to hydrolysis of imine groups and subsequent chain scission, resulting in the formation of degradation products.[98-100]

LBL assembled films containing PANI have been constructed based on electrostatic interactions and hydrogen bonding interactions, and the conductivity and doped spectral absorbance of these materials was described by Rubner and co-workers.[22,23] This advance provided a method for applying robust, conformal PANI thin films onto essentially any planar or nonplanar substrate. Other efforts have expanded the range of PANI-containing LBL assembled composites.[46,101,102] In some cases, these studies have touched on the electrochromic nature of PANI,[102] but until recently there has been no in-depth study of the electrochromic properties in particular.

In this chapter, a survey is presented of the electrochromic properties of PANI within various LBL assembled film architectures. As a pH-sensitive polycation and a strong hydrogen bonding donor/acceptor, PANI can be assembled into a wide variety of LBL assembled composites (see Figure 2.12). The polyanions poly(2-acrylamido-2-methyl-1-propanesulfonic acid) (PAMPS), the perfluoronated ionomer Nafion, the polysaccharide carageenan, and strongly sulfonated, self-doping PANI (SPANI) can be LBL assembled with PANI based on electrostatic interactions. Hydrogen bonding donor/acceptors such as poly(acrylic acid) (PAA, here assembled at low pH so that it is fully protonated), poly(acrylamide) (PAAm), and poly(ethylene oxide) (PEO), can be assembled with PANI via hydrogen bonding interactions. Finally, in order

to explore the possibility of an all-polycation LBL assembled film, we assembled PANI with a hydrogen bonding polycation, ethoxylated poly(ethylene imine) (ePEI). This last case assesses the capability of a strong hydrogen bonding system to overcome electrostatic repulsion between two charged polycations in a LBL thin film. This wide range of "partner" polymer character provides a great deal of variety in the properties of the finished PANI composites, providing the opportunity to assess the relative contributions of such properties as hydrophilicity and dielectric constant on the behavior of PANI coloration and switching.

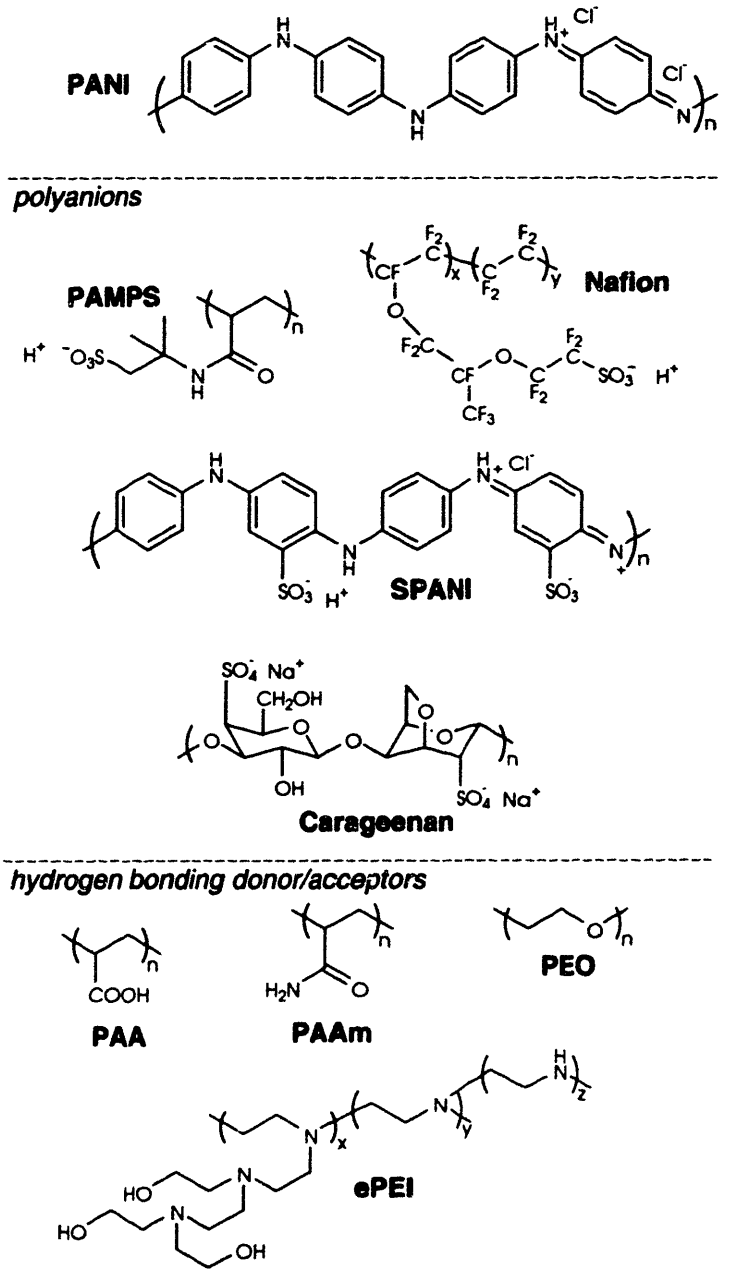

Figure 2.12. Molecular structures of the polyelectrolytes and nonionic polymers employed in PANI LBL studies.

2.3.2 Experimental details for poly(aniline) studies

2.3.2.1 Materials

The electroactive polymer was PANI (Aldrich). PANI films were LBL assembled with PAMPS (Aldrich), Nafion 117 (Fluka), Carageenan (Fluka), SPANI (Aldrich), PAA (Aldich MW), PAAm (Polysciences), and ePEI (MW, Aldrich). Polymer solutions were made using Milli-Q (Millipore deionized, >18.2 Ωcm, 0.22 μm filtered) water, and pH adjusted using NaOH or HCl. The PANI solution was 10mM (all polymer solution concentrations are respect to the molecular weight of the repeat unit). PANI solutions were formulated using a 1:9 dimethylacetamide and water solvent pair as described by Rubner and co-workers.[22,23] PAMPS and Nafion solutions were formulated at 2mM, while all other polymer solutions were formulated at 20 mM. The pH of all deposition baths was adjusted to pH 2.5. ITO-glass substrates with dimensions 0.7 cm × 5 cm (Delta Technologies, 6 Ω/square) were cleaned by ultrasonication in a series of solvents: dichloromethane, methanol, acetone, and Milli-Q water for 15 minutes each, followed by a 5-minute oxygen plasma etch (Harrick PCD 32G) to provide a clean, hydroxyl-rich surface.

2.3.2.2 Assembly

Film assembly was automated with a Carl Zeiss HMS DS-50 slide stainer. The substrates were exposed to polycation solution for 15 minutes, followed by copious water rinsing for 4 minutes in three consecutive Milli-Q water baths, and then exposed to polyanion solution for 15 minutes and again rinsed. This cycle was repeated for 15 layer pairs for each PANI-containing LBL system.

2.3.2.3 Measurement

Electrochemical analysis was performed using an EG&G 263A potentiostat/galvanostat. These measurements were performed in a flat cell of 30 mL volume and approximately 0.3 cm^2 working electrode area. The electrolyte used was aqueous 0.1 M sulfuric acid with a pH of approximately 1.1. The counterelectrode was 4 cm^2 platinum foil, and reference was a K-type saturated calomel electrode. CV was performed with potential limits of –0.2 V and 0.6 volts, at scan rates of 25, 50, 100, and 200 mV/s. Double potential step chronoamperomtery was performed by stepping between –0.2 V and 0.6 V vs. SCE, with 5 seconds per step and 10 seconds per cycle, with approximately 20 cycles performed sequentially before the measurement cycle. Spectral characterization was performed on a rail-mounted Oriel UV-Vis spectrophotometer with a 75 W Xe lamp, 300 L/mm, 300 nm blaze grating and InstaSpec IV CCD. For

spectroelectrochemistry, potential control was provided by EG&G 263A, with the polymer-coated ITO-glass substrate positioned in a quartz cell and immersed in electrolyte, along with a platinum wire counter electrode, and SCE reference.

2.3.3 Results and discussion for poly(aniline) LBL assembled films

2.3.3.1 Assembly of poly(aniline) LBL assembled films

The PANI-containing films assembled in this study featured a linear increase in thickness with the number of layer pairs deposited, as was described previously by Rubner and co-workers for some systems of this type.[22,23] Film thickness and roughness are shown in Table 2-7. Thickness of electrostatic films varied from 2.5 to 5.1 nm per layer pair, well in agreement with previous work on the PANI/poly(styrene sulfonate) system.[22,23] The thickest film assembled by electrostatics was found to be PANI/Nafion, most likely owing to high equivalent weight of Nafion as compared to the other strong polyanions employed.

Table 2-7. Thickness of several PANI LBL assembled films.

system	final thickness (per layer pair) (nm)		R_q rms roughness (nm)
$(PANI/PAMPS)_{15}$	53.0	(3.5)	2.6
$(PANI/Nafion)_{15}$	77.2	(5.1)	2.3
$(PANI/carageenan)_{15}$	60.8	(4.1)	3.6
$(PANI/SPANI)_{15}$	37.9	(2.5)	2.5
$(PANI/PAA)_{15}$	111.9	(7.5)	8.3
$(PANI/PAAm)_{15}$	452.5	(30.2)	16.9
$(PANI/PEO)_{15}$	221.9	(14.8)	8.9
$(PANI/ePEI)_{15}$	13.6	(0.9)	1.5

Hydrogen bonded films assembled in this study are far thicker than those studied earlier by Rubner and co-workers.[23] In particular, the PANI/PAAm and the PANI/PEO systems are two to four times thicker. This difference may be due to the use of an ITO substrate rather than organosilane- or PEI-treated silica. The hydroxyl surface of ITO provides strong Lewis acidity that has stronger attractive interactions with polyimines than the Brönsted acid silica surface, especially at lower pH conditions. Due to this advantage, PANI deposits in thicker layers onto ITO – an effect which propagates throughout the film in hydrogen bonded systems because growth is less self-limiting than electrostatics. Greater thickness could also stem from differences in nonionic polymer dipping solution pH, which was ambient in Rubner's work,[23] yet adjusted to 2.5 in our work, which could have strengthened the interactions of nonionic polymers by providing a fully protonated PANI surface. The roughness of hydrogen bonded LBL assembled films is greater than that of electrostatically LBL assembled films, possibly due to instabilities arising from the deposition of these extremely thick layers.

The PANI/ePEI system is thinner than any other system due to the inherent electrostatic repulsion between PANI and ePEI, both of which possess protonated and cationic groups at the assembly pH of 2.5. Despite the repulsion, hydrogen bonding between PANI amine/imine groups and ePEI hydroxyls and amines is strong enough to facilitate the growth of a very thin film. This example is a surprising result of the complex interplay of attractive/repulsive forces in LBL assembled films.

2.3.3.2 Electrochemistry - cyclic voltammetry

The general electrochemical behavior of PANI-containing LBL assembled composites were assessed using CV. The potential limits of –0.2 to 0.6 V vs. SCE were chosen to eliminate oxidative degradation while still accessing the full color change between the reduced, pale yellow leucoemeraldine base to the oxidized green/blue emeraldine salt/base.[98] The CV results are shown in Figure 2.13. In general, the electroactive behavior of PANI is similar to that reported from other sources, with strong oxidation and reduction peaks centered at 0.11-0.12 V vs. SCE. This potential is consistent with the desired transition in this pH range.[103] There is no strong shift in the redox potential when PANI is complexed with stronger polyacids (e.g. Figure 2.13a,b) or weaker polyacids (e.g. Figure 2.13e), indicating that the polyanions ionically crosslinked with PANI are primarily in salt form and thus do not provide a strongly acidic internal film environment(pH<1), which would shift the redox potential of this transition to higher values for greater acidity.[103]

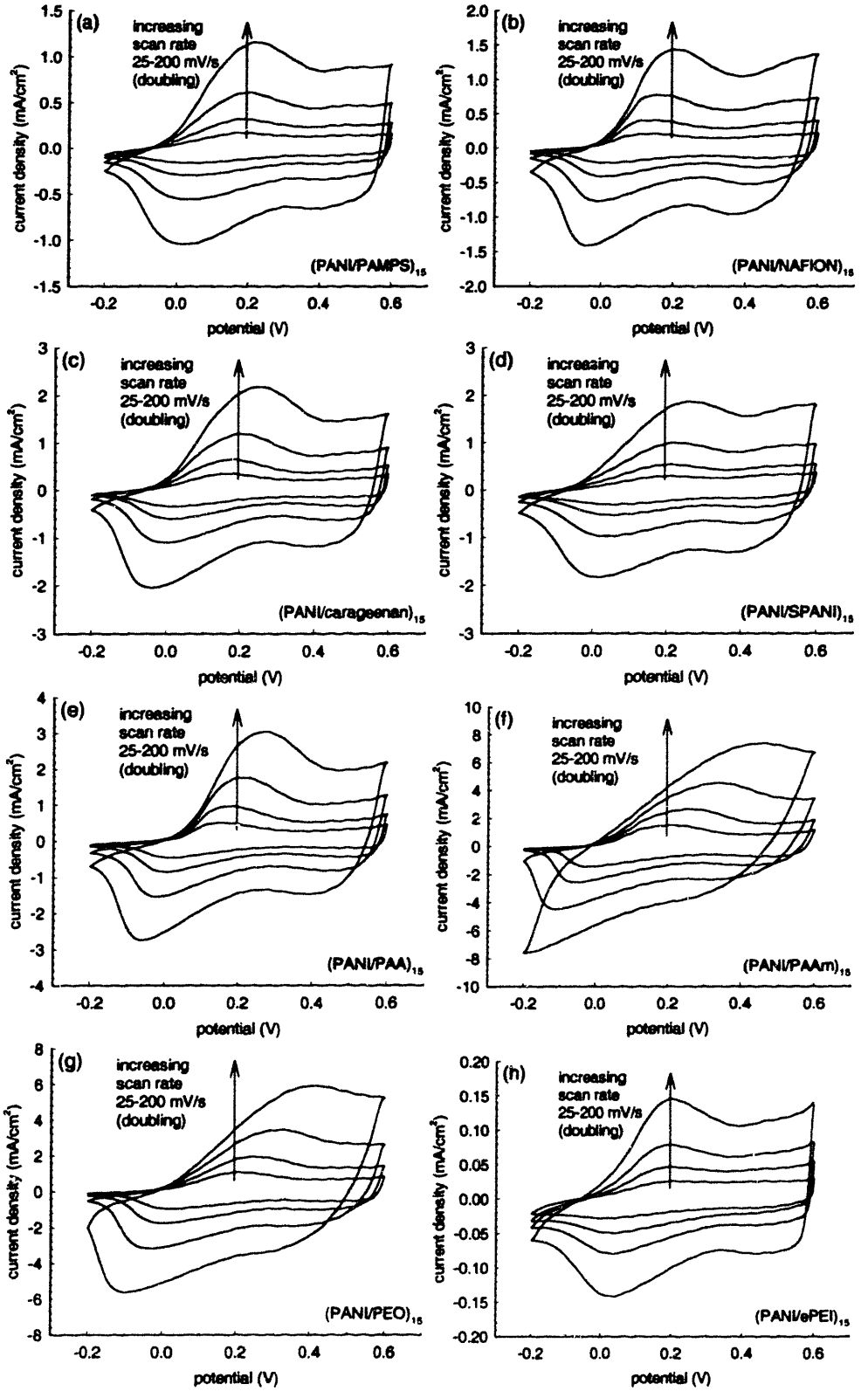

Figure 2.13. Cyclic voltammetry of PANI LBL assembled films.

While the PANI is undergoing reduction and oxidation throughout the CV experiment, ions travel through the thickness of the film to balance the changing electrostatic charge of PANI. For neat PANI and hydrogen bond LBL assembled PANI films, the mobile species would be small polyanions – in our case sulfate anions. PANI within electrostatically LBL assembled films is paired with polyanions, so the mobile species in those systems would be small cations - in our case protons - moving in and out of association with the polyanionic dopant.[33] The speed of this ionic exchange can be qualitatively assessed from the oxidative and reductive CV peak currents at different scan rates, as shown in Figure 2.14. The peak height increases linearly with scan rate in all cases. This linear increase indicates that the redox reaction is confined to the thin film and not limited by diffusion. There is a very slight nonlinearity in the response of the very thick hydrogen bonded LBL assembled films (notably PANI/PAAm), indicating a small resistance to counterion diffusion. Even very thick LBL assembled films present an open and ion permeable morphology, a result that has also been found in other electroactive polymer LBL systems.[55] These results contrast with studies that show severely restricted ion permeation in highly-charged LBL assembled films due to intrinsic charge compensation and a lack of free ion exchange sites.[104] In those studies, electrolyte exposure increased the number of exchange sites, though the ionic strength required for significant permeation was much higher than the ionic strength of our own electrolyte.[104] Facile ion permeation in these PANI-containing systems may be attributed to the low cationic charge density of PANI, which may naturally assemble into a more loopy, open morphology.

Another transport phenomenon occurring within the films during CV switching is the movement of the redox front - the transfer of electrons at the ITO/PANI interface and within the film interior. A qualitative characterization of this phenomemon may be made by examining the hysteresis between CV oxidation and reduction peaks shown in Figure 2.13. For most systems the hysteresis between these peaks grows with increasing scan rate, indicating a non-Nernstian condition at the reactive front caused by internal resistance (the iR drop) within the LBL assembled film structure. The hysteresis is greatest for the thickest LBL assembled films, where the outermost PANI layers are isolated and less electrochemically available. The large individual layer thickness may limit redox propagation by insulating PANI between thick layers of resistive polymer. The thinnest film, PANI/ePEI, shows a small hysteresis that does not increase, indicating that the PANI within this film is immediately electrochemically available.

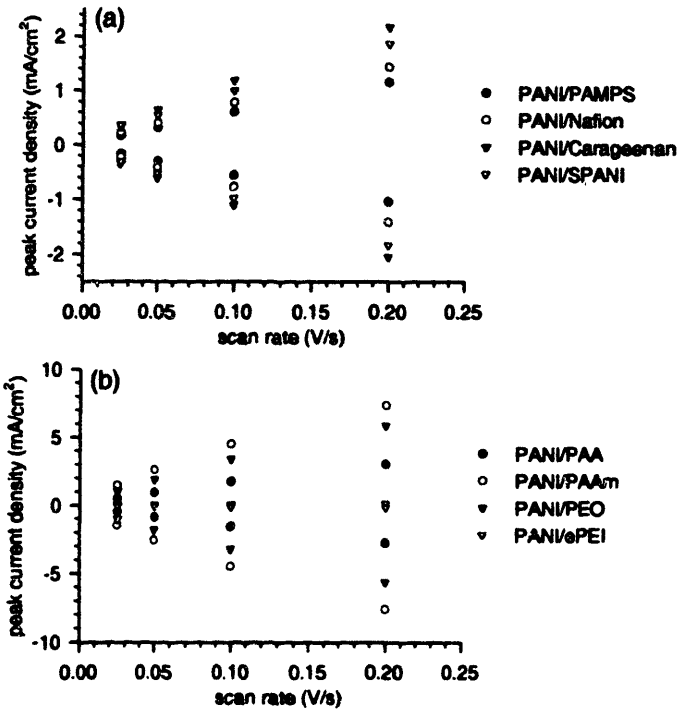

Figure 2.14. Oxidative (positive) and reductive (negative) peak currents for (a) electrostatic and (b) hydrogen bonded PANI LBL assembled films linearly increase with scan rate.

2.3.3.3 Electrochemistry – square wave switching

The electrochemical technique of double potential step chronoamperomtery (DPSCA) was used to investigate the electrochemical accessibility of PANI and composite switching time. A square wave between –0.2 V and 0.6 V vs. SCE with 5 seconds at each potential was applied while monitoring current. The dynamics of current change and the integrated charge injected/withdrawn are plotted as a function of time in Figure 2.15.

Electrostatically assembled PANI films switch faster than hydrogen-bonded films, an effect due primarily to film thickness that may also be influenced by the different mobile species (sulfate vs. proton). The final charge capacity scales well with expectations based on thickness, indicating similar PANI "loading" in all LBL assembled composites. PANI/SPANI has a higher charge capacity than other systems due to the inclusion of a reactive SPANI polyanion. The PANI/PAAm system has less charge density than may be expected, indicating that outer PANI layers in this extremely thick composite may not be fully accessible.

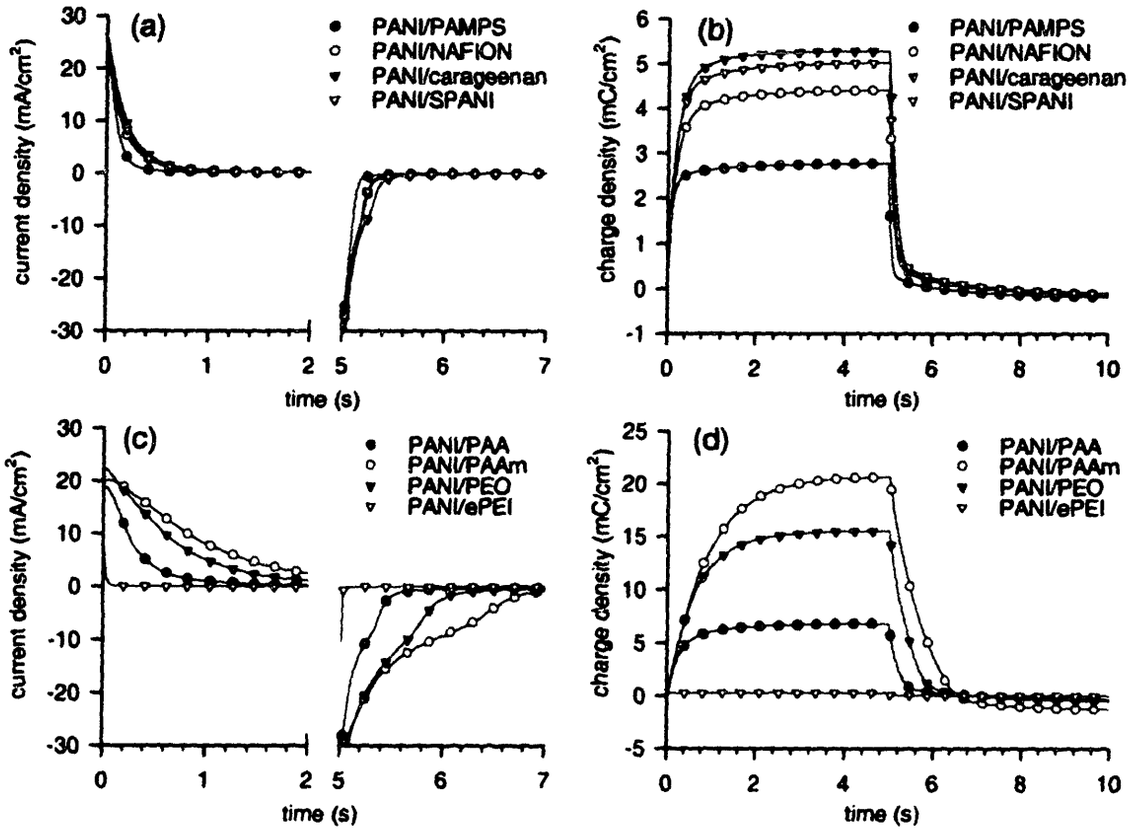

Figure 2.15. Square wave switching for (a,b) electrostatic and (c,d) hydrogen-bonded PANI LBL assembled films.

2.3.3.4 Spectroelectrochemistry

The full electrochromic properties of the PANI LBL assembled films were examined using spectroelectrochemistry, taking a UV-Vis "snapshot" of each film at equilibrated potentials between –0.6 and 0.2 V, with results shown in Figure 2.16. At very cathodic potentials, leucoemeraldine PANI exhibits a single absorbance maximum at 340 nm, with essentially no additional absorbance in the visible region. At more anodic potentials, emeraldine PANI evinces a 700 nm peak, with broad visible absorbance.

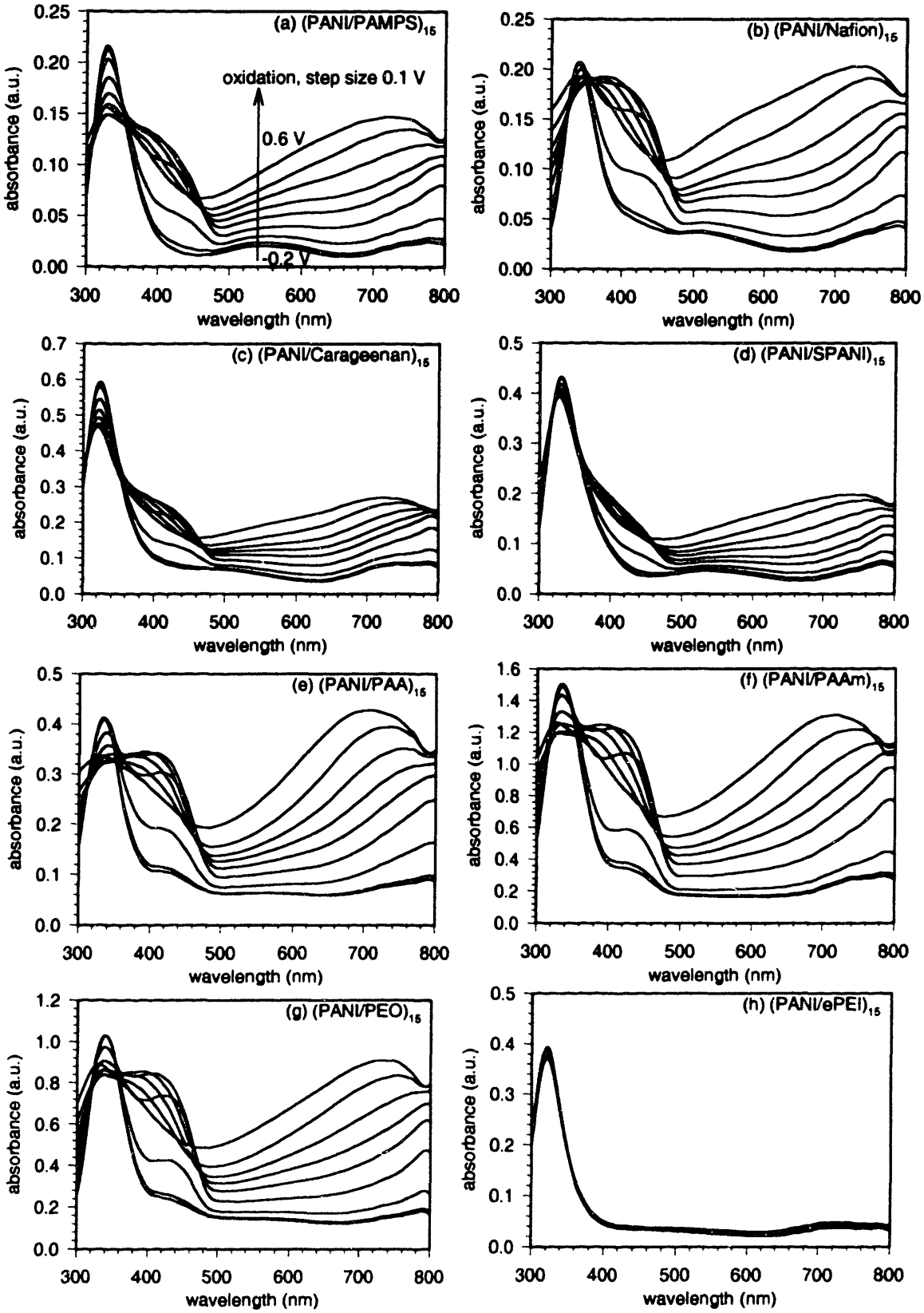

Figure 2.16. Spectroelectrochemistry of PANI LBL assembled films.

The primary spectral differences between the various LBL assembled composites described in Figure 2.16 are the intensities of leucoemeraldine and emeraldine peaks. In general, the emeraldine peak absorbance scales mostly linearly with the film thickness and Faradaic charge capacity, but there is some small variation in extinction coefficient. The calculated extinction coefficients are shown in Table 2-8. It should be noted that the concentrations shown in Table 2-8 are not concentrations of PANI monomer, but rather the concentrations of redox centers (as determined from square wave switching in Figure 2.15) that may be distributed over several monomer units and might be considered a macro-chromophore. As can be seen, the concentration of these centers for PANI/SPANI is approximately double that seen for the other composites, as would be expected because both polycation and polyanion are redox-active.

What is especially notable from the trends in Table 2-8 is that the *electrostatically assembled* PANI films consistently display extinction lower than the *hydrogen bond assembled* PANI films. In fact, the extent of acidity can be correlated to some degree with the caliber of extinction; Nafion the superacid has the lowest extinction of the redox-inert sulfonic acids. Another factor introduced by the strong polyacids is the appearance of a small peak at 500-550 nm that can be seen clearly in the –0.2 V absorbance spectrum of the electrostatically assembled PANI films in Figure 2.16. Together, these two phenomena suggest that the acidity of the counterpolymer has a direct influence on the properties of PANI. This acidity may influence the equilibrium between emeraldine salt and emeraldine base in the oxidized composite; at the pH of the electrolyte, both should be present but emeraldine salt should dominate. The emeraldine base form is more prevalent at higher pH conditions and features greater absorbance in the red region of the spectrum, therefore displaying a more blue color, while the emeraldine salt form is more prevalent at lower pH conditions and features greater absorbance in the 400 nm range, resulting in a greener color (for images of LBL PANI films, look ahead to Figure 2.18). In PANI films assembled with strong polyacids, the additional acidity provided by the acid appears to shift the equilibrium to the emeraldine salt so that less absorbance is observed in the 700 nm range. In PANI films assembled with hydrogen-bonding polymers, there is no additional acidity and the oxidized PANI takes on an equilibrium composition influenced entirely by the electrolyte that features a greater amount of the emeraldine base.

The emeraldine peak that is preserved in the reduced electrostatic PANI films must be due to continued doping by the polyacid even when the film is polarized to a potential that should result in complete conversion to leucoemeraldine PANI. This phenomenon has been noted for PANI|PAMPS interfaces and is one of the reasons these materials are employed in tandem in electrochemical cells.[105-107] This effect may be enhanced by polyacid enthalpic

resistance to protonation under these pH conditions and the potential entropic loss due to re-association of a free proton with the polyacid.

A final phenomenon that should be noted is that the extinction of PANI/SPANI is poorer than any of the other composites. SPANI coloration has been found to be inferior to that of PANI, which in general explains this lowered absorbance.[46,51] PANI/ePEI is not sufficiently absorbing for full detection.

Table 2-8. PANI LBL assembled film redox center concentration and extinction.

system	PANI centers (mmol/cm³)	ε ($M^{-1}cm^{-1}$) at 700 nm
$(PANI/PAMPS)_{15}$	5.5	4618
$(PANI/Nafion)_{15}$	6.0	4264
$(PANI/carageenan)_{15}$	9.1	4814
$(PANI/SPANI)_{15}$	13.7	3627
$(PANI/PAA)_{15}$	6.5	5575
$(PANI/PAAm)_{15}$	5.0	5306
$(PANI/PEO)_{15}$	7.4	5141
$(PANI/ePEI)_{15}$	7.6 *	3473 *

* questionable data from ultrathin film

2.3.3.5 Optical switching

The dynamics of switching were investigated using in situ fast spectral scans during square wave switching. Absorbance switching of an isolated wavelength is shown in Figure 2.17. In general, the absorbance switching mirrors the Faradaic charge switching described in Figure 2.15.

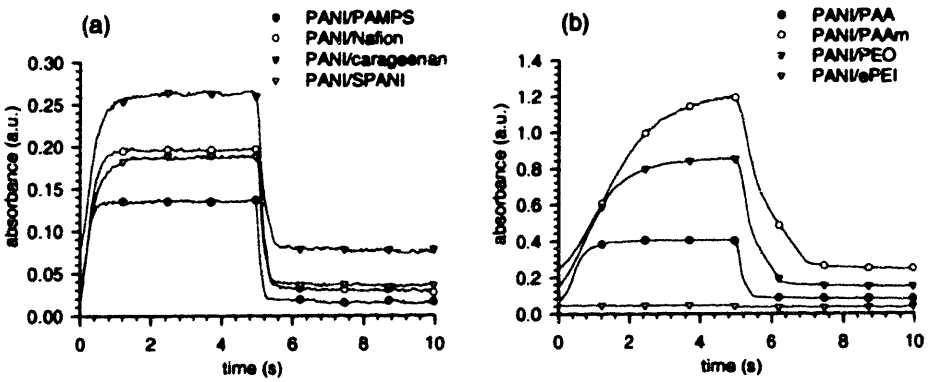

Figure 2.17. Optical switching at 700 nm for (a) electrostatic and (b) hydrogen-bonded PANI LBL assembled films.

Primary performance metrics for electrochromic polymer films are response time and contrast. Contrast can be evaluated by many measures; maximum transmittance change is often used. Contrast and response times for the PANI LBL assembled composites surveyed herein are presented in Table 2-11. Response time is based on the time required for 90% of full transmittance change. In general, films of similar thickness performed similarly, indicating that their commonality - PANI - must direct the connectivity and ion mobility of the constructed

films, especially as the counterpolymers possess such a diverse range of dielectric constant, hydrophilicity, and acidity. The maximum contrast was exhibited by PANI/PAAm and PANI/PEO. With similar extinction coefficient and PANI loading, this maximum contrast is achieved in films near a simple optimum thickness, which may lie between 250 and 400 nm. The best combination of fast switching and high contrast was found in PANI/PAA, which is thinner than both PANI/PAAm and PANI/PEO. It should be noted that the contrasts achieved from these LBL assembled composites are quite high when compared to other electrochromic polymer films, due to freedom from defects even in very thick films. A comparison of switching photographs of two of the films studied in this work is shown in Figure 2.18. The PANI/PAMPS composite shows slightly less coloration than does the PANI/SPANI composite, even though the thickness of the latter is much less. The PANI/SPANI composite may be considered a LBL "dual electrochrome" in that both polycation and polyanion are electrochromic polyions; this combination results in a greater concentration of redox centers within the LBL matrix, that outweigh the slightly lower extinction of those redox centers due to the incorporation of SPANI. The possibilities of extending this dual electrochrome concept to combine very dissimilar electrochromic polycations and polyanions to achieve strongly enhanced contrast and multiple colors will be fully described in the following chapter.

Table 2-9. Switching time and contrast of PANI LBL assembled films.

system	bleach / color time (s)	$\Delta\%T_{max}$ (bleach – colored, loc.)
$(PANI/PAMPS)_{15}$	0.25 / 0.41	26% (98% - 72%, 688 nm)
$(PANI/Nafion)_{15}$	0.41 / 0.62	31% (95% - 64%, 682 nm)
$(PANI/carageenan)_{15}$	0.50 / 0.74	34% (92% - 58%, 649 nm)
$(PANI/SPANI)_{15}$	0.41 / 0.83	29% (94% - 62%, 687 nm)
$(PANI/PAA)_{15}$	0.50 / 0.91	49% (87% - 38%, 687 nm)
$(PANI/PAAm)_{15}$	2.0 / 2.2	61% (68% - 7%, 649 nm)
$(PANI/PEO)_{15}$	1.3 / 1.7	62% (78% - 14%, 686 nm)
$(PANI/ePEI)_{15}$	<0.15 / <0.05	2% (93% - 91%, 688 nm)

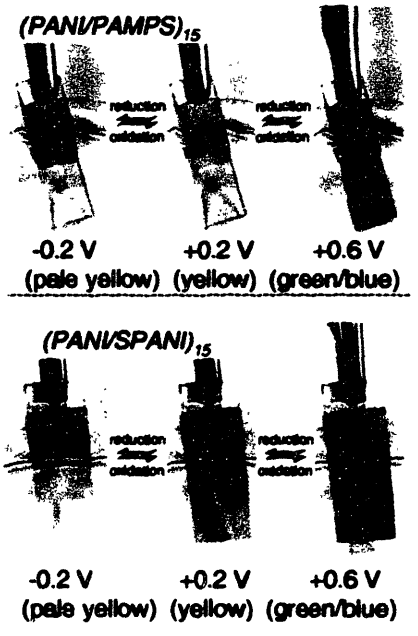

Figure 2.18. Photograph of electrochromism in PANI LBL assembled films.

2.3.4 Conclusions from poly(aniline) studies

A survey of the electrochemical and optical properties of a wide variety of PANI LBL assembled electrochromic films has been presented. Different counterpolymers do influence the electrochemical and spectral properties. For the first time it has been shown that the acidity of the LBL counterpolymer can be used to directly manipulate the coloration of PANI films by influencing local pH conditions and shifting the equilibrium between PANI emeraldine salt and emeraldine base forms. However, PANI appears to control the overall morphology - in particular the connectivity of the electroactive species and the ion mobility environment - because films of very different composition yet similar thickness possess similar electrochemical kinetics and switching behavior. This behavior is in contrast to that of PXV, which exhibited a distinct kinetic dependence on counterpolyion. These PANI composites switch extremely fast and display high contrast owing to the high thickness that can be achieved with low roughness in LBL assembled films. The performance capabilities of these films are of sufficient caliber to support the recommendation that the LBL process be considered generally superior for the fabrication of electrochromic PANI films as compared to traditional techniques.

2.4 PEDOT LBL assembled films

2.4.1 Introduction to PEDOT

Given the success of the PANI-containing LBL assembled films, it is natural to extend the assembly concept to other conjugated systems, in order to enhance the available "library" of LBL assembled electrode films that can be realized. One conducting polymer that has been gaining notoriety of late is poly(3,4-ethylene dioxythiophene) (PEDOT).[108,109] PEDOT was initially developed commercially by Bayer AG with an ethylenedioxy moiety bound to the 3- and 4-position carbons on thiophene as protecting groups to produce a polythiophene with no beta coupling interruptions of the conjugated structure.[110,111] The resultant polymer displayed a high conductivity - on the order of 300 S/cm - and the chemical modification introduced by the beta-position electronegative oxygens was discovered to lower the conjugated polymer bandgap to such an extent that introduction of carriers upon oxidative doping redshifted the primary absorbance band from the visible to the near IR spectral region. Thus PEDOT is essentially completely transparent in its oxidatively doped state, and it colors upon reduction to a dark blue insulating state. This combination of high conductivity and transparency has resulted in a wide variety of applications including antistatic coatings,[112] supercapacitor electrodes,[113,114] and many other electronic applications.[115] The electrochromic behavior of PEDOT has been exploited by many researchers, and in fact the highest contrast electrochromic polymer films reported to date have been based on covalent chemical modification of the PEDOT monomer before electrochemical polymerization.[13,116]

In order to provide easy processing, PEDOT is produced commercially as an aqueous colloidal suspension of the normally aqueous insoluble conjugated polymer combined with an excess of the polyanionic dopant poly(styrene sulfonate) (SPS) (the suspension trade name: Baytron P). This suspension is apparently produced by simple oxidative polymerization of the EDOT monomer utilizing iron chloride or ammonium persulfate in the presence of excess acid form SPS. This excess of SPS acts to charge-stabilize the colloid by providing negative polyvalency. It was discovered in the course of this thesis work that the excess polyanion can then be exploited to create electrochromic PEDOT:SPS-containing LBL assembled films by pairing the colloid with appropriate polycations. The PEDOT:SPS pairing is maintained in a three-component LBL assembled film. An electrochromic film based on the LBL assembly of a self-doping sulfonated PEDOT was subsequently developed by other investigators.[55]

PEDOT appears to be particularly sensitive to specific environments – in particular, an effect that has come to light in recently years is that adding glycerol to the commercial

PEDOT:SPS colloidal suspension reduces visible-range optical absorbance of the doped state and enhances electronic conductivity.[68,69] The specific nature of the effect has not been completely elucidated. However, one might assume that the effect is due to morphological and secondary chemical interactions. Glycerol is a strongly hydrogen-bonding small hydrocarbon liquid. It is possible that glycerol plasticizes the PEDOT:SPS film to a degree that allows the conducting polymer greater linearity, increasing effective conjugation length and lowering the local bandgap energy of previously "kinked" chains. This effect would reduce visible color absorbance and enhance electronic conductivity. It is also possible that hydrogen-bonding interactions between β-position oxygens on PEDOT and hydroxyl hydrogens on glycerol are responsible for the effect.

As the PEDOT:SPS colloid can be successfully LBL assembled, it is natural, then, to attempt to mimic the effect of glycerol in a LBL assembled film. This would require a polycation that possesses similarities in physical and chemical properties to the glycerol molecule. Plasticization is difficult to introduce into a LBL assembled film via the introduction of a polycation, so our efforts focused on introducing hydrogen bonding functionality. To this end, polycations for combination with PEDOT:SPS were chosen based on suitability as hydrogen bonding donors. These polycations included linear poly(ethylene imine) (LPEI), branched poly(ethylene imine) (BPEI), poly(dimethylamine-co-epichlorohydrin) (PDAE), poly(diallyl dimethyl ammonium chloride) (PDAC), and 80% ethyoxylated poly(ethylene imine) (ePEI). Polycations such as ePEI and PDAE in particular should provide a polyhydroxyl environment similar to glycerol (see Figure 2.19).

To fully examine PEDOT:SPS-containing LBL systems, the colloid was first assembled in a series of films with LPEI. As can be seen from section 2.3 on PANI films, the thickness of films can have a profound effect on the electrochemical behavior and spectral performance of the resultant films. The LPEI/PEDOT:SPS series provided information concerning the behavior of films of increasing thickness and also explored the peculiarities of this colloidal LBL assembly mechanism. Individual films of BPEI/PEDOT:SPS, ePEI/PEDOT:SPS, PDAC/PEDOT:SPS, and PDAE/PEDDOT:SPS were compared to LPEI/PEDOT:SPS films of similar thicknesses in order to isolate effects that might be due to the character of the counterpolycation. Results confirm that electrochromically coloring PEDOT:SPS electrode films can be constructed and optimized using the LBL technique. Furthermore, there exist indications that the counterpolycation may indeed influence coloration to some extent. Importantly, these results can serve as a template for the inclusion of normally aqueous insoluble conjugated polymers into LBL assembled films using the vehicle of a soft colloidal dispersion. Employing this strategy, a wider variety of electrode systems may be able to capture the advantages of the technique.

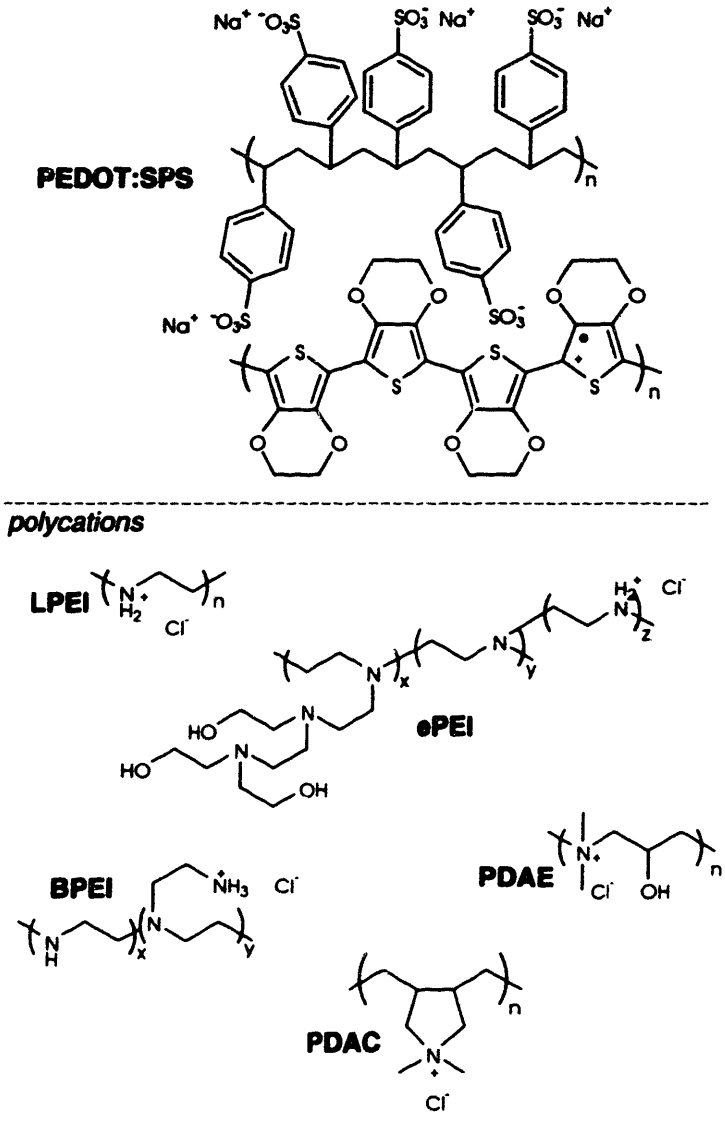

Figure 2.19. Molecular structures of the polyelectrolytes employed in PEDOT LBL studies.

2.4.2 Experimental details for PEDOT studies

2.4.2.1 Materials

BAYTRON P, the commercial PEDOT:SPS colloid formulation, was generously donated by Bayer AG. The PEDOT:SPS colloid as received consists of 2% solids in deionized water. The PEDOT:SPS ratio in the colloid is 1:1.6 by mass, so that excess negative charge stabilizes the suspension. The PEDOT:SPS colloidal suspension was diluted 1:10 to result in a solution of 0.2% solids. Additionally, sufficient dimethylacetamide (DMAc) was added to create a final solvent composition of 10% DMAc. This addition of this polar organic solvent was found to enhance the solubility of the thiophene component of the colloid and result in films with a higher PEDOT

content. Solutions of the polycations LPEI (Polysciences MW 25k), PAH (Aldrich MW 70k), BPEI (Aldrich MW 25k), PDAE (Aldrich MW unknown), PDAC (Aldrich, MW 25k), and ePEI (Aldrich 80% ethoxylated MW 70k) were formulated at 10 mM with respect to the polyelectrolyte equivalent weight (weight of charged repeat unit). The PEDOT:SPS and polycation solutions were adjusted to pH 4 using sodium hydroxide and hydrochloric acid solutions.

Substrates were 7×50×0.7 mm passivated, polished float glass cuvette slides, $In_2(Sn)O_x$ coated on one side with sheet resistance of 6 ± 2 Ω, obtained from Delta Technologies (hereafter ITO slides). Substrates were cleaned by ultrasonication in 1) dichloromethane, 2) acetone, 3) methanol, and 4) water for 15 minutes each in a Bransonic ultrasonic cleaner. All water used for cleaning was MilliQ purified deionized water. This cleaning regimen was followed by an oxygen plasma etch for 5 minutes in a Harrick PCD 32G cleaner/sterilizer.

2.4.2.2 Assembly and Measurement

Assembly and film assessment follow the equipment and procedures described in detail in section *2.3 Poly(aniline) LBL assembled films*, subheading *2.3.2 Experimental.*

2.4.3 Results and discussion for PEDOT LBL assembled films

2.4.3.1 Assembly of PEDOT LBL assembled films

The first study of PEDOT:SPS-containing LBL assembled electrode films involved the assembly of a single system – LPEI/PEDOT:SPS – at several layer pair numbers in order to determine the general assembly behavior and isolate thickness effects from the effects of polycation identity. The thickness as measured by profilometry for this system is shown below in Figure 2.20. There appears to be first an exponential growth regime followed by a linear growth regime. The earliest films are thin – on the order of 2-3 nm per layer pair, which is typical for a model polcation/polycanion LBL assembled film. Unlike model systems, the LPEI/PEDOT:SPS series increases exponentially in thickness from 5 to approximately 15-20 layer pairs, when linear growth is established outwards to 40 layer pairs at approximately 75 nm per layer pair. Roughness as shown in the Figure 2.20 inset, increases approximately linearly with film thickness and follows approximately the same trend as thickness. The generally large thickness of these films may be attributed to the partially charged nature of LPEI at pH 4; very few charges on the LPEI backbone lead to a greater amount of deposited LPEI, and a loopy or globular LPEI morphology. The PEDOT:SPS colloid may also contribute to the thick film as the inherent ionization density on SPS chains is smaller that it would be typically due to the binding of

PEDOT. The only literature value available for a comparison of thickness profiles involves the LBL assembly of PEDOT:SPS as a hole injection layer for LED devices that was performed concurrently with the work in this thesis.[43] This work employed a strongly cationic, permanently quaternized polyamine with a resultant film thickness of a 5 layer pair film being approximately 5 nm, or 1 nm per layer pair. The study was not extended to greater layer pair numbers to investigate whether nonlinear growth was apparent. A less apt comparison can be made between this system and the poly(allylamine hydrochloride) / sulfonated PEDOT (PAH/PEDOT-S) system investigated by Cutler and Reynolds, which showed linear, 4.5 nm per layer pair growth at pH 2.8.[55]

It is notable that very thin LPEI/PEDOT:SPS films do not show evidence of the deposition of colloidal particles in spheres or hemispheres. As characterized by profilometry, the films are thin and smooth as might be expected from the LBL assembly of a fully soluble polycation / polyanion pair. This would indicate that PEDOT:SPS as provided by Bayer is not a hard colloidal suspension but rather a soft dispersion of partly soluble PEDOT:SPS complexes that can extend or unwind onto a polycation surface to satisfy surface charge and provide a smooth, anionic surface. However, as the film grows exponentially in thickness, so does the roughness; this trend indicates that there may be some three-dimensional character to the depositing colloid. With each PEDOT:SPS deposition step, surface roughness increases, and therefore the surface area should also increase. This increased area would be capable of adsorbing additional polycation, which in turn would adsorb more PEDOT:SPS, further enhancing surface roughness. Deposition does become linear after a certain thickness is reached, indicating that there exists a certain limiting surface roughness at which additional (exponentially increasing) deposition is impossible, possibly because further increase in surface area would render some parts of that surface inaccessible for deposition.

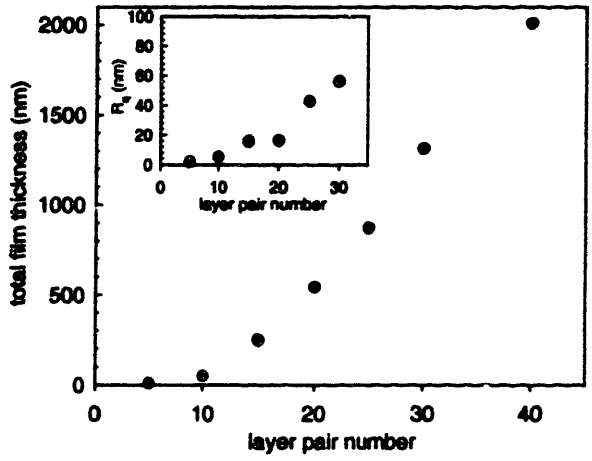

Figure 2.20 Correlation of film thickness to layer pair number for the LPEI/PEDOT:SPS series.

Table 2-10 Thickness results for different PEDOT LBL assembled composites

system	final thickness (per layer pair) (nm)	R_q rms roughness (nm)
$(BPEI/PEDOT:SPS)_{40}$	242.4 (6.1)	2.5
$(ePEI/PEDOT:SPS)_{40}$	977.0 (24.4)	13.4
$(PDAC/PEDOT:SPS)_{40}$	91.0 (2.30)	2.6
$(PDAE/PEDOT:SPS)_{40}$	732.5 (18.3)	12.6

After the assembly of the LPEI/PEDOT:SPS series, the other polycations were also assembled with PEDOT:SPS, and the thickness results for those single films are shown Table 2-10 above. It is important to note that the per layer pair thickness as shown in the table does not necessarily reflect the thickness that might be achieved at intermediate layer pair numbers because we expect that these systems may also show an initial exponential growth tendency. The BPEI/PEDOT:SPS and ePEI/PEDOT:SPS systems both assemble into layers that are thinner than those deposited by LPEI/PEDOT:SPS – this difference could be due to the lower chain ionization density on both of these polycations due to extensive branching. The PDAC/PEDOT:SPS thickness is on the order of that discovered in the other work that involved strong polycations.[43] However, it is surprising that the PDAE system is so much thicker than the PDAC system considering that the PDAE repeat unit MW is less than that of PDAC and therefore one would expect that films incorporating this polycation would be thinner due to the greater chain ionization density. This disparity may be evidence of contributions of secondary interactions such as hydrogen bonding between PDAE hydroxy units and PEDOT β-position oxygens. A similar argument could explain why ePEI/PEDOT:SPS films are almost four times thicker than BPEI/PEDOT:SPS films even though both are branched poly(ethylene imines); the only difference between the two polymers is the ethoxylation of ePEI. Indeed, it is possible that hydrogen bonding is strongest with LPEI, which would contain the greatest density of hydrogen

bonding donating protons (from secondary amines), followed by ePEI (from ethoxylated terminal amines), and finally BPEI (from terminal amines). The roughnesses of all of the films described in Table 2-10 fall within the trend described by LPEI/PEDOT in the inset to Figure 2.20, suggesting a similar assembly mechanism.

2.4.3.2 Electrochemistry - cyclic voltammetry

CV was performed on the LPEI/PEDOT series for all of the films that were assembled. The character of the resultant voltammograms followed a distinct trend, which is illustrated below in Figure 2.21. In part (a) of this figure, the 5-layer pair film displays the general electrochemistry of PEDOT, yet is partially obscured by proton reduction in the aqueous electrolyte at negative potentials, which causes a strong current draw in that portion of the curve. The general electrochemistry of these systems is better described by part (b), which shows the electrochemistry of a 15 layer pair film. The onset of oxidation is clearly at approximately –0.1 V, while the onset of reduction is broader, but appears to be in the same potential range. As the scan rate is increased, the peak hysteresis increases slightly, but the peak height continues to increase linearly with scan rate, indicating a fast, thin film electrode reaction that is not limited by ion diffusion. In part (c), the 30 layer pair shows increasing skew due to the increased film thickness and thus increased resistance to reduction and oxidation throughout the film thickness. However, linearity between scan rate and height persists. Finally, at 40 layer pairs, internal resistance overcomes the sharp oxidation peak at high scan rates, and a fast electrode reaction is no longer apparent. The combination of resistance to redox propagation through this thick film combined with an apparent limitation of ion diffusion into the film limit the speed of the electrochemical reaction, and thus the electrochemistry is less apparent in part (d) of this figure.

The electrochemistry evinced in Figure 2.21 is strikingly similar to that found for oxidative doping and reductive undoping of electropolymerized PEDOT[109] and cast PEDOT:SPS[117,118] with respect to the location of the redox peaks and the general shape of the voltammograms, even including the more resistive electrochemistry in Figure 2.21d. The electrochemistry of the LPEI/PEDOT:SPS system appears more well-defined that that of PAH/PEDOT-S system recently investigated by Cutler and Reynolds, which shows no discernable redox peaks.[55]

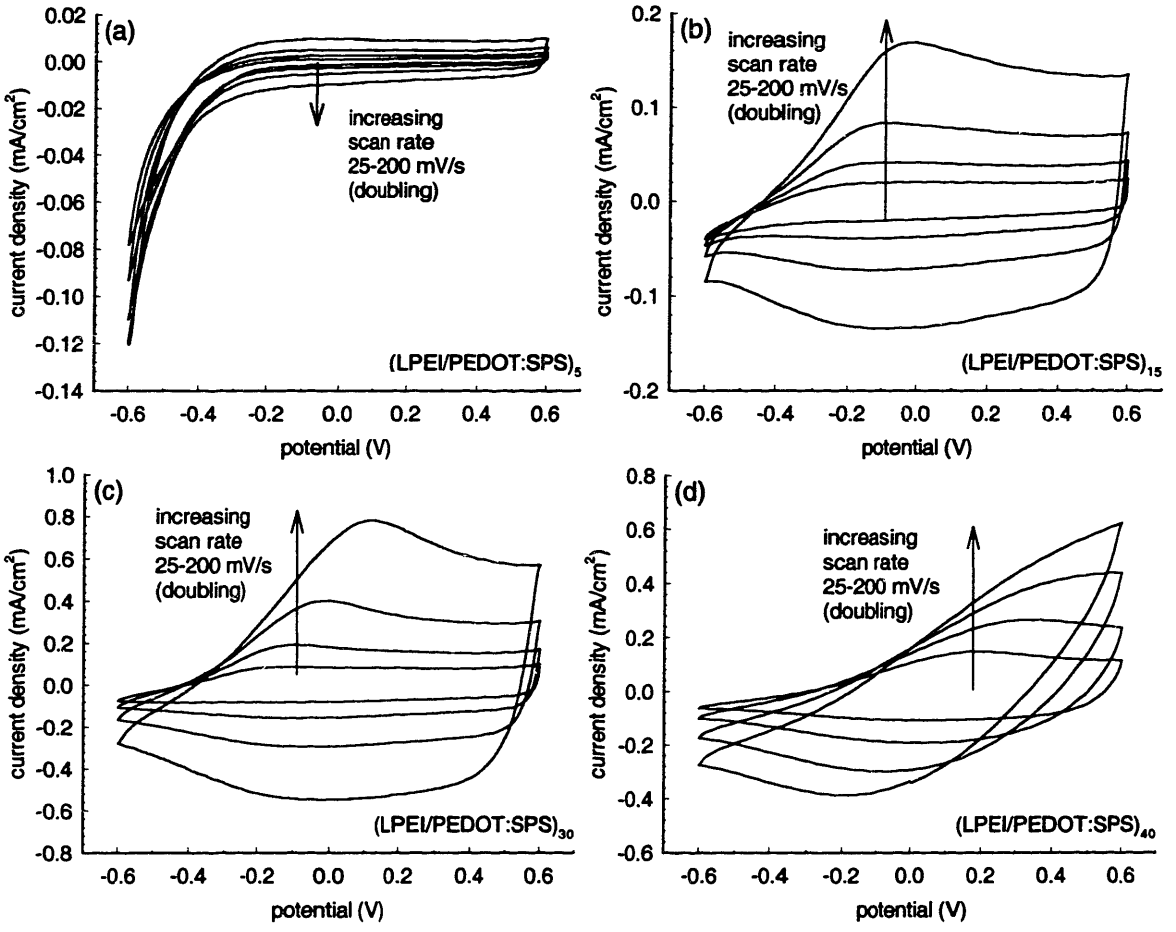

Figure 2.21 Cyclic voltammetry of the LPEI/PEDOT:SPS series.

The electrochemistry of the LPEI/PEDOT:SPS series can be compared to that of the other PEDOT:SPS composites; CVs of those composites are shown in Figure 2.22. It is clear from examination that these films also contain PEDOT:SPS and do not include additional peaks or electrochemistry. The thinner films BPEI/PEDOT:SPS and PDAC/PEDOT:SPS show similar skew and height trends to those of LPEI/PEDOT:SPS films of similar thickness. However, the thicker ePEI/PEDOT:SPS and PDAE/PEDOT:SPS composites show far more resistive electrochemistry than their LEPI/PEDOT:SPS thickness counterparts.

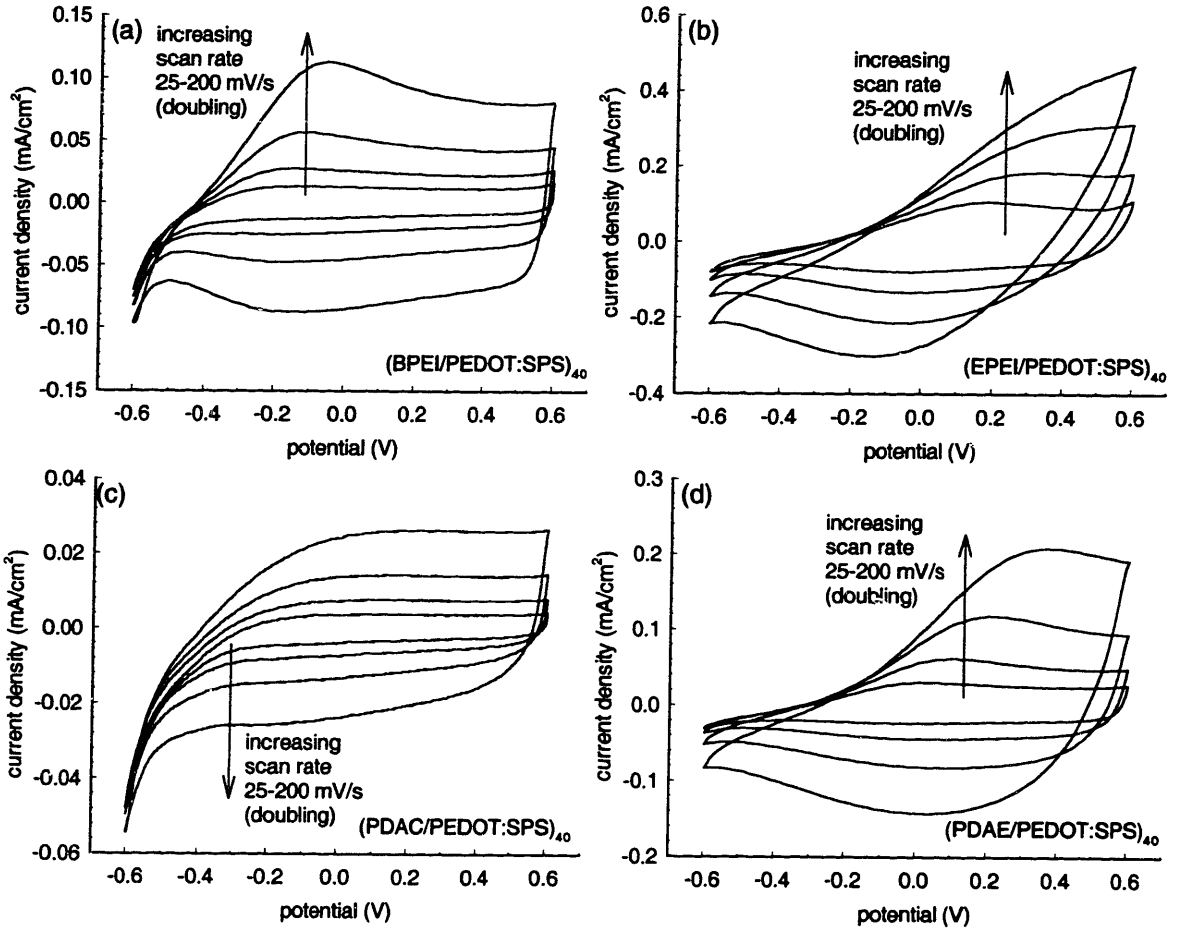

Figure 2.22. Cyclic voltammetry of other PEDOT:SPS LBL assembled films.

2.4.3.3 Electrochemistry - square wave switching

The second electrochemical test that was performed on the LPEI/PEDOT:SPS series was to apply a potential step function to the films and observe the resultant current and charge waves. The potential was switched between a 0.6 V oxidizing potential and –0.6 V reducing potential. The resultant Faradaic current and charge responses are shown in Figure 2.23. The increasing resistivity of the films with increasing layer pair number (and increasing thickness) is clear in these plots as the current decays much more slowly for the thicker films. It is also clear from the current decay plots that the oxidation of PEDOT proceeds much more rapidly than reduction. In general, the films reach their equilibrium charge density quite quickly, except for the thicker films, especially the 40-layer pair film.

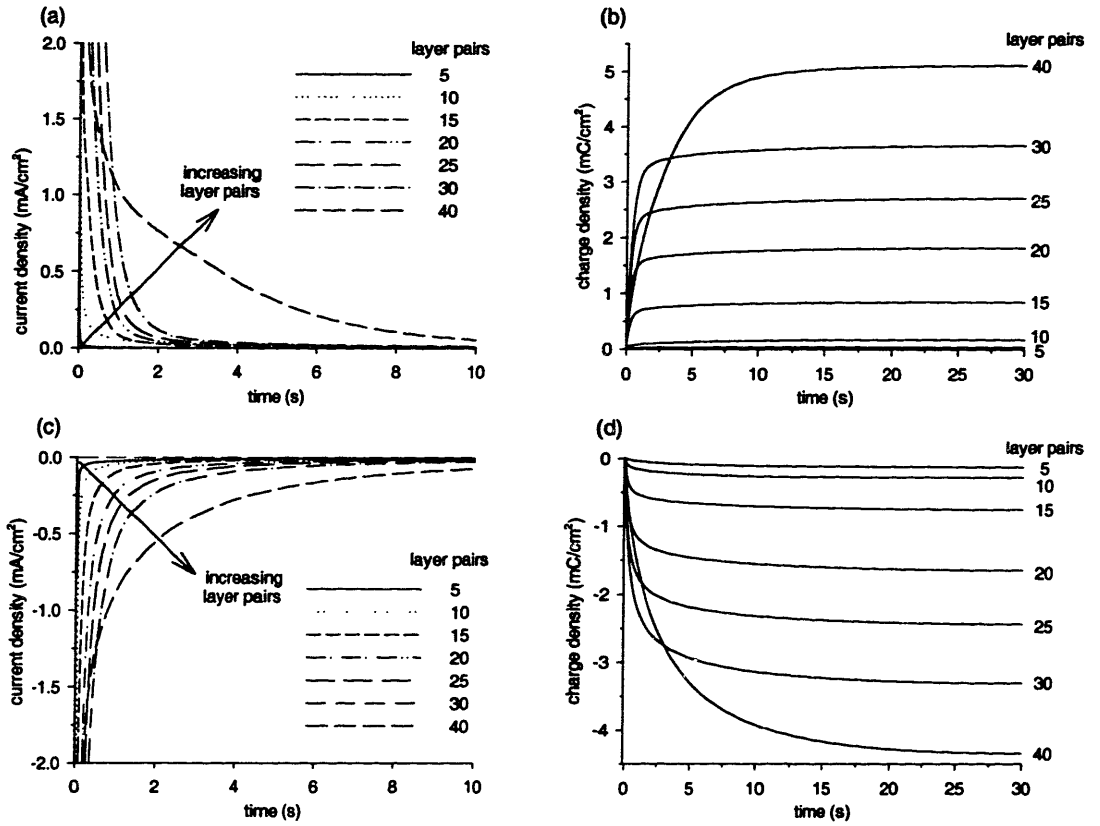

Figure 2.23. Square wave switching of the LPEI/PEDOT:SPS series.

Accounting the Faradaic charge uptake of the films during reduction and oxidation provides a method for determining the relative amount of redox-accessible species within the films. An absolute accounting like that of PXV is more difficult with PEDOT because the exact extent of a single reaction center is less clear – it is most likely confined over 4 or so PEDOT molecular repeats (whereas with PXV the reaction center is confined to a single bipyridilium moiety). If all of the redox centers within the LPEI/PEDOT:SPS film are accessible and there are no strong variations in the amount of PEDOT within the film or the ratio of LPEI to PEDOT:SPS as deposition proceeds, then the Faradaic coulomb uptake of the films should be exactly linear with the film thickness. As can be seen in Figure 2.24, this trend is accurate for films of 5-20 layer pairs. From the linear region, the effective concentration of redox centers within LPEI/PEDOT:SPS films would be 0.34 mmol/cm^3, approximately one order of magnitude less than that found in PXV and PANI LBL assembled films. Thus the conjugated polymer "loading" of PEDOT films very low, as might be expected based on the assembly mechanism; PEDOT is present only by virtue of strong binding with SPS, and the layers are presumably primarily composed of the polyion pair LPEI and SPS.

At higher layer numbers, both the oxidative and reductive Faradaic charge densities decrease from what would be expected based on the total film thickness. As this decrease in effective charge density appears in films that are within the regime of linear film growth, one would not expect strong variations in composition, so this deviation from the linear trend must be due to a lessening of the *accessibility* of the PEDOT within the LBL construct. That is, the absolute amount of PEDOT does increase linearly with film thickness, but after a certain limiting thickness, the accessibility of the additional PEDOT decreases, and PEDOT in the outermost portions of the film cannot be "reached" by the applied potential at the ITO electrode, and thus that PEDOT does not participate in redox switching. If LPEI/PEDOT films were constructed to even greater thicknesses, one would expect an eventual plateau or even a decrease in the effective Faradaic charge density due to the limitation of ion diffusion into the film by a thick barrier.

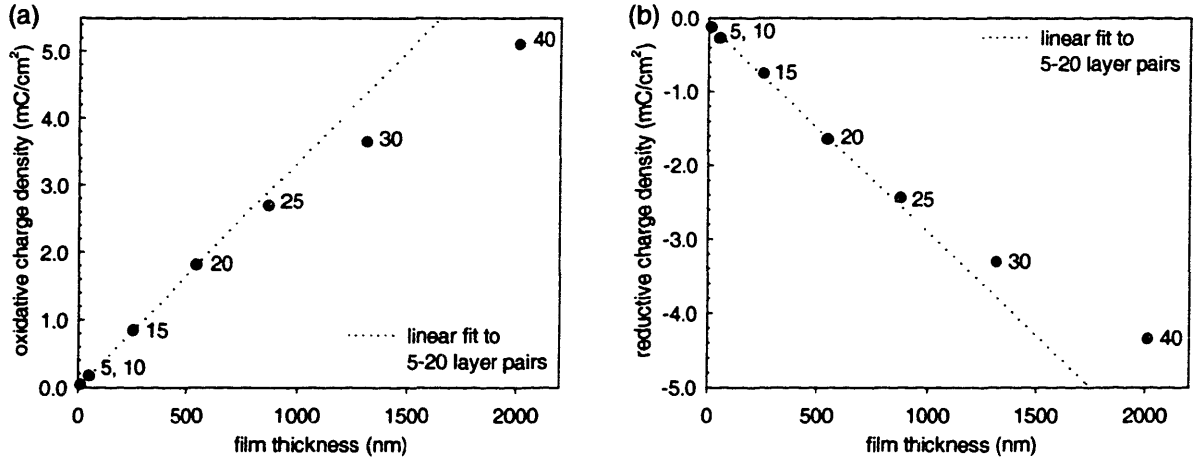

Figure 2.24. Correlation of (a) oxidative and (b) reductive Faradaic charge capacity to film thickness for the LPEI/PEDOT:SPS series.

The square wave experiments on the LPEI/PEDOT:SPS series were continued on the other PEDOT:SPS-containing films, with results shown in Figure 2.25. The thicker systems again show very resistive behavior, with slow current decays and slow approaches to equilibrium charge density. By accounting the Faradaic charge, it is possible to compare the PEDOT density of LPEI-containing LBL assembled films with the PEDOT density in LBL assembled films containing other polycations, as shown in Figure 2.26. It is clear that none of the other LBL assembled films contain a greater density of accessible redox centers than LPEI/PEDOT:SPS. There are two possible reasons for this result. The first possibility is that the LPEI/PEDOT:SPS films inherently contain more PEDOT than the other films. As LPEI has the highest chain ionization density of any of the polycations employed in this study (PDAC has the lowest), this explanation appears sufficient to explain this result. An alternative explanation could be that

films with other polycations are more resistive than LPEI/PEDOT:SPS. Thus they may contain similar PEDOT density to LPEI/PEDOT:SPS, but less PEDOT may be accessible if the polycations provide a more resistive environment. Both explanations could apply - a lower intrinsic PEDOT "loading" will lead to a more resistive environment because PEDOT chains will be less dense in the LBL assembled film, and redox transfers between chains will be less likely and will require more energy. This is quite possibly the case for PDAE/PEDOT:SPS, which has a low chain ionization density (leading to less PEDOT and more resistance to redox transfers) and a molecular structure that is most likely not conducive to fast ion migration (leading to higher resistance to ion motion). Together these effects combine to limit the amount of accessible PEDOT in PDAE/PEDOT:SPS dramatically. A lower intrinsic loading of PEDOT within the ePEI and PDAE containing LBL assembled films no doubt contributes to the more resistive electrochemistry (as seen in Figure 2.22) that is observed in these films relative to LPEI/PEDOT:SPS films of the same thickness.

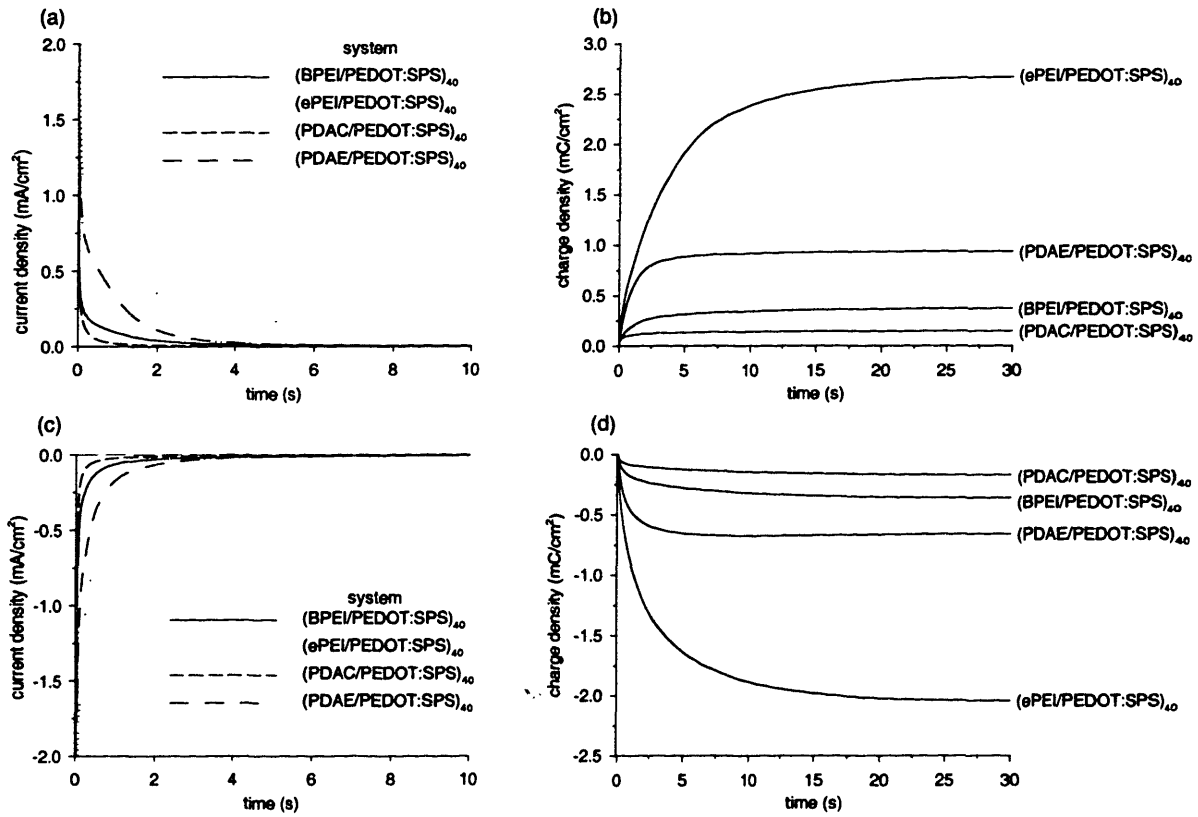

Figure 2.25. Square wave switching of other PEDOT LBL assembled films.

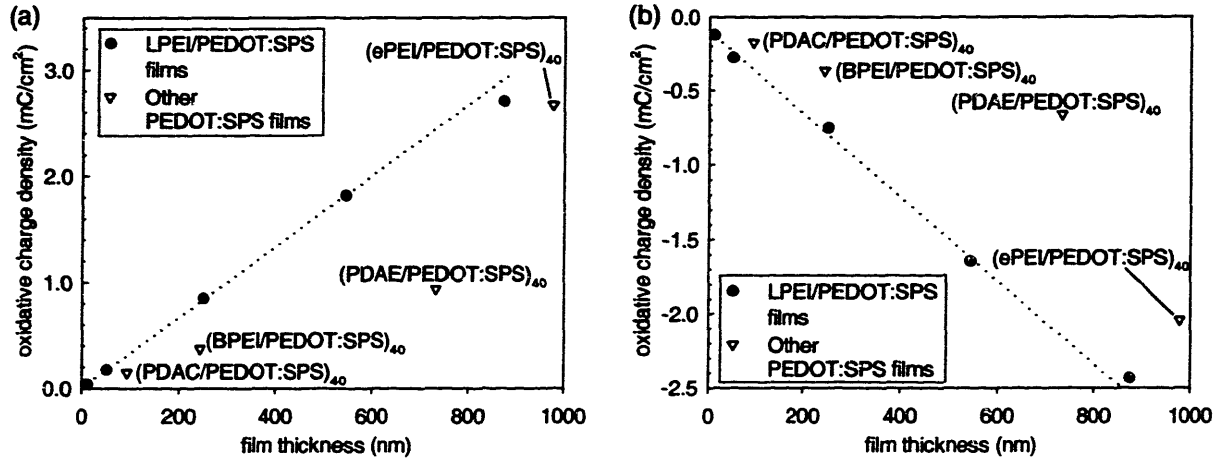

Figure 2.26. Correlation of (a) oxidative and (b) reductive Faradaic charge capacity to film thickness for all PEDOT LBL assembled films.

2.4.3.4 Spectroelectrochemistry

Following electrochemistry, the LPEI/PEDOT:SPS films were then subjected to spectroelectrochemistry in order to directly observe absorbance changes in the films during reduction and oxidation. The spectroelectrochemistry of a representative LPEI/PEDOT:SPS film is shown in Figure 2.27(a); the equilibrium absorbance increases as potential is stepped from +0.6 V to –0.6 V in 0.1 V increments. The bleached state presents very little visible absorbance as the primary polaron absorbance peak would be expected at 2000 nm.[109] A sloping shoulder of this polaron absorbance does extend slightly into the visible range; because of this shoulder, the oxidized films appear a pale blue color rather completely clear. The reduced, colored state presents a strong peak at 650 nm, which is consistent with other observations, but at somewhat lower energy – the peak absorbance is typically found closer to 610 nm.[108,109] The fully colored, reduced spectrum of the entire LPEI/PEDOT:SPS series is shown in Figure 2.27(b). As would be expected, the spectra and peaks are very self-similar except with regard to magnitude.

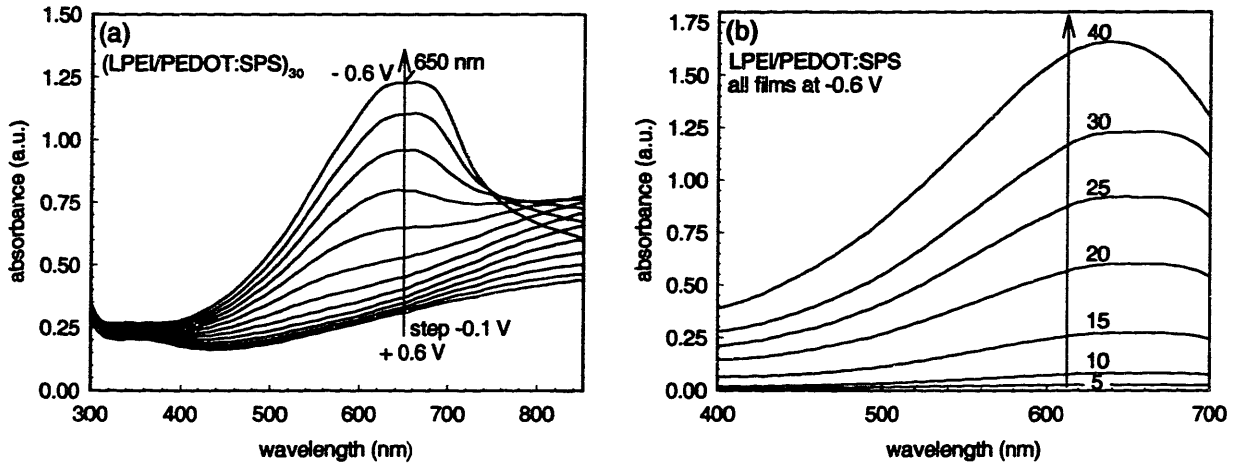

Figure 2.27. (a) Spectroelectrochemistry of (LPEI/PEDOT)$_{30}$ (b) fully colored absorbance of the LPEI/PEDOT series.

Like charge capacity, film absorbance can also be used to quantify the number of chromophores within the film. By the Beer-Lambert law, film absorbance should increase linearly with the total population of chromophores. Figure 2.28 provides the trends in bleached and colored absorbance at 650 nm with film thickness for the LPEI/PEDOT:SPS series. The bleached absorbance increases linearly with film thickness. This indicates conclusively that the solid concentration of PEDOT within these films does not vary significantly over their growth. The colored state absorbance at 650 nm follows the exact same trend as the charge density – initial linearity for 5-20 layer pairs, and then a deviation to lower-than-expected coloration. This spectral evidence is further confirmation that the PEDOT within these thicker LBL assembled films is present but not electrochemically accessible, and therefore not colored during film switching.

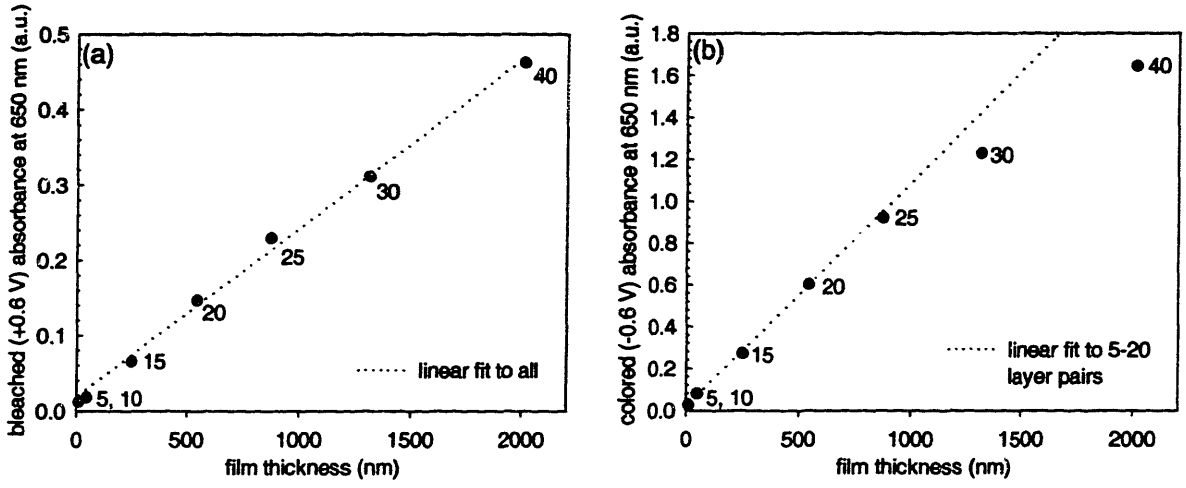

Figure 2.28. Correlation of (a) fully bleached and (b) fully colored peak absorbance to film thickness for the LPEI/PEDOT:SPS series.

The charge and absorbance-based quantification of the density of PEDOT within the LBL assembled films can be compared directly as shown in Figure 2.29. The bleached state absorbance is not directly linearly correlated with the Faradaic charge capacity due to the electrochemical unavailability of the outermost PEDOT in the film. Assembled while bleached, this PEDOT contributes to bleached state absorbance while not participating in electrochemical color switching. As would be expected, the colored absorbance of the film does increase completely linearly with increasing Faradaic charge capacity as would be expected for increasing populations of accessible redox centers. This result confirms an accounting balance; the entire Faradaic current contributes directly to coloration in thick or thin films. The results from Figure 2.29(b) can be used to determine an effective extinction coefficient of 31,900 $M^{-1}cm^{-1}$ based on the solid concentration of chromophores determined from potential step work. This extinction coefficient must be considered to apply to concentration of a nominal "chromophores" that in reality consist of the several EDOT units over which a charge carrier site would be distributed at oxidative potentials. This extinction coefficient is 3-4 times greater than that determined for PXV. Thus although PEDOT-containing LBL assembled films contain very little PEDOT, this lack of material is somewhat compensated for by high extinction of the colored state. This comparison of extinction coefficients is analogous to the comparison of "coloration efficiencies" that is often found in electrochromic film studies,[116,119] though coloration efficiency is more of an extrinsic, thickness-dependent performance metric and provides less intrinsic physical property information.

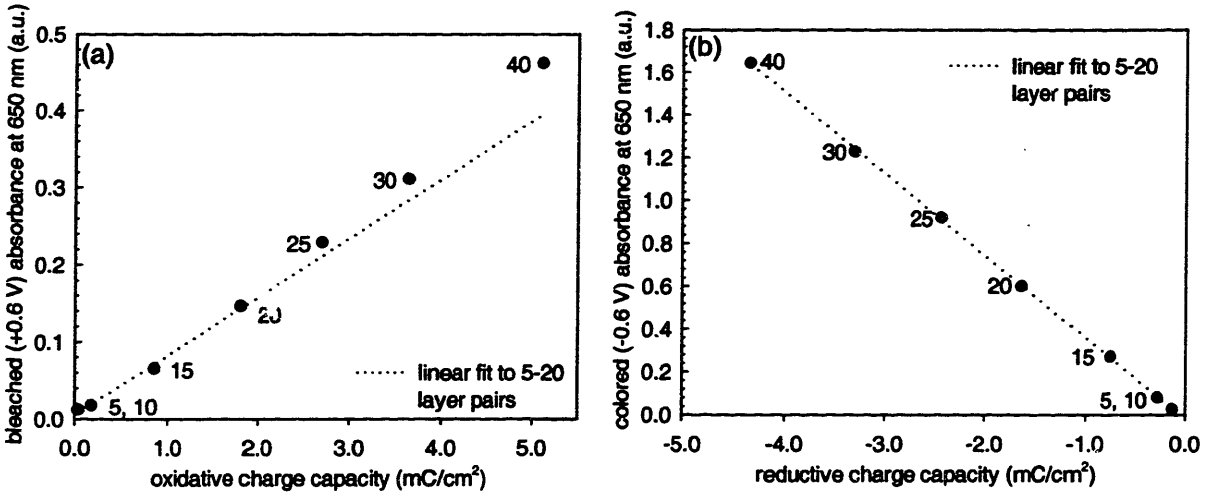

Figure 2.29. Correlation of peak absorbance to Faradaic charge capacity in the LPEI/PEDOT:SPS series.

Spectroelectrochemistry was also collected for the other PEDOT:SPS-containing LBL assembled films. The results of these experiments are shown in Figure 2.30. In general, the curves are very similar to that of LPEI/PEDOT:SPS and show few deviations in terms of peak location or curve shift with potential.

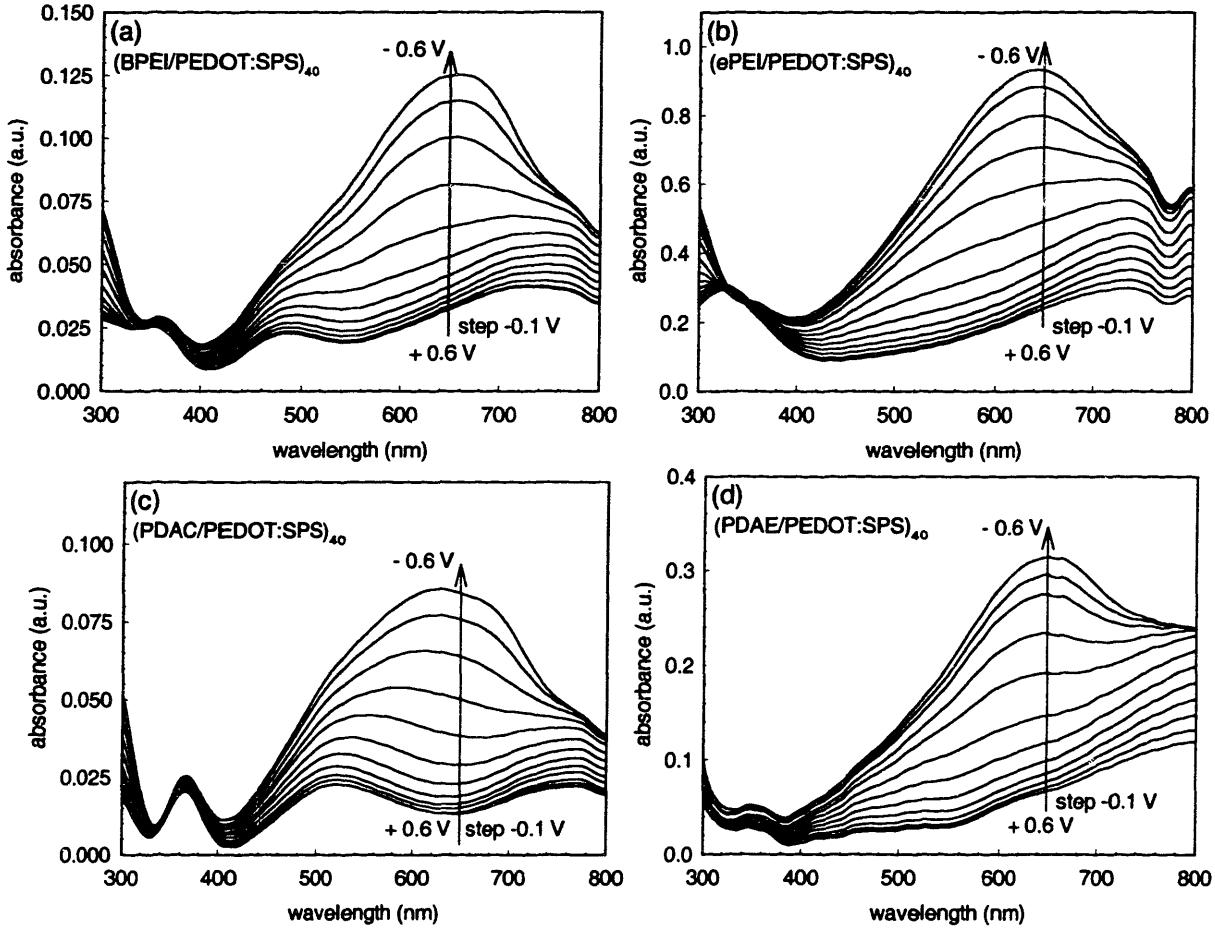

Figure 2.30. Spectroelectrochemistry of other PEDOT LBL assembled films

Of nigh interest in this study is the possibility of absorbance suppression of PEDOT within a LBL structure by the incorporation of hydroxylated polycations mimicking the effects glycerol. The electrochemical and spectral evidence collected thus far allow the full determination of whether this effect is apparent. If there is increased bleaching of the film, then the film should show disproportionately low absorbance for the same Faradaic charge uptake. That is, the extinction coefficient of absorbance should be lowered so that the absolute absorbance is less than would be expected based on the electrochemical response, which should be independent of this effect. An investigation can be made using a similar format to that shown in Figure 2.29. This analysis is shown in Figure 2.31, which correlates absorbance to Faradaic charging for all PEDOT LBL assembled films.

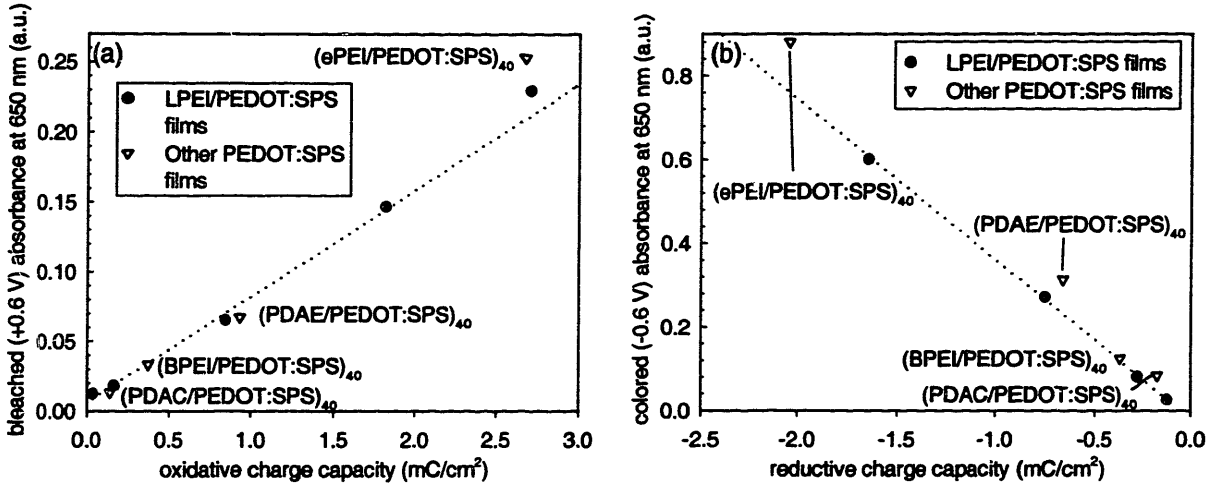

Figure 2.31. Correlation of peak absorbance to Faradaic charge capacity for all PEDOT LBL assembled films.

Based on Figure 2.31(a) it is clear that there is no strong suppression of PEDOT absorbance in the bleached state for any of the composites of this study. In fact, the ePEI composite shows a disproportionately high absorbance, though this is probably due to the electrochemical inaccessibility of outerlying PEDOT:SPS as was seen for thicker LPEI/PEDOT:SPS films. Interestingly, it can be seen in Figure 2.31(b) that the colored absorbance of most of the composites in this study was higher than LPEI/PEDOT for the same charge capacity. This would seem to indicate that the LPEI/PEDOT:SPS film has a loss of absorbance in the *colored* state that may be attributable to an effect analogous to that of glycerol. Although intriguing, this effect has a negative impact upon electrochromic film performance and is of little use in creating functional electronically conductive or color-switching films.

2.4.3.5 Optical switching

The final battery of tests applied to the LBL assembled films was the determination of electrochromic performance and potential utility in electrochromic devices. This testing was performed by monitoring the film peak absorbance at 650 nm during square wave switching of the film potential from +0.6 V to –0.6 V. The switching of the LPEI/PEDOT:SPS series is displayed in Figure 2.32. In general, the films reach close to the equilibrium peak absorbances displayed in Figure 2.27(b) within the 30-second reducing potential application. Differences in the speed of switching can be seen in the figure as well. With the selection of an achieved 90% change in the total absorbance span as the criterion for complete switching, the exact switching time for each film can be calculated as shown in Table 2-11.

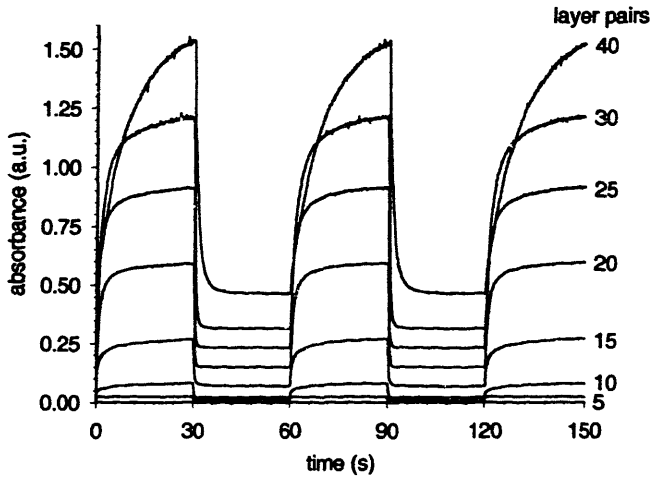

Figure 2.32. Optical switching of the LPEI/PEDOT series

Table 2-11. Switching time and contrast of the LPEI/PEDOT series.

layer pairs	color time (s)	bleach time (s)	Δ%T
5	0.4	< 0.1	3.0%
10	11.8	0.7	12.3%
15	10.9	1.0	32.6%
20	6.6	0.9	46.0%
25	6.8	0.7	47.0%
30	10.9	1.2	42.9%
40	20.8	3.5	31.9%

From the above table, it is clear that there is not a monotonic variation in switching time with layer pair number. However, the resulting bimodal variation is smooth and not attributable to a single outlier (the 5-layer pair number may be disregarded as it represents a film that is little more than a colloidal monolayer). The switching time at first decreases until about 20 layer pairs, and then increases again up to 40 layer pairs. This bimodal trend suggests competition between two factors. One obvious factor is the film thickness. As film thickness increases, the switching time should be slower, even if the film resistance remains constant. The second factor should be the intrinsic film resistance, which could vary over the growth cycle. As the PEDOT solid concentration has been shown not to vary over the growth cycle, then the only contribution to film resistance that could vary is the ionic resistance. Ionic resistance is highly coupled to film morphology, and as seen earlier in this section, there is an indication that the film growth mechanism changes at 20-25 layer pairs (where the switching time trend reverses), so it logical then to suggest that the second variable influencing switching time is more properly the film internal morphology.

If the effect of increasing thickness is to *decrease* switching time with increasing layer pairs, then the effect of morphology must be to *increase* switching time with increasing layer

pairs. Given the thickness of the layer pairs in each regime, we would expect the thinner layers at less than 15 layer pairs to be flatter and more tightly crosslinked while the thicker layers at greater layer pairs numbers should be loopier and less tightly crosslinked. From this consideration it appears that the flat, tightly crosslinked, thinner LPEI/PEDOT:SPS layers present a high resistance to ion motion, while the loopier, less tightly crosslinked layers present a lower resistance. Competition between morphology and thickness bring about the bimodal variation in switching time – at first switching is slow due to the highly resistive, tightly crosslinked film, then switching becomes faster as the morphology changes, and finally switching becomes slower again as increasing thickness inhibits the speed of electrochemistry within the film.

It is worth noting that with our current understanding of LBL processes, the thicker LPEI/PEDOT:SPS films should still contain the thin, highly resistive layer pairs interposed between the less resistive layers and the ITO substrate. However, switching in thicker composites is still accelerated. This result suggests that the entire film may undergo some type of rearrangement during assembly so that thin layers are partially or completely changed to the morphology of the thicker layers. This type of rearrangement, accompanied by polyion diffusion into and throughout the growing film, has been found accountable for superlinear growth processes in other systems[120-122] and very likely is occurring in this one as well.

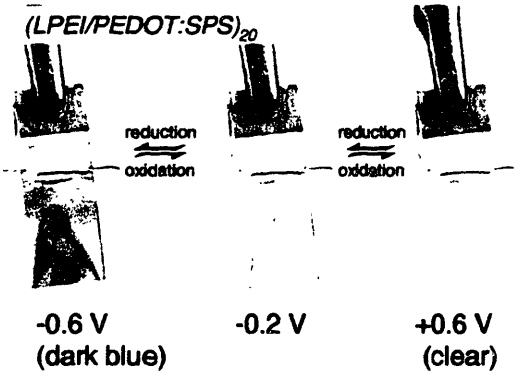

Figure 2.33. Photograph of (LPEI/PEDOT:SPS)$_{15}$ electrochromism.

A final step in the examination of the PEDOT-containing LBL assembled films was a comparison of the switching of the other composites with that of LPEI/PEDOT. The switching profiles of the other films are shown in Figure 2.34, and the switching times are shown in Table 2-12. It appears that the BPEI/PEDOT:SPS and PDAC/PEDOT:SPS films switch significantly faster than LPEI/PEDOT:SPS films of the same thickness and contrast. ePEI/PEDOT:SPS and PDAE/PEDOT:SPS films switch slower than LPEI/PEDOT:SPS films of the same thickness. The exact factors that influence these switching variations are unclear, but given the thickness-

dependent morphology and switching time of the LPEI/PEDOT:SPS system, the variation is likely linked to the architecture of the underlying films. Full series of each system would be required to completely elucidate all influences.

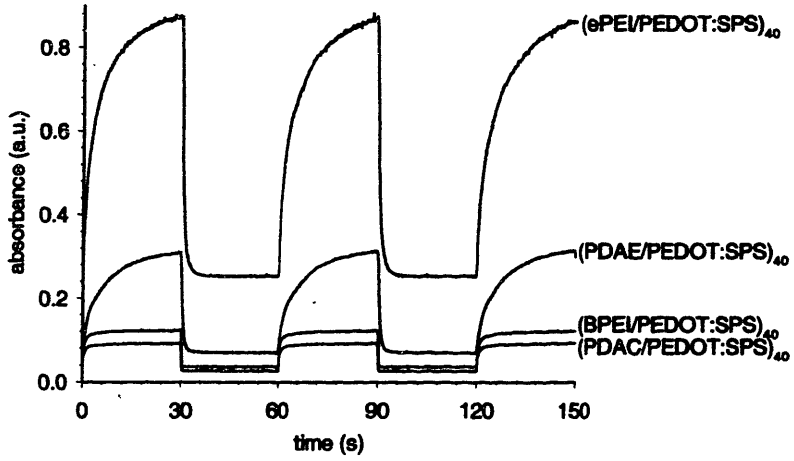

Figure 2.34. Optical switching of other PEDOT LBL assembled films.

Table 2-12. Switching time and contrast of other PEDOT LBL assembled films.

layer pairs	color time (s)	bleach time (s)	Δ%T
BPEI	5.4	0.5	17.3%
ePEI	16.9	1.6	43.1%
PDAC	4.0	0.3	13.8%
PDAE	16.7	1.5	37.1%

In terms of contrast and electrochromic performance, it is clear that PEDOT-containing films can provide reasonable contrast with somewhat reasonable switching times. Contrast is limited by the inherently low PEDOT "loading" within the film. Very thick films are required to achieve significant coloration, and these thick films also feature substantial color in the bleached state, lowering the effective contrast. Because of these competing effects, the maximum contrast for PEDOT-containing LBL assembled films appears to be a transmittance change of approximately 50% at 650 nm. This performance is on par with but does not exceed that of PEDOT films fabricated by other methods.

2.4.3.6 A note on electronic conductivity

Because PEDOT is an electronically conducting polymer in its oxidized state, conductivity tests were performed on thicker LPEI/PEDOT:SPS films deposited onto glass substrates. These tests were made using gold-coated, spring-loaded four point probes in a row arrangement with 1 mm spacing between probes. The conductivity was found to be quite low, causing a great deal of noise in the voltage measurement. However, a mean conductivity of about $2 \cdot 10^{-5}$ S/cm was

discovered with error of perhaps ±50%. There was found to be no influence of polycation identity within the LBL pairs that could be distinguished from the noise of the measurement. Conjugated polymer electroniuc conductivity is typically considered by orders of magnitude ("high" electronic conductivity is described as anywhere from 0.01 to 500 S/cm, depending on the investigator), so this result is by no means inconclusive – even with high error the conductivity is unmistakably lower than 1-10 S/cm found for PEDOT:SPS[111,112] or the maximum 400 S/cm that has been claimed for neat PEDOT films. Importantly, conductivities of this magnitude are fully expected for films that contain a small concentration of the PEDOT polymer. In fact, conductivities of exactly this magnitude have been measured for PEDOT loadings of less than 10% in solution cast films of PEDOT:SPS and poly(vinyl pyrrolidone) blends.[123,124]

2.4.4 Conclusions from PEDOT studies

Electrochromic PEDOT-containing LBL assembled films provide a contrast from PANI LBL assembled films because film morphology appears to strongly influence electrochemical properties. This morphology variation is notable at the outset from assembly; unlike most polycation/polyanion LBL assemblies, the LPEI/PEDOT:SPS system has an exponential growth regime that extends out to approximately 20 layer pairs, at which point film growth becomes more linear. Initial electrochemistry indicates that a substantial amount of PEDOT in the thicker films is electrochemically inaccessible, though UV-Vis spectroscopy confirms that it is present. The "cutoff" for electrochemical inaccessibility in the LPEI/PEDOT:SPS system appears to be approximately 1 μm, that is, films thicker than 1 μm contain inaccessible material. This result is by no means generalizable to other systems, as the ePEI/PEDOT:SPS system shows definite inaccessible PEDOT even though its thickness is less than 1 μm. Thus each system may have somewhat unique morphology that contributes both to the general speed of electrochemical reactions and to the accessibility of material within the layers. Furthermore, this film morphology seems to vary depending on the layer number. For the LPEI/PEDOT:SPS system, early layers that are presumably very thin and tightly crosslinked provide greater resistance to electrochemical reaction (though all of the PEDOT remains accessible), while the later layers that are presumably thicker and loopier present less resistance (though outerlying PEDOT eventually becomes inaccessible). The trend of morphology variation with thickness appears to vary for different systems, and does not appear generalizable even based on polycation type (weak or strong).

In all, the spectral features and electrochemistry of PEDOT can be attained in LBL assembled films by depositing the Bayer colloid, and the richness of electrochemical variation

provided by morphology changes only adds to the level of control that can be exercised by the LBL researcher. The contrast and switching times of the resultant films, while not outstanding, are sufficient for application consideration. PEDOT:SPS thus continues to be a strong candidate for LBL assembled electrochromic film research, and becomes a unique member of the library of LBL-capable electrochromic species because of its colloidal identity. Utilizing the LBL assembly of such colloids could lead to the inclusion of a wider variety of electrochromic conjugated polymers in LBL film structures; this work may provide a paradigm for such a powerful general strategy.

2.5 Prussian Blue LBL assembled films

2.5.1 Introduction to Prussian blue

Prussian blue (PB) is the prototype compound of one of the oldest families of inorganic pigments in existence. This family is composed of transition metal hexacyanometallates in which two similar or dissimilar metal ion centers are bridged by cyano ligands in a typically cubic crystalline lattice. Color is introduced as photoexcited electrons can freely oscillate between the low-spin and high-spin metal centers by virtue of the electron-rich cyano bridges. PB is the most well-known and well-researched of these compounds, consisting of iron(III) hexacyanoferrate(II) and possessing a brilliant blue color – the original "cyan" that has been employed for centuries as an inexpensive pigment in paints and inks.

Given the elegant simplicity of the PB crystal structure and its many possible uses aside from pigmentation, it is surprising that details regarding its electrochemical behavior and other detailed aspects such its uses in photo- or electro-catalysis[125-129] or magnetic storage[29,130-132] have been elaborated only very recently. This research vacuum exists because it is very difficult to construct PB thin films for experimentation; when synthesized chemically it is a friable crystal. There are two well-known forms of the PB crystal, the aptly named "insoluble" PB with the formula $Fe(III)_4[Fe(II)(CN)_6]_3$ and the poorly named "soluble" PB $KFe(III)Fe(II)(CN)_6$. Actually, both forms are completely insoluble in water and all common solvents. This insolubility is one of the primary difficulties in film formation, because PB cannot be controllably crystallized onto a substrate. However, "soluble" PB contains potassium inclusions that can dissociate in aqueous media, leading to a net negative charge on the crystal surface and allowing a stable dispersion to be formed if the crystals are sufficiently small. Dispersions of this type have been the basis for most cyanotype pigments historically.

Research on PB increased profoundly in the early 1980s when an electrochemical synthesis for PB films was introduced by Neff.[24,133] This electrochemical synthesis, which involves the electroreduction of a solution/slurry of mixed iron(III) ions and hexacyanoferrate(III) ions, allowed for the first time the formation of PB thin films for electrochemical and spectroscopic measurements. Employing these films, the electrochromism of PB was first demonstrated.[133] Electrodeposited PB thin films based on the same process are by far the most common PB films studied today. Thus, despite the persistence of PB pigments throughout history, electrochromism and other application aspects of these materials became well-known during the same period that aspects of conjugated polymer applications such as electronic conductors and electrochromic displays were first being developed.

The electrochromism of PB (and PB analogs) is quite simple: a valence change of one of the component metal centers in the crystal causes a concomitant change in the energy of charge transfer oscillation, and thus the color of the crystal changes. Due to its long history, colloquial names have been attached to the various redox states of PB, as listed below.

Table 2-13. Common names for "soluble" Prussian blue redox states.

state	name	acronym
$Fe(III)[Fe(III)(CN)_6]$	Prussian brown	PX
$Fe(III)[Fe(III)(CN)_6]$ / $KFe(II)[Fe(III)(CN)_6]$	Berlin green (intermediate)	BG
$KFe(II)[Fe(III)(CN)_6]$	Prussian blue	PB
$K_2Fe(II)[Fe(II)(CN)_6]$	Prussian white or Everitt's salt	PW

As can be seen from the table, compounds derived from all possible combinations of iron redox states in PB are well known. All of these states are thought to be chemically stable, though exposure to appropriately strong chemical oxidizing or reducing agents can change the redox state of the system.[134] As all of these states are electrochemically accessible, PB has recently become a popular functional material in the construction of electrochromic devices, both as the single functional species[25,27,135-140] and in combination with polymer electrochromes.[26,141,142] The highest-contrast and most commonly exploited electrochromic transition of PB is the conversion between the completely reduced PW state, which features essentially no optical absorbance, and the deeply cyan-colored PB state.

In recent years, a chemical synthesis for PB films that is based on LBL assembly has appeared from several research efforts.[63-67] This chemical synthesis, described variously as "successive ion adsorption," "directed assembly," or "multiple sequential adsorption," involves the alternating exposure of a substrate to aqueous solutions (typically) of a soluble iron salt followed by exposure to an aqueous solution of potassium ferricyanide. Upon each exposure, a greater amount of the insoluble complex is formed on the substrate by complexation. Although the assembly is nominally electrostatic in nature as the two reagents feature opposite charges, the complexation mechanism bears some hallmarks of covalently LBL assembled films – in particular, in many of the efforts noted above, the thickness of each layer begins to falter as the film increases in thickness beyond a certain limit due to an incomplete reaction yield at each step. The resultant films are zeolitic and completely inorganic.

The work in this thesis has focused on preparing PB-containing LBL assembled films as polymer / inorganic composites assembled entirely by electrostatic interactions. The primary PB form of interest for this work is the "soluble" PB nanoparticle dispersion. The stability of this dispersion in water is due to the polyvalent negative charges intrinsic on the particle surface. These particles can be LBL assembled with polycations to create polymer/inorganic

nanocomposites containing PB or PB analogs. As compared to the LBL synthesis of all-inorganic PB films, this method allows greater flexibility; film properties can be controlled by the particle formation technique and particle properties, and by the choice of component polymer and LBL deposition conditions. Thus far these are no published descriptions of this type of PB LBL assembled films, so this work represents the first effort to assemble and characterize these high-contrast and fast switching electrochromic polymer/inorganic composites.

2.5.2 Experimental details for Prussian blue studies

2.5.2.1 Materials

PB was synthesized by the addition of 35 mL of a 0.01 M aqueous solution of $FeCl_2$ (Aldrich) dropwise to a 35 mL solution containing 0.05 M potassium ferricyanide (Aldrich) and 0.05 M KCl. After complete addition, the liquid was vigorously agitated for 1 minute and then immediately subjected to filtration.

Filtration was performed using an Amicon 50 mL volume ultrafiltration apparatus with magnetic agitator. A Millipore membrane with nominal molecular weight cutoff of 3k and constructed of regenerated cellulose was used in the filtration. Filtrate side hydrostatic pressure was maintained at 50 psi for approximately 48 hours for the elution of at least 1000 mL of permeate. Permeate color was initially yellow, turning to clear after 250 mL of permeate was collected indicating the removal of excess potassium ferricyanide. Absence of any blue hue in the permeate confirmed that no significant amount of PB passed the membrane. The ultrafiltration retentate was used in LBL assembly as collected immediately after filtration, after pH adjustment to pH 4 by the addition of several drops of a saturated aqueous solution of potassium hydrogen phthalate.

Aqueous solutions containing dissolved polycation LPEI (Polysciences MW 25k) were formulated at 10 mM with respect to the polyelectrolyte equivalent weight (weight of charged repeat unit). The pH was adjusted to pH pH 4 using sodium hydroxide and hydrochloric acid solutions.

ITO-glass substrates with dimensions 0.7 cm × 5 cm (Delta Technologies, 6 Ω/square) were cleaned by ultrasonication in a series of solvents: dichloromethane, methanol, acetone, and Milli-Q water for 15 minutes each, followed by a 5-minute oxygen plasma etch (Harrick PCD 32G) to provide a clean, hydroxyl-rich surface.

2.5.2.2 Assembly

Film assembly was automated with a Carl Zeiss HMS DS-50 slide stainer. The substrates were exposed to LPEI solution for 10 minutes, followed by copious water rinsing for 4 minutes in three consecutive Milli-Q water baths, and then exposed to PB dispersion for 10 minutes and again rinsed. This cycle was repeated for the required number of layer pairs.

2.5.2.3 Measurement

Thickness measurements on ITO substrates were performed with a Tencor P10 profilometer by scoring the film and profiling the score. A tip force of 5 mg was used to avoid penetrating the polymer film.

Electrochemical analysis was performed using an EG&G 263A potentiostat/galvanostat. These measurements were performed in a flat cell of 30 mL volume and approximately 0.3 cm^2 working electrode area. The electrolyte used was aqueous 0.1 M potassium hydrogen phthalate with a pH of exactly 4. The counterelectrode was 4 cm^2 platinum foil, and reference was a K-type saturated calomel electrode. CV was performed with potential limits of –0.2 V and 0.6 volts, at scan rates of 25, 50, 100, and 200 mV/s. Double potential step chronoamperomtery was performed by stepping between –0.2 V and 0.6 V vs. SCE, with 30 seconds per step and 60 seconds per cycle, with approximately 20 cycles performed sequentially before the measurement cycle. Spectral characterization was performed with a StellarNet EPP2000 concave grating UV-Vis-NIR spectrophotometer with combined incandescent and deuterium lamp sources. For spectroelectrochemistry, potential control was provided by EG&G 263A, with the polymer-coated ITO-glass substrate positioned in a quartz cell and immersed in electrolyte, along with a platinum wire counter electrode, and SCE reference.

2.5.3 Results and discussion for PB LBL assembled films

2.5.3.1 Nanoparticle synthesis

Unlike most nanoparticles that are synthesized by controlled condensation methods, PB nanoparticles are synthesized by a step growth mechanism. The individual unit crystals are composed of two units that are individually and separately soluble in water. When these two solutions are physically mixed at room temperature, step growth takes place in three dimensions (rather than one for a polymer chain), and crystals nucleate and increase in size.

Early efforts in this work focused on maintaining stoichiometric parity between reactants in order to maintain the soluble form of PB that possesses a 1:1 ratio between Fe^{+2} and Fe^{+3} centers. These early efforts created suspensions that were often unstable or became unstable rather rapidly after mixing. Based on analogy with polymer step growth, it becomes clear that

stoichiometric parity between reactants is a condition of large, uniform crystal growth. Later efforts recognized this fact and adjusted the reactant ratio to include a large excess of a single reactant to force the crystal size to be smaller. The final ratio used was a 5:1 molar ratio of potassium ferricyanide to iron (II) chloride. The reaction scheme is shown below for clarity.

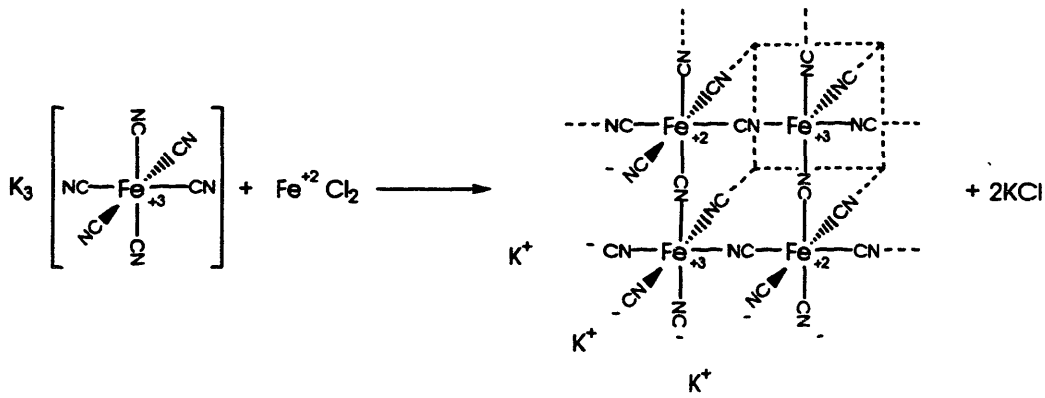

Figure 2.35. Synthesis of PB nanoparticles.

The resultant suspension was then subjected to ultrafiltration against a 3k cellulose membrane to remove the excess reagent. No color signature from the PB was noticeable in the permeate. Constant-volume filtration was completed to 10 equivalent volumes, which should result in the reduction in the concentration of permeable species by a factor of e^{-10}.

This scheme produced dark blue aqueous suspensions that did not scatter light and were stable apparently indefinitely without agitation or stabilizer addition. Even though these particles were thought to be quite small, dynamic light scattering results, as shown in Figure 2.36, indicated an average particle size of 70-75 nm. However, light scattering is well known for providing particle sizes based on loose agglomerates or aggregates; no distinction to the finer crystal size is possible.

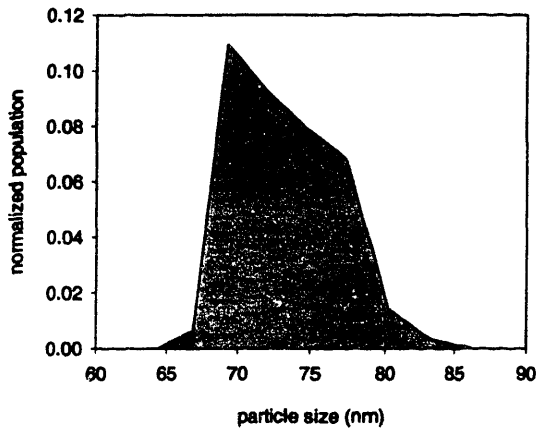

Figure 2.36. Particle size distribution of PB nanoparticles by dynamic light scattering.

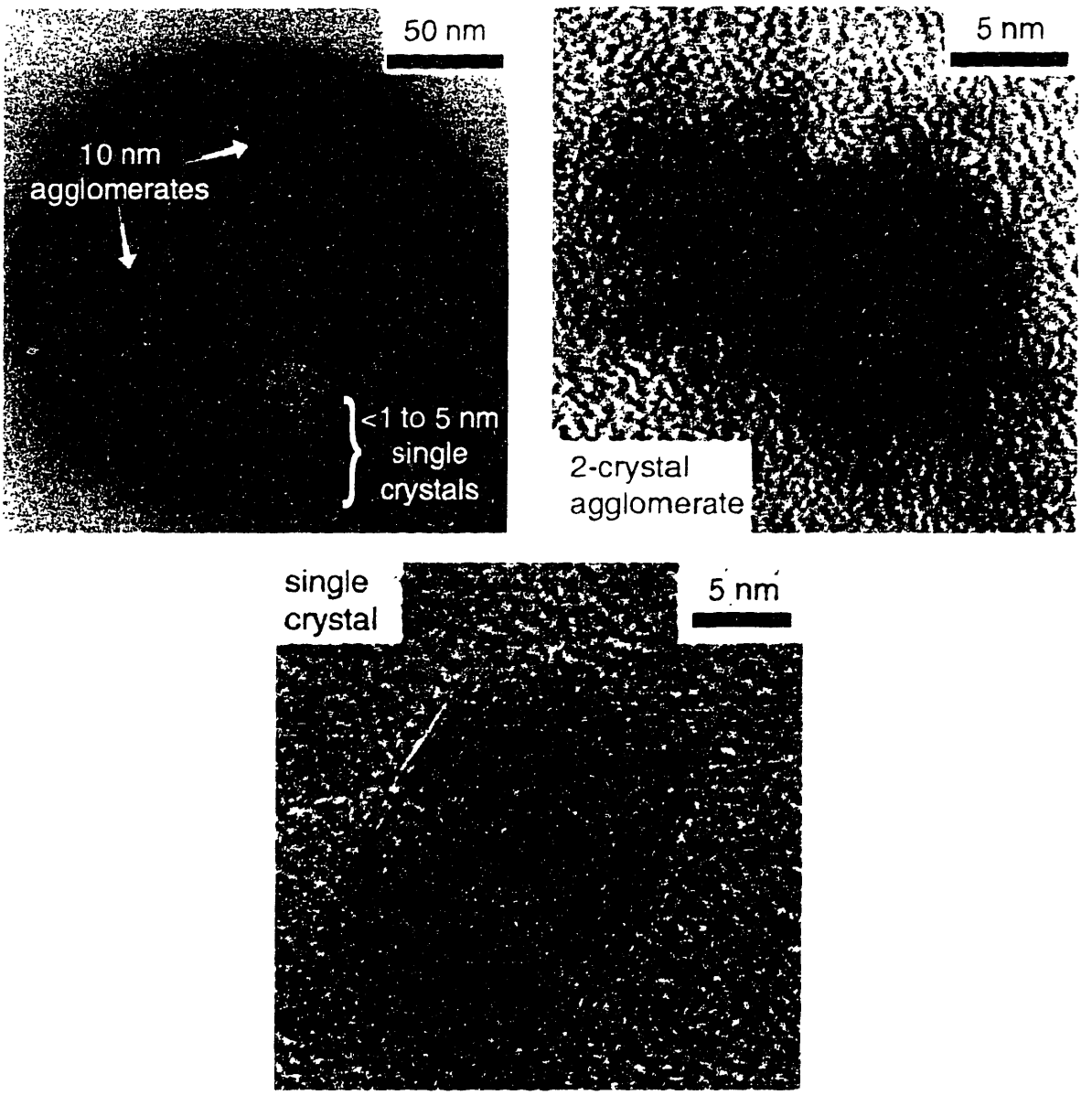

Figure 2.37. TEM images of PB nanoparticles. (Thanks to Mark Johnson for these images).

As an alternative to the poor fidelity of dynamic light scattering, a more accurate particle size could be determined by transmission electron microscopy (TEM), as shown in Figure 2.37. The lower magnification image shows a dried droplet of PB suspension – several different particle sizes are apparent, ranging from 15 nm to ~1 nm, though it is not clear whether larger particles are aggregates, agglomerates or single crystals. Some of the larger crystals of approximately 6–10 nm could be magnified, the FCC crystal lattice of PB is clearly visible in these images.

2.5.3.2 Assembly

The PB suspension described above was LBL assembled with the polycation linear polyethylene imine (LPEI) at pH 4. Growth was apparent with the formation of extremely

smooth, pale blue films after 10 layer pairs had been deposited. The full growth profile of the LPEI/PB system is shown below in Figure 2.38. Growth is reproducibly linear at approximately 4.1 nm per layer pair even up to 60 layer pairs, and roughness remains less than 4 nm.

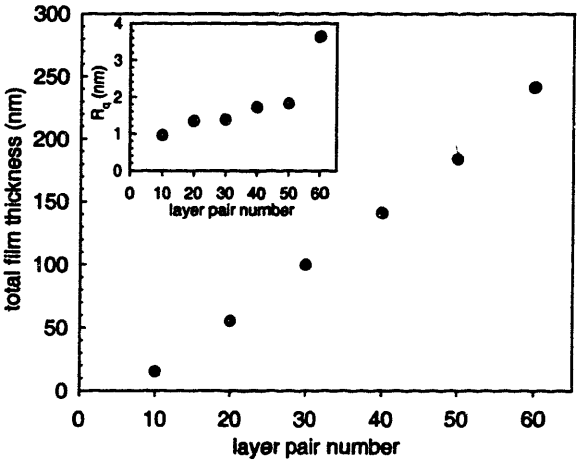

Figure 2.38. Correlation of film thickness to layer pair number for the LPEI/PB series.

One remarkable feature of the LBL assembly is that the film thickness indicates a depositing particle size of far less than the 70 –75 nm that was suggested by dynamic light scattering. In fact, given the layer pair dimensions and allowing for some LPEI within the layers, the PB particle size can be no greater than 4 nm in diameter. The smoothness of LPEI/PB films rules out the possibility that larger particles deposit to span several nominal layers. This evidence of a truly nano-sized dispersion is fully consistent with the smaller crystals observed in the TEM images. As the particles of size <4 nm are clearly single crystals from the TEM images, then from the layer thickness, the depositing PB particles must indeed be single crystals.

Quite surprisingly, the layer-pair thickness of LPEI/PB is actually far less than that observed from the electrostatic/covalent growth of an all-PB film from successive ion adsorption,[66] indicating that the LPEI/PB system allows a finer degree of control than that technique. Indeed, the successive ion adsorption technique appears to result in the formation of rough nanodomains on the film surface rather than a continuous film; the domains appear to grow in three dimensions, resulting in films that are far thicker than a single PB unit crystal monolayer.[66]

2.5.3.3 Electrochemistry – cyclic voltammetry

Once assembled, the LPEI/PB series was subjected to electrochemistry around the potential range expected for the primary transition of PB: between–0.2 and 0.6 V (just as for PANI). Some representative voltammograms are shown in Figure 2.39. All show the primary

reversible transition of PB to PW, at an $E_{1/2}$ of approximately 0.15 V, consistent with PB electrochemistry described elsewhere, although slightly more cathodic than the 0.2 V that are typically reported.[24,66,143,144] It is unclear what aspect of LPEI/PB films might shift the redox potential; one possibility is that LPEI has replaced potassium as counterion for most of the PB particle, and therefore the effective composition of the particle is far different than that of pure PB films. The use of non-potassium counterions has been shown by others to strongly affect the redox potential for PB films. Importantly, the replacement of monovalent electrolytes such as KCl with electrolytes containing divalent metal ions such as $CaCl_2$ often results in a shifting of the formal redox potential for PB and PB analogues to more cathodic potentials.[64] The mechanism of the reduction potential shift may be attributed to a greater Coulombic interaction between the negative crystal surface and the polyvalent cation that adds stability to the oxidized state so that a greater free energy is required to reduce the crystal. As LPEI might be considered a polyvalent countercation to PB crystal surfaces within the LPEI/PB LBL assembled film, it seems reasonable that there could be some shifting of the potential in this manner.

The sharp nature of the redox peak is typical of small molecule or inorganic redox-active species and contrasts with the more distributed peaks seen in CVs of PANI and PEDOT. The nature of the PB peaks seen here is broader than that observed for completely inorganic PB films.[24,143] This general effect in electrochemically active films has been attributed by Peerce and Bard to nonequivalent electrochemical sites in the film.[145] It follows that LPEI/PB films may have a greater distribution of site character than pure PB films, which is not surprising considering that surface sites on PB nanocrystals will be coordinated with LPEI cations, while interior sites may remain coordinated with potassium cations (or no cations if the sites are "insoluble" PB). Just as for other single-electrochrome LBL assembled films, the increasing skew in the LPEI/PB CVs is indicative of increasing resistance in the film due to increasing thickness. This effect has also been observed in pure PB films.[24,143] In general, peak height appears to increase linearly with scan rate, indicating that the films are ion-permeable and the electrochemistry is not diffusion-controlled, though there is some deviation from this trend for thicker films.

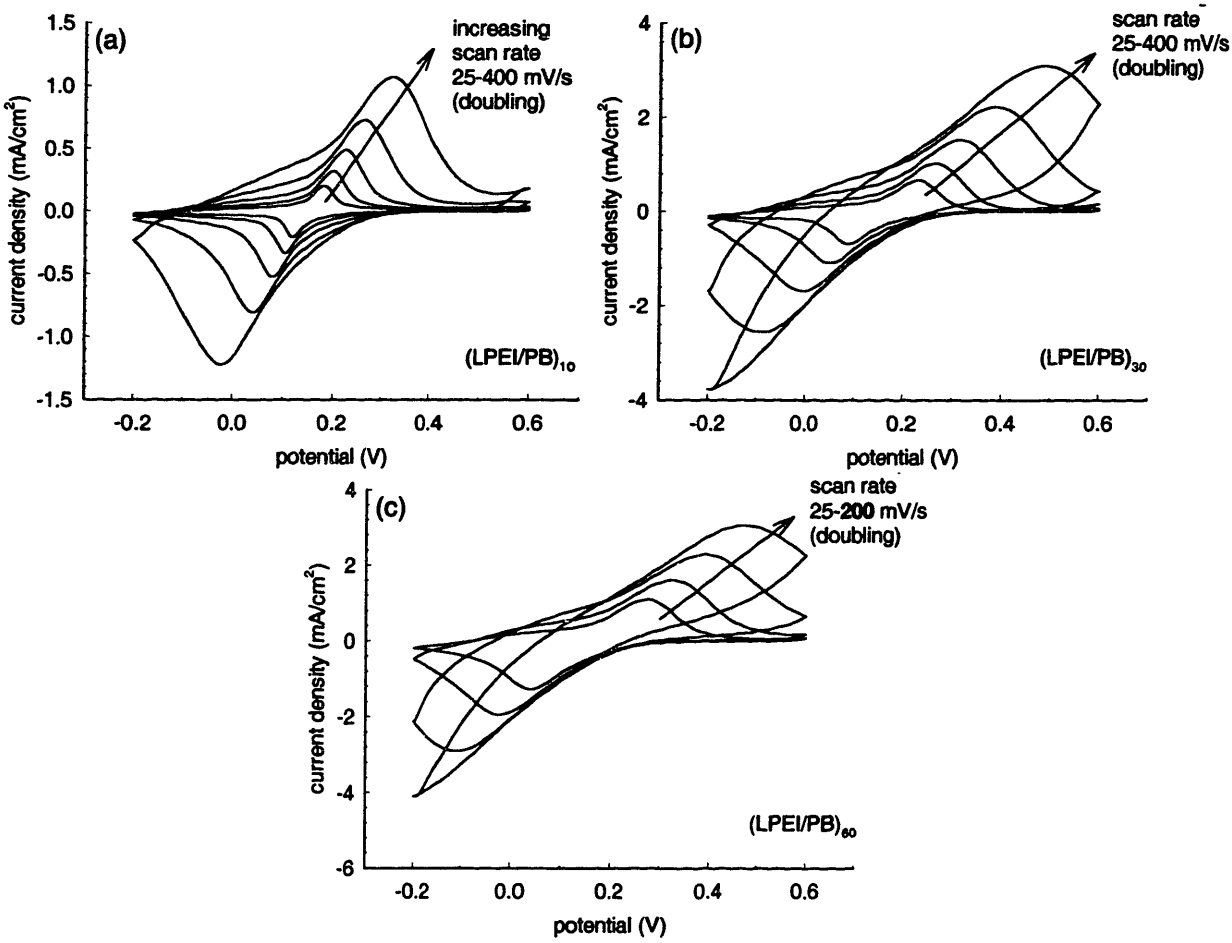

Figure 2.39. Cyclic voltammetry of the LPEI/PB series.

2.5.3.4 Electrochemistry – square wave switching

The second test applied to the LPEI/PB series was the application of a square wave switch between the oxidizing and reducing potentials. The results of this square wave test are shown in Figure 2.40. Slower switching times for greater layer pair numbers can be observed from the slower decay of current profiles. There exists a linear increase in charge density of the film as it increases linearly in thickness. Unlike the LPEI/PEDOT:SPS system, the entire LPEI/PB film appears to be accessible even up to 60 layer pairs. This difference is most likely due to the thinner assembly behavior of LPEI/PB; these films are not nearly as thick as the 1-2 μm films from LPEI/PEDOT:SPS.

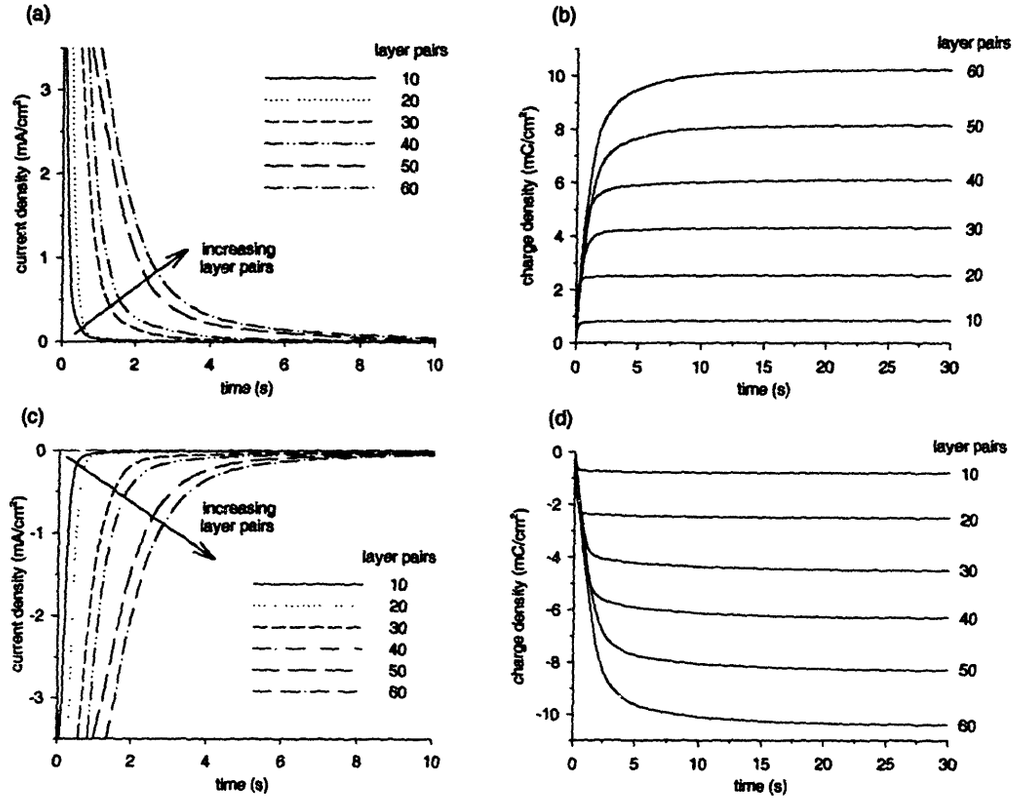

Figure 2.40. Square wave switching of the LPEI/PB series.

Based on the linear trend in Faradaic charge uptake of these LBL assembled films, it is possible to estimate a solid concentration of redox centers within the LBL structure. For the LPEI/PB system, this concentration is consistently 4.6 mmol/cm^3. This concentration is far higher than that found in the polymer LBL assembled electrochromic films studied so far in this thesis because the solid density of PB is heavier than that of most polymers. This density is expected to be approximately 1.75-1.80 g/cm^3, based on crystallography of "insoluble" PB,[146] while the PB unit crystal mass of 268 g/mol is similar to the repeat molecular weight of polymers such as PXV. Based on the solid concentration of redox centers, and using the density quoted above, it is possible to estimate a compositional profile for the LPEI/PB system because each unit crystal within a PB particle would be expected to contribute one electron to the Faradaic charge capacity. A concentration of 4.6 mmol/cm^3 PB within the film corresponds to 1.2 g/cm^3 PB, or a volume fraction of 0.68. Assuming that the density of LPEI remains 1.2 g/cm^3, then the concentration of LPEI molar repeats in the film would be 6.1 mmol/cm^3. This calculation leads to a LPEI:PB unit pairing ratio of 1.48, or approximately 3 LPEI repeats per every 2 PB unit crystals. This ratio is very reasonable considering that LPEI is only partially charged at the assembly pH of 4.

It should be noted that the PB might be composed of mixed "insoluble" and "soluble" forms. This consideration changes the composition profile only slightly; even if all of the PB crystals were of the insoluble type, the LPEI:PB ratio would be 1.41 rather than 1.48. This compositional range, which is based on only two very reasonable density assumptions and therefore presumably quite accurate, must not necessarily be taken to indicate an absolute ratio of ion pairing. As some part of the PB may be in the "insoluble" form and therefore nonionic, a LPEI:PB unit ratio of 1.4-1.5 does not necessarily indicate that LPEI is 67-70% ionized at pH 4.

2.5.3.5 Spectroelectrochemistry

Following the electrochemistry, the LPEI/PB series was then subjected to spectroelectrochemistry. The shift of coloration in the PB-containing LBL assembled film is much more abrupt than that of the more distributed conjugated polymers. Beginning at –0.2 V, the PW composite shows almost no absorbance in the visible range. As the potential becomes increasingly positive, absorbance increases, with the largest jump in absorbance coming between 0.1 V and 0.2 V, which span the formal redox potential determined from CV. Fully oxidized, colored PB is attained at 0.3 V, and has a well-defined absorbance peak at almost exactly 700 nm, as has been previously observed in inorganic PB films.[24,143] Like the charge capacity, the peak absorbance of PB increases perfectly linearly with increasing layer pair number, indicating that the extinction coefficient remains constant during growth and again, that all material is redox-active in the film.

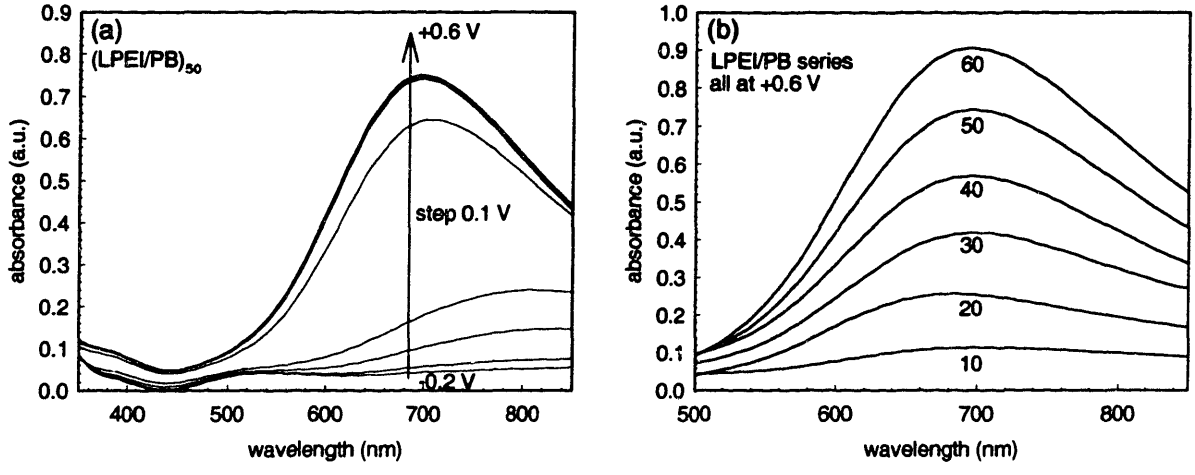

Figure 2.41. Spectroelectrochemistry of the LPEI/PB series.

Given the excellent linearity in thickness, Faradaic charging, and absorbance for the LPEI/PB system, it is a simple task to calculate the molar extinction coefficient for a PB unit cell. For this system, extinction at 700 nm would be 8700 $M^{-1}cm^{-1}$, very similar to that discovered in

PXV LBL assembled films near 550 nm. However, because of the greater density of PB chromophores, thinner films of PB absorb more light in their colored states than most electrochromic films composed exclusively of polymers.

2.5.3.6 Opticai switching

Optical switching was applied to the LPEI/PB series as well. The switching, which can be seen below, trends as would be expected. Thinner films switch extremely fast, with profiles resembling square waves, while thicker films have more rounded switching profiles indicative of slower switching. The peak absorbances shown in Figure 2.42 emphasize the linearity of the LPEI/PB system and the potential for achieving a desired film thickness, charge capacity, and absorbance by simply varying the layer pair number.

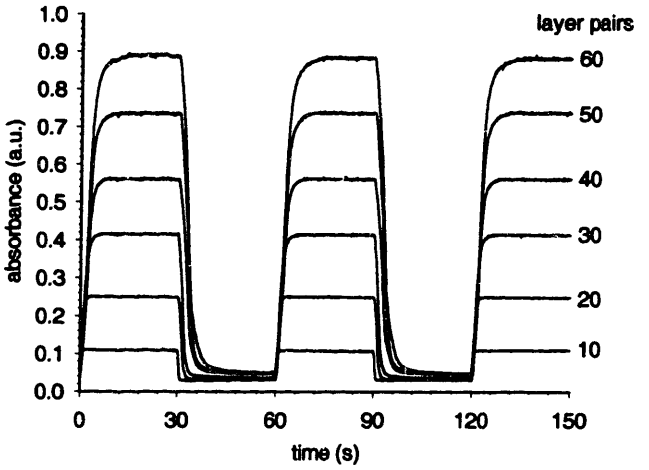

Figure 2.42. Optical switching of the LPEI/PB series.

The switching time of the LPEI/PB system in Table 2-14 was determined using the same criterion as was used for the evaluation of other electrochromic films in this report, namely the time required to reach a 90% change in total absorbance span of each film.

Table 2-14. Switching time and contrast of the LPEI/PB series.

layer pairs	color time (s)	bleach time (s)	Δ%T (λ = 700nm)
10	0.63	0.83	16.5%
20	1.55	2.15	37.6%
30	2.84	2.78	54.0%
40	3.98	4.98	63.3%
50	4.60	5.10	72.4%
60	5.48	5.88	77.4%

The LPEI/PB system performs very well compared to the other single electrochrome systems studied in this work, both in terms of contrast and in terms of switching time. Switching time increases linearly, as would be expected from this film, indicating no changes in morphology as

were discovered in PEDOT-containing LBL assembled films. Notably, these switching times are far faster than the 30-120 seconds described for many electrochromic devices containing PANI and PB Due to the very low coloration of the bleached state PW, contrast continues to increase with film thickness as well, so that it is as yet undiscovered what maximum contrast might be achievable. This high-contrast coloration is demonstrated in Figure 2.43, which shows the same 60-layer pair LPEI/PB film at oxidizing and reducing potentials. The change in color is both dramatic and aesthetic.

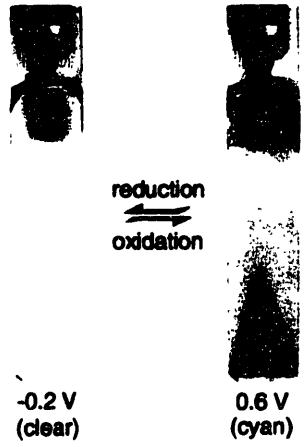

Figure 2.43. Photograph of $(LPEI/PB)_{60}$ electrochromism.

2.5.3.7 Extended potential range

The potential range of the electrochemical testing of LPEI/PB can be extended to include additional colored states. In particular, at more oxidizing potentials, the iron(III) hexacyanoferrate (III) PX form can be accessed. This "Prussian brown" is in reality a golden color, and the combination of PB and PX at intermediate potentials creates the olive green colored BG state.

An extended potential range was applied in a CV waveform to a 50-layer pair film of LPEI/PB, with the result shown below in Figure 2.44. From this CV, the oxidation of PB to PX has a potential $E_{½}$ of 0.85 V. Although the peaks for this oxidation have a lower magnitude than those for PB reduction to PW, they are broader, so that the ratio of peak areas (which corresponds to charge passed) for PB→PX to PB→PW, is almost exactly 1.0. This ratio indicates that the PB is present primarily in the "soluble" form because the "insoluble" form should show a ratio of 0.75 due to the asymmetry of Fe(III) and Fe(II) populations in the crystal (it is essentially already partially oxidized to PX).

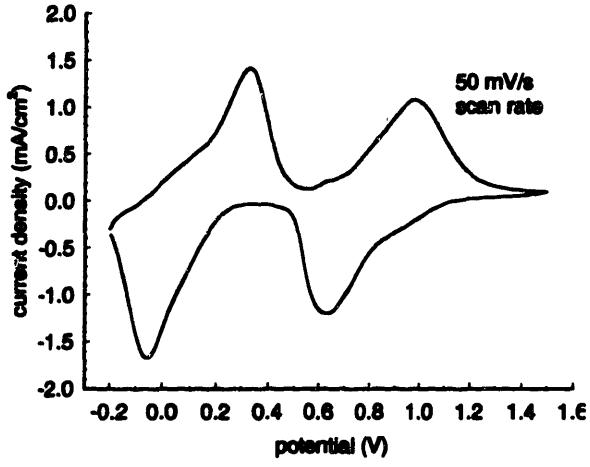

Figure 2.44. Cyclic voltammetry of $(LPEI/PB)_{30}$ over an extended potential range.

The spectroelectrochemistry for the transition from PB to PX is shown in Figure 2.45. The peak at 700 nm gradually decreases, with a concomitant increase in absorbance at 450 nm that is the origin of the golden yellow PX coloration. The color state at ~1.0 V, which features peaks at both 700 and 540 nm, is the BG state that is not a formal oxidation state but rather an intermediate or transition state between PB and PX. The PX absorbance at 450 nm has a molar extinction coefficient of 2550 $M^{-1}cm^{-1}$, far lower than that for the PB state absorbance at 700 nm. It is for this reason that the transition between the PW state and the PB state is most widely employed in electrochromic devices; the PX coloration presents far lower contrast.

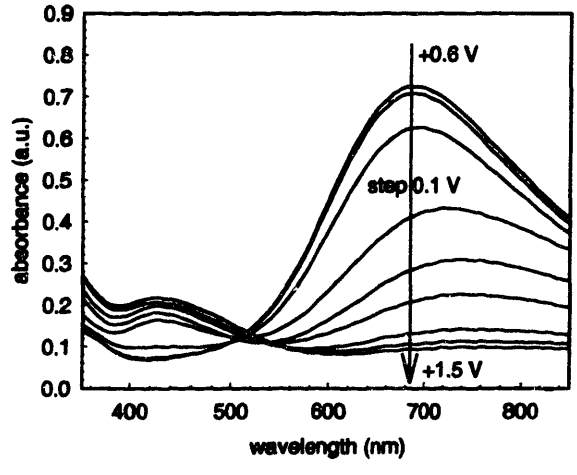

Figure 2.45. Spectroelectrochemistry for $(LPEI/PB)_{30}$ over an extended potential range.

Visualization of the color states of the LPEI/PB electrode film over the extended potential range is provided in Figure 2.46, which features color photographs of the same 50-layer pair film at equilibrium coloration at each potential listed. The photographs were taken in an

electrochemical cell, and several minutes were allowed for the films to reach equilibrium at each potential. The different colors of the LPEI/PB system are clearly discernable by the human eye.

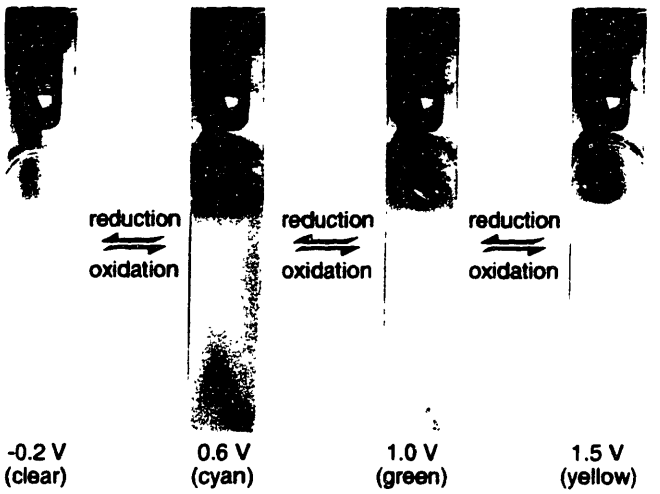

Figure 2.46. Photograph of $(LPEI/PB)_{50}$ electrochromism over an extended potential range.

Although the LPEI/PB composite shows promising, multiply colored behavior over the extended potential range, tests of optical switching between PB and PX for many cycles reveal a critical flaw. As seen in Figure 2.47, when the LPEI/PB film is repeatedly switched between +0.6 V (PB - high absorbance at 700 nm) and +1.5 V (PX – low absorbance at 700 nm), coloration of the composite as monitored by absorbance at 700 nm steadily decreases with each cycle. As this loss cannot be a result of chemical or electrochemical degradation - the PB, BG, and PX states are all chemically stable at these potentials - clearly the film is losing PB nanoparticles during this switching process.

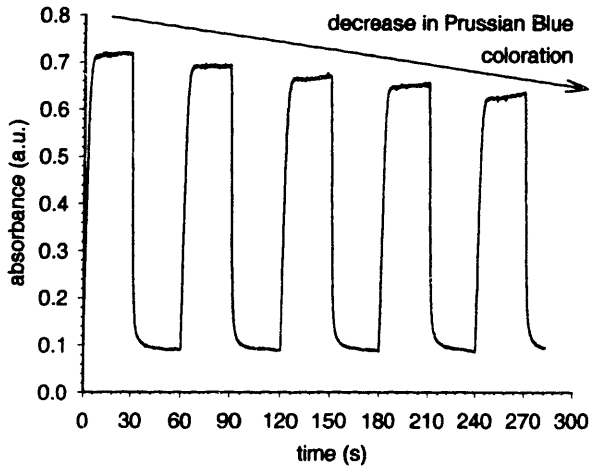

Figure 2.47. Optical switching of $(LPEI/PB)_{50}$ over an extended potential range showing decreasing response.

Modulation of the ionization of PB nanorparticles during switching explains the probable reason for particle loss. The oxidation of PB produces PX - iron (III) hexacyanoferrate (III) – a crystal that is fully charge-balanced within the ferrocyanide crystal and thus possesses no potassium substitution. Put differently, PX nanocrystals in aqueous environments have *no surface or interior ionization.* Once these particles lose ionization, there remains no strong binding force to the LPEI matrix. If the particles were not completely non-dispersable and fairly hydrophobic in the PX state, they might diffuse into the electrolyte. Instead, the PX particles remain but no longer provide negative polyvalency for attraction to LPEI, and LPEI can easily become charge-charge repulsed by adjacent LPEI chains, causing the entire film to rupture and desorb (presumably the PX particles are physically carried away from the film by desorbing LPEI). This is the most likely scenario to explain the loss of PB/PX nanocrystals from the film during repeated switching.

This situation has not occurred in any of the systems studied thus far; PXV has two charges per repeat when oxidized and one charge when reduced and thus remains crosslinked, PANI is charged in both its oxidized and reduced forms (at the proper pH) and thus remains crosslinked, and PEDOT remains within the permanently crosslinked polycation/SPS matrix. In the case of PB, however, the oxidation of a negatively polyvalent electrochrome results in total charge removal, ionic crosslinks are eliminated, and the film breaks up. This phenomenon is a type of controlled release, and could realistically be considered for pharmaceutical delivery if more inert redox-active materials could be employed.

2.5.3.8 PB analogues

Ruthenium Purple

The PB nanoparticle system is created by a simple synthesis that can easily be tailored to the development of several different types of PB analogues. These analogues can be prepared by simple substitution of other hexacyano transition metal complexes or other soluble transition metal salts in the synthesis. Perhaps one of the best studied of the PB analogues is the so-called "Ruthenium purple" (RuP), which is synthesized by substitution of potassium ferricyanide with ruthenium ferrocyanide and substitution of a soluble iron (II) salt with a soluble iron(III) salt. The synthesis for RuP is shown below for clarity.

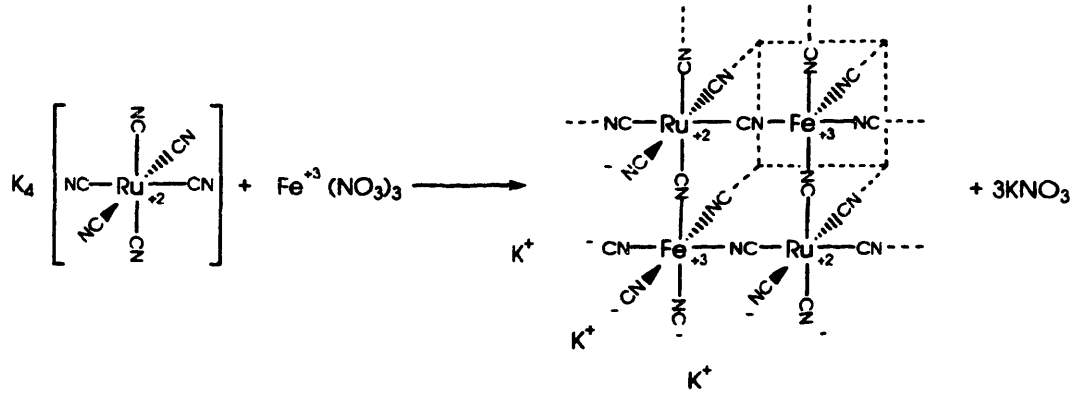

Figure 2.48. Synthesis of RuP nanoparticles.

A nanoparticulate RuP dispersion can easily be combined with LPEI in a LBL fashion, and a series of films analogous to the LPEI/PB series has been fabricated. In general, RuP assembly behavior is almost identical to that of PB, except that the RuP dispersion shows a greater tendency toward aggregation after standing several days, though this aggregation can be discouraged by diligent sonication of the aqueous dispersion.

The most notable difference between RuP and other PB analogues and PB itself is that the primary absorbance wavelength of the $metal_1$(II)$metal_2$(III)hexacyanoferrate state is greatly shifted due to the presence of transition metal ions other than iron within the charge transfer complex. The spectroelectrochemistry of a 60-layer pair film of LPEI/RuP is shown in Figure 2.49. With a peak absorbance at 550 nm, the RuP complex creates a violet/purple color similar to that of the poly(viologens) examined earlier, though the RuP absorbance peak is more well-defined and slightly more blue (indicating a redder reflected/transmitted color). When reduced, the LPEI/RuP complex returns to a completely colorless state that is analogous to PW. A photograph of the switching behavior of the 60-layer pair film of LPEI/RuP is shown in Figure 2.50.

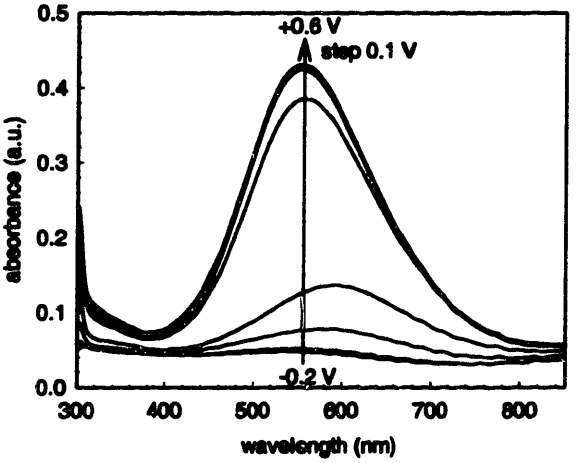

Figure 2.49. Spectroelectrochemistry of (LPEI/RuP)$_{40}$

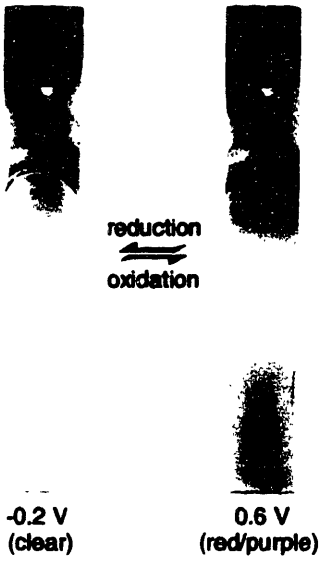

Figure 2.50. Photograph of (LPEI/RuP)$_{40}$ electrochromism.

Nickel hexacyanoferrate

In a manner similar to the synthesis of RuP, a nickel-containing hexacyanoferrate (NiHCF) can be synthesized by substitution of a soluble nickel salt in the place of iron (II). The synthesis is shown below for clarity.

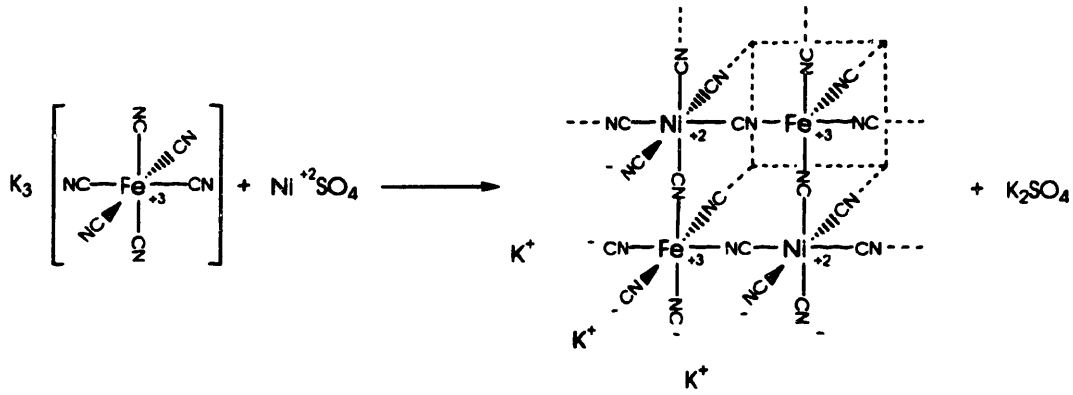

Figure 2.51. Synthesis of NiHCF nanoparticles.

The NiHCF suspension LBL assembles in a manner completely similar to that of the RuP and PB systems, though it shows an even greater tendency than either to agglomeration, necessitating careful changing of the deposition bath every 12 hours during an assembly cycle.

Spectroelectrochemistry of a 60-layer pair film of LPEI/NiHCF is shown in Figure 2.52. This complex has shifted absorbance to even higher energies so that the absorbance peak is approximately 400 nm, resulting in a vibrant yellow coloration. Like PB and RuP, the complex returns to an essentially colorless state when reduced. A photograph of this color change is shown in Figure 2.53.

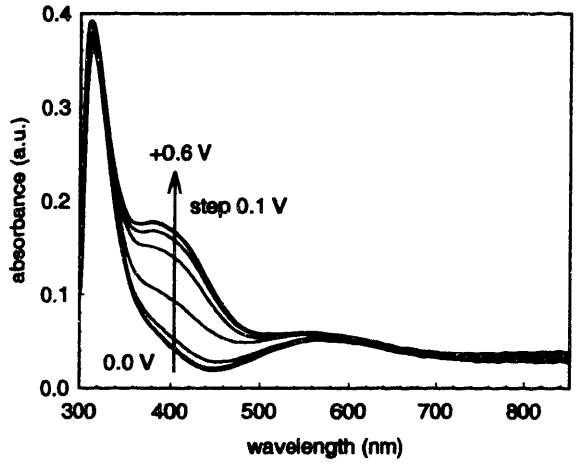

Figure 2.52. Spectroelectrochemistry of (LPEI/NiHCF)$_{60}$

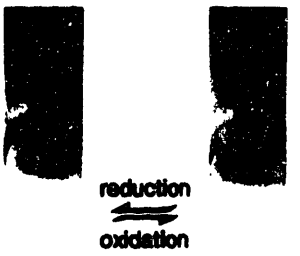

Figure 2.53. Photograph of $(LPEI/NiHCF)_{40}$ electrochromism.

2.5.4 Conclusions from Prussian blue studies

PB and its analogs can be LBL assembled from ionized nanoparticle suspensions. Films assembled with these suspensions and LPEI show extremely ideal LBL assembly behavior, with total film thickness, Faradaic reductive and oxidative charge capacity, and film absorbance all increasing linearly with the number of layer pairs for films up to 250 nm thick. By measuring Faradaic charge capacity, the composition of these films can be ascertained. The molar extinction coefficient for the PB state is similar in magnitude to that of PXV, but the greater density of PB allows for greater absorbance from thinner films. Both in terms of switching time and contrast, the LPEI/PB system displays extremely competitive electrochromic performance, switching between the saturated cyan PB state and the optically clear PW state. The contrast of this hybrid system is superior to that of most polymer electrochromes that are described in literature; the hybrid system also appears to exhibit a significant switching speed increase over conventional, fully-crystalline PB films.

If the potential range for LPEI/PB electrochemistry is extended to more anodic potentials, the BG and PX states can be accessed, providing multiple color electrochromism. Repeated switching between PB and PX results in a loss of ionization on PX nanoparticles that eventually leads to desorption and release of LPEI and PX from the LBL assembled film.

PB analogues provide an attractive route to systematic variation of colored states in these inorganic/polymer composite electrochromic films because they are easily formed by substituting different transition metal ion centers into the PB nanocrystal framework. LPEI/RuP reversibly switches between a purple/red oxidized color and a clear reduced color while LPEI/NiHCF reversibly switches between a yellow oxidized color and a clear reduced color. Together, the LPEI/PB, LPEI/RuP, and LPEI/NiHCF LBL assembled films closely satisfy the three colors

required for fabrication of a switchable reflective display, namely Cyan, Magenta, and Yellow (also known as the CMYK triad, see Figure 2.54). As each of these composites switches between a completely clear state and its corresponding color, it is conceivable that a fully switchable, full-color reflective display might be built using these three films. Even more advanced electrochromic properties might be evinced should the LPEI be replaced with a redox-active, color changing material. The wide-ranging possibilities of such dual-electrochrome LBL assembled films containing PB will be discussed in the following chapter.

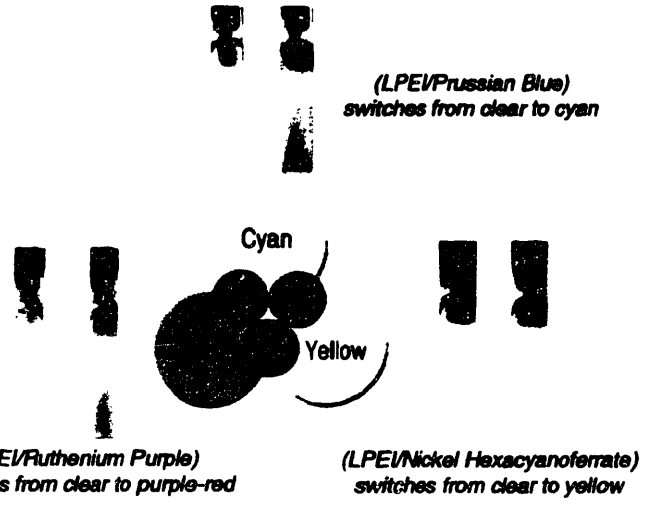

Figure 2.54. The CMYK color scale and appropriate polymer/inorganic electrochromic LBL assembled films.

2.6 Cited literature

(1) Simon, M. S.; Moore, P. T. *J. Polym. Sci. Pol. Chem.* **1975**, *13*, 1-16.
(2) Sato, H.; Tamamura, T. *J. Appl. Polym. Sci.* **1979**, *24*, 2075-2085.
(3) Bird, C. L.; Kuhn, A. T. *Chem. Soc. Rev.* **1981**, *10*, 49-82.
(4) Itaya, K.; Akahoshi, H.; Toshima, S. *Journal of Physical Chemistry* **1981**, *85*, 818-822.
(5) Laurent, D.; Schlenoff, J. B. *Langmuir* **1997**, *13*, 1552-1557.
(6) Stepp, J.; Schlenoff, J. B. *J. Electrochem. Soc.* **1997**, *144*, L155-L157.
(7) Monk, P. M. S. *The Viologens*; John Wiley & Sons Ltd.: West Sussex, England, 1998.
(8) Schlenoff, J. B.; Laurent, D.; Ly, H.; Stepp, J. *Chem. Eng. Technol.* **1998**, *21*, 757-759.
(9) Monk, P. M. S.; Delage, F.; Vieira, S. M. C. *Electrochim. Acta* **2001**, *46*, 2195-2202.
(10) Reynolds, J. R.; Sapp, S. A.; Sotzing, G. A.; Reddinger, J. L. *Polym. Mater. Sci. Eng.* **1996**, *75*, 414-415.
(11) Sapp, S. A.; Sotzing, G. A.; Reddinger, J. L.; Reynolds, J. R. *Adv. Mater.* **1996**, *8*, 808-811.
(12) Sapp, S. A.; Sotzing, G. A.; Reynolds, J. R. *Chem. Mater.* **1998**, *10*, 2101-2108.
(13) Welsh, D. M.; Kumar, A.; Meijer, E. W.; Reynolds, J. R. *Adv. Mater.* **1999**, *11*, 1379-1382.
(14) Rudge, A.; Raistrick, I.; Gottesfeld, S.; Ferraris, J. P. *Electrochim. Acta* **1994**, *39*, 273-287.
(15) Meeker, D. L.; Mudigonda, D. S. K.; Osborn, J. M.; Loveday, D. C.; Ferraris, J. P. *Macromolecules* **1998**, *31*, 2943-2946.
(16) Brotherston, I. D.; Mudigonda, D. S. K.; Osborn, J. M.; Belk, J.; Chen, J.; Loveday, D. C.; Boehme, J. L.; Ferraris, J. P.; Meeker, D. L. *Electrochim. Acta* **1999**, *44*, 2993-3004.
(17) Cheung, J. H.; Fou, A. F.; Rubner, M. F. *Thin Solid Films* **1994**, *244*, 985-989.
(18) Ferreira, M.; Cheung, J. H.; Rubner, M. F. *Thin Solid Films* **1994**, *244*, 806-809.
(19) Rubner, M. F. *Macromolecules Rep.* **1994**, *A31*, 805-809.
(20) Ferreira, M.; Rubner, M. F. *Macromolecules* **1995**, *28*, 7107-7114.
(21) Fou, A. C.; Rubner, M. F. *Macromolecules* **1995**, *28*, 7115-7120.
(22) Cheung, J. H.; Stockton, W. B.; Rubner, M. F. *Macromolecules* **1997**, *30*, 2712-2716.
(23) Stockton, W. B.; Rubner, M. F. *Macromolecules* **1997**, *30*, 2717-2725.
(24) Ellis, D.; Eckhoff, M.; Neff, V. D. *Journal of Physical Chemistry* **1981**, *85*, 1225-1231.
(25) Itaya, K.; Shibayama, K.; Akahoshi, H.; Toshima, S. *J. Appl. Phys.* **1982**, *53*, 804-805.
(26) Duek, E. A. R.; Depaoli, M. A.; Mastragostino, M. *Advanced Materials* **1992**, *4*, 287-291.
(27) Habib, M. A.; Maheswari, S. P. *J. Electrochem. Soc.* **1992**, *139*, 2155-2157.
(28) Pyrasch, M.; Toutianoush, A.; Jin, W. Q.; Schnepf, J.; Tieke, B. *Chem. Mater.* **2003**, *15*, 245-254.
(29) Ikeda, K.; Ohkoshi, S.; Hashimoto, K. *J. Appl. Phys.* **2003**, *93*, 1371-1375.
(30) Kuhn, A.; Anson, F. C. *Langmuir* **1996**, *12*, 5481-5488.
(31) Liu, S. Q.; Kurth, D. G.; Mohwald, H.; Volkmer, D. *Adv. Mater.* **2002**, *14*, 225-+.
(32) Moriguchi, I.; Fendler, J. H. *Chem. Mater.* **1998**, *10*, 2205-2211.
(33) Schlenoff, J. B.; Ly, H.; Li, M. *J. Am. Chem. Soc.* **1998**, *120*, 7626-7634.
(34) Kim, T. S.; Crooks, R. M.; Tsen, M.; Sun, L. *J. Am. Chem. Soc.* **1995**, *117*, 3963-3967.
(35) Pigoislandureau, E.; Nicolau, Y. F.; Delamar, M. *Synth. Met.* **1995**, *72*, 111-119.
(36) Tian, J.; Wu, C. C.; Thompson, M. E.; Sturm, J. C.; Register, R. A. *Chem. Mater.* **1995**, *7*, 2190-2198.
(37) Kim, D. S.; Char, C.; Hong, J. D.; Yu, S. H.; Jin, J. I. *Polym.-Korea* **1996**, *20*, 915-924.
(38) Zhou, P. G.; Samuelson, L.; Alva, K. S.; Chen, C. C.; Blumstein, R. B.; Blumstein, A. *Macromolecules* **1997**, *30*, 1577-1581.
(39) Cassagneau, T.; Mallouk, T. E.; Fendler, J. H. *J. Am. Chem. Soc.* **1998**, *120*, 7848-7859.
(40) Neumann, R.; Davidov, D. *Acta Polym.* **1998**, *49*, 642-651.
(41) Tarabia, M.; Hong, H.; Davidov, D.; Kirstein, S.; Steitz, R.; Neumann, R.; Avny, Y. *J. Appl. Phys.* **1998**, *83*, 725-732.

(42) Ram, M. K.; Salerno, M.; Adami, M.; Faraci, P.; Nicolini, C. *Langmuir* **1999**, *15*, 1252-1259.
(43) Ho, P. K. H.; Kim, J. S.; Burroughes, J. H.; Becker, H.; Li, S. F. Y.; Brown, T. M.; Cacialli, F.; Friend, R. H. *Nature* **2000**, *404*, 481-484.
(44) Kovtyukhova, N. I.; Gorchinskiy, A. D.; Waraksa, C. *Mater. Sci. Eng. B-Solid State Mater. Adv. Technol.* **2000**, *69*, 424-430.
(45) Raposo, M.; Oliveira, O. N. *Langmuir* **2000**, *16*, 2839-2844.
(46) Sarkar, N.; Ram, M. K.; Sarkar, A.; Narizzano, R.; Paddeu, S.; Nicolini, C. *Nanotechnology* **2000**, *11*, 30-36.
(47) Li, D.; Lutt, M.; Shi, X.; Fitzsimmons, M. R. *Mater. Res. Soc. Symp. Proc.* **1998**, *488*, 401-406.
(48) Lukkari, J.; Salomaki, M.; Viinikanoja, A.; Aaritalo, T.; Paukkunen, J.; Kocharova, N.; Kankare, J. *J. Am. Chem. Soc.* **2001**, *123*, 6083-6091.
(49) Zotti, G.; Schiavon, G.; Zecchin, S.; Berlin, A.; Giro, G. *Synth. Met.* **2001**, *121*, 1381-1382.
(50) Zotti, G.; Zecchin, S.; Berlin, A.; Schiavon, G.; Giro, G. *Chem. Mater.* **2001**, *13*, 43-52.
(51) Baba, A.; Park, M. K.; Advincula, R. C.; Knoll, W. *Langmuir* **2002**, *18*, 4648-4652.
(52) Ferreira, M.; Zucolotto, V.; Huguenin, F.; Torresi, R. M.; Oliveira, O. N. *J. Nanosci. Nanotechnol.* **2002**, *2*, 29-32.
(53) Xin, H.; Li, F. Y.; Huang, Y. Y.; Huang, C. H. *J. Rare Earths* **2002**, *20*, 333-338.
(54) Zhai, L.; McCullough, R. D. *Adv. Mater.* **2002**, *14*, 901-905.
(55) Cutler, C. A.; Bouguettaya, M.; Reynolds, J. R. *Adv. Mater.* **2002**, *14*, 684-688.
(56) Caruso, F.; Kurth, D. G.; Volkmer, D.; Koop, M. J.; Muller, A. *Langmuir* **1998**, *14*, 3462-3465.
(57) Schutte, M.; Kurth, D. G.; Linford, M. R.; Colfen, H.; Mohwald, H. *Angew. Chem.-Int. Edit.* **1998**, *37*, 2891-2893.
(58) Caruso, F.; Schuler, C.; Kurth, D. G. *Chem. Mater.* **1999**, *11*, 3394-3399.
(59) Kurth, D. G.; Schutte, M.; Wen, J. *Colloid Surf. A-Physicochem. Eng. Asp.* **2002**, *198*, 633-643.
(60) Liu, S. Q.; Kurth, D. G.; Bredenkotter, B.; Volkmer, D. *J. Am. Chem. Soc.* **2002**, *124*, 12279-12287.
(61) Liu, S. Q.; Kurth, D. G.; Volkmer, D. *Chem. Commun.* **2002**, 976-977.
(62) Xu, L.; Zhang, H. Y.; Wang, E.; Kurth, D. G.; Li, Z. *J. Mater. Chem.* **2002**, *12*, 654-657.
(63) Millward, R. C.; Madden, C. E.; Sutherland, I.; Mortimer, R. J.; Fletcher, S.; Marken, F. *Chem. Commun.* **2001**, 1994-1995.
(64) Chen, S. M. *J. Electroanal. Chem.* **2002**, *521*, 29-52.
(65) Zamponi, S.; Kijak, A. M.; Sommer, A. J.; Marassi, R.; Kulesza, P. J.; Cox, J. A. *J. Solid State Electrochem.* **2002**, *6*, 528-533.
(66) Moriguchi, I.; Kamogawa, H.; Hagiwara, K.; Teraoka, Y. *Chem. Lett.* **2002**, 310-311.
(67) Pyrasch, M.; Tieke, B. *Langmuir* **2001**, *17*, 7706-7709.
(68) Makinen, A. J.; Hill, I. G.; Shashidhar, R.; Nikolov, N.; Kafafi, Z. H. *Appl. Phys. Lett.* **2001**, *79*, 557-559.
(69) Kim, B. H.; Jung, J. H.; Hong, S. H.; Joo, J.; Epstein, A. J.; Mizoguchi, K.; Kim, J. W.; Choi, H. J. *Macromolecules* **2002**, *35*, 1419-1423.
(70) Michaelis, L.; Hill, E. S. *J. Gen. Physiol.* **1933**, *16*, 859.
(71) Monk, P. M. S.; Mortimer, R. J.; Rosseinsky, D. R. *Electrochromism: Fundamentals and Applications*; Weinheim: New York, 1995.
(72) Anderson, T. *Leibig's Ann. Chem.* **1855**, *94*, 358.
(73) Menshutkin, N. *Z. Phys. Chem.* **1890**, *5*, 589.
(74) Raposo, M.; Pontes, R. S.; Mattoso, L. H. C.; Oliveira, O. N. *Macromolecules* **1997**, *30*, 6095-6101.

(75) Krasemann, L.; Tieke, B. *J. Membr. Sci.* **1998**, *150*, 23-30.
(76) Cochin, D.; Laschewsky, A. *Macromol. Chem. Phys.* **1999**, *200*, 609-615.
(77) Lvov, Y.; Ariga, K.; Onda, M.; Ichinose, I.; Kunitake, T. *Colloid Surf. A-Physicochem. Eng. Asp.* **1999**, *146*, 337-346.
(78) Chen, W.; McCarthy, T. J. *Macromolecules* **1997**, *30*, 78-86.
(79) Phuvanartnuruks, V.; McCarthy, T. J. *Macromolecules* **1998**, *31*, 1906-1914.
(80) Hosoda, N.; Ohno, H.; Tsuchida, E. *Polymer* **1984**, *25*, 1302-1306.
(81) Hu, S. S.; Xu, C. L.; He, Y. B.; Meng, L. Z.; Cui, D. F. *Microchem. J.* **2000**, *65*, 311-317.
(82) Sun, W. L.; Xue, J.; Chen, J. S.; Mao, L. Q.; Jin, L. T.; Yamamoto, K.; Tao, S. G.; Jin, J. Y. *Talanta* **1999**, *49*, 345-356.
(83) Caruso, F.; Niikura, K.; Furlong, D. N.; Okahata, Y. *Langmuir* **1997**, *13*, 3422-3426.
(84) Caruso, F.; Furlong, D. N.; Ariga, K.; Ichinose, I.; Kunitake, T. *Langmuir* **1998**, *14*, 4559-4565.
(85) Kosower, E.; Cotter, J. L. *J. Am. Chem. Soc.* **1964**, *86*, 5524.
(86) Poizat, O.; Sourisseau, C.; Mathey, Y. *Journal of the Chemical Society-Faraday Transactions I* **1984**, *80*, 3257-3274.
(87) Borgarello, E.; Pelizzetti, E.; Mulac, W. A.; Meisel, D. *Journal of the Chemical Society-Faraday Transactions I* **1985**, *81*, 143-159.
(88) Poizat, O.; Sourisseau, C.; Corset, J. *J. Mol. Struct.* **1986**, *143*, 203-206.
(89) Oyama, N.; Ohsaka, T.; Yamamoto, H.; Kaneko, M. *Journal of Physical Chemistry* **1986**, *90*, 3850-3856.
(90) Johansen, O.; Loder, J. W.; Mau, A. W. H.; Rabani, J.; Sasse, W. H. F. *Langmuir* **1992**, *8*, 2577-2581.
(91) Diaz, A. F.; Logan, J. A. *J. Electroanal. Chem.* **1980**, *111*, 111-114.
(92) MacDiarmid, A. G. *Synth. Met.* **1997**, *84*, 27-34.
(93) Deberry, D. W. *J. Electrochem. Soc.* **1984**, *131*, C302-C302.
(94) Sekine, I.; Kohara, K.; Sugiyama, T.; Yuasa, M. *J. Electrochem. Soc.* **1992**, *139*, 3090-3097.
(95) Trochnagels, G.; Winand, R.; Weymeersch, A.; Renard, L. *J. Appl. Electrochem.* **1992**, *22*, 756-764.
(96) Gustafsson, G.; Cao, Y.; Treacy, G. M.; Klavetter, F.; Colaneri, N.; Heeger, A. J. *Nature* **1992**, *357*, 477-479.
(97) Yang, Y.; Heeger, A. J. *Appl. Phys. Lett.* **1994**, *64*, 1245-1247.
(98) Kobayashi, T.; Yoneyama, H.; Tamura, H. *J. Electroanal. Chem.* **1984**, *161*, 419-423.
(99) Huang, W. S.; Humphrey, B. D.; MacDiarmid, A. G. *J. Chem. Soc.-Faraday Trans.* **1986**, *82*, 2385-2400.
(100) Huang, W. S.; Macdiarmid, A. G. *Polymer* **1993**, *34*, 1833-1845.
(101) Onoda, M.; Yoshino, K. *Jpn. J. Appl. Phys. Part 2 - Lett.* **1995**, *34*, L260-L263.
(102) Li, D.; Jiang, Y.; Li, C.; Wu, Z.; Chen, X.; Li, Y. *Polymer* **1999**, *40*, 7065-7070.
(103) MacDiarmid, A. G.; Humphrey, B. D.; Huang, W.-S. *J. Chem. Soc., Faraday Trans. 1* **1986**, *82*, 2385-2400.
(104) Farhat, T. R.; Schlenoff, J. B. *Langmuir* **2001**, *17*, 1184-1192.
(105) Jelle, B. P.; Hagen, G.; Sunde, S.; Odegard, R. *Synth. Met.* **1993**, *54*, 315-320.
(106) Jelle, B. P.; Hagen, G.; Nodland, S. *Electrochim. Acta* **1993**, *38*, 1497-1500.
(107) Goff, A. H.-L.; Bernard, M.-C.; Zang, W. *Electrochim. Acta* **1998**, *44*, 781-796.
(108) Groenendaal, B. L.; Jonas, F.; Freitag, D.; Pielartzik, H.; Reynolds, J. R. *Adv. Mater.* **2000**, *12*, 481-494.
(109) Pei, Q.; Zuccarello, G.; Ahlskog, M.; Inganäs, O. *Polymer* **1994**, *35*, 1347-1351.
(110) Jonas, F.; Schrader, L. *Synth. Met.* **1991**, *41*, 831-836.
(111) Heywang, G.; Jonas, F. *Adv. Mater.* **1992**, *4*, 116-118.
(112) Lerch, K.; Jonas, F.; Linke, M. *J. Chim. Phys. Phys.-Chim. Biol.* **1998**, *95*, 1506-1509.

(113) Ghosh, S.; Inganas, O. *Adv. Mater.* **1999**, *11*, 1214-1218.
(114) Ferraris, J. P.; Eissa, M. M.; Brotherston, I. D.; Loveday, D. C. *Chem. Mater.* **1998**, *10*, 3528-3535.
(115) Granlund, T.; Nyberg, T.; Roman, L. S.; Svensson, M.; Inganas, O. *Adv. Mater.* **2000**, *12*, 269-273.
(116) Krishnamoorthy, K.; Ambade, A. V.; Kanungo, M.; Contractor, A. Q.; Kumar, A. *J. Mater. Chem.* **2001**, *11*, 2909-2911.
(117) Li, G.; Pickup, P. G. *Phys. Chem. Chem. Phys.* **2000**, *2*, 1255-1260.
(118) Lefebvre, M.; Qi, Z. G.; Rana, D.; Pickup, P. G. *Chem. Mater.* **1999**, *11*, 262-268.
(119) Rauh, R. D.; Wang, F.; Reynolds, J. R.; Meeker, D. L. *Electrochim. Acta* **2001**, *46*, 2023-2029.
(120) Picart, C.; Lavalle, P.; Hubert, P.; Cuisinier, F. J. G.; Decher, G.; Schaaf, P.; Voegel, J. C. *Langmuir* **2001**, *17*, 7414-7424.
(121) Lavalle, P.; Gergely, C.; Cuisinier, F. J. G.; Decher, G.; Schaaf, P.; Voegel, J. C.; Picart, C. *Macromolecules* **2002**, *35*, 4458-4465.
(122) Picart, C.; Mutterer, J.; Richert, L.; Luo, Y.; Prestwich, G. D.; Schaaf, P.; Voegel, J. C.; Lavalle, P. *Proc. Natl. Acad. Sci. U. S. A.* **2002**, *99*, 12531-12535.
(123) Ghosh, S.; Inganas, O. *Synth. Met.* **1999**, *101*, 413-416.
(124) Ghosh, S.; Rasmusson, J.; Inganas, O. *Adv. Mater.* **1998**, *10*, 1097-+.
(125) Abe, T.; Shiroishi, H.; Kinoshita, K.; Kaneko, M. *Macromol. Symp.* **1998**, *131*, 81-86.
(126) Ogura, K.; Endo, N.; Nakayama, M.; Ootsuka, H. *J. Electrochem. Soc.* **1995**, *142*, 4026-4032.
(127) Uchida, H.; Sasaki, T.; Ogura, K. *J. Mol. Catal.* **1994**, *93*, 269-277.
(128) Katakis, D. F.; Mitsopoulou, C.; Konstantatos, J.; Vrachnou, E.; Falaras, P. *J. Photochem. Photobiol. A-Chem.* **1992**, *68*, 375-388.
(129) Christensen, P. A.; Harriman, A.; Neta, P.; Richoux, M. C. *Journal of the Chemical Society-Faraday Transactions I* **1985**, *81*, 2461-2466.
(130) Sato, O.; Gu, Z. Z.; Etoh, H.; Ichiyanagi, J.; Iyoda, T.; Fujishima, A.; Hashimoto, K. *Chem. Lett.* **1997**, 37-38.
(131) Entley, W. R.; Treadway, C. R.; Girolami, G. S. *Mol. Cryst. Liq. Cryst. Sci. Technol. Sect. A-Mol. Cryst. Liq. Cryst.* **1995**, *273*, 153-166.
(132) Ferlay, S.; Mallah, T.; Ouahes, R.; Veillet, P.; Verdaguer, M. *Nature* **1995**, *378*, 701-703.
(133) Neff, V. D. *J. Electrochem. Soc.* **1978**, *125*, 886-887.
(134) Somani, P. R.; Radhakrishnan, S. *Mater. Chem. Phys.* **2003**, *77*, 117-133.
(135) Honda, K.; Ochiai, J.; Hayashi, H. *J. Chem. Soc.-Chem. Commun.* **1986**, 168-170.
(136) Habib, M. A.; Maheswari, S. P.; Carpenter, M. K. *J. Appl. Electrochem.* **1991**, *21*, 203-207.
(137) Su, L. Y.; Fang, J. H.; Liang, B. J.; Lu, Z. H. *Jpn. J. Appl. Phys. Part 2 - Lett.* **1997**, *36*, L684-L686.
(138) Su, L. Y.; Fang, J. H.; Lu, Z. H. *J. Appl. Polym. Sci.* **1998**, *70*, 1955-1958.
(139) Ho, K. C. *Electrochim. Acta* **1999**, *44*, 3227-3235.
(140) Chen, L. C.; Huang, Y. H.; Ho, K. C. *J. Solid State Electrochem.* **2002**, *7*, 6-10.
(141) Duek, E. A. R.; Depaoli, M. A.; Mastragostino, M. *Adv. Mater.* **1993**, *5*, 650-652.
(142) DePaoli, M. A.; Zanelli, A.; Mastragostino, M.; Rocco, A. M. *J. Electroanal. Chem.* **1997**, *435*, 217-224.
(143) Rajan, K. P.; Neff, V. D. *Journal of Physical Chemistry* **1982**, *86*, 4361-4368.
(144) Liu, S. Q.; Xu, J. J.; Chen, H. Y. *Electrochem. Commun.* **2002**, *4*, 421-425.
(145) Peerce, P. J.; Bard, A. J. *J. Electroanal. Chem.* **1980**, *114*, 89-115.
(146) Buser, H. J.; Schwarzenbach, D.; Petter, W.; Ludi, A. *Inorg. Chem.* **1977**, *16*, 2704-2710.

Chapter 3. Layer-by-layer dual electrochrome concepts

Contents

Figures

Tables

3.1 Introduction to dual electrochrome electrodes

The single-electrochrome work of this thesis has demonstrated for the first time the directed application of LBL assembly to the engineering of desirable properties and performance in electrochromic electrode films. Thick and smooth electrode films incorporating a wide variety of electrochromic materials were deposited using this versatile technique. The resultant films possessed very different properties depending on the nature of the counterpolyion employed, and a wide variety of spectral and electrochemical behavior were observed, leading to general conclusions and strategies for the intelligent design of electrochromic films for specific applications.

Despite the advantages of LBL assembled electrochromic films, in most functional LBL assembled films an inert polymer is employed as the counterpolyion for the functional species. This counterpolyion is typically chosen from the short list of model polyelectrolytes: poly(diallyl dimethylammonium chloride) (PDAC), poly(allylamine hydrochloride) (PAH), poly(acrylic acid)(PAA), or poly(styrene sulfonate) (SPS), although this selection has been enhanced by some of the more unusual inert polyions explored within this thesis work. There have been previous successful efforts to create electroactive LBL assembled films in which the polycation and polyanion are both conjugated,[1] however such efforts have not yet been extended to electrochromic composites. The inclusion of inert material reduces the performance of LBL assembled electrochromic films because inert polyions scatter or absorb light without contributing to contrast. Such polyions can also be resistive and can hinder electron or ion mobility within the film.

In this chapter, we present completely novel "dual electrochrome" composites in which the polycation and polyanion species within the LBL assembled film are both electrochromic species. These dual electrochromes were designed two different and distinct strategies. In the first section of this chapter, contrast and switching speed enhancement are attained by combining PXV and PEDOT:SPS, two electrochromic species that cathodically color to the similar final absorbance states. A schematic of this design strategy is illustrated in Figure 3.1. The additive contributions of PXV and PEDOT coloration should result in greater coloration of the combined composite over a larger range of potentials. In the second part of this chapter, multiple hued states within the same electrode are attained by combining PANI and the PB nanoparticle dispersion, two electrochromic species that anodically color to different final absorbance states over the same potential range. Additive absorbance contributions at midrange potentials should result in a green color, while absorbance when fully colored should be blue. This second design strategy is illustrated in Figure 3.2.

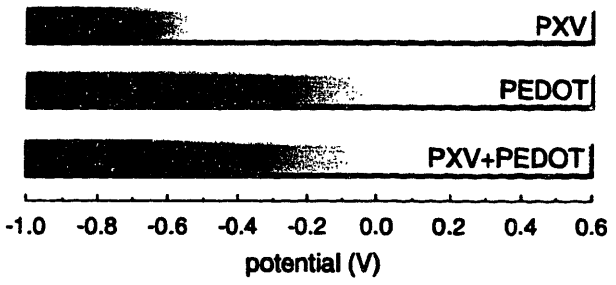

Figure 3.1. Coloration design schematic for a high-contrast electrochromic electrode from LBL assembly.

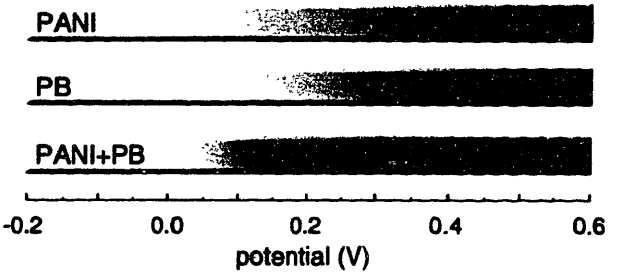

Figure 3.2. Coloration design schematic for a multiple hue electrochromic electrode from LBL assembly.

Together, these two design strategies represent alternative possibilities allowed by the LBL fabrication of electrochromic electrodes. In addition, the results derived from each of these studies revealed very different phenomena within electroactive LBL assembled films. The first part of the chapter that describes the high-contrast electrode indicates a LBL construct in which there is a *high degree of interaction* between the two component electroactive species, resulting in behavior not seen in single-electrochrome films of the component materials. By contrast, the second part of this chapter describes a multi-hue system in which the two component redox-active materials display almost *no interactions* whatsoever, and instead behave entirely as would be expected from a linear combination of single-electrochrome behavior. Results indicate clearly that both of these strategies can be successful, and moreover present no obstacles to the further conception, development, and optimization of dual electrochrome electrodes to meet an even greater variety of display applications at a commercial level of performance.

3.2 The PXV/PEDOT:SPS system

3.2.1 Introduction to PXV/PEDOT:SPS

In the first system studied in this chapter, the polycation PXV is combined with the anionic PEDOT:SPS colloid. PXV is colored in the reduced state due to the formation of a charge transfer complex,[2] while PEDOT:SPSderives color upon reduction from undoping of the conducting state.[3] Both electrochromic polymers switch from transparent oxidized states to dark blue reduced states. The chemical structures of these two electrochromic polymers are reviewed in Figure 3.3.

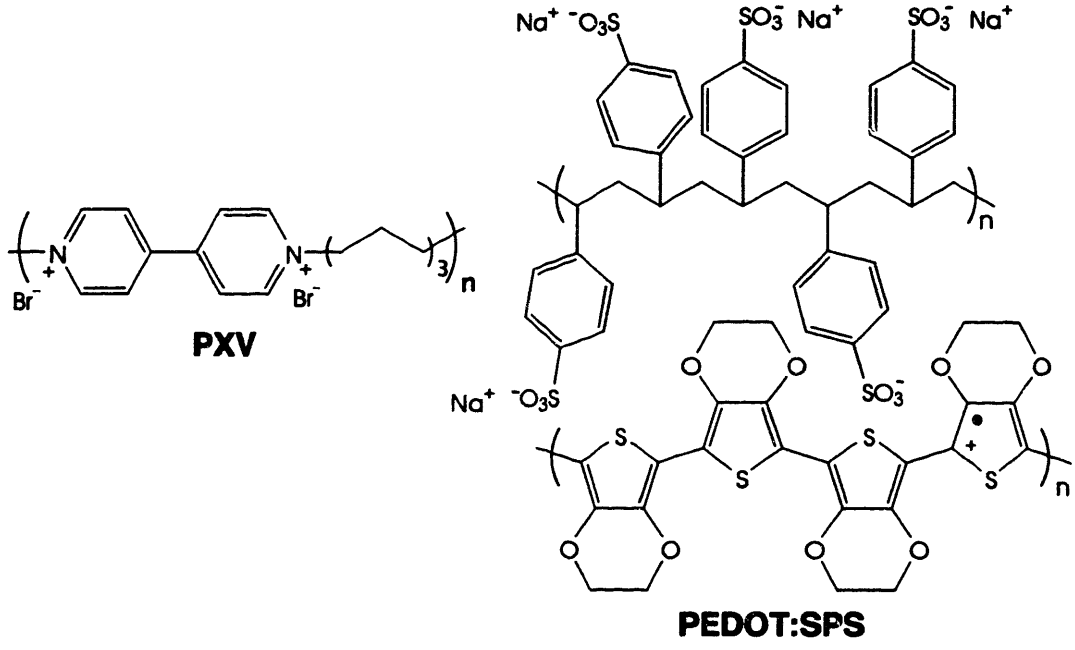

Figure 3.3. Molecular structures of PXV and PEDOT:SPS.

Our investigation into this novel dual electrochrome composite first compares it with single-electrochrome LBL assembled films containing the individual electrochromic polymers paired with inert polyions. Comparison of the PXV component was made with PXV/SPS, whereas comparison of the PEDOT component was made with LPEI/PEDOT:SPS. Particular comparisons were drawn from the results of cyclic voltammetry and spectroelectrochemistry.

The electrochemical and optical properties of the dual electrochrome system PXV/PEDOT:SPS were then elaborated using a variety of additional voltammetric and spectroscopic techniques, including voltage stepping and in situ monitoring of absorbance during switching. This study of the composite reveals complex behavior not found in single-electrochrome films that is caused by interactions between the two electrochromic polymers. After optimization, the contrast of this new electrochromic material actually surpasses that of

almost all polymers synthesized specifically for electrochromic applications, and in fact, at this time there is only one polymeric electrochrome that has been reported to exhibit contrast higher than this dual electrochrome system.[4] These promising results further strengthen the position of this new assembly technique as a means of fabricating lightweight and flexible electrochromic films, as well as other types of redox based devices.

3.2.2 Experimental details for PXV/PEDOT:SPS

3.2.2.1 Materials

Polycations included LPEI (25k, Polysciences), and PXV, which was synthesized in dry, boiling acetonitrile from 1,6-bromohexane and 4,4'-bipyridine (both from Sigma-Aldrich) and then recrystallized from cold methanol with an overall yield of approximately 50%. PXV is fully oxidized at ambient conditions, providing two positive charges per monomer repeat unit. Polyanions included SPS (70k, Aldrich), and PEDOT:SPS (BAYTRON P, Bayer Corporation). BAYTRON P is described by the manufacturer as roughly 0.8 % SPS and 0.5 % PEDOT by mass, indicating approximately equimolar monomer amounts with a slight (~22%) SPS excess. As PEDOT doping does not involve oxidation of every PEDOT repeat, there is a substantial excess of unpaired SPS, providing stabilization and enabling coulombic interactions with polycations in LBL assembly.

Polymer solutions were made using Milli-Q (Millipore deionized, >18.2 Ωcm, 0.22 μm filtered) water, and adjusted to pH 5 using NaOH or HCl. PEDOT:SPS colloidal suspsension was diluted 1:10 with an aqueous cosolvent. The cosolvent was 90% water and 10% dimethylacetamide as described by Rubner.[5] LPEI and SPS solutions were 0.02 M, and PXV solutions were 0.01 M (polymer concentrations with respect to repeat unit). ITO-coated float glass substrates with dimensions 0.7 cm × 5 cm (Delta Technologies, 6 Ω/square) were cleaned by ultrasonication in a series of solvents including dichloromethane, methanol, acetone, and Milli-Q water at 15 minutes each, followed by a 5-minute oxygen plasma cleaning (Harrick PCD 32G). Silicon substrates (research grade <100>, SiTech) were similarly etched to provide a hydrophilic silica surface.

3.2.2.2 Assembly

Film assembly was automated with a Carl Zeiss HMS DS-50 slide stainer. The substrates were exposed to polycation solution for 15 minutes, rinsed for 4 minutes in several Milli-Q water baths, then exposed to polyanion solution for 15 minutes and again rinsed. This cycle was repeated for the desired number of layer pairs. PXV/PEDOT:SPS systems employed a base coat

of (LPEI/PEDOT:SPS)$_2$, to promote adhesion. After assembly, a ~ 1 mg sample was collected from films of several thicknesses by scraping, dried under vacuum at 150°C for 48 hours, and then sent for C-H-N-S elemental analysis at Desert Analytics, Inc.

3.2.2.3 Testing

Electrochemical potential control and current sensing were performed using an EG&G 263A potentiostat/galvanostat. Electrolyte was 0.1 M NH_4Cl, counterelectrode was 4 cm^2 platinum foil, and reference was K-SCE. CV was performed by cyclic between 0.5 V and -0.9 V at 0.025 V/s, 0.05 V/s, 0.1 V/s, and 0.2 V/s. Square wave switching was performed by stepping between -0.9 V and 0.5 V vs. SCE, with 10 seconds per step and 20 seconds per cycle. Approximately 20 cycles were performed sequentially before the measurement cycle. Spectral characterization was performed with a rail-mounted Oriel UV-Vis spectrophotometer with a 300 L/mm, 300 nm blaze grating and InstaSpec IV CCD. Films assembled atop ITO were positioned in a quartz cell with electrolyte, platinum working electrode, and SCE.

3.2.3 Results and discussion for PXV/PEDOT:SPS

3.2.3.1 Assembly of PXV/PEDOT:SPS.

The assembly of PXV- and PEDOT- containing single electrochrome films has been well covered in this thesis thus far, and will only be briefly reviewed. PXV LBL assembled films appear to assemble with a linear increase in film thickness with increasing layer pairs, and electrochemical accounting for Faradaic charge capacity demonstrated that each PXV remains bound to a single bromide counterion within the LBL assembled film, with the other cationic site on the viologen moiety bound to the polyanion species. General film thickness varied depending on polyanion chain ionization density; PXV/SPS films showed growth of 4.3 nm per layer pair. LPEI/PEDOT:SPS films by contrast exhibited an extended regime of superlinear growth to approximately 20-25 layer pairs at which point thickness increased linearly with layer pair number resulting in growth of approximately 75 nm per layer pair.

The LBL assembly of PXV together with the PEDOT:SPS colloid into plasma-etched silicon substrates proved problematic at first as no film deposition could be observed. It was concluded that the growth inhibition culprit was a mismatch between the effective ionization charge densities of PXV and PEDOT:SPS because much of the SPS within the PEDOT colloid remains bound to PEDOT cationic sites and thus the chain ionization density of this SPS is less than that of SPS in free solution. The resolution to this deposition inhibition was found by reducing the effective chain ionization density of PXV by the addition of the anionic surfactant

sodium dodecyl sulfate (SDS). Increasing amounts of SDS were added to the PXV deposition solution. LBL assembled film growth was observed at low ~10^{-5} M surfactant concentrations, and layer pair thickness increased with increasing SDS concentrations to a thickness plateau reached at 10^{-4} M SDS. Film quality suffered at SDS concentrations greater than $5 \cdot 10^{-4}$ M due to a loss of PXV solubility and wholesale precipitation occurred at 10^{-3} M SDS. The addition of SDS proved to be more effective than the addition of salt for thickness enhancement because SDS binds and shields cationic sites on PXV and also presents a hydrophobic alkane tail to solution, reducing the effective ionization density of the polyion and leading to a more globular solution morphology. The addition of 10^{-4} M SDS was thereafter chosen as a standard condition for PXV exposure solutions due to the resultant reproducibly thick LBL assembled film.

The PXV/PEDOT:SPS series was assembled in 10, 20, 30, 40, 50 and 60-layer pair systems onto ITO-coated float glass. The LBL growth profile for this system is shown in Figure 3.4. Rather than a linear growth profile, which is typical for most electrostatically LBL assembled polymer films, the PXV/PEDOT:SPS system demonstrates an exponential growth profile, with total film thickness ranging from approximately 40 nm for a 10 layer pair film to almost 2 μm for a 60 layer pair film. The per-layer pair thickness for this system is not a single value, but rather increases from less than 4 nm/layer pair to greater than 100 nm/layer pair. Nonlinear regression gives the relation between t, the thickness in nm, and n, the layer pair number, as $t = 22.7e^{0.0736 \cdot n}$ with an R^2 value over 0.999, indicating that the total thickness of a PXV/PEDOT:SPS film roughly doubles with every 10 layer pairs that are deposited. The regression line connects the film thickness points on Figure 3.4. A similar curve was obtained using quartz crystal microbalance (QCM) monitored deposition with results shown in Figure 3.5, confirming the deposition of exponentially increasing mass.

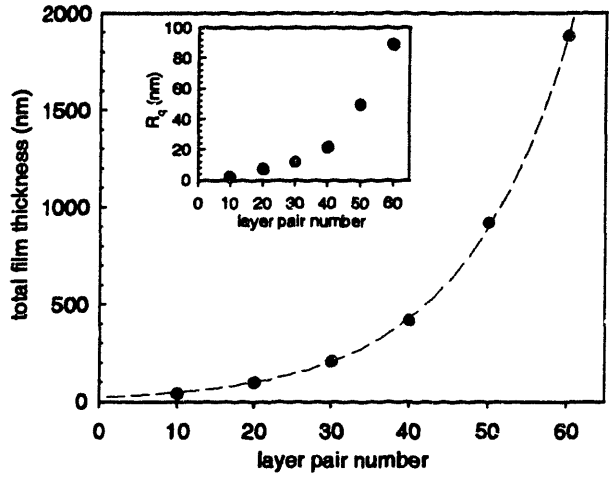

Figure 3.4. Correlation of film thickness to layer pair number for the PXV/PEDOT:SPS series

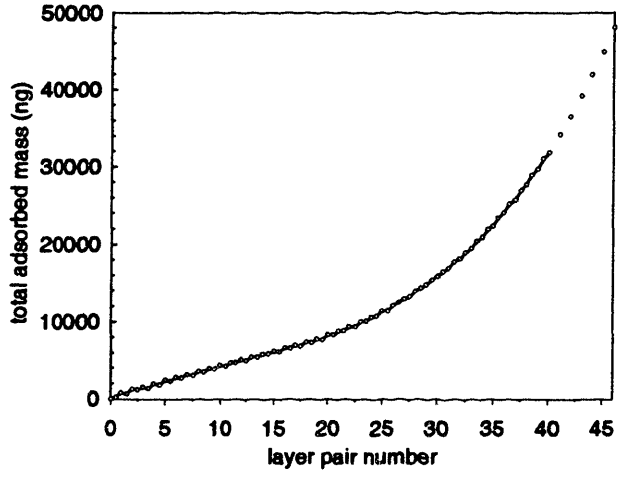

Figure 3.5. Correlation of PXV/PEDOT:SPS film mass to layer pair number monitored in-situ by QCM.

As was explained for the LPEI/PEDOT:SPS system, nonlinear growth profiles in polyelectrolyte LBL assembled films are well-established phenomena. Even in "model" polyelectrolyte LBL systems PAH/SPS[6] and PDAC/SPS,[7,8] superlinear growth has been observed when deposition solutions are at medium to high ionic strengths (>0.1 - 0.3 M). Exponential thickness growth appears to be especially common in the LBL assembly of many biologically derived polyelectrolytes even in the absence of added electrolyte.[9-11] Explanations of the exact exponential assembly mechanism vary. One explanation, offered for the case of high ionic strength deposition, suggests that the superlinear growth is due to increasing surface roughness, which in turn presents an increasing surface area that permits deposition of increasing amounts of material.[6] Increasing roughness in these systems is provided by the deposition of polyelectrolytes in the globular morphology that is assumed in solution at high ionic strengths.

More recent efforts by other groups have suggested that the mechanism is related to polyelectrolyte diffusion into and out of the film as well as surface interactions.[9-11] In the case of PXV/PEDOT:SPS, we believe the exponential growth to be a consequence of the nature of the PEDOT:SPS colloidal dispersion, which should deposit in a manner similar to globular polyelectrolytes, forming an increasingly rough and larger surface area. Our supposition of increasing "fractal" surface area is supported by roughness measurements shown in the Figure 3.4 inset, which increase approximately linearly with total film thickness and exponentially with layer pair number.

This consistent exponential growth appears to be an extension of the exponential growth regime of LPEI/PEDOT:SPS (as described in the previous chapter) to even greater layer numbers; the growth of PXV/PEDOT:SPS never becomes linear within the scope of this study. Comparing these two systems, we can conclude that the PEDOT:SPS colloid is predisposed to superlinear growth when LBL assembled, most likely because of its colloidal nature, but the magnitude and extent of this superlinear growth are highly dependent on the character of the polycation. With the PXV/PEDOT:SPS system, the addition of SDS to the PXV deposition solution may also play a role in extending the exponential growth regime due to the globular morphology that charge-shielded PXV would *also* assume in solution. Thus if both polycation and PEDOT:SPS possess a globular morphology, the extent and magnitude of superlinear growth may be enhanced. This effect may explain why highly charged and unshielded polycations such as PDAC form extremely thin films with the PEDOT:SPS colloid while partially charged LPEI or shielded polycations form extremely thick films. Regardless of the assembly mechanism, PXV/PEDOT:SPS films with this novel architecture display unique electrochemical and optical properties, as described in further detail in a later section of this chapter.

3.2.3.2 Compositional analysis.

Given the rather unusual architecture of PXV/PEDOT:SPS films, the composition was determined to better analyze the resultant film properties. Because of the difficulties inherent in compositional estimation from simple thickness or mass measurements, sample scrapings were taken from multiple films of varying thickness and subjected to elemental analysis. As a result of the exponential growth of these films, the collected sample best represents the composition of the thickest films. Elemental analysis revealed a sulfur:nitrogen atomic ratio of 0.83. Assuming that PXV is the sole source of nitrogen and that the PEDOT:SPS complex is the sole source of sulfur, and given the PEDOT:SPS molar repeat unit ratio of 0.45:0.55 as provided by the manufacturer, a PXV:PEDOT:SPS molar repeat unit ratio of 0.38:0.28:0.34 was calculated. We assume that this

bulk composition represents the film throughout growth, though we recognize that composition may vary at earlier or later stages of film deposition. Given that there are two quaternized, cationic ammonium sites on each PXV repeat, these results indicate that over half of these sites are not paired with SPS; this effect is consistent with the adsorption of PXV as loopy layers due to shielding of charged groups with either salt anions or hydrophobic surfactant. The sulfur:carbon and sulfur:hydrogen ratios indicate that these sites are *not* coordinated with the surfactant SDS - in fact there is no significant amount of SDS in the final film, confirming that PEDOT:SPS is the sole source of sulfur; thus, these cationic sites must remain paired with their bromide counterions. (This conclusion could not be confirmed, as a prohibitively large sample is required for bromide analysis). SPS is assumed to be fully ionically paired with either PEDOT or PXV, and PEDOT cationic sites are assumed to be electrostatically balanced by the SPS dopant.

3.2.3.3 Electrochemistry - cyclic voltammetry.

The first electrochemical test that was applied to the electroactive LBL assembled films assembled in this study was cyclic voltammetry (CV), to identify redox potential ranges and elucidate general electrochemical behavior. Because PEDOT and PXV have very different redox potentials, the scanning range was quite large: between -0.9 V and 0.5 V vs. SCE, in a supporting electrolyte of aqueous 0.1 M NH_4Cl. Working electrodes consisted of LBL assembled films assembled onto ITO-coated float glass. In order to assess the electrochemical accessibility of the redox polymers within the films, the CV dependency on scan rate was determined for each film.

single electrochrome films

Electroactive behavior of PXV and PEDOT containing films has been described in the previous chapter of this thesis. The redox behavior of the PXV/SPS composite is generally similar to that of poly(viologen)-containing LBL assembled films studied by Schlenoff.[12,13] A sharp redox wave appears with $E_{½}$ = -0.66V, corresponding to the first reduction of bipyridilium moieties in the PXV polymer backbone. The peak is sharp due to the insulating nature of the alkyl spacer; the polymer is a covalently bonded collection of discrete redox centers each with a well-defined redox potential. The hysteresis between oxidative and reductive peaks increases with scan rate, due to slow electron transfer from ITO to the polyviologen or more likely resistance to redox propagation in the bulk of the film. Oxidation and reduction peak heights do not scale linearly with scan rate and instead scale almost perfectly with the square root of scan rate, indicating that slow ion diffusion into the film controls the reaction rate of reduction and oxidation. This in turn suggests that the LBL assembled film does not have an open, ion permeable morphology, but rather a more tightly knit, hydrophobic interior. This character would be expected for a LBL

assembled film such as PXV/SPS which contains two highly charged polyelectrolytes;[14] in particular as SPS presents a very hydrophobic main-chain.

The CV characterization of the LPEI/PEDOT:SPS series features a broad redox wave centered at $E_{1/2} \approx 0.15$V, corresponding to the reductive elimination and oxidative creation of distributed cationic polaron charge carriers on the PEDOT polymer backbone. The broad nature of these peaks is due to the extended conjugation of PEDOT; redox potential varies depending on polaron environment and proximity to other charge carriers. Like PXV/SPS, this system displays an increasing hysteresis between oxidation and reduction peaks with increasing scan rate, again indicating internal resistance in the film. High internal resistance in this system is not surprising considering the low PEDOT "loading" that we have observed in this and previous work[15] - the film is composed primarily of resistive polyions LPEI and SPS (a primary motivation for considering the dual electrochrome approach). However, unlike the PXV/SPS CV, the oxidation and reduction peak heights for LPEI/PEDOT:SPS scale nearly linearly with scan rate, indicating less ion resistance and a more open film morphology.

dual electrochrome films

Films of PXV/PEDOT:SPS ranging from 20 layer pairs to 60 layer pairs were subjected to CV under the same experimental conditions as the single-electrochrome films. As shown in Figure 3.6, the CV curves exhibit electrochemical signatures of both the polyviologen and the PEDOT. In particular, a sharp PXV peak centered at approximately -0.65 V and a broader PEDOT peak centered near 0.0 V are clearly visible, and correspond to peaks obtained from the separate CV scans shown in the previous chapter. In the dual electrochrome scans, the polyviologen peak predominates in thinner films while the PEDOT contribution appears to become larger at higher layer pair numbers. Thus, both materials are electrochemically accessible, though the relative contributions of the two materials vary with the total layer pair number and film thickness. Furthermore, the PEDOT peak is partially obscured by the presence of a strong new peak that appears in the oxidative scan. Thus, the combination is successful, though the behavior of the combined composite is far more complex than that of simpler single-electrochrome systems.

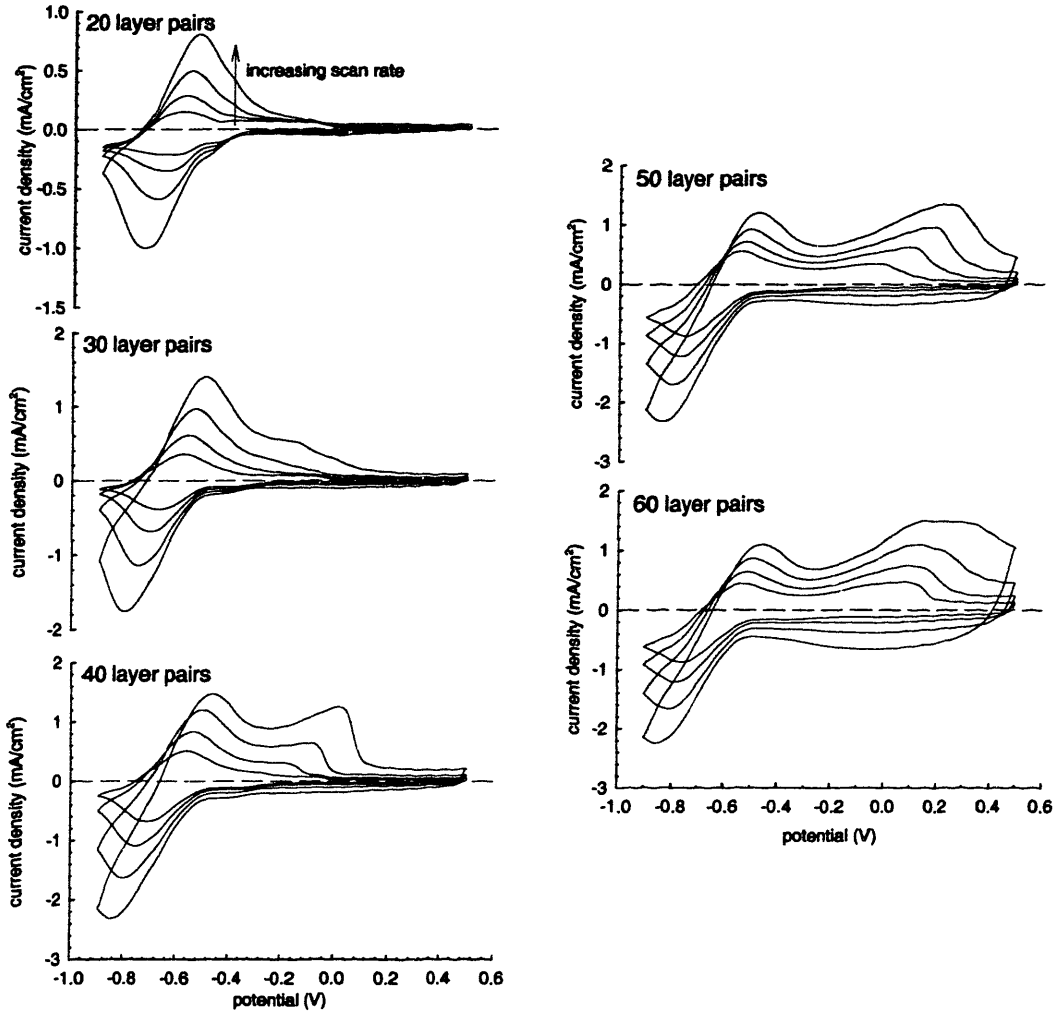

Figure 3.6. Cyclic voltammetry of the PXV/PEDOT:SPS LBL series.

Because this new oxidation peak does not appear in CVs of the single-electrochrome composites, it must be the product of interactions between PEDOT:SPS and PXV. The new peak first appears as a sloping shoulder in the 0.2 V/s CV scan of $(PXV/PEDOT:SPS)_{30}$, and it grows broader and more prominent in scans of films with more layer pairs. There is no reductive wave for this peak, and the peak location and height are extremely scan-rate dependent. One explanation for this behavior is that PXV might facilitate PEDOT oxidation as has been observed for other conjugated polymers,[16,17] resulting in a more localized and stronger PEDOT oxidation peak. One possible mechanism for this facilitation is shown in Figure 3.7.

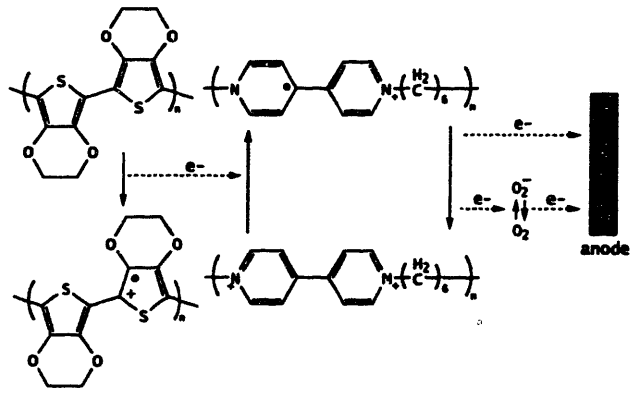

Figure 3.7 Possible mechanism of PEDOT oxidation facilitation by PXV.

This hypothesis does not, however, explain the large size of the peak or its appearance only in thicker films. Furthermore, the new peak should also appear in CV scans at potentials too anodic for PXV reduction, as shown in Figure 3.8; however, such a peak does not appear in these scans. Indeed, these scans appear exactly similar to those of other polycation/PEDOT:SPS LBL assembled films of similar thickness that were investigated in the previous chapter.

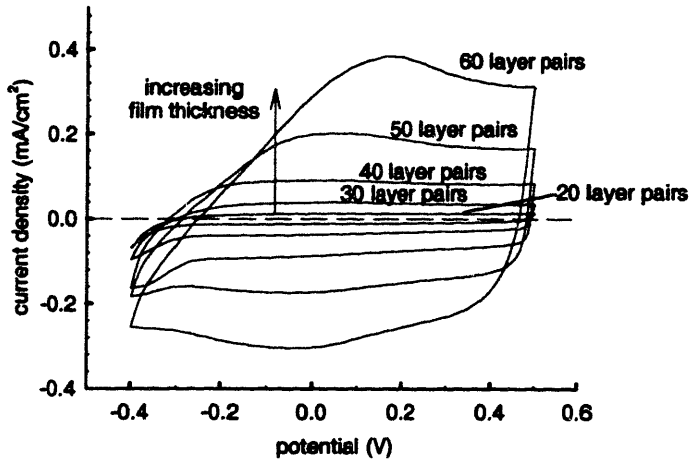

Figure 3.8. Cyclic voltammetry of PXV/PEDOT:SPS films over a more limited potential range.

A more consistent hypothesis is that the new peak is due to the release of charge trapped states within the LBL construct. Charge-trapping is a phenomenon that has been observed in specially fabricated, spatially separated heterogeneous redox-active systems consisting of a bilayer film of two different materials.[18] The oxidation state of the inner layer controls electron transfer to the outer layer and thus regulates the outer layer oxidation state. One model charge-trapping system that has been studied in detail is composed of a polythiophene inner layer and a polyviologen outer layer.[19] Although charge-trapping has not yet been described within polyelectrolyte LBL assembled films, it stands to reason that the PXV/PEDOT:SPS LBL system might be considered as

a "stack" of charge-trapping bilayers. However, the growth profile for this system is almost perfectly exponential, so that the thin, highly interpenetrated inner layers of PXV/PEDOT:SPS should behave as a homogenous blend with no charge-trapping, while much thicker outer layers should behave as more well-defined domains and allow for redox mediation. The fact that these large domains are stacked in series within the LBL assembled film should further enhance charge-trapping, allowing for greater mediation with each subsequent layer pair. This hypothesis explains why the new oxidation peak is not observed in thinner PXV/PEDOT:SPS films, yet becomes prominent in films of greater thickness, where the individual layers are thicker and presumably more discrete.

The charge trapping mechanism is illustrated in Figure 3.9, which compares CV curves of PXV/PEDOT:SPS films of 20-, 40-, and 60-layer pair thickness at a scan rate of 0.2 V/s. The cathodic scan begins at point A where all films are oxidized. From point A to point B, PEDOT reduction occurs, which appears to be essentially complete by -0.5 V. PEDOT appears to be electrochemically accessible even in thick films as the peak current of this reduction wave appears to increase proportionally with film thickness. From point B to point C, PXV becomes reduced, though in the thick 60-layer pair film, PXV appears to be only partially accessible and outer portions may not become reduced – this is especially clear as the 40- and 60- layer pair films show reduction peaks of similar magnitude, even though the 60-layer pair film contains nearly four times more PXV. Point C is the endpoint of the cathodic scan.

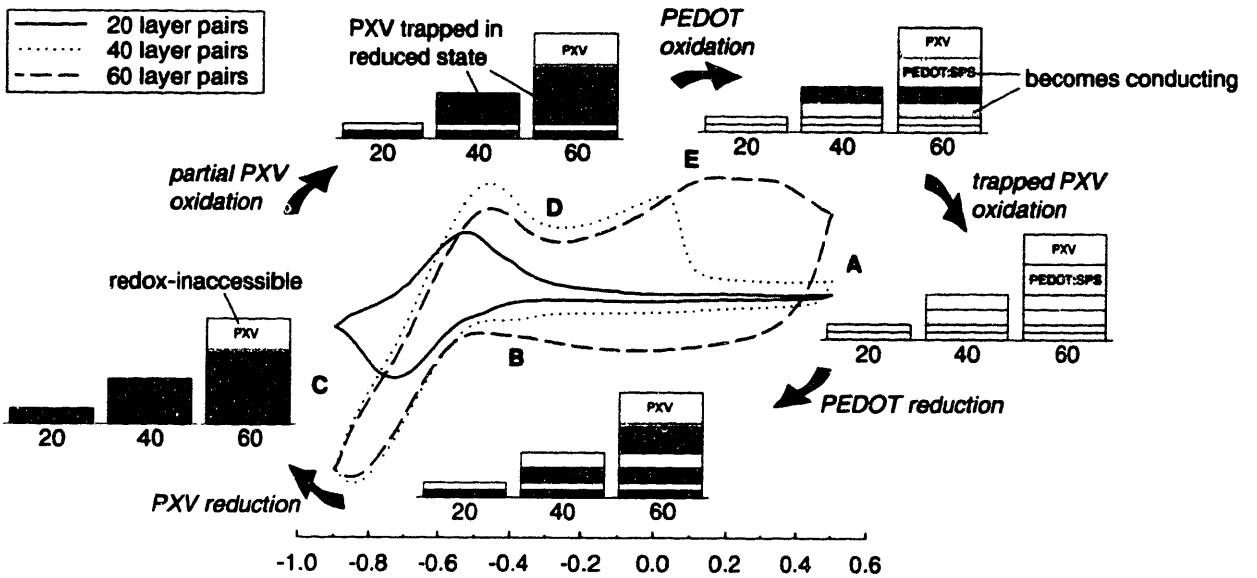

Figure 3.9. Suspected charge trapping mechanism depicting cyclic voltammograms of the PXV/PEDOT:SPS series. Illustrations representing the suspected state of the films begin at point A and proceed clockwise through points A-E following the discussion in the text.

From point C to point D, the anodic scan begins and PXV becomes re-oxidized. In thicker films (40 and 60 layer pairs), it is clear that re-oxidation is only partial because the oxidation peak is far smaller than the reduction peak. The PXV that remains reduced is suspected to reside in a trapped state located in the outer portions of the film, insulated by reduced PEDOT:SPS. From point D to point E, PEDOT becomes re-oxidized. After oxidation, PEDOT becomes electronically conducting and reduced PXV remaining in the outer portions of the film becomes immediately redox-accessible and re-oxidizes. The re-oxidation of trapped PXV takes place between point E and point A, and follows immediately or is simultaneous with PEDOT oxidation, resulting in the appearance of the strong new CV peak in thicker films.

3.2.3.4 Electrochemistry - cyclic absorptometry.

The charge-trapping effect was also investigated spectroelectrochemically by performing fast spectral scans of films *in situ* while applying the potential ramp waveform used for CV. This technique provides information about the hysteresis of light absorbance during CV, which directly correlates to the polymer film oxidation state. A single wavelength of 560 nm was chosen to represent the oxidation state of both PEDOT and PXV. This wavelength was isolated from the fast spectral scans, resulting in the cyclic absorptometry shown in Figure 3.10. These scans were performed at a scan rate of 0.1 V/s; slower scans produced less hysteresis, though it was not eliminated. The cathodic scan shows two regions of increasing absorbance: one near the PEDOT reduction onset at 0.2 V, and one near the polyviologen reduction onset at -0.6 V. The anodic scan also shows two vertical inflections: one small decrease in absorbance at -0.7 V and one very large decrease in absorbance at -0.1 V. The differences in the location and magnitude of these inflections between the anodic and cathodic scans create two regions of hysteresis. These hystereses are not observed in the $(PXV/PEDOT:SPS)_{20}$ scan, but become significant in thicker films.

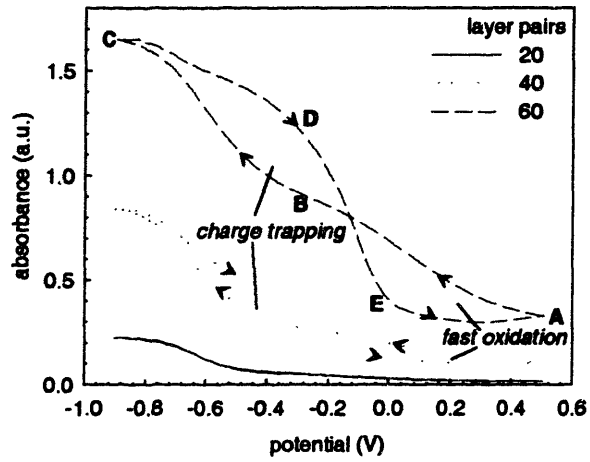

Figure 3.10. Cyclic absorptometry at 560 nm and 0.1 V/s for the PXV/PEDOT:SPS series. Labels A – E correlate to labels in Figure 3.9.

The hysteresis at negative potentials is clear evidence of the existence of charge-trapped states. As was elaborated by electrochemical means, charge-trapping does not appear in the 20-layer pair film but is significant within 40- and 60-layer pair films. During the anodic scan, starting at point C, the PXV undergoes a small oxidation at -0.7 V (point D) but remains substantially reduced until the sudden inflection at -0.1 V (point D to point E, corresponding to PEDOT oxidation), where light absorbance suddenly decreases as the charge-trapped states are released (point D through point A). The second and opposite hysteresis at positive potentials is due to the fact that the PEDOT oxidation proceeds much faster and at a more cathodic potential than the initial PEDOT reduction (point A to point B). The oxidative bleaching of PEDOT is typically far faster than its reductive coloration, yet it is also possible that PXV is indeed facilitating PEDOT oxidation, as was suggested previously in this chapter.

3.2.3.5 Electrochemistry – square wave switching.

The electrochemical properties of the PXV/PEDOT:SPS system were further investigated using double potential step chrono-amperometry (DPSCA) in order to confirm the results of CV and to investigate the response time and charge capacity (columbic charge uptake/removal) of each film. In the DPSCA scans, the PXV/PEDOT:SPS films were subjected to a continuous square-wave pulse that switched the film potential between 0.5 V and -0.9 V with a period of 20 seconds and a duration of 10 seconds at each potential. A current wave was reproduced with every step, which was found not to vary significantly over at least 100 full cycles. A single current wave was isolated for oxidation and reduction of each film, and integrated to show the charge

response. These results are compared in Figure 3.11. The reduction step shown in Figure 3.11a and Figure 3.11b shows a generally slower response time with increasing layer pair number. The final charge density at 10 seconds from Figure 3.11b indicates the total charge capacity of the film.

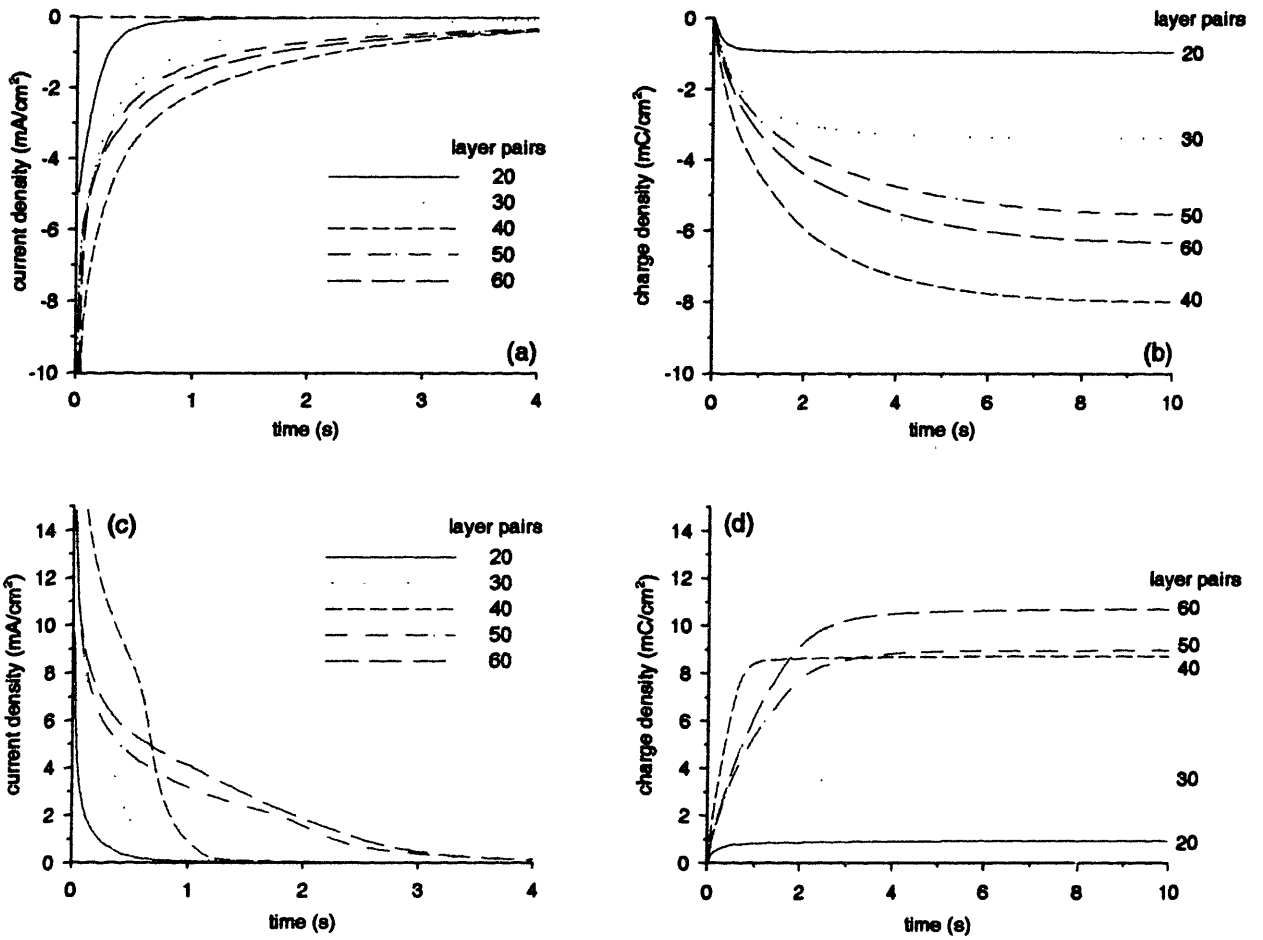

Figure 3.11. Square wave switching of the PXV/PEDOT:SPS series.

Given the compositional data obtained through elemental analysis, it is possible to estimate the percentage of redox-accessible sites in the finished film at various film thicknesses. Assuming a thin film density of 1.2 g/cm^3, as has been previously verified for similar polyelectrolyte LBL-assembled films,[20,21] and assuming that each PXV repeat unit remains coordinated to one bromide anion, an estimated number of total redox sites and percent accessed were calculated, with results shown in Table 3-1. The estimated sites were based on the sum of PXV and PEDOT repeat units, a calculation which considers a single PXV reduction and complete PEDOT reduction/oxidation, though one would not expect full oxidation or reduction of every monomer unit on the PEDOT chain. Results shown are for 30-60 layer pairs, where bulk

composition data are most accurate. Initially half of the redox sites present are accessible; this number decreases above 40 layer pairs due to increasing electronic resistance and ion impermeability in the thicker films.

Table 3-1. Estimated redox accessibility of films of varying thickness.

layer pair number	est. sites (mC/cm^2)	reduced sites (mC/cm^2)	oxidized sites (mC/cm^2)
30	7.0	3.4 (48%)	3.5 (50%)
40	14	7.8 (54%)	8.7 (61%)
50	31	5.5 (18%)	9.0 (29%)
60	64	6.3 (10%)	10 (17%)

3.2.3.6 Spectroelectrochemistry.

Following the electrochemical tests, the optical properties of the electrochromic LBL assembled composites were evaluated using spectroelectrochemistry. For these investigations, LBL assembled films assembled onto transparent working electrodes were inserted into a cuvette electrochemical cell and a UV-Vis spectrum was measured through the films at different potentials. The results are presented as a series of UV-Vis absorbance curves correlated to film potential. The potential range and other electrochemical experimental conditions were identical to those used for CV and DPSCA. The scan for spectroelectrochemistry was made cathodically, proceeding from 0.5 V to -0.9 V, and two-minute equilibration at each stepped potential was employed to minimize transient effects.

Single electrochrome films

In PXV containing LBL assembled films, the characteristic visible absorbance of the singly-reduced state of PXV can be observed at 550 nm. The reduction appears to begin suddenly at -0.5 V and continues essentially to completion by -0.8 V. The sharp transition from bleached to colored state is consistent with the sharp nature of the CV peak, and the potential of the optical absorbance increase is in good agreement with the reduction potential determined from the CV scan. The spectroelectrochemistry of PEDOT reduction proceeds quite differently, with a much more gradual transition over the entire potential range. A substantial portion of the reaction appears to take place between 0.3 V and -0.4 V. This behavior is again consistent with a broad CV peak and is expected for a polymer with extended conjugation.

Dual electrochrome films

In Figure 3.12, we present spectroelectrochemistry of the dual electrochrome $(PXV/PEDOT:SPS)_{40}$, which clearly shows absorbance features of both PEDOT and PXV. At positive potentials, the entire composite is bleached. Immediately on applying a more cathodic potential, the film begins to color. From 0.5 V to -0.5 V, the gradual coloration is due primarily

to the reduction of PEDOT. In fact, at -0.5 V, the spectrum of $(PXV/PEDOT:SPS)_{40}$ appears nearly identical to that of $(LPEI/PEDOT:SPS)_{40}$. At negative potentials beyond -0.5 V, the reduction of PXV suddenly begins, and absorbance increases profoundly. The final colored state clearly displays three broad absorbance peaks: two due to PXV at 550 nm and 620 nm, and one due to PEDOT at approximately 670 nm. The separation of redox potentials within this composite provides a unique breadth of grayscale control, with adjustable absorbance over the entire potential range studied. The inclusion of PXV with PEDOT provides significantly more coloration than PEDOT alone, and the combination clearly provides broader absorbance throughout the visible range. Due to this wide band absorbance, very thick PXV/PEDOT:SPS films appear nearly black at negative potentials.

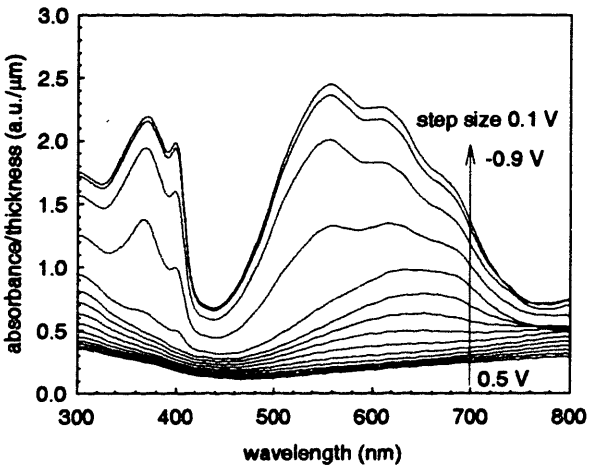

Figure 3.12. Spectroelectrochemistry of $(PXV/PEDOT:SPS)_{40}$

3.2.3.7 Optical switching.

The kinetics of color change within PXV/PEDOT:SPS films were investigated spectroelectrochemically by performing fast spectral scans *in situ* while applying the potential step DPSCA waveform. This technique provides information about the kinetics of color-switching as shown in Figure 3.13, which demonstrates the absorbance change of an isolated wavelength (560 nm) from the fast spectral scans. The 20-, 30-, and 40-layer pair films all display minimum and maximum absorbance that is linear with respect to film thickness and exponential with respect to layer pair number. The thicker films such as 50- and 60- layer pair films do not have this linear relationship, confirming the inaccessibility of PXV in outer regions of the film that was determined by electrochemical means.

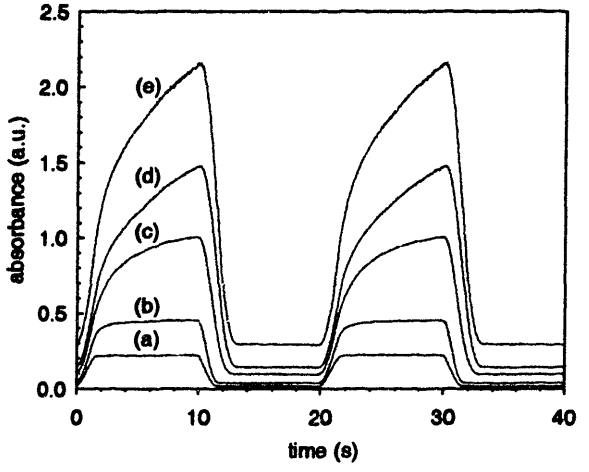

Figure 3.13. Optical switching at 560 nm for PXV/PEDOT:SPS films. Films of 20, 30, 40, 50, and 60 layer pairs correspond to plots a-e, respectively.

The absorbance profiles shown in Figure 3.13, as well as the charge density DPSCA response presented in Figure 3.13 can be used to determine switching time, an important figure of merit for electrochromic composites. Different metrics are often used to define the switching time. If switching time were defined as the time that is required to reach 90% of the full change in absorbance after switching the potential, then these composites would require 1.3-7.4 seconds for coloration, and 1.2-2.3 seconds for bleaching. If the definition were changed to refer to reaching 90% of the full change in *transmittance*, then coloration would require 1.3-3.1 seconds and bleaching would require 1.2-2.7 seconds. Switching time can also be based on the charge response of the film. A full tabulation of switching times based on these metrics is reported in Table 3-2.

Table 3-2. Switching times for PXV/PEDOT:SPS composites.

	bleaching time (s)			coloring time (s)		
layer pair number	%T*	abs	charge†	%T*	abs	charge†
20	1.2	1.2	1.2	1.3	1.3	0.6
30	1.1	1.2	0.6	1.8	2.2	2.2
40	2.2	1.9	0.7	3.1	5.5	3.7
50	2.6	2.3	2.2	3.1	7.3	4.8
60	2.7	2.3	2.3	2.0	7.4	4.6

* from Figure 3.13
† from Figure 3.11

Switching times of 1-2 seconds are typical for electrochromic polymer films, though the times shown here are somewhat slower than the subsecond switching times reported for some high-contrast electrochromic polymers.[22] Importantly, the PXV/PEDOT:SPS films are far thicker than those with subsecond switching,[22] and the slower switching of this composite is thought to be due

to slow ion permeation and internal resistance in thicker films that was described earlier by electrochemical investigation. Importantly, the switching time of this dual electrochrome is shorter than the switching time of either PXV or PEDOT:SPS assembled separately in a single electrochrome composite. This faster switching must be due to the establishment of a less interrupted continuum of redox active polymer that transmits the electrochemical potential field faster throughout the film thickness. Of course, with increasing layer numbers, the switching time does increase, but still remains faster than the single electrochrome films. This slight disadvantage in thicker PXV/PEDOT:SPS films is by no means prohibitive. Furthermore, the application possibilities for static displays are undiminished due to the coloration and high contrast that can be achieved with this composite.

3.2.3.8 Coloration study.

Coloration in PXV/PEDOT:SPS is demonstrated in Figure 3.14, which shows digital images of films at different potentials. The composite switches from a transmissive, sky-blue color when oxidized, to a deeply absorptive purple/blue color when reduced. Increasing the composite thickness results in a slightly darker color in the bleached state, and a far more saturated colored state. The grayscale of this composite is demonstrated at -0.4 V, where most of the PEDOT is reduced, but PXV remains oxidized. Aside from saturation, there is a slight difference in color between -0.4 V and -0.9 V because reduced PEDOT only absorbs in the red portion of the visible spectrum, producing a pure blue color, while the PXV features an additional, higher energy visible absorbance that produces a more purple color. Due to the dramatic coloration to an intensely saturated purple/blue at full reduction, these films have obvious applications as electronic inks or in other types of static display technologies.

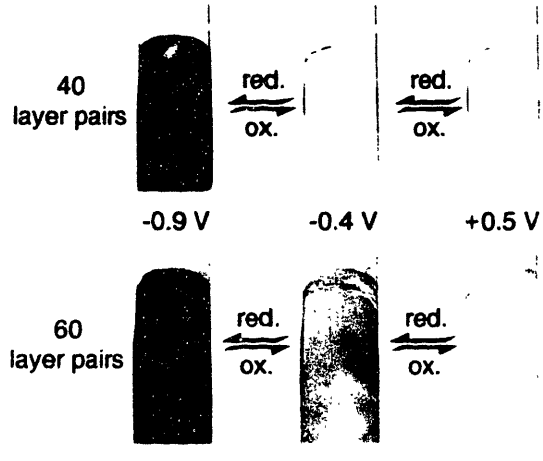

Figure 3.14. Photographs of PXV/PEDOT:SPS electrochromism.

3.2.3.9 Optimization for electrochromic applications.

The most important figure of merit for electrochromic materials is the contrast between oxidation and reduction. From examination of the plot shown in Figure 3.13 and the images of Figure 3.14, it is clear that the contrast achieved is strongly dependent on the number of layer pairs. Furthermore, both colored and bleached absorbance increase with increasing layer number, so there must exist an optimum film thickness at which the contrast is maximized. The probable location of this maximum can be determined by comparing the contrast of the films studied spectroelectrochemically using a suitable metric. There are several metrics for contrast determination, however the most commonly used are $\Delta\%T(\lambda)$ and the optical density, $OD(\lambda)$. One rather recent criterion has been the comparison of colorimetric luminance, which we may pursue in future studies.[23] The quantity $\Delta\%T(\lambda)$ is the change in transmittance between the colored and bleached states at a specific wavelength. The $OD(\lambda)$ is the logarithm of the ratio of bleached transmittance to colored transmittance at a specific wavelength - not a suitable measure for evaluating strongly coloring films such as PXV/PEDOT:SPS because thicker films invariably have a greater OD. Instead of OD, the quantity $\Delta\%T_{max}$, the maximum value of $\Delta\%T(\lambda)$, was determined for each of the PXV/PEDOT:SPS films. The values of this measure are shown in Figure 3.15, along with the transmittance of bleached and colored states at the $\Delta\%T_{max}$ wavelength. The value of $\Delta\%T_{max}$ increases from about 35% for a 20-layer pair film to a maximum of greater than 70% for a 40-layer pair film. Although these contrast values are already quite high, it is clear that an even greater maximum contrast might be achievable in a film of thickness between 40 and 50 layer pairs.

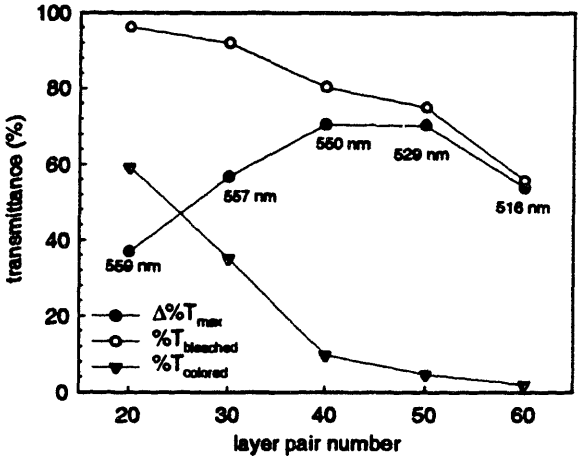

Figure 3.15. Optimization of PXV/PEDOT:SPS film thickness and layer pair number. The wavelength of $\Delta\%T_{max}$ is recorded for each point, and the $\%T_{bleached}$ and $\%T_{colored}$ at that wavelength (wavelength of $\Delta\%T_{max}$) are plotted.

In order to achieve this maximum, several PXV/PEDOT:SPS films were assembled in the range of 40-50 layer pairs, fine-tuning the optimum film thickness. A $(PXV/PEDOT:SPS)_{45}$ film with a thickness of approximately 550 nm was found to display higher contrast than either the 40- or 50-layer pair films. The spectroelectrochemistry of this film is shown from the transmittance perspective in Figure 3.16.

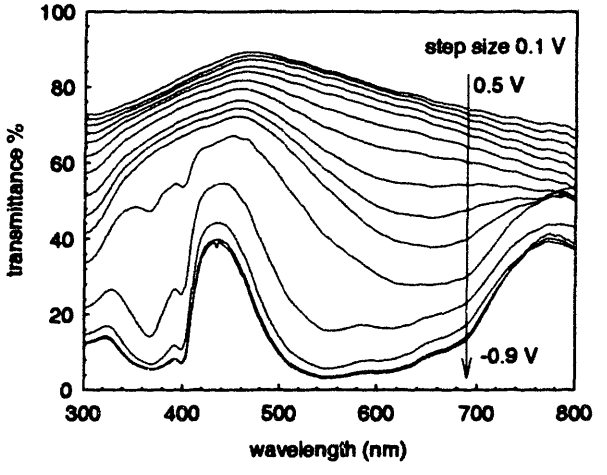

Figure 3.16. Spectroelectrochemistry of $(PXV/PEDOT:SPS)_{45}$ presented from the transmittance perspective.

The bleached state of this film transmitted more light than $(PXV/PEDOT:SPS)_{40}$ due to the addition of a ultrasonic rinsing step during the deposition process that resulted in a smoother film. As expected, the colored state transmittance of $(PXV/PEDOT:SPS)_{45}$ was between that of the 40- and 50- layer pair films. The maximum contrast of $(PXV/PEDOT:SPS)_{45}$ is $\Delta\%T_{max}$ =

82.1% at 525 nm; this contrast is higher than that of any reported electrochromic polymer film with the exception of one.[4,22] Because of the very wide band absorbance, Δ%T is greater than 50% over the range of 450 nm to 700 nm.

The fact that PXV/PEDOT:SPS can provide a greater contrast than many specially synthesized materials is a testament to the power of the LBL processing technique to provide new high-performance electrochromic composites. We anticipate that elegant monomer design and polymer synthesis efforts to provide water-soluble electrochromic polymers that are capable of aqueous assembly by electrostatic or other forces will broaden the color and performance capabilities of these exciting new LBL assembled composite materials. A combination of new materials design and innovative polymer processing using the LBL assembly process as a means of tailoring these systems will lead to new advancements in this area.

3.2.4 Conclusions from PXV/PEDOT:SPS studies

A new high contrast dual electrochrome composite has been developed based on the LBL assembly of two cathodic electrochromic polymers - PXV, a discrete electrochromic polymer that colors based on charge transfer complex formation, and PEDOT, a conjugated polymer doped with SPS that colors based on the reduction of electronically conducting polaron and bipolaron states. Unlike most LBL assembled films, the PXV/PEDOT:SPS system grows exponentially in thickness with increasing layer pair number, providing smooth and robust films that double in thickness every 10 layer pairs. As the PXV/PEDOT:SPS films become thicker, PXV becomes less electrochemically available and charge-trapping appears where PEDOT controls the PXV oxidation state in the outlying film portions. In contrast to PXV, PEDOT appears to remain redox-accessible even in very thick films. Spectroelectrochemical investigations confirm that both PXV and PEDOT contribute to electrochromic coloration, and additional optical/electrochemical investigation corroborates the charge-trapping effect and also reveals accelerated PEDOT oxidation. These interaction effects do not negatively impact performance and in fact may be positive; charge trapping enhances colored state stability, and accelerated oxidation causes faster electrochromic bleaching.

The performance of PXV/PEDOT:SPS as an electrochromic material was extremely competitive. Color change response times vary depending on metric, but in general range from 1-4 seconds for coloration and bleaching, which is similar to other electrochromic polymers, but slower than the fastest-switching. PXV/PEDOT:SPS provides high contrast, switching between a transmissive light-blue oxidized state to a deeply saturated purple/blue reduced state. The LBL approach provides a convenient means to optimize the polymer film thickness based on layer

pair number, and optimum contrast performance was manifested by $(PXV/PEDOT:SPS)_{45}$, which exhibited a maximum transmittance change of 82.1% at 525 nm, exceeding that of all but one reported electrochromic polymer film to date.

Future directions of this work involve enhancing the response time of LBL assembled electrochromic composites by evaluating the effects of different assembly mechanisms and morphologies. In addition, the LBL method provides a simple processing platform to create complex composites with multiple colored states from assembly of simpler electrochromic films with a single bleached/colored transition. Development in this area will be accelerated with the realization that aqueous solubility and functionality for intermolecular interactions are worthy of consideration by the synthetic polymer chemist regardless of application, because investigators can then avail themselves of this and other similar processing techniques to extend the utility and application of newly synthesized and/or existing electro-optical materials.

3.3 The PANI/PB system

3.3.1 Introduction to PANI/PB

Following the development of a contrast-enhanced, cathodically coloring dual electrochrome from LBL assembly, an anodically coloring dual electrochrome was conceived using an alternative strategy. From the work in Chapter 2 of this thesis, it is clear that PANI and the PB colloid are anodically coloring electrochromic materials that possess opposite ionizable charge and are dissimilarly colored when oxidized. The development of a dual electrochrome electrode based on these two materials was thus pursued, with the intent of achieving multiple colored states within the same electrochromic electrode film.

PANI derives color upon the oxidative doping of the leucoemeraldine state, typically in a low pH environment. The final color that PANI achieves when oxidized ranges from green to blue depending on the ambient pH. PB nanocrystals color to cyan upon oxidation of the clear PW state due to a change in iron center valence from iron (II) to iron (III). It is important to note that PANI passes through an intermediate greenish yellow state while the PB passes through a pale blue intermediate state over the same potential range.

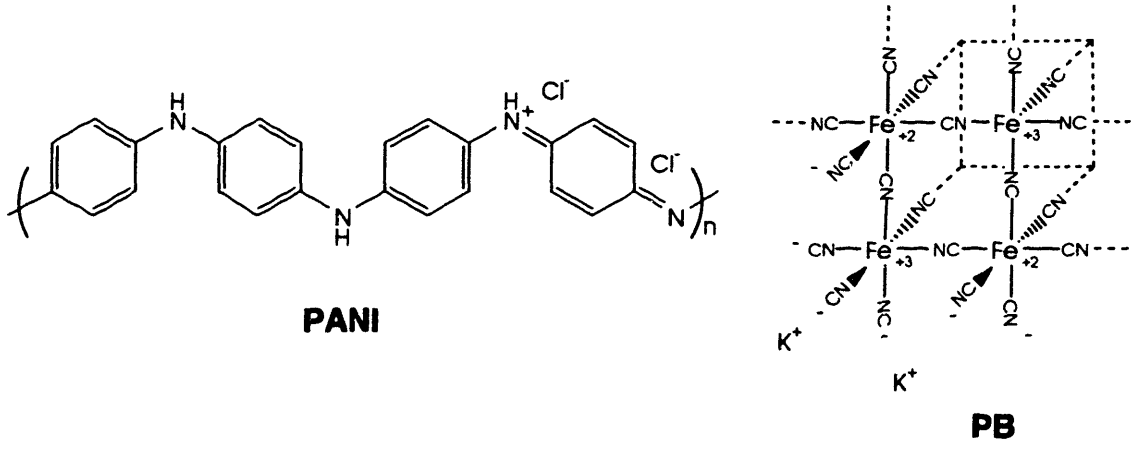

Figure 3.17. Molecular structures of PANI and PB.

Thus from the standpoint of the intelligent design of electrochromic electrodes, this system presents an opportunity: both materials eventually color to blue, but do so by passing through different color states. The combination of these intermediate color states in an electrode should, by virtue of the additive pigment color palette, result in a different intermediate color that neither material possesses by itself. This strategy is illustrated in Figure 3.2. This work is not the first to combine the electrochromic capabilities of PANI and PB; the first example of this combination is most likely that published by Leventis,[24] who was involved with some of the

earliest efforts to commercialize electrochromic displays and devices. Since that publication, there have been several other electrochromism studies examining PANI and PB, most commonly in the fabrication of complete electrochromic cells. In all of these cases, PANI and PB are electrodeposited. Only a few of these examples employ PANI and PB within the same electrode;[24-27] some employ PANI and PB as opposing cathode and anode (respectively) during coloration in a rather curious and low-contrast green-to-blue electrochromic cell scheme.[28,29] In one notable study, Jelle and Hagen determined that the simultaneous or "intermixed" electrochemical deposition of PANI and PB onto a single electrode resulted in superior coloration and stability over a PANI + PB bilayer electrode,[30] a result that provides impetus for the application of the LBL method, which provides far greater control over such intermixing. No description of multihued electrochromism has been put forth in any of this previous work. Thus far there have been no published efforts to combine these two materials in a self-assembled composite, and in fact there have been no efforts to self-assemble PB nanocrystals in a LBL assembled film as was described in the previous chapter of this thesis.

Thus PANI/PB is the first LBL assembled electrochromic electrode of its kind, designed to provide multiple colors at different redox potentials. Results from this study validate the viability of this concept, and suggest that the paradigm might be extended to additional types of electrochromic materials eventually to provide an array of multiply colored electrochromic electrodes that may satisfy the demands of applications such as multiple color display elements or cheap, flexible elements of color-adaptive raiment.

3.3.2 Experimental details for PANI/PB

3.3.2.1 Materials

The electroactive polymer was PANI (Aldrich). Polymer solutions were made using Milli-Q (Millipore deionized, >18.2 Ωcm, 0.22 μm filtered) water, and adjusted to pH 2.5 using HCl. The PANI solution was 10mM with respect to the repeat unit molecular weight. PANI solutions were formulated using a 1:9 dimethylacetamide and water solvent pair as described by Rubner and co-workers.[5,31]

PB was synthesized by the addition of 35 mL of a 0.01 M aqueous solution of $FeCl_2$ (Aldrich) dropwise to a 35 mL solution containing 0.05 M potassium ferricyanide (Aldrich) and 0.05 M KCl. After complete addition, the liquid was vigorously agitated for 1 minute and then immediately subjected to filtration.

Filtration was performed using an Amicon 50 mL volume ultrafiltration apparatus with magnetic agitator. A Millipore membrane with nominal molecular weight cutoff of 3k and

constructed of regenerated cellulose was used in the filtration. Filtrate side hydrostatic pressure was maintained at 50 psi for approximately 48 hours for the elution of at least 1000 mL of permeate. Permeate color was initially yellow, turning to clear after 250 mL of permeate was collected indicating the removal of excess potassium ferricyanide. Absence of any blue hue in the permeate confirmed that no significant amount of PB passed the membrane. The ultrafiltration retentate was used in LBL assembly as collected immediately after filtration, after pH adjustment to pH 2.5 by the addition of 1 M HCl.

ITO-glass substrates with dimensions 0.7 cm × 5 cm (Delta Technologies, 6 Ω/square) were cleaned by ultrasonication in a series of solvents: dichloromethane, methanol, acetone, and Milli-Q water for 15 minutes each, followed by a 5-minute oxygen plasma etch (Harrick PCD 32G) to provide a clean, hydroxyl-rich surface.

3.3.2.2 Assembly

Film assembly was automated with a Carl Zeiss HMS DS-50 slide stainer. The substrates were exposed to PANI solution for 10 minutes, followed by copious water rinsing for 4 minutes in three consecutive Milli-Q water baths, and then exposed to PB dispersion for 10 minutes and again rinsed. This cycle was repeated for the required number of layer pairs.

3.3.2.3 Testing

Electrochemical potential control and current sensing were performed using an EG&G 263A potentiostat/galvanostat. Electrolyte was 0.1 M H_2SO_4, counterelectrode was 4 cm^2 platinum foil, and reference was K-SCE. CV was performed by cycling between 0.6 V and -0.2 V at 0.025 V/s, 0.05 V/s, 0.1 V/s, and 0.2 V/s. DPSCA was performed by stepping between -0.2 V and 0.6 V vs. SCE, with 10 seconds per step and 20 seconds per cycle. Approximately 20 cycles were performed sequentially before the measurement cycle. Films assembled atop ITO were positioned in a quartz cell with electrolyte, platinum working electrode, and SCE. Spectral characterization was performed with a StellarNet EPP2000 concave grating UV-Vis-NIR spectrophotometer with combined incandescent and deuterium lamp sources. For spectroelectrochemistry, potential control was provided by EG&G 263A, with the polymer-coated ITO-glass substrate positioned in a quartz cell and immersed in electrolyte, along with a platinum wire counter electrode, and SCE reference.

3.3.3 Results and discussion for PANI/PB

3.3.3.1 Assembly of PANI/PB.

The PANI/PB films were assembled in a manner identical to the assembly of LPEI/PB films, except for the pH environment, which in this case was maintained at pH 2.5 for both deposition solutions and rinse baths. Proper pH maintenance enhanced the LBL assembled film smoothness and uniformity by ensuring that PANI retained a net positive charge and solubility or semi-solubility in the aqueous media. No destabilization of the PB dispersion was observed at this pH, though greater destabilization in RuP dispersions was observed in attempts to create PANI/RuP films. Subjecting the films to an ultrasonically agitated deionized water rinse after the PANI deposition step further enhanced smoothness; this step was found to reduce film roughness by at least 50%.

The growth of PANI/PB films under these conditions is classically linear as was observed for the growth of LPEI/PB films. The correlation of total film thickness to layer pair number is shown in Figure 3.4. The PANI/PB series shows a linear increase in film thickness of approximately 6.9 nm per layer pair, which is substantially thicker than that of the LPEI/PB series, mostly likely due to the partially charged nature and lesser ionization density of PANI as compared to LPEI. The roughness of this series is slightly higher than that of LPEI/PB most likely for the same reasons. It should be noted that the roughness of PANI/PB remains less than or equal to the ~4 nm depositing particle size that was suspected based on the thickness of the LPEI/PB series. This linear growth indicates the successful combination of the PANI and PB electrochromes without the complications arising from superlinear growth exhibited by systems such as PXV/PEDOT:SPS.

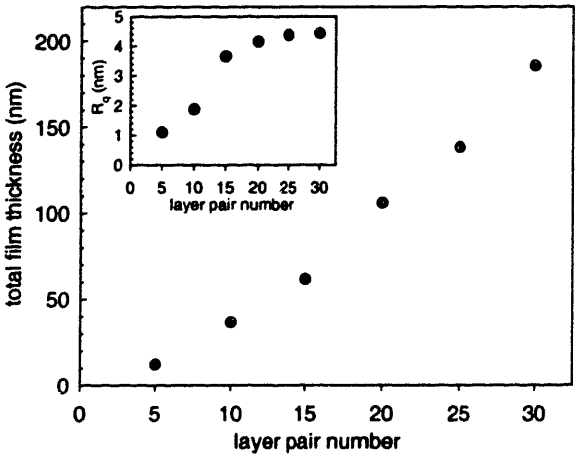

Figure 3.18. Correlation of film thickness to layer pair number for the PANI/PB series.

3.3.3.2 Electrochemistry - cyclic voltammetry.

Cyclic voltammetry (CV) was applied to the PANI/PB system over the same potential range that was used for PANI and PB-containing single-electrochrome films. CVs of some films of the PANI/PB series are shown in Figure 3.19. In general there is an increasing resistance to reduction and oxidation with increasing film thickness, just as for all of the LBL assembled electrochromic films investigated in this thesis. This increasing resistance is reflected by an increasing hysteresis between oxidative and reductive current waves as scan rates increase. In general, however, linearity is maintained between the scan rates and peak heights, indicating that the reaction is not limited by ionic diffusion into the electrode but rather is hampered by internal resistance to redox transfers within the layers. However, the resistance in this case is not nearly as great as that seen in single electrochromes and the PXV/PEDOT:SPS dual electrochrome; this is one of the least resistive systems studied in this thesis. This conclusion is not surprising from the standpoint that there is no redox-inactive material within these LBL assembled films; both PANI and PB are redox-active in this potential range. The resistance that is observed is most likely internal resistance of PB crystals as the redox reactions propagates through the solid matrix. As would be expected, the resistance observed in the PANI/PB composite is far less than that observed in LPEI/PB; the PANI within the matrix appears to greatly facilitate the conduction of electrons throughout the film during oxidation and reduction.

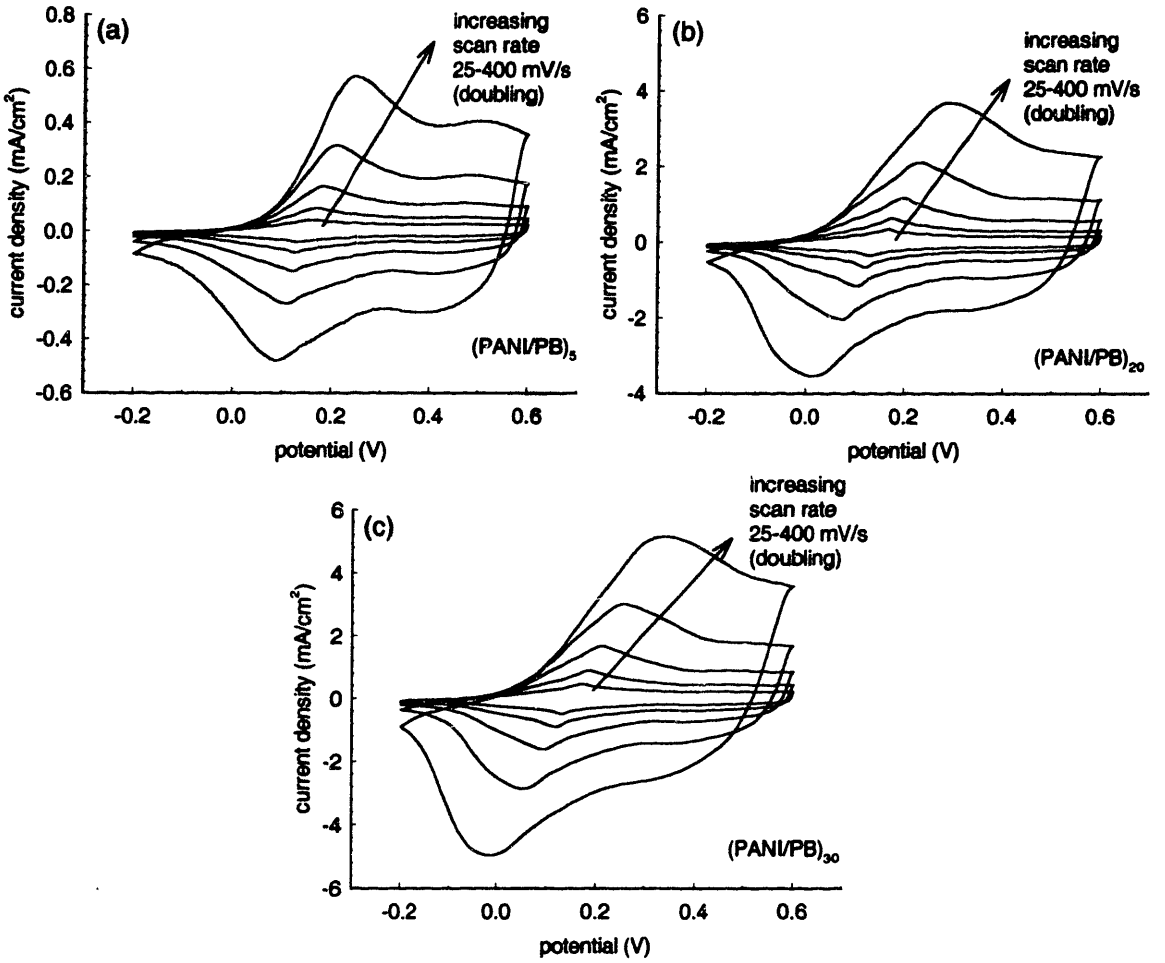

Figure 3.19. Cyclic voltammetry of the PANI/PB series.

Although it is not immediately obvious from the data presented in Figure 3.19, both the PANI and PB electrochemistry are well represented in the CV tests. The reason that both contributions cannot be immediately distinguished is that the electrochemistry for both materials occurs over very similar potential ranges so that the waves for electrochemistry are almost exactly superimposed. This is in direct contrast to the PXV/PEDOT:SPS system, where the electrochemical contributions of each material could be easily separated because of the great separation in formal redox potential of the two components. It is possible to distinguish individual contributions of PANI and PB at slower scan rates; a comparison is offered in Figure 3.20. This figure compares CV scans of the 30-layer pair PANI/PB composite, the 15-layer pair PANI/PAMPS composite, and the 20-layer pair LPEI/PB composite. Individual contributions of PANI and PB within the PANI/PB composite are clearly visible as the nature of the two redox peaks is different. The PANI provides broad reduction and oxidation peaks, with large, sloping shoulders, while the PB provides sharper, better defined peaks. In the scan of the PANI/PB

composite, the sloping broad peaks of PANI dominate the CV *except* at the exact expected potentials of PB electrochemistry, where the PB peaks "emerge" from the broader PANI electrochemistry and become clearly visible. These CV curves are consistent with those produced from earlier studies of PANI+PB electrochemistry, though the deconvolution of individual contributions from this LBL assembled composite are even more clear.[24] This comparison shows definitively that both materials are electrochemically accessible within the LBL assembled film, and both show explicit electrochemical signatures without the creation of unusual effects such as the charge trapping that was observed in the PXV/PEDOT:SPS composite.

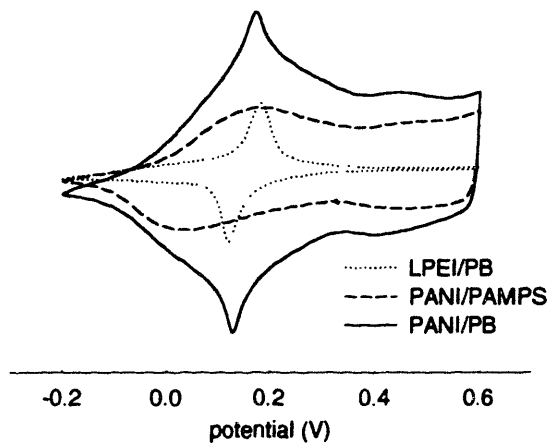

Figure 3.20. Comparison of cyclic voltammetry of the PANI, PB, and the PANI/PB composite at 25 mV/s.

3.3.3.3 Electrochemistry – square wave switching.

Square wave switching was next applied to the PANI/PB composites to determine whether the separate and distinct electrochemistries of PANI and PB remained completely accessible even in very thick films. The potential range of switching was the same as that used for the PANI and PB single electrochrome films. Results of switching are shown in Figure 3.21. As expected, the switching speed as observed by current decay decreases with increasing film thickness. The Faradaic charge density of the films increased extremely linearly with increasing film thickness, indicating that the PANI and PB within the films remain equivalently accessible within PANI/PB films regardless of thickness or layer pair number. From this linear trend, a concentration of 3.9 mmol/cm^3 of redox-active sites can be calculated for the PANI/PB series, which is slightly less than that found for the LPEI/PB series. This would seem to indicate that there is some amount of PANI within the layers that is not electrochemically accessible, especially

considering the high Faradaic charge density found in PANI-containing films in Chapter 2 of this thesis.

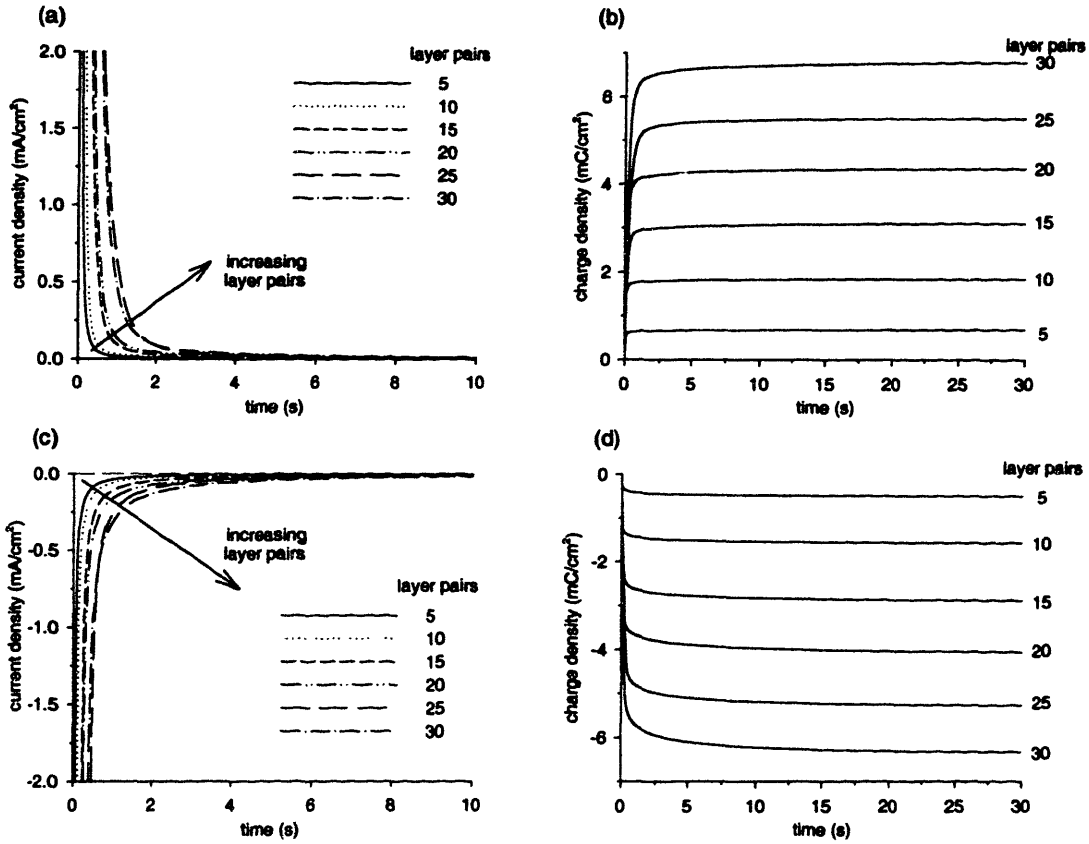

Figure 3.21. Square wave switching of the PANI/PB series.

3.3.3.4 Spectroelectrochemistry.

In Figure 3.22, we present spectroelectrochemistry of the PANI/PB dual electrochrome series. The spectroelectrochemistry shows a complete conversion from a pale yellow, transparent state to a highly colored blue state with a peak absorbance at approximately 750 nm. The absorbance at reducing potentials is not indicative of any electrochemically inaccessible PANI within the layers, as might be expected from the calculation of Faradaic charge concentration. The oxidized state features a very broadband absorbance that increases linearly with film thickness, showing no profound shifts in peak location or spectral character. At an intermediate potential of 0.2 V, the spectrum in Figure 3.22(a), shows absorbance both at 400-450 nm and at broad absorbance at 600-800 nm. These absorbances indicate yellow and blue colorations, respectively; the combination should result in a green hue.

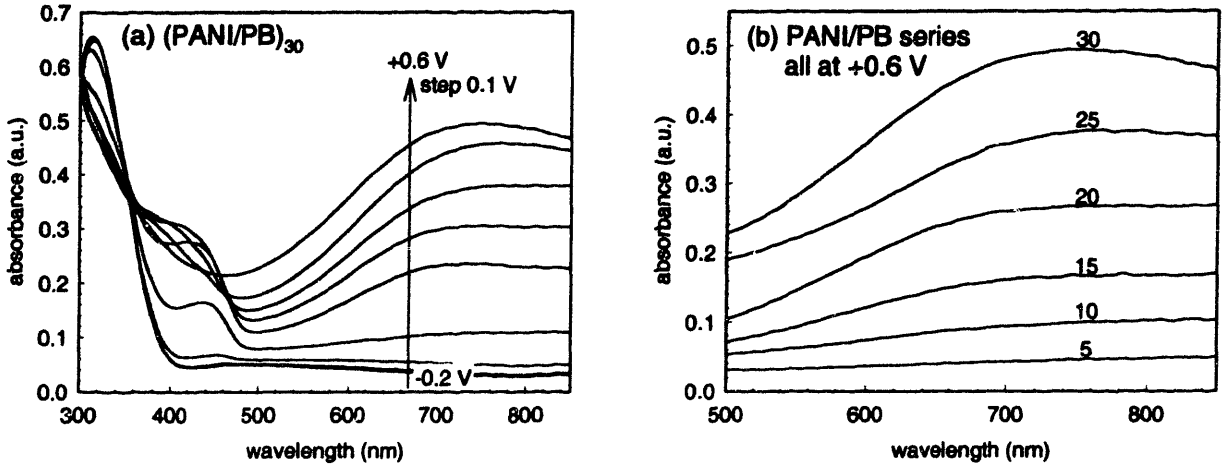

Figure 3.22. Spectroelectrochemistry of the PANI/PB series.

Individual contributions to the absorbance character of these dual electrochrome films can be distinguished from the UV-Vis absorbance spectra of the films in the fully colored, oxidized state. Figure 3.23 offers a comparison of the dual electrochrome absorbance spectrum with spectra of single electrochrome films representative of PANI and PB spectra. The coloration of PANI/PB is clearly the result of the addition of the two chromophores. The characteristic absorbance of PANI at 300 nm is reproduced in the PANI/PB composite, as is the PB peak at 700-800 nm. The PB peak location is red-shifted in the PANI/PB composite due the addition of the PANI shoulder from 600-800 nm. One important aspect of this combination is that PB enhances red absorbance of oxidized PANI relative to blue absorbance, resulting in a darker and truer blue than the usual blue/green PANI hue.

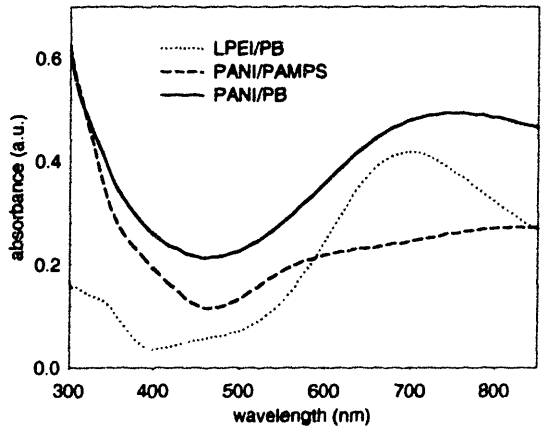

Figure 3.23. Comparison of fully oxidized spectra of PANI, PB, and the PANI/PB LBL assembled film.

As the strong absorbance at 600-800 nm is the sum of PANI and PB coloration, the contributions of each can be determined. From the concentration of redox centers based on the

Faradaic charge uptake of PANI/PB, the extinction coefficient for the oxidized state of this system is 7040 $M^{-1}cm^{-1}$ at 750 nm and 6690 $M^{-1}cm^{-1}$ at 700 nm. From PANI work, a counterpolymer-dependent extinction coefficient of 4260-5570 $M^{-1}cm^{-1}$ at 700 nm was found, with an average of ~4950 $M^{-1}cm^{-1}$. The LPEI/PB system displayed an extinction coefficient of 8020 $M^{-1}cm^{-1}$ at this wavelength. Based on these figures, and assuming that the extinction of PB and PANI are not significantly altered in the dual electrochrome composite as compared to the single electrochrome composite, then the relative coloration contribution of PANI to PB is calculated to be 0.43:0.57, or approximately 0.77 PANI chromophores per PB chromophore. Each PB chromophore is well defined as a single unit cell of a PB nanocrystal, but the chromophore definition is less precise in the case of the PANI conducting polymer where one molar chromophore unit might be distributed over several repeats. A full composition profile cannot be determined without additional information concerning the extent of oxidation or reduction of PANI.

3.3.3.5 Optical switching.

The optical switching of the PANI/PB series can be measured at the peak wavelength of 750 nm with results as shown in Figure 3.24. Based on the square-wave appearance of the spectral response to potential switching, it is clear that PANI/PB series switches extremely fast compared to most of the electrochromic thin films investigated so far in this thesis. Quantification of switching times can be made using the criterion of achieving a change in 90% of the total absorbance span as indicating switching completion. A tabulation of the switching times based on this criterion is shown in Table 2-14. With switching time consistently lower than 1.5 seconds, these films present the fastest switching of any of the LBL assembled electrochrome composites studied in this thesis work aside from PANI-containing single electrochrome composites. The contrast is extremely high for such thin films, especially as compared to the PXV/PEDOT:SPS system, which required films more than twice as thick to achieve similar contrasts. PANI/PB switches far faster than devices incorporating PANI and PB, which appear to switch in 3-120 seconds, though these devices may be slower due to the inclusion of a WO_3 complementary coloring counterelectrode.

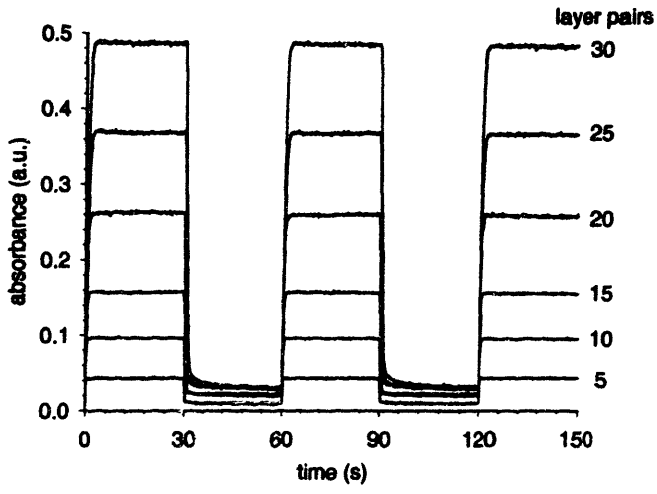

Figure 3.24. Optical switching of the PANI/PB series.

Table 3-3. Switching time and contrast of the PANI/PB series.

layer pairs	color time (s)	bleach time (s)	Δ%T (λ=750 nm)
5	0.31	0.49	8.2%
10	0.66	0.66	15.4%
15	0.90	0.66	26.4%
20	1.15	0.85	39.7%
25	1.58	1.28	55.5%
30	1.62	1.52	61.1%

The coloration in PXV/PEDOT:SPS is demonstrated in Figure 3.14, along with the coloration of PANI and PB single-electrochrome composites. The origins of multiple hue electrochromism are clear upon consideration of these photographs. In the reduced state, both PANI and PB are non-absorbing, resulting in a PANI/PB color that is almost clear. At an intermediate potential of 0.2 V, the PANI composite has a darker yellow color; the strong absorbance at 500-700 nm is not yet apparent at this potential. The PB single electrochrome composite has a pale blue color at this intermediate potential because some, but not all, of the PB within the film is oxidized. The combination of these two intermediate colors results in an intermediate color of almost pure green for the PANI/PB composite, as was suspected based on the two absorbance peaks seen in Figure 3.22(a). This type of additive electrochromism strategy is generalizable, especially with materials such as the conducting polymers that show electrochemical reactions over a very distributed potential range, as the various levels of grayscale for each coloration reaction can be combined with other grayscale colors.

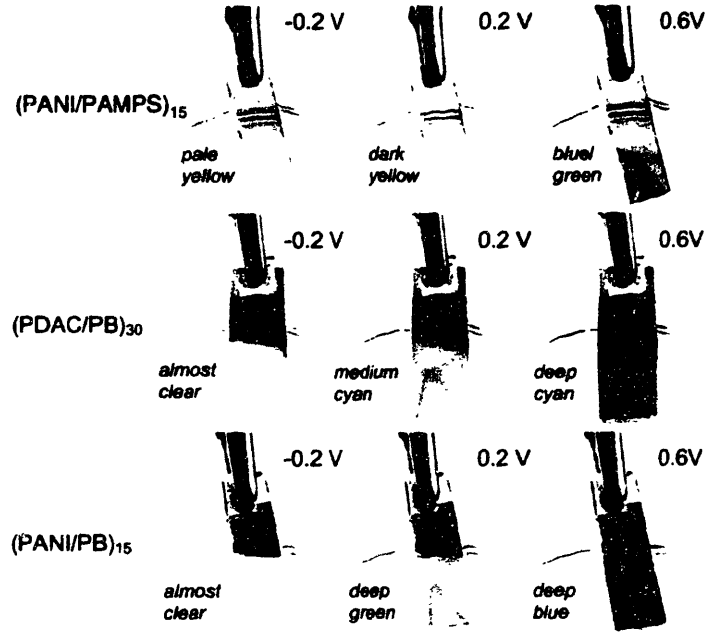

Figure 3.25. Photographs of the electrochromism of PANI/PB and the origins of multiple color electrochromism in this dual electrochrome composite.

3.3.4 Conclusions from PANI/PB studies

A new multiple-hue dual electrochrome composite has been developed based on the LBL assembly of two anodically electrochromic materials - PANI , a conjugated polymer that colors based on the oxidative creation of electronically conducting polaron and bipolaron states, and an inorganic nanoparticle dispersion of PB that colors based on the oxidative change in charge transfer pair from Fe(II)-Fe(II) to Fe(II)-Fe(III). The PANI/PB series grows linearly in thickness with layer pair number, providing extremely smooth films with roughness no greater than 4 nm.

As PANI/PB increases in thickness, both PANI and PB within the layers remain completely electrochemically accessible as indicated by a linear increase in the Faradaic charge capacity with increasing layer thickness. By cyclic voltammetry, the films do become more resistive to electrochemical oxidation and reduction, but in general remain less resistive than most thick redox-active polymer films. Clear contributions from both materials are visible in CV scans of PANI/PB composites at slower scan rates. Spectroelectrochemistry also confirms clear contributions from colored absorbances of both components, and the absorbance of the dual electrochrome film increases linearly with the increase in thickness for this system, indicating no shift of extinction with increasing film thickness. The extinction coefficient of this system was between those of PANI and PB, and allowed a chromophore ratio of PANI:PB to be calculated as 0.77. With information describing the extent of PANI oxidation, an exact composition profile could be calculated from this quantity.

The PANI/PB system was engineered with the expectation of multiple hues due to the different coloration grayscale responses of PANI and PB. This expectation was fully substantiated; the color of the dual electrochrome composite changes from a completely clear reduced state to an intermediate partially oxidized green color to a navy blue fully oxidized color. This result confirms the validity of this strategy for the design of multiple-hue electrochromic electrodes; the technique can be extended to even more useful colors, initially taking advantage of the wide color spectrum of hexacyanoferrate nanoparticle suspensions, and perhaps later extending to differently colored states based on unusual poly(viologens) or water-soluble or dispersable conjugated polymer systems, which have been shown to cover a great color spectrum as well.

Aside from multiple-hue electrochromism, the performance of PANI/PB as an electrochromic material was superior to most other electrochromic films. Color change response times ranged from 0.5 to 1.5 seconds for coloration and bleaching, which is faster than many electrochromic polymers. High contrast is also achievable in these composites, due to the high density of electrochromic material and substantial extinction of each switching chromophore. With these results, the true power of the LBL technique is truly established. From the PXV/PEDOT:SPS work, exceptionally high contrast was realized, while now from the PANI/PB work, multiple colors can be achieved. The LBL assembly technique provides almost limitless possibilities regarding the combination of electrochromic species into intelligently designed composites that can meet a host of applications. This work may impact commercial considerations of electrochromic device construction, as proper application could lead directly to the formation of high contrast and multiple color display elements conceived and constructed via LBL assembly. Extension of the application of these complex electrodes may follow, and it might be envisioned that this technology could impact bio- and electro-catalysis, magnetic storage, and sensing, leading to even more advanced and intricately designed LBL assembled electroactive electrodes in the years to come.

3.4 Cited literature

(1) Zotti, G.; Zecchin, S.; Berlin, A.; Schiavon, G.; Giro, G. *Chem. Mater.* **2001**, *13*, 43-52.
(2) Monk, P. M. S. *The Viologens*; John Wiley & Sons Ltd.: West Sussex, England, 1998.
(3) Groenendaal, B. L.; Jonas, F.; Freitag, D.; Pielartzik, H.; Reynolds, J. R. *Adv. Mater.* **2000**, *12*, 481-494.
(4) Krishnamoorthy, K.; Ambade, A. V.; Kanungo, M.; Contractor, A. Q.; Kumar, A. *J. Mater. Chem.* **2001**, *11*, 2909-2911.
(5) Cheung, J. H.; Stockton, W. B.; Rubner, M. F. *Macromolecules* **1997**, *30*, 2712-2716.
(6) Ruths, J.; Essler, F.; Decher, G.; Riegler, H. *Langmuir* **2000**, *16*, 8871-8878.
(7) Clark, S. L.; Montague, M.; Hammond, P. T. *Supramol. Sci.* **1997**, *4*, 141-146.
(8) McAloney, R. A.; Sinyor, M.; Dudnik, V.; Goh, M. C. *Langmuir* **2001**, *17*, 6655-6663.
(9) Picart, C.; Lavalle, P.; Hubert, P.; Cuisinier, F. J. G.; Decher, G.; Schaaf, P.; Voegel, J. C. *Langmuir* **2001**, *17*, 7414-7424.
(10) Picart, C.; Mutterer, J.; Richert, L.; Luo, Y.; Prestwich, G. D.; Schaaf, P.; Voegel, J. C.; Lavalle, P. *Proc. Natl. Acad. Sci. U. S. A.* **2002**, *99*, 12531-12535.
(11) Lavalle, P.; Gergely, C.; Cuisinier, F. J. G.; Decher, G.; Schaaf, P.; Voegel, J. C.; Picart, C. *Macromolecules* **2002**, *35*, 4458-4465.
(12) Laurent, D.; Schlenoff, J. B. *Langmuir* **1997**, *13*, 1552-1557.
(13) Stepp, J.; Schlenoff, J. B. *J. Electrochem. Soc.* **1997**, *144*, L155-L157.
(14) Farhat, T. R.; Schlenoff, J. B. *Langmuir* **2001**, *17*, 1184-1192.
(15) DeLongchamp, D.; Hammond, P. T. *Adv. Mater.* **2001**, *13*, 1455-1459.
(16) Zhao, B. Z.; Neoh, K. G.; Liu, F. T.; Kang, E. T.; Tan, K. L. *Synth. Met.* **2001**, *123*, 263-266.
(17) Ng, S. W.; Neoh, K. G.; Sampanthar, J. T.; Kang, E. T.; Tan, K. L. *J. Phys. Chem. B* **2001**, *105*, 5618-5625.
(18) Abruna, H. D.; Denisevich, P.; Umana, M.; Meyer, T. J.; Murray, R. W. *J. Am. Chem. Soc.* **1981**, *103*, 1-5.
(19) Hillman, A. R.; Mallen, E. F. *J. Chem. Soc.-Faraday Trans.* **1991**, *87*, 2209-2217.
(20) Caruso, F.; Niikura, K.; Furlong, D. N.; Okahata, Y. *Langmuir* **1997**, *13*, 3422-3426.
(21) Caruso, F.; Furlong, D. N.; Ariga, K.; Ichinose, I.; Kunitake, T. *Langmuir* **1998**, *14*, 4559-4565.
(22) Welsh, D. M.; Kumar, A.; Meijer, E. W.; Reynolds, J. R. *Adv. Mater.* **1999**, *11*, 1379-1382.
(23) Thompson, B. C.; Schottland, P.; Zong, K.; Reynolds, J. R. *Chem. Mater.* **2000**, *12*, 1563-1571.
(24) Leventis, N.; Chung, Y. C. *J. Electrochem. Soc.* **1990**, *137*, 3321-3322.
(25) Jelle, B. P.; Hagen, G. *Sol. Energy Mater.* **1999**, *58*, 277-286.
(26) Jelle, B. P.; Hagen, G.; Birketveit, O. *J. Appl. Electrochem.* **1998**, *28*, 483-489.
(27) Jelle, B. P.; Hagen, G. *J. Appl. Electrochem.* **1998**, *28*, 1061-1065.
(28) Duek, E. A. R.; Depaoli, M. A.; Mastragostino, M. *Adv. Mater.* **1992**, *4*, 287-291.
(29) Duek, E. A. R.; Depaoli, M. A.; Mastragostino, M. *Adv. Mater.* **1993**, *5*, 650-652.
(30) Jelle, B. P.; Hagen, G. *J. Appl. Electrochem.* **1998**, *28*, 1061-1065.
(31) Stockton, W. B.; Rubner, M. F. *Macromolecules* **1997**, *30*, 2717-2725.

Chapter 4. Electrochromic cell employing layer-by-layer electrodes

Contents

Figures

Tables

4.1 Introduction to electrochromic cells

There has been a large interest in the development of low-cost, portable, chromic devices suitable for consumer products, flexible or wearable displays, smart windows, electronic paper, and other applications.[1-3] As the use of information technology continues to grow expansively, the need for smaller, portable displays for new applications has continued to increase. The desire for inexpensive but stable materials systems has led to investigation of liquid crystal displays (LCDs) and organic light emitting diode (OLED) devices. However, LCD's generally provide angle-dependent viewing, and often require a backlight, which adds to weight and energy costs. OLED technology is quickly meeting the needs of many applications for radio, dashboard and other displays; however, these systems often require more expensive, specifically designed organic or polymer systems to achieve performance and stability, and remain most appropriate for small area or high-end products. Electrochromic cells can provide reasonable contrast without angle dependence, backlights or extensive materials synthesis efforts.[4,5] These devices are particularly well-suited to large area displays due to their low power consumption.

Electrochromic cells are full electrochemical cells such as those found in batteries. Thus they contain two electrodes, nominally a cathode and an anode, though these identities can be reversed depending on the cell bias. The two electrodes are separated by an electrolyte that can be a solid or a liquid containing mobile ions. These ions are required to balance the electrochemical reactions on either side of the cell. The electrolyte also functions as a separator for the two electrodes, preventing unwanted discharge or shorting of the cell. Thus the electrolyte must be electronically resistive, while retaining facile ion conduction. The electrodes of the cell can be films of the redox-active, color-changing species, or the color-changing species can be dissolved directly in the electrolyte and the electrodes can be bare electronic conductors. For the purposes of this thesis, only cells supporting solid, electrochromic electrode films were considered. In theory, these devices should feature faster switching as the electrochemical reactions should not be limited by diffusion of the reactive species.

The cathode and anode electrodes of electrochromic cells may be combined in several architectures. One fabrication strategy is to combine a single electrochromic electrode on one side of the cell with a transparent counterelectrode on the other side of the cell. Transparent counterelectrodes can undergo redox reactions to satisfy the ion and electron balances required for the full cell reaction, while not contributing to cell coloration; the oxidized and reduced states of transparent counterelectrodes are both colorless. Some examples of transparent counterelectrodes are found in the transition metal oxides; V_2O_5 is often used for this purpose as

it features reduction intercalation electrochemistry that results in only a very faint bluish coloration.

A more powerful cell fabrication strategy is to combine two electrochromic electrodes in a complementary coloring electrochromic cell. In the complementary configuration, the coloration of both electrodes is harnessed; both color and bleach simultaneously. The cathode and anode of the cell therefore must be very different materials because one must color when oxidized whilst the other must color when reduced. A reversal of the cell bias must result in both materials bleaching. Cells containing complementary coloring electrochromic materials must be fabricated more carefully than those containing single electrochromic materials. The materials must be chosen to have additive coloration and the number of redox sites within each film must be carefully balanced.

This chapter presents a fully functional and switchable electrochromic device in which complementary coloration is achieved from LBL assembled films containing poly(aniline) (PANI) and poly (3,4-ethylenedioxythiophene) (PEDOT). This device was constructed early in the progress of this thesis work to investigate the feasibility of the use of LBL assembly in the creation of films for incorporation into display devices or electrochromic windows. At that time, the PANI and PEDOT films were the only available LBL assembled films with fully characterized electrochromic properties. PANI films feature anodic coloration – that is they color when oxidized, while PEDOT films feature cathodic coloration – that is they color when reduced. Thus PEDOT and PANI are suitable choices as the anode and cathode of a complementary coloring electrochromic device. The general architecture that such a device should possess is shown below, with element thickness exaggerated for clarity.

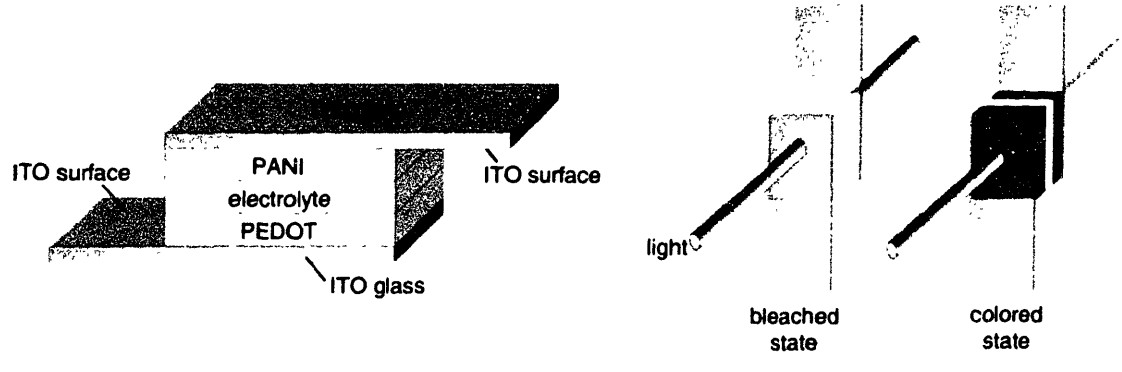

Figure 4.1. Architecture of a complementary coloring electrochromic device employing PANI and PEDOT.

The configuration of the device shown in Figure 4.1 is that of an electrochromic *window* because it should be completely transmissive in the bleached state and absorbing in the colored state. The

most appropriate configuration for an electrochromic display device would be a reflective arrangement, in which one of the transparent ITO glass electrode film supports is replaced with a white, specularly reflective electrode such as roughened aluminum or ITO with adsorbed nanoparticulate TiO_2. The transmissive configuration shown above is most straightforward to characterize and thus was chosen as the most appropriate configuration for prototype work.

Using the LBL technique, the PANI and PEDOT films shown in the display architecture in Figure 4.1 were assembled directly upon ITO glass supports. The selected PANI LBL system was PANI/PAMPS, while the selected PEDOT LBL system was LPEI/PEDOT. After electrode assembly, the device was laminated utilizing a gel electrolyte, hydrated PAMPS, which has found use in several other PANI-containing electrochromic devices. The molecular structures of the component materials in the device are shown in Figure 4.2.

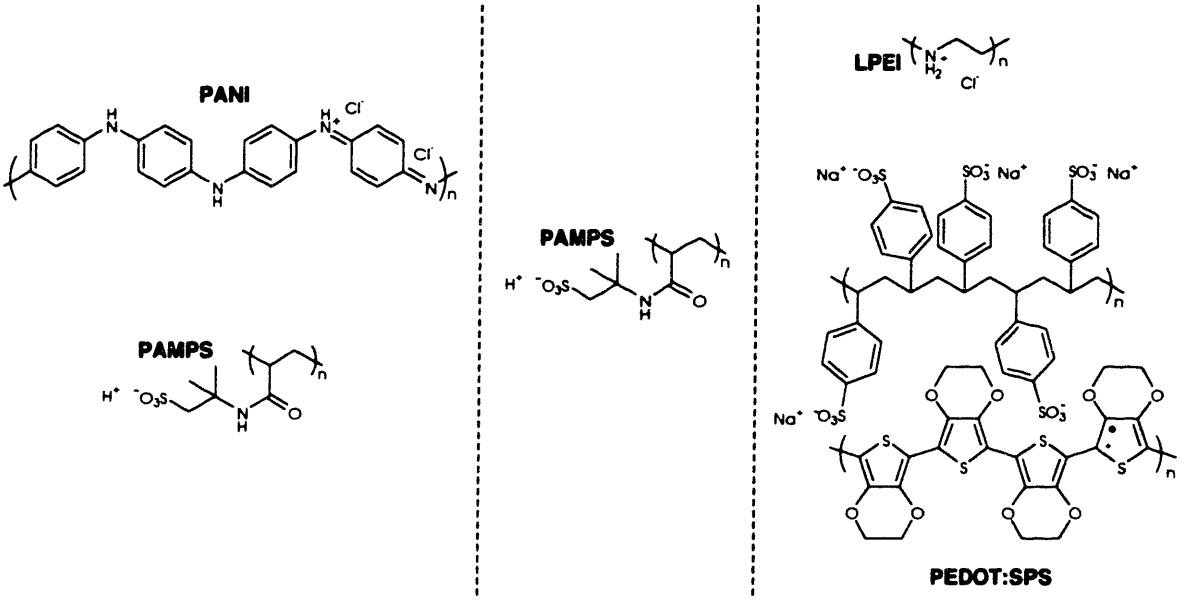

Figure 4.2. Molecular structures of the component polymers in the prototype device.

After fabrication, the device was characterized and performance was assessed. Performance of this device is quite reasonable for a first-generation prototype, and confirms that the LBL assembly method is a viable alternative to traditional electrochromic film-forming techniques for the creation of full electrochromic cells. Results show that the performance of the device is completely commensurate with expectations based on the characterization of single PANI and PEDOT films. It is important to note that this prototype device could be further optimized or extended to contain any of the electrochromic films represented in Chapters 2 and 3 of this thesis. This exercise has been left to future researchers because the result of this work conclusively showed that device performance can be predicted based on single-film behavior and

therefore in most cases device fabrication is not truly necessary except to demonstrate the full power of the technique in the manufacture of high contrast and fast switching electrochromic windows or display devices.

4.2 Experimental

4.2.1 Materials

Polymers included PANI (Aldrich), LPEI (Polysciences), PAMPS (Aldrich), and PEDOT:SPS (BAYTRON P, Bayer Corporation). Polymer solutions were made using Milli-Q (Millipore) water. PANI and PEDOT:SPS solutions were prepared with an aqueous cosolvent including dimethylacetamide at 10 mM polymer as described by Rubner[6] (polymer concentrations with respect to repeat unit). LPEI solutions were 20 mM. PAMPS solutions were 2mM. ITO-glass substrates were cleaned by ultrasonication in surfactant solution and Milli-Q water, followed by a 5-minute oxygen plasma etch (Harrick PCD 32G). Gold milli-electrodes were prepared by evaporating 99.99% gold shot (American Metals) through a shadow mask onto polyolefin plates.

4.2.2 Assembly

Film assembly was automated with a modified Carl Zeiss HMS DS-50 slide stainer. The substrates were dipped in polycation solution for 15 minutes, rinsed for 4-minutes in Milli-Q, and then dipped in polyanion solution for 15 minutes and then rinsed again. This cycle was repeated 20 times for 20 bilayers. Polymer electrolyte was prepared by casting PAMPS from aqueous solution that had been adjusted to pH 3 using lithium hydroxide. PAMPS films were equilibrated at 65% relative humidity. Electrodes were then pressure laminated. Devices were stored at 65% RH.

4.2.3 Characterization

Film thickness was measured by Tencor profilometer. Cyclic voltammetry and chronocoulometry were performed using an EG&G 263A potentiostat/galvanostat. Assembled devices were electrically characterized using the EG&G 263A in two-electrode configuration with a sense electrode. Devices were optically characterized using an Oriel UV-Vis spectrophotometer with a 1200 L/mm, 300 nm blaze Oriel grating and InstaSpec IV CCD, with grating angle adjusted manually for full range.

4.3 Results and discussion

4.3.1 Description of component films

The component films of the device were assembled as described in Chapter 2 of this thesis. Two sets of electrochromic electrodes were assembled for cell fabrication; one set of 20-layer pair electrodes and one set of 40-layer pair electrodes. Because the fabrication of these cells was performed earlier in the timeline of this thesis, there existed some differences in assembly conditions from the work described in Chapter 2. Importantly, the LPEI/PEDOT:SPS films assembled for use in this device were fabricated at pH 5 rather than pH 4, which resulted in a thinner film–the 20-layer pair LPEI/PEDOT:SPS film has a thickness of 168 nm at pH 5, which is closer to the expected thickness of a 15-layer pair LPEI/PEDOT film at pH 4. The 40-layer pair film at pH 5 is slightly more than double the 20-layer pair thickness at pH 5, indicating that the superlinear growth regime is still present at this assembly pH condition. This condition was later refined to produce the films described in Chapter 2. This refinement focused on decreasing the roughness of the films, which for these early LPEI/PEDOT:SPS films (assembled at pH 5) was approximately 10% of the total film thickness.

Despite the small difference in assembly conditions, there appeared to be no significant differences in terms of UV-Vis absorbance spectra or electrochemistry between these films and the PANI and PEDOT LBL assembled films described in Chapter 2, aside from the absolute magnitude of electrochemistry and absorbance as regulated by the thickness of the electrochromic LBL assembled films.

4.3.2 Device fabrication and testing

The two LBL assembled electrochromic electrodes were separated by a film of a proton-conducting polyelectrolyte, PAMPS, at 35% water content, ca. 200μm thick. PAMPS at this water content is a clear, gel-like solid. The cells were bracketed by ITO-glass plates, so that, when bleached, the devices would be optically transparent windows as shown in Figure 4.1. In electrochemical cell notation, these cells would be described as:

$(PANI/PAMPS)_{20}|PAMPS \cdot H_2O|(LPEI/PEDOT:SPS)_{20}$ - hereafter $Cell_{20}$

$(PANI/PAMPS)_{40}|PAMPS \cdot H_2O|(LPEI/PEDOT:SPS)_{40}$ - hereafter $Cell_{40}$

These cells can be considered solid state, with the exception of water plasticization in the solid PAMPS electrolyte gel.

4.3.2.1 Device electrochemistry – cyclic voltammetry

These cells operate by simultaneous oxidation of one electrochromic element and reduction of the other. Considering that the redox-active polymers are doped with immobile polyacids in these devices, protons or lithium cations are expected to shuttle between SPS and PAMPS; such an operation mode is unusual for electrochromic devices consisting of conjugated polymers, as mobile ions are more typically anions associated directly with conjugated polymers species *as* dopants rather than cations associated with an immobile dopant.

The character of cell electrochemistry was investigated using cyclic voltammetry (CV). Some expectations can be formulated considering single-film behavior. From CV work in Chapter 2, PANI and PEDOT films proved to have large peak hystereses indicating a lack of electrochemical reversibility. However, the average of the reduction and oxidation peaks $E_{1/2}$ may still be regarded as nearly equivalent the formal reduction potential $E^{o'}$ for the purposes of cell potential estimation. Thus PANI/PAMPS has an reduction potential of ~0.15 V while LPEI/PEDOT:SPS has a reduction potential of ~0.05 V, both vs. K-SCE. The full cell then has a formal cell potential based on half-cell potentials as follows:

$$E_{cell} = E_{red}(cathode) - E_{red}(anode)$$

As PANI has a more positive reduction potential (e.g. the free energy required to reduce oxidized PANI under standard conditions is less than that required to reduce oxidized PEDOT), the PANI electrode serves as the nominal cathode. The formal potential of the cell is thus ~0.1 V. When the cell is biased at 0.1 V or more positive potentials (as measured from the PANI electrode), then the cell should color, with PANI oxidizing and PEDOT reducing. When the cell is biased at negative potentials, then the cell should bleach with PANI reducing and PEDOT oxidizing. An alternative description of this cell is that when PANI is primarily oxidized and PEDOT is primarily reduced, the device behaves as a *galvanic cell* producing power at a potential of 0.1 V. Applying a more negative potential across the cell hastens "discharge" bleaching of this cell, though bleaching could also be accomplished by simply shorting the cell. When PANI is oxidized and PEDOT is reduced, the device behaves as an *electrolytic cell* that requires power at a potential of greater than 0.1 V for "recharge" coloration.

Cyclic voltammetry of $Cell_{20}$ shown in Figure 4.3 exhibits broad current peaks consistent with the estimation of formal cell potential. In particular, a peak indicating the onset of cell recharge can be seen in the anodic scan at small positive potentials. It was observed that crossing this potential peak was accompanied by visible color increase. In a sacrificial device, a second

peak was apparent at 0.85 V, corresponding to the oxidative degradation of PANI discussed earlier in Chapter 2. In order to accelerate device switching while avoiding PANI degradation, we chose an operating cell overpotential of ± 0.8 V.

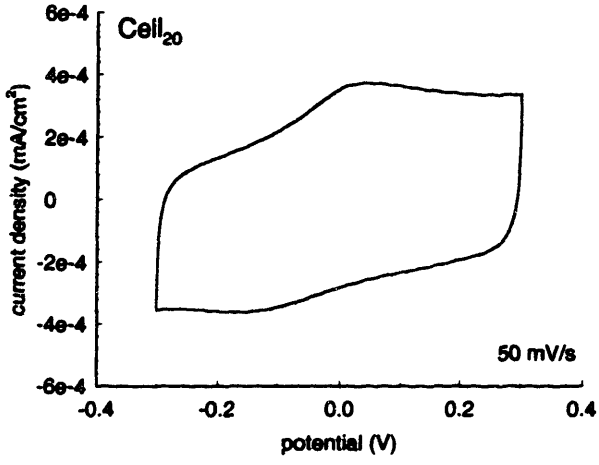

Figure 4.3. Cyclic voltammetry of Cell$_{20}$

4.3.2.2 Device electrochemistry – square wave switching

Square wave switching reveals an important area for cell optimization. The current and charge density profiles for cell switching between the overpotential values of ± 0.8 V are shown in Figure 4.4. Slower current decay in Cell$_{40}$ indicates slower switching, not unexpected for films of greater thickness and more resistivity. A critical optimization theme is revealed when considering the full Faradaic charge capacity of each cell, which is directly analogous to the number of redox reactions taking place within. The injected/removed Faradaic charge density was 0.69 mC/cm^2 for Cell$_{20}$ and 0.92 mC/cm^2 for Cell$_{40}$. By comparison, a (PANI/PAMPS)$_{20}$ film has charge density of 3.3 mC/cm^2 while a (LPEI/PEDOT:SPS)$_{20}$ film assembled at pH 5 would have a capacity of 0.49 mC/cm^2. Clearly the charge density of Cell$_{20}$ more closely resembles that of the PEDOT LBL assembled electrode film. Thus device switching is bounded by the smaller amount of PEDOT, which is essentially the limiting reagent in a balanced electrochemical reaction. As the PEDOT is present in only a small amount due to the low loading of PEDOT that has been established in these films, then there is a much more shallow switching extent than might otherwise be observed. Ideally, the charge capacity of the two electrochromic films should be equal, and the capacity of the device should be that capacity. Future attempts to create devices should leverage the capabilities of the LBL technique to vary the number of layers, and composition of each layer, to improve charge capacity balance.

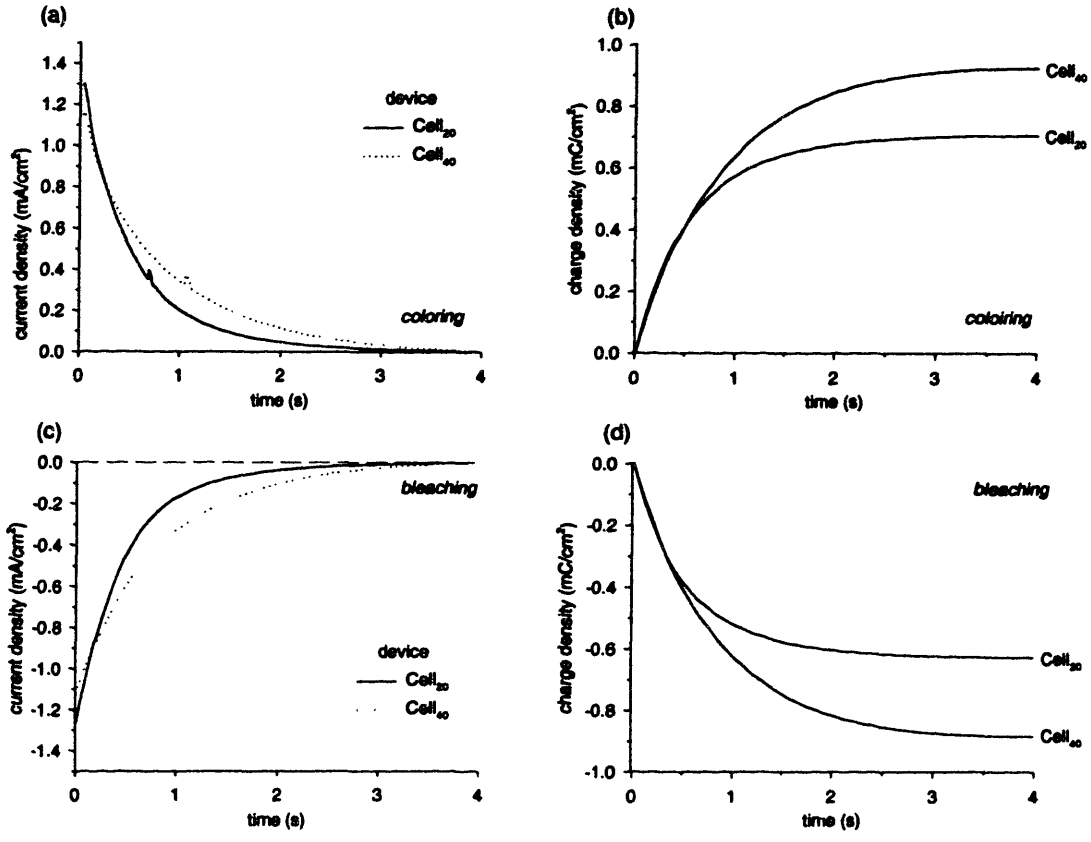

Figure 4.4. Square wave switching of $Cell_{20}$ and $Cell_{40}$

It is important to note that because switching of the device is limited by the small PEDOT present, then there remains a significant amount of PANI within the device that cannot undergo electrochemical reaction to either a completely oxidized or completely reduced state. Inaccessible PANI, which may be as much as 80% of the PANI present in the device, must remain in the intermediate state assumed by freshly LBL assembled PANI films. From observations made during device assembly and extensive work with single PANI films, the intermediate state appears to resemble a combination of leuoemeraldine and emeraldine PANI, with a greenish-yellow coloration that is lighter in color than blue/green fully oxidized PANI and darker than pale yellow fully reduced PANI.

4.3.2.3 Device spectroelectrochemistry

The spectroelectrochemical properties of the devices were characterized by inserting the device in a collinear beam of white light and measuring the absorbance of the cells as compared to a reference cell that contained only ITO glass and electrotrolyte. In general, this characterization method proved successful for cell evaluation. From the spectroelectrochemistry of $Cell_{20}$, the individual contributions of PEDOT and PANI can be ascertained. A comparison is

shown in Figure 4.5 to deconvolute these contributions. The bleached state absorbance exhibits an absorbance peak due to leucoemeraldine PANI at about 350 nm, and a strong influence from the PEDOT film is especially notable as a linearly increasing absorbance from 500 to 800 nm. This linearly increasing absorbance in the bleached state is due to the polaron absorbance shoulder in oxidized PEDOT that was described in Chapter 2.

Notably, the leucoemeraldine PANI peak at 350 nm is lower than expected for bleached $Cell_{20}$, while absorbance between 500-800 nm is higher than expected. In addition, a peak shoulder is clearly visible at approximately 450 nm. The presence of these features in the bleached spectrum is consistent with the hypothesis that not all of the PANI within the cell can be accessed. Unbalanced PANI remains primarily in its native mixed state, and contributes to excessive coloration in the nominally bleached state of the device, hampering contrast performance. This hypothesis is further supported by the appearance of a peak at 450 nm in the bleached $Cell_{20}$ spectrum, which is a spectral signature of yellow-green, emeraldine salt PANI, often observed at intermediate potentials in PANI spectroelectrochemistry (see for example the PANI/PB system in Chapter 3).

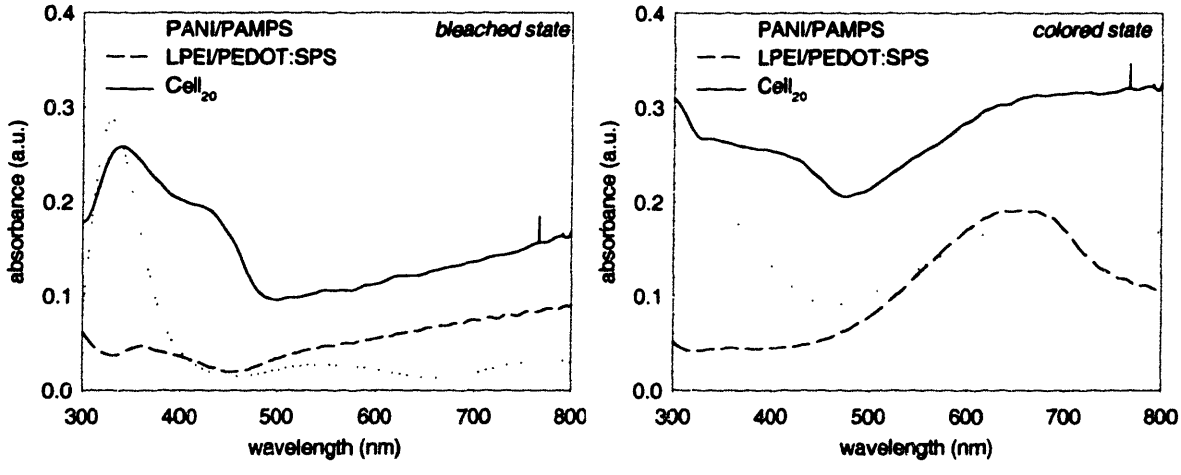

Figure 4.5. Comparison of $Cell_{20}$ spectroelectrochemistry with that of single films.

The colored state absorbance of $Cell_{20}$ clearly results from the combination of PANI and PEDOT colored states. Absorbance between 300 and 450 nm is due to the PANI emeraldine salt form, while the broad absorbance at 600-800 nm is due to a combination of the PANI emeraldine absorbance and the undoped PEDOT absorbance. The combination of absorbance results in no truly distinct peak but rather broadband absorbance over the entire red sector of the visible spectrum. Notably, the colored absorbance of the device is slightly less than might be expected from full oxidation of both component films. This observation is again consistent with the

hypothesis that some PANI within the device is inaccessible due to charge balance issues, and remains in the native intermediate state throughout switching. Absorbance in both the colored and bleached states for $Cell_{40}$ is approximately doubled as shown in Figure 4.6.

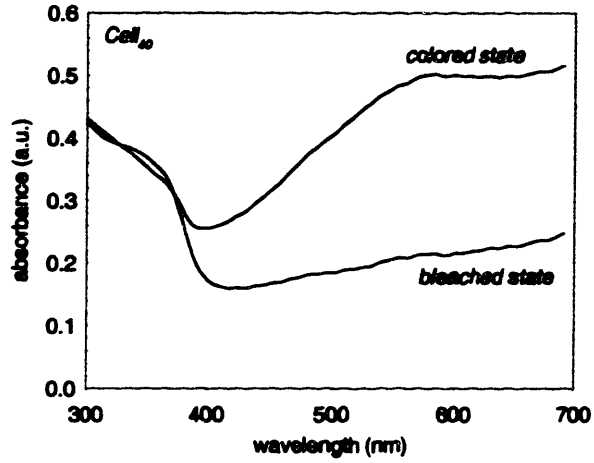

Figure 4.6. $Cell_{40}$ spectroelectrochemistry.

Based on the spectroelectrochemistry, the device contrast can be directly calculated. The maximum contrast for $Cell_{20}$ was reached between 650nm and 670nm, with a Δ%T at these wavelengths of 24%. $Cell_{40}$ had increased contrast, with a maximum contrast between 640nm and 680nm and Δ%T at these wavelengths of 30%. Although these contrasts are reasonable, they are far below the maximum contrasts observed for many individual films studied in this thesis (especially the high-contrast, dual electrochrome films), and are not substantially greater than what might be observed for the single component films that make up $Cell_{20}$ and $Cell_{40}$. Contrast is reduced because complementary films within an electrochromic cell exhibit additive absorbance in their bleached states, leading to excessive light absorbance. Additive residual absorbance greatly diminishes the overall contrast that can be achieved. A simple calculation can be performed to elucidate this matter:

Table 4.1. Calculation of the loss of contrast with residual coloration in the bleached state.

	films with absorbance:		one film	two films
Δabs	bleached	colored	Δ%T	Δ%T
0.25	0.01	0.26	43%	65%
	0.10	0.35	35%	43%
	0.50	0.75	14%	7%
0.50	0.01	0.51	67%	86%
	0.10	0.60	54%	57%
	0.50	1.00	22%	9%
1.00	0.01	1.01	88%	95%
	0.10	1.10	71%	62%
	0.50	1.50	28%	10%

The calculation results shown in Table 4.1 consider hypothetical devices that have one electrode or two electrodes performing identically. Absorbances in the bleached and colored states are shown for these electrodes, and the transmittance contrast, which is best correlated to the sensitivity of the human eye, is indicated for single films (correlating to solution testing or a device with a single electrochromic electrode) and double films (correlating to a complementary device). For a constant change in absorbance, the transmittance contrast decreases with increasing residual coloration. A point can be reached where the single electrochrome configuration displays greater contrast than the complementary configuration. Thus the complementary coloring electrochromic device is not necessarily the most gainful configuration for electrochromic electrodes, if there be significant coloration in the bleached state. It should be noted that bleached state coloration can arise from many sources, including electrode supports and electrolyte. If these contributions are not "referenced out," during evaluation then the measured contrast will be even lower. Electrochromic device construction should not focus on adding increasing coloration, but must consider even more important the removal of unwanted color.

4.3.2.4 Optical switching

Despite unwanted coloration in the bleached state, the contrasts of $Cell_{20}$ and $Cell_{40}$ are easily sufficient to be seen by the human eye. A photograph of the electrochromism of $Cell_{40}$ is shown in Figure 4.7. As depicted in the photograph, the cell reversibly switched between a deep blue-green colored state and a yellow bleached state. The bleached state does appear to have significant residual coloration, especially as compared to photographs of bleached PANI and PEDOT films as shown in Chapter 2. However, the blue-green colored state is highly absorbing and the contrast between the two states may be sufficient for a simple display.

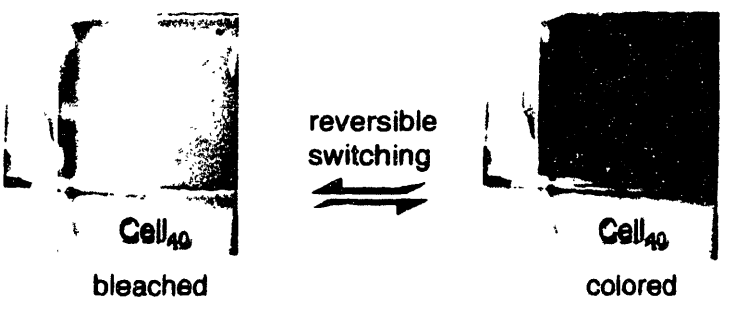

Figure 4.7. Photograph of $Cell_{40}$ electrochromism (get enhanced contrast one from somewhere).

Cell stability and switching times were competitive with other solid-state electrochromic devices. $Cell_{20}$ retained visible switching for over 35,000 deep coloring/bleaching cycles, though the exact contrast retained was not assessed. Switching time was evaluated by real-time UV-Vis spectrophotometry while applying a ± 0.8 V overpotential square wave to the device. The response at a 660 nm wavelength is shown in Figure 4.8. Switching time was defined as the time required to achieve 90% of the desired response. Based on this criterion, $Cell_{20}$ had a bleaching time of 0.8 seconds and a coloring time of 2.3 seconds. Faster bleaching is expected because the bleaching process represents "discharge" of the cell to its lowest free energy state. $Cell_{40}$ had a bleaching time of 1.3 seconds and a coloring time of 2.8 seconds. Although additional layers in $Cell_{40}$ enhanced the optical contrast, switching speed suffered due to hindered ion and electron transport in the thicker electrochromic films.

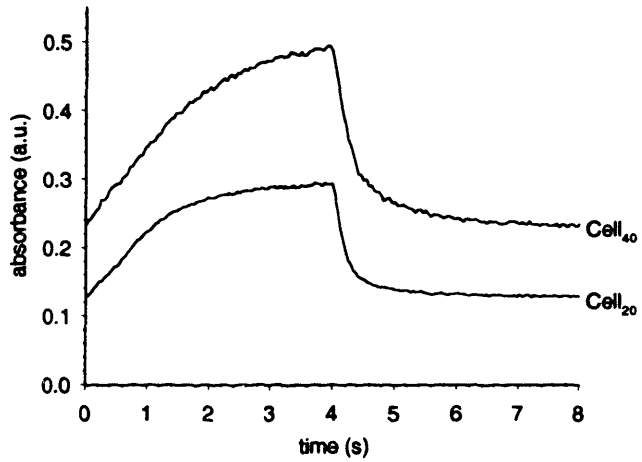

Figure 4.8. Square wave switching of $Cell_{20}$ and $Cell_{40}$ at 660 nm.

The switching times for both cells are on par with the individual film switching times for PANI LBL assembled films and are significantly faster than the switching times determined for PEDOT LBL assembled films. Enhancement in switching speed is most likely related to the presence of the solid PAMPS electrolyte near the PEDOT film. Because PAMPS was solution-cast directly upon an already-assembled PEDOT LBL assembled film, it is possible that there was some commingling of PAMPS with the LPEI/PEDOT:SPS matrix, especially because PAMPS gel was formulated at pH 3, while LPEI/PEDOT:SPS was assembled at pH 5. When exposed to lower pH PAMPS gel, LPEI should further ionize, with new cationic sites becoming available for ionic crosslinking with PAMPS. As demonstrated in the next chapter of this thesis, the LPEI/PAMPS complex is highly ion conducting even at intermediate hydration levels. Enhanced ionic

conduction from LPEI/PAMPS may accelerate switching of the thinner, typically more resistive LPEI/PEDOT:SPS films that were employed in this full cell study.

4.4 Conclusions

In summary, working electrochromic devices have been constructed for the first time with two complementary chromic layer-by-layer polymer systems. Initial results are promising, indicating that highly stable, uniform films can be incorporated into full electrochromic cells that switch between colored and bleached states in under 3 seconds. The cells have been shown to undergo over 35,000 cycles without failure utilizing a PAMPS/H_2O electrolyte. These results introduce a viable and potentially lucrative electrochromic device fabrication method to the field, which can be applied to a number of electrochromic materials. The speed and high stability of the devices make them good candidates for smart windows or large area, long term displays. The contrast in these devices is not optimal, particularly in comparison with the high contrast dual electrochromes that have been developed in this thesis; however, by changing the electrochromic system and fine-tuning the bilayer number, we expect that such performance could be achieved in full electrochromic cells.

These results serve to provide a template for the design of electrochromic devices by combining the various electrochromic electrodes that have been developed during the course of this thesis work. Because the devices examined in this chapter performed as expected considering the electrochemical and spectral properties of the component films, further device work is not truly necessary. If there is a requirement for a device to serve a particular application or to contain particular electrochromic elements, then the results gained within this chapter should provide a framework for device construction and analysis. Future incorporation of LBL engineered electrochromic electrodes into single-film or complementary arrangements should result in extremely high contrast and fast switching devices appropriate for use as solar windows, static electrochromic signage, and perhaps even dynamic displays.

4.5 Cited literature

(1) Dagani, R. *Chem. Eng. News* **2001**, *79*, 40-43.
(2) Seeboth, A.; Schneider, J.; Patzak, A. *Sol. Energy Mat. Sol. Cells* **2000**, *60*, 263-277.
(3) Green, M. *Chem. Ind.* **1996**, *17*, 641-644.
(4) Monk, P. M. S.; Mortimer, R. J.; Rosseinsky, D. R. *Electrochromism: Fundamentals and Applications*; Weinheim: New York, 1995.
(5) Mortimer, R. J. *Electrochim. Acta* **1999**, *44*, 2971-2981.
(6) Cheung, J. H.; Stockton, W. B.; Rubner, M. F. *Macromolecules* **1997**, *30*, 2712-2716.

Chapter 5. Layer-by-layer assembled polymer electrolytes

Contents

Figures

Tables

5.1 Introduction to LBL assembled polymer electrolytes

Solid polymer electrolytes are rapidly attaining notoriety as high-performance materials for a wide range of applications. The industrial manufacture of batteries (including fuel cells), sensors, and electrochromic devices increasingly employs solid polymer electrolytes because they feature easier processing, enhanced chemical compatibility, and better mechanical properties over liquid electrolytes. The development of these materials focuses on increasing ionic conductivity while maintaining favorable mechanical and chemical properties,[1] which leads to higher battery power density and faster electrochromic film switching speeds. Applying new materials and processing techniques has been a successful strategy for enhancing polymer electrolyte performance.

Just as for electrochromic electrode films, the LBL technique offers unique advantages for the design and development of ionically conductive films for use as solid polymer electrolytes. LBL assembled polymer films are inherently amorphous solids with superior mechanical properties to gels and crystalline solids – they do not flow or easily deform, yet remain flexible. They can be applied very thin and defect-free, which can lead to thinner solid electrolytes in devices, increasing the overall conductance of the electrolyte layer. Unlike roll-casting, solvent-casting, or spin-coating, the LBL technique can uniformly coat nonplanar surfaces, allowing for a diverse range of cell geometries. Finally, LBL assembled films can be easily tailored on the nanometer scale to create composition gradients or surface passivation, incorporating a wide variety of materials to achieve chemical compatibility and high performance.

This chapter addresses the directed fabrication of polymer electrolyte films using the LBL processing technique. The first section of this chapter includes an examination of the properties of electrostatically LBL assembled films of several systems chosen specifically to achieve high ionic conduction levels. The second section of this chapter involves the exploration of hydrogen bond LBL assembled systems that feature weaker crosslinks and therefore can potentially possess greater short-range segmental mobility and thus faster ion conduction. Together these sections represent the first effort to directly engineer enhanced ionic conductivity in LBL assembled films. The results gained from these studies indicate that high performance polymer electrolytes can indeed be fabricated utilizing the LBL assembly process, and key directions can be identified to further develop the capabilities of these new composite films.

5.2 Electrostatically LBL assembled polymer electrolytes

5.2.1 Introduction to electrostatically LBL assembled polymer electrolytes

Despite the many potential advantages of the LBL assembly of polymer electrolytes, early ionic conductivity results for electrostatically LBL assembled films were disappointing. The dielectric and ion conduction properties of LBL assembled films were first investigated by Durstock and Rubner,[2] following limited earlier studies on cast polycation/polyanion complexes.[3,4] The first LBL investigation evaluated films of poly(allyl amine hydrochloride) (PAH) with poly (styrene sulfonate) (SPS) and poly(acrylic acid) (PAA). These composites demonstrated ionic conductivity with a maximum of 2×10^{-7} S/cm at room temperature and high hydration,[2] which is too low for most electrochemical applications. The low ionic conductivity of typical electrostatically LBL assembled films can be explained using the general relation:

$$\sigma = \sum_{i=1}^{\text{all ion types}} n_i q_i \mu_i \qquad \textit{Equation 1}$$

where i is the ion type, σ is ionic conductivity, n is the number of mobile ions, q is the ion charge, and μ is the ion mobility. The ion number and mobility are potentially limited by the LBL assembly technique.

The limited number of mobile ions is due to the large extent of polyion pairing and rejection of residual small ions from the LBL assembled film bulk, which is especially notable in strong polyion systems such as poly(diallyl dimethyl ammonium chloride) (PDAC)/SPS.[5] In general, an electrostatically LBL assembled film *cannot* contain as many dissociable small counterions as a neat film of either polyion, which would contain one counterion per monomer unit. In addition, hydrophobic aspects of common model polyelectrolytes such as PAH, PDAC, or SPS limit the potential for residual or added salt to dissolve into the film.

Limited mobility is due to an inherently high crosslink density, which has been shown to decrease ionic conductivity in polyether networks.[6] The underlying mechanism of such poor conductivity is the constraint of small-segment polymer dynamics, which are widely recognized as being coupled to ion mobility.[7] Furthermore, each ion pair within a LBL assembled film can behave as a "coulomb trap," slowing migration by temporary association with the migrating ion.

This work addresses the design of LBL assembled films with high ionic conductivity by maximizing small ion concentration and minimizing crosslink density. The first design step was the choice of the polycation linear (polyethylene imine) (LPEI). LPEI is a hydrophilic, hard Lewis base with high donicity that can solvate hard Lewis acids such as alkali metal cations and

has been employed as a polymer scaffold in several polymer electrolytes.[8,9] In addition, the crosslink density in LPEI-containing films can be modulated by adjusting assembly pH. LPEI was paired with three polyacids to create three LBL assembled polymer electrolyte composites (Figure 5.1). The first polyacid chosen was Nafion, which was employed because of its well-known proton conduction through hydrophilic pores. The second polyanion chosen was poly(2-acrylamido-2-methyl-1-propanesulfonic acid) (PAMPS), a hydrophilic sulfonic acid commonly used in electrochromic devices, which was chosen to increase polymer matrix dielectric constant and plasticity. Finally, to increase the number of mobile counterions, the weak polyelectrolyte PAA was used under acidic conditions, so that it would remain partially protonated.[2,10,11]

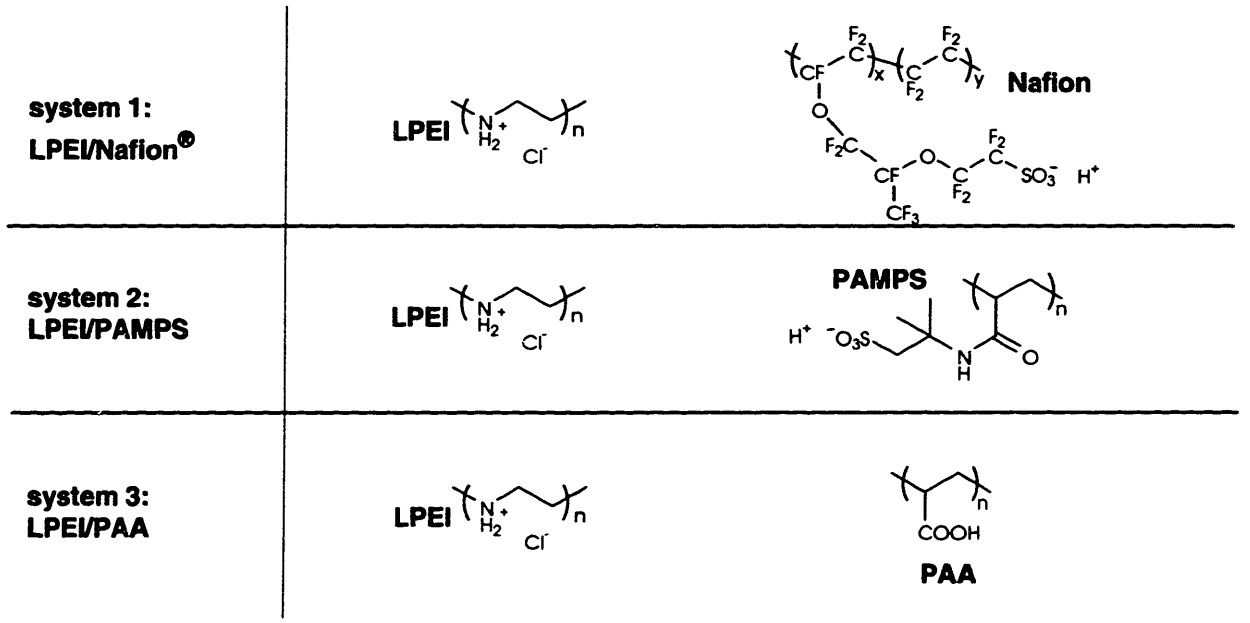

Figure 5.1. The three electrostatically LBL assembled polymer electrolyte systems assembled and tested in this section.

These three composites were optimized by varying assembly conditions and assessing effects on film thickness and ionic conductivity. For strong polyacid systems LPEI/Nafion and LPEI/PAMPS, the effects of ionic screening of the assembly solution were evaluated. Adding salt to polyelectrolyte systems causes deposition in thicker, loopy layers, a phenomenon termed screening enhanced adsorption.[12-15] The ionically screened morphology may be more plastic or less crosslinked than the extended and flat adsorbed state attained in the absence of added small ions. For the weak polyelectrolyte system LPEI/PAA, pH effects were studied. Modulating assembly pH can influence film composition as well as morphology and crosslink density, due to changes in degree of ionization with pH.[10,11] Using this pH modulation, films with differing

relative amounts of LPEI and PAA can be assembled, and relative contributions to ionic conductivity can be assessed.

In addition to the polymer matrix improvements, an easily dissociable salt with a low lattice energy and delocalized anion charge ($LiCF_3SO_3$)[16,17] was added into already-assembled films to provide additional mobile species. Using these comprehensive design strategies, LBL assembled films with strongly enhanced ionic conductivity were developed. Moreover, clear future development directions were ascertained, so that the high ionic conductivity and applicability of these materials might be even further extended.

5.2.2 Experimental details for electrostatically LBL assembled polymer electrolytes

5.2.2.1 Materials.

The polycation LPEI (25,000 M_w, Polysciences, Inc.) was used as-received as were polyanions PAA (90,000 M_w, Polysciences), PAMPS (Aldrich), and Nafion 117 (Fluka). The polyelectrolytes were dissolved in MilliQ-filtered deionized water and then pH adjusted with dilute HCl or NaOH solutions. PAMPS solutions were 0.002 M; PAA and LPEI solutions were 0.020 M (polyelectrolyte concentrations are with respect to repeat unit). The Nafion 117 solution as received from Fluka was 5% polymer solution in light alcohols, (an mixture of isopropyl alcohol, 1-propanol, and methanol in an unspecified ratio), with 1100 Da equivalent weight (MW per sulfonic acid group of Nafion 117), and unspecified polymer M_w. The as-received solution was diluted with MilliQ-filtered deionized water to 0.002 M Nafion (with respect to the 1100 Da equivalent weight), for a final solvent alcohol composition of 4.4%. Substrates were 1"×2" indium-tin oxide (ITO) coated glass purchased from Donelly Applied Films and patterned by DCI, Inc to form multiple 3 mm ITO stripes. ITO film resistance was measured to be 28 Ω/square after patterning. The ITO substrates were cleaned by ultrasonication in a series of solvents including detergent, deionized MilliQ-filtered water, acetone, methanol, and 1,1,1-trichloroethane, for 15 minutes each. Immediately before use, the ITO glass substrates were plasma etched in a Harrick PCD 32G plasma cleaner with oxygen bleed for 5 minutes.

5.2.2.2 Assembly.

Films were constructed using a modified Carl Ziess DS50 programmable slide stainer. Substrates were exposed first to polycation solution for 15 minutes, followed by 4 minutes of rinsing in three MilliQ water baths, then exposed to polyanion solution for 15 minutes, rinsed, and then the cycle was repeated for 30 layer pairs. The $(LPEI/Nafion)_{30}$ system was assembled at pH 4 and films were made with at several levels of ionic strength between 0.025 M and 0.4 M by

adding NaCl to polycation and polyanion solutions. The $(LPEI/PAMPS)_{30}$ system was also assembled at pH 4 at several levels of ionic strength between 0.025 M and 3.0 M by adding NaCl. The $(LPEI/PAA)_{30}$ system was assembled with polyelectrolyte solutions at pH conditions between pH 2 and pH 7. In each trial, the ionic strength and pH of the polycation and polyanion solutions were equivalent. Thickness and roughness measurements were performed with a Tencor P10 profilometer using a 2 μm stylus and 5 mg stylus force. Following analysis of film assembly, films for ionic conductivity evaluation were fabricated. $(LPEI/ Nafion)_{30}$ films were assembled at pH 4 with no NaCl added and with 0.1 M NaCl added to deposition solutions. $(LPEI/PAMPS)_{30}$ films were assembled at pH 4 with no NaCl added and with 0.2 M NaCl added to deposition solutions. Finally, $(LPEI/PAA)_{30}$ films were assembled with deposition solutions at pH 2 and pH 5.

5.2.2.3 Test bed fabrication.

After assembly, films for ionic conductivity evaluation were dried at 110°C for 24 hours, which has been shown to effectively remove water from LBL assembled films.[18] The drying was followed by thermal evaporation through a custom designed shadow mask of 2mm wide, 1000 Å thick gold electrodes perpendicular to the 3mm wide patterned ITO stripes. This technique creates 2-electrode test beds of 6 mm^2 area in which the LBL assembled film is sandwiched between ITO and gold electrodes. The dimensions allowed 8 such cells per substrate. The cells were profiled to verify the absence of significant gold penetration into the LBL assembled film.

5.2.2.4 Testing.

Following fabrication, the cells were exposed to a controlled humidity environment. First the cells were exposed to a chamber that contained anhydrous $CaSO_4$ (Drierite) the solid-vapor equilibrium of which controls humidity to approximately 17% relative humidity (RH), as measured by a VWR pen thermometer/hygrometer (all RH measurements ±2%) at a room temperature of 25°C. The chamber was approximately 0.05 m^3 and contained a fan recirculating at 0.15 m^3/min; equilibrium RH at any humidity level was reached within approximately 5 minutes with this configuration. The cells were exposed to this relatively dry environment for 7 days. After this equilibration period, ionic conductivity was evaluated within the chamber by impedance spectroscopy. Substrates were accessed by means of electrodes built into the chamber wall.

Impedance spectroscopy was performed using a Solartron 1260 scanning from 1 MHz to 1 Hz. Due to noise at low frequency and high impedance, the lowest frequency included in analysis was variable and typically greater than 1 Hz; the lowest frequency was chosen so that the

measurement would be within the <2% error region of impedance measurement for the instrument. The initial signal amplitude was 10 mV with no bias; amplitude was increased to 100 mV for each sample to reduce noise and increase the effective measurement range. Results at 100 mV amplitude were compared with the earlier 10 mV measurement to ensure no artifacts from increasing amplitude above kT (or approximately 25 mV at 25°C), which in some cases can cause nonlinearity in the impedance response, especially in the interfacial component.[19] Fitting of the impedance results is described in the Results and discussion section of this publication. The absence of any cell shorting, even for rough samples, further substantiated that evaporation-deposited gold did not penetrate the LBL assembled film.

Following impedance spectroscopy, the anhydrous calcium sulfate was replaced with a saturated solution of $Mg(NO_2)_2 \cdot 6H_2O$ (Aldrich) in MilliQ water, the vapor-liquid equilibrium of which controls relative humidity to 52% RH at 25°C.[20] After 7 days the ionic conductivity was again evaluated by impedance spectroscopy. Finally, the $Mg(NO_2)_2 \cdot 6H_2O$ solution was replaced with pure MilliQ water for 100% RH at 25°C, with 7-day equilibration and subsequent ionic conductivity evaluation. Following the 100% RH measurement, substrates were immersed in MilliQ water overnight and then evaluated "dripping wet" by impedance spectroscopy using an apparatus that maintained a constant slow drip of MilliQ water over the substrate surface, ensuring that the surface was continuously wetted. During this last process the gold electrodes atop the two $(LPEI/PAMPS)_{30}$ samples delaminated and thus impedance measurements could not be made on these two samples.

LBL assembled films were invested with salt by soaking the films in aqueous solutions of $LiCF_3SO_3$ overnight and then drying without rinsing. The films were first soaked in a solution of 0.01 M $LiCF_3SO_3$. The two $(LPEI/PAMPS)_{30}$ samples delaminated and could not be tested. Following drying, the films were equilibrated for 7 days at 52% RH and 25°C and then tested using the procedure described above. The process was repeated for a $LiCF_3SO_3$ concentration of 0.1 M. After the samples were tested at 52% RH, they were exposed to the 100% RH environment and the ionic conductivity was evaluated a final time. $LiCF_3SO_3$ crystallization was not observed on or in the polymer films after drying.

5.2.3 Results and discussion

5.2.3.1 Assembly behavior.

The LBL systems employed in this study were designed to be high performance solid electrolytes - they have not been previously studied and they are quite unlike most model polyelectrolyte LBL systems. Characterization of assembly is therefore both appropriate and

necessary. Each system that was studied exhibits a unique response to assembly conditions, giving insight into the morphological and compositional character of the resultant films, and illuminating appropriate conditions for the assembly of high-performing polymer electrolyte systems.

The first step was to determine the ideal pH for assembly of LPEI/Nafion and LPEI/PAMPS. As LPEI is a weak polycation, pH influences the assembly of these systems. At low pH, LPEI charge density increases due to increasing secondary amine protonation, and at more basic pH, LPEI charge density decreases. A range of assembly pH conditions were evaluated between pH 1 and pH 5, with both dipping solutions at the same pH. At pH less than 2, LPEI/PAMPS and LPEI/Nafion LBL assembled films were thinner than 10 Å per layer pair and RMS roughness was 20-30% of thickness as observed by profilometry, which indicated a roughened, almost granular surface. The most favorable pH was determined to be pH 4, where films are 50-200 Å per layer with RMS roughness less than 1% of thickness. This pH corresponds with the solution isoelectric point of LPEI, which has been described as pH 4 - pH 5.[21-23] At this condition, film growth is reproducibly linear with layer pair number after approximately 5 layer pairs.

After determining the optimum pH, the response of LPEI/Nafion assembly to changing ionic strength could then be explored. Films were LBL assembled from LPEI and Nafion deposition solutions at pH 4 that contained different NaCl concentrations, and the resultant 30-bilayer films were thickness profiled, with results shown in Figure 5.2. With increasing ionic strength, film thickness first increases and then decreases. The increase in thickness is termed *screening-enhanced* adsorption, and is generally attributed to a change in polymer solution conformation; upon charge screening, the polymer transforms from an extended conformation to a more globular, coiled conformation that deposits far more thickly. The reduction in thickness is termed *screening-reduced* adsorption, and is generally attributed to binding competition and coulombic shielding at the deposition surface from the highly concentrated small ions, which effectively block polyelectrolyte adsorption. Both screening-enhanced and screening-reduced adsorption have been observed in many other systems,[12-15] though typically the maximum thickness is found at much higher salt concentrations than the 0.025 M for LPEI/Nafion. The dramatic thickness increase of the LPEI/Nafion system at low ionic strength may be because the water/alcohol solvent pair is an exceptionally poor solvent for the perfluorinated ionomer Nafion. Nafion solution for LBL assembly is prepared by the addition of water to dilute Nafion in alcohol for a final alcohol/water solvent pair that is only 4% alcohol. Though there is no noticeable precipitation or aggregation after even one year of shelf storage, we

suspect that the "solution" is more accurately a dispersion that may not be thermodynamically stable. Higher salt concentrations result in a gradual loss of Nafion solubility; at 0.4 M NaCl, there is visible cloudiness and at 1.0 M NaCl Nafion solid precipitates. Due to this poor solubility, screened LPEI/Nafion composites with different thickness and roughness can be attained even at very low ionic strengths.

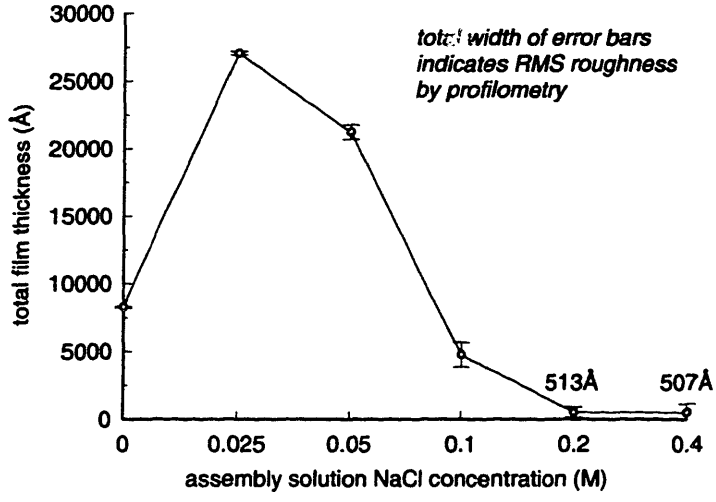

Figure 5.2. Correlation of total film thickness of (LPEI/Nafion)$_{30}$ films to deposition solution ionic strength.

The response of LPEI/PAMPS to screening is more complex than that of LPEI/Nafion, as shown in Figure 5.3. Film growth without salt at pH 4 results in smooth, thick films. Adding a small amount of salt to the pH 4 deposition solutions abruptly inhibits adsorption at 0.05M NaCl. At 0.2 M NaCl and greater, more traditional screening effects are observed, with screening-enhanced adsorption up to a maximum at 0.4 M, and then screening-reduced adsorption with total inhibition at 3 M NaCl. This surprising bimodal behavior suggests two assembly forces at work, one weak force and one strong force. A weak interaction might be completely screened at a low ionic strength, while a strong interaction would be screened at a higher ionic strength. Upon consideration of molecular structures (Figure 5.1), it appears that hydrogen bonding is the most likely possibility for the weak interaction. Hydrogen bonding is possible between adjacent PAMPS amide moieties and also between PAMPS amide moieties and LPEI, as shown in Figure 5.4. Thus LPEI/PAMPS assembly may be initially facilitated by hydrogen bonding that, being a weak electronic interaction, is completely screened upon the addition of a very small amount of salt. After hydrogen bonding is screened, film assembly is due entirely to electrostatic interactions and the resultant films are quite thin due to the high charge density of the polymer chains. Upon addition of further salt, these electrostatic interactions also

eventually become screened, and film thickness once again increases to a maximum. Regardless of the identity of the weak interaction, it is clear that by varying ionic strength, the unique response of LPEI/PAMPS films may be exploited to attain films assembled by different subsets of interactions. These films may display very different ion conduction behavior due to altered crosslink character and density.

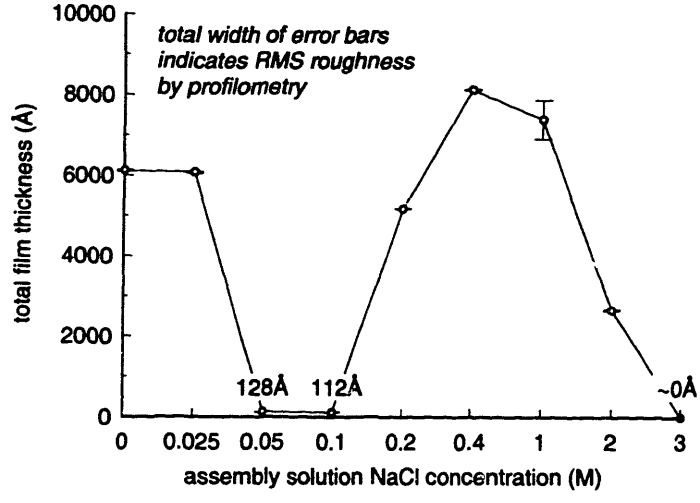

Figure 5.3. Correlation of total film thickness of (LPEI/PAMPS)$_{30}$ films to deposition solution ionic strength.

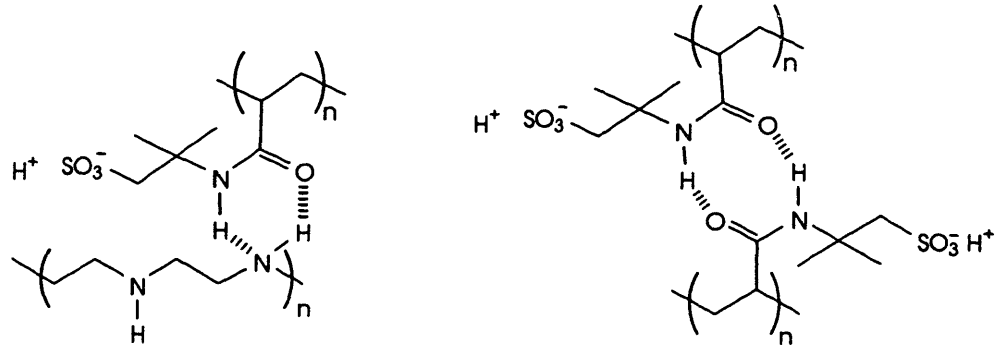

Figure 5.4. Possible weak, nonionic interactions in the LPEI/PAMPS system.

For systems containing two weak polyions such as LPEI/PAA, changing assembly pH can influence the final character of the films even more profoundly than ionic screening.[10,11] To explore the influence of pH on this particular polyamine system, LPEI and PAA assembly solutions were adjusted to the same pH over a range of 2 to 7, and 30-bilayer films were formed at each pH, with thickness results shown in Figure 5.5. Film thickness first increases with increasing pH up to pH 4, and then decreases, becoming ultra-thin at pH 7. At pH greater than 7, LPEI/PAA assemblies become increasingly thin and eventually fail to assemble.

These thickness variations are due to changes in degree of ionization that have been studied in other LBL systems using FTIR methods,[11] which generally show ionization greater than that in solution due to intimate polyacid/polybase contact. In LPEI/PAA films, PAA ionization increases as LPEI ionization decreases with increasing pH. This in turn increases the proportion of LPEI in the film and decreases the proportion of PAA. Morphology also changes in a manner similar to screening; weakly ionized polyions form thick, loopy conformations on the surface. As seen in Figure 5.5, at low pH, LPEI is fully ionized, and only PAA deposits thickly. The thickness of the LPEI/PAA system steadily increases up to pH 4, where both LPEI and PAA are partially ionized, and thick, loopy layers of *both* polymers are formed on adsorption. Thickness again decreases at higher pH as PAA gains further ionization and only LPEI deposits thickly. This trend is identical to that determined for selective LPEI/PAA assembly on acid surfaces by Clark and Hammond, who observed intermediate thickness at pH 2.5, maximum thickness at pH 4.8, and ultrathin film formation at pH 7.[24]

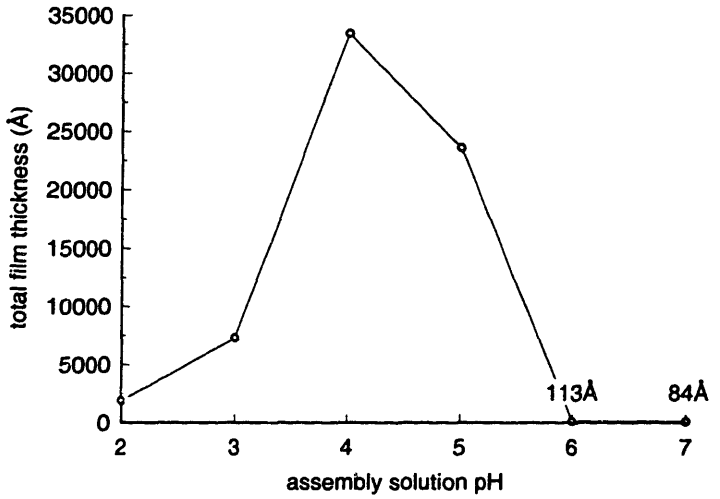

Figure 5.5. Correlation of total film thickness of (LPEI/PAA)$_{30}$ films to deposition solution pH. RMS roughness from profilometry was less than 20Å.

In the case of the LPEI/PAA films adsorbed atop ITO that were investigated in this study, secondary interactions must play a substantial role in assembly, as the final thickness of 30-bilayer films is close to 3 μm, indicating a per layer pair thickness close to 1000 Å, which is far thicker than that of most electrostatically LBL assembled systems. Thicknesses in this range have been observed for LBL systems based on hydrogen bonding interactions between poly(ethylene oxide) (PEO) and PAA.[25] As LPEI is the nitrogen analog of PEO, similar interactions and

assembly behavior could be expected between LPEI and PAA, especially at pH conditions where LPEI is less protonated.

Despite the contributions of secondary interactions, the pH behavior of the LPEI/PAA system is remarkably consistent with the study of PAH/PAA by Rubner and co-workers.[10,11] The PAH/PAA system, as described where pH of polycation and polyanion solutions are equivalent, features two thickness maxima: one at pH 5, where PAA is partially ionized, and one at pH 9, where PAH is partially ionized, and a minimum in between at pH 6 – pH 7.5 where both polymers are fully charged. The pK_a of LPEI (pH 4- pH 5)[21-23] is substantially lower than that of PAH, so that for LPEI/PAA there is no pH region where polycation and polyanion are fully charged. The LPEI/PAA system instead presents a single thickness maximum at pH 4-pH 5 where both LPEI and PAA are partially ionized. The variation of composition and morphology of LPEI/PAA with pH provides a simple tool with which to construct acid-rich and amine-rich polymer electrolyte films and compare relative ionic conductivity performance.

5.2.3.2 Ionic conductivity evaluation.

Following the examination of deposition solution condition effects, the performance of these three LBL systems as polymer electrolyte membranes was tested using impedance spectroscopy. Polyelectrolytes in the dry state are generally expected to be very resistive due to clustering of polar groups, with ionic conductivities of 10^{-15}-10^{-12} S/cm,[26] so a plasticizer was chosen to enhance ion conductivity in our three LBL systems. The preferred plasticizer for polyelectrolyte systems is water, which dissociates ionic clusters and enhances ion mobility.[1,26] Therefore, the ionic conductivity of the LBL assembled films was evaluated at three levels of hydration by changing the room temperature relative humidity of the measurement environment. Future studies will explore the use of nonaqueous plasticizers to apply these LBL assembled solid electrolytes to water-intolerant applications such as lithium batteries. To fully explore the potential of these films with water plasticization, two deposition conditions with very different film character were chosen for each system based on assembly behavior.

Impedance spectroscopy data was collected as real (Z') and imaginary (Z") components of the complex impedance. Representative raw data plots from this study are shown in Figure 5.6. Ionic conductivity can be determined from these plots by fitting to a simple equivalent circuit shown in Figure 5.7, which represents idealized components of the real system, in particular a bulk polymer electrolyte sandwiched between blocking electrodes.[27,28] Bulk electrolyte polarization and resistance to ion motion are represented as the parallel combination of a constant phase element (CPE_B) and resistance (R_B), respectively; in the complex impedance plots

(Figure 5.6b, Figure 5.6c), these elements are represented as a depressed semicircle at high frequency. R_B is the semicircle diameter. As was described in Chapter 1 of this thesis, electrolyte polarization is represented as a CPE rather than a capacitance to better capture non-ideality, particularly a dielectric relaxation time distribution within the bulk polymer electrolyte.[19,29] Interface polarization and double layer formation (C_I) cause a low frequency spike in the impedance response, and parasitic lead resistance causes a small, positive translation of the complex impedance along the real axis (R_I, typically < 20 Ω). The value of the individual equivalent circuit elements was determined by nonlinear least squares fitting using ZPlot/ZView© software. Fitting and the analytical expressions involved have been very well reviewed.[19,29,30] We fit CPE_B and R_B separately from the interface elements, a practice that can be employed if the time constants for each relaxation contribution (bulk and surface in our case) are greater than 2 orders of magnitude apart.[19] Once determined, R_B was transformed into conductivity using the thickness-dependent cell constant.

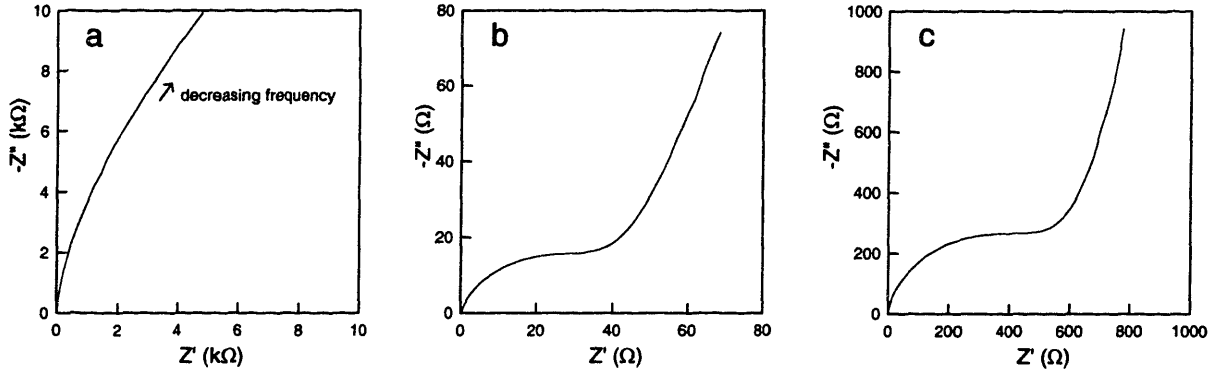

Figure 5.6. Complex impedance raw data plots at 52% RH. a) $(LPEI/Nafion)_{30}$ no added NaCl; b) $(LPEI/PAMPS)_{30}$ no added NaCl; c) $(LPEI/PAA)_{30}$ at pH 5. These plots are representative raw data and are not normalized with respect to cell constant.

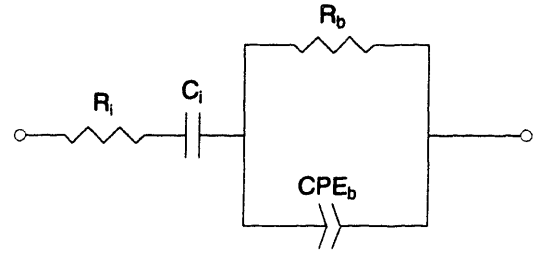

Figure 5.7. Equivalent circuit used for fitting impedance data.

Ionic conductivity of LPEI/Nafion.

The perfluorinated ionomer Nafion (see Figure 5.1), manufactured by DuPont, is widely used in proton exchange membrane (PEM)-type fuel cells. Nafion has also been used as an electrolyte in electrochromic devices.[31] Commercial Nafion in its most common form is a proton conducting membrane with 5 to 10 nm diameter water-filled hydrophilic pores or ion "clusters" in a perfluorinated matrix through which protons travel by hopping between adjacent sulfonic acid sites.[1,32] Fast ion conductivity (10^{-1}-10^{-2} S/cm) is facilitated through these pores.[33-35] High mechanical strength and chemical resistance coupled with high proton conductivity are key to Nafion's commercial success. The two deposition conditions chosen for LPEI/Nafion were 1) with no salt added and 2) with 0.1 M salt, representing unscreened and screened morphologies (see Figure 5.2).

The combination of Nafion with LPEI via the LBL method resulted in polymer electrolyte films with ionic conductivity lower than that of commercial Nafion membranes, but similar to that previously seen in LBL assembled films of strong polyacids. As shown in Table 5-1, the dry ionic conductivity was almost 10^{-11} S/cm. This performance is similar to the 10^{-12}-10^{-11} S/cm obtained for dry PAH/SPS by Durstock and Rubner.[2] Ionic conductivity increased by three orders of magnitude to about 10^{-8} S/cm at full plasticization (100% RH), again very similar to PAH/SPS. The ionic conductivity of LPEI/Nafion under running water is approximately equivalent to that at 100% RH, implying that the film is saturated with water at 100% RH. This saturation behavior was generally observed for all LBL assembled films tested in this study.

It is important to note that the ionic conductivity of LPEI/Nafion in the fully hydrated state is actually only <u>one</u> order of magnitude lower than values determined for hydrated solution-cast Nafion films,[36] suggesting that processing plays an important part in the formation of ion-transporting pores. Atomic force microscopy (not shown) of LPEI/Nafion reveals a roughened but nonporous surface. Thus the nanoporous morphology of commercial Nafion membranes is not expressed in LBL assembled films; the sulfonic acid sites are tightly bound to protonated secondary amines so that morphological rearrangement to a nanoporous secondary structure is impossible.

The difference in performance between the ionically screened and unscreened LPEI/Nafion films suggests an improvement in performance with additional screening. This improvement is especially notable under conditions where the measurement is most accurate (52 and 100% RH). The screened morphology may present voids or large domains of either polyelectrolyte, enhancing ion conduction. Additional salt present in screened polyelectrolyte solutions could also dissolve within the film to associate with LPEI and provide additional charge carriers.

Table 5-1. Room temperature (25°C) ionic conductivity of the systems investigated in this study, each assembled at two different conditions and studied under varying humidity. Uncertainty indicates 95% confidence intervals.

measurement environment:	17% RH	52% RH	100% RH	Wet
system	ionic conductivity (S/cm)			
$(LPEI/Nafion)_{30}$ No Salt	$5.0 \pm 1.5 \cdot 10^{-11}$	$3.4 \pm 0.4 \cdot 10^{-11}$	$2.9 \pm 0.1 \cdot 10^{-9}$	$4.8 \pm 0.1 \cdot 10^{-9}$
$(LPEI/Nafion)_{30}$ 0.1 M NaCl	$1.2 \pm 0.2 \cdot 10^{-11}$	$8.3 \pm 0.4 \cdot 10^{-11}$	$6.9 \pm 0.4 \cdot 10^{-9}$	$3.8 \pm 0.3 \cdot 10^{-9}$
$(LPEI/PAMPS)_{30}$ No Salt	$1.5 \pm 0.5 \cdot 10^{-9}$	$9.4 \pm 0.7 \cdot 10^{-6}$	$1.0 \pm 0.1 \cdot 10^{-5}$	delaminated
$(LPEI/PAMPS)_{30}$ 0.2 M NaCl	$2.7 \pm 0.4 \cdot 10^{-12}$	$1.3 \pm 0.0 \cdot 10^{-8}$	$1.5 \pm 0.2 \cdot 10^{-5}$	delaminated
$(LPEI/PAA)_{30}$ pH 2	$6.7 \pm 0.3 \cdot 10^{-12}$	$5.6 \pm 0.6 \cdot 10^{-10}$	$1.2 \pm 0.1 \cdot 10^{-6}$	$9.7 \pm 0.8 \cdot 10^{-7}$
$(LPEI/PAA)_{30}$ pH 5	$2.8 \pm 0.2 \cdot 10^{-11}$	$6.4 \pm 0.2 \cdot 10^{-9}$	$1.0 \pm 0.0 \cdot 10^{-5}$	$5.8 \pm 0.2 \cdot 10^{-6}$

Ionic conductivity of (LPEI/PAMPS).

PAMPS is a proton/cation conductor most widely used as a hydrated gel in polymer electrochromic devices.[31,33,37] Amorphous polyelectrolyte hydrogels of this type present an ionic conductivity of about 10^{-2}-10^{-3} S/cm at full hydration. However, at this hydration level, PAMPS is a viscous fluid with very poor mechanical properties. When PAMPS is combined with LPEI using the LBL method, robust films can be formed that show very unusual ionic screening behavior, revealing the contributions of two different assembly interactions (see Figure 5.3). To exploit this behavior, the two deposition conditions chosen for LPEI/PAMPS were 1) with no salt added, representing assembly by weak interactions plus electrostatic interactions, and 2) with 0.2 M salt, representing assembly by only electrostatics.

The performance of LPEI/PAMPS as presented in Table 5-1 far surpasses that of LPEI/Nafion and in fact surpasses all other LBL assembled polymer electrolytes evaluated to date, reaching greater than 10^{-5} S/cm when water-saturated. Films with this level of performance are suitable for application in electrochromic devices and electrochemical sensors. In addition, films of LPEI/PAMPS assembled using different interactions exhibit clear differences in ion conduction behavior. This system does lose mechanical properties under flowing water, resulting in delamination of the gold top electrodes, but this composite does not require such high plasticizer loading to achieve high ionic condition.

The ionic conductivity of unscreened LPEI/PAMPS is consistently several orders of magnitude greater than that of screened LPEI/PAMPS at low and intermediate humidity levels. This disparity suggests a clear difference in the film character, reinforcing the proposition that the films are assembled by different interaction subsets under different screening conditions. The

crosslink density in the unscreened film may be significantly lower due to the weaker assembly interaction, and hydrogen bond crosslinks would be far less rigid than electrostatic crosslinks, allowing some degree of rearrangement and greater plasticity. It is also possible that some unbound sulfonic acid groups exist within the film if a PAMPS monomer unit should be bound by interactions rather than electrostatics, though the strongly acidic nature of PAMPS would preclude an abundance of unbalanced negative charge within the film. The unscreened composite becomes saturated with water at much drier conditions than the screened composite, indicating an increased capacity for adsorbing and binding water and suggesting a highly polar and hydrogen-bonding interior. The high ionic conductivity of unscreened LPEI/PAMPS at 52% RH is greater than that of any other LBL assembled film at this intermediate level of hydration.

The ionic conductivity of dry, screened LPEI/PAMPS is similar to that obtained for LPEI/Nafion. However, conductivity increases greatly at 52% RH, and at full humidity exceeds that of LPEI/Nafion by three orders of magnitude. Even though LPEI/PAMPS appears to be assembled by electrostatic interactions just as LPEI/Nafion, this higher ionic conductivity was expected in LPEI/PAMPS because PAMPS was chosen for its very hydrophilic, polar nature. As compared to unscreened LPEI/PAMPS, the screened composite becomes water-saturated at a higher relative humidity, indicating a more tightly crosslinked and less water-accessible interior. However, screened LPEI/PAMPS outperforms unscreened LPEI/PAMPS at full hydration, possibly due to increased salt uptake from screened polyelectrolyte assembly solutions.

Ionic conductivity of (LPEI/PAA).

The LPEI/PAA system was assembled for comparison with the systems containing strong polyanions PAMPS and Nafion. PAA contains carboxylic acids that, when assembled under acidic conditions, remain protonated, and may provide dissociable and mobile protons in a PAA-containing LBL assembled polymer electrolyte. Based on assembly characterization (see Figure 5.5), the two deposition conditions chosen for LPEI/PAA films were pH 2, to yield a large number of free acid groups, and pH 5, to achieve composites containing an increased number of free amine groups. Though relative amounts of acid and amine were not precisely determined in this study, the expectation of acid-rich and amine-rich characteristics is strongly supported by studies on PAH/PAA;[10,11] detailed FTIR studies of LPEI/PAA are planned to confirm this hypothesis.

The ionic conductivity of LPEI/PAA exceeds 10^{-5} S/cm and is higher than that of all other LBL assembled polymer electrolytes studied thus far except for LPEI/PAMPS. The LPEI/PAA system is more mechanically robust than LPEI/PAMPS and remains fully laminated under

running water. In addition, there are definite assembly condition influences on ionic conduction, which suggest the relative importance of acid and amine functionality in the fully assembled polymer electrolyte film.

LPEI/PAA composites assembled at pH 5 exhibit ionic conductivity one order of magnitude greater than that those assembled at pH 2, suggesting that the incorporation of greater amounts of uncoordinated LPEI into the LBL matrix is more advantageous than incorporation of free acid groups. The cation complexation capability and hydrophilic nature of the heteroatomic LPEI backbone, as well as the mobility allowed by the lower number of crosslinks in the pH 5 composite appear to enhance ionic conduction. This suggestion is further supported by comparison with the PAH/PAA system, which demonstrated the opposite trend: higher ionic conductivity when assembled under acidic conditions.[2] The conductivity of LPEI/PAA is two orders of magnitude greater than that of PAH/PAA, suggesting that the nature of the polycation is largely responsible for the conductivity increase. Evidently the hydrophobic polymer backbone of PAH is not conducive to ion association or motion, as adding greater amounts of PAH hinders ion motion, while adding of greater amounts of LPEI enhances ion motion. This great disparity truly emphasizes the importance of the molecular architecture of the LPEI and PAH near-isomers.

Salt-exposure post assembly.

To investigate the possibility that ion conductivity is limited in LBL assembled films by the absence of ions, intrinsic ion concentration was increased by adding a salt with potential high solubility in the solid polymer matrix. To add this additional salt, substrates were immersed into aqueous solutions of $LiCF_3SO_3$ and then dried without rinsing. Ion conduction results, shown in Table 5-2, do not include LPEI/PAMPS films, which delaminate in salt solution. Salt dissolution into the film is controlled by partitioning between film and solution; the degree of partitioning was not possible to determine in this study.

Table 5-2. Room temperature (25°C) ionic conductivity of the salt-exposed systems investigated in this study, which are based on LPEI/Nafion and LPEI/PAA. Uncertainty indicates 95% confidence intervals.

measurement environment:		52% RH	100% RH
system	$LiCF_3SO_3$ soak (M)	ionic conductivity (S/cm)	
$(LPEI/Nafion)_{30}$ No Salt	none	$3.4 \pm 0.4 \cdot 10^{-11}$	$2.9 \pm 0.1 \cdot 10^{-9}$
	0.01	$2.4 \pm 0.6 \cdot 10^{-10}$	-
	0.10	$2.3 \pm 0.6 \cdot 10^{-10}$	$2.9 \pm 0.0 \cdot 10^{-9}$
$(LPEI/Nafion)_{30}$ 0.1 M NaCl	none	$8.4 \pm 0.3 \cdot 10^{-11}$	$6.9 \pm 0.4 \cdot 10^{-9}$
	0.01	$1.7 \pm 0.0 \cdot 10^{-9}$	-
	0.10	$1.2 \pm 0.6 \cdot 10^{-9}$	delaminated
$(LPEI/PAA)_{30}$ pH 2	none	$5.6 \pm 0.6 \cdot 10^{-10}$	$1.2 \pm 0.1 \cdot 10^{-6}$
	0.01	$1.3 \pm 0.1 \cdot 10^{-8}$	-
	0.10	$1.1 \pm 0.1 \cdot 10^{-8}$	$8.1 \pm 0.0 \cdot 10^{-7}$
$(LPEI/PAA)_{30}$ pH 5	none	$6.4 \pm 0.2 \cdot 10^{-9}$	$1.0 \pm 0.0 \cdot 10^{-5}$
	0.01	$3.6 \pm 0.0 \cdot 10^{-8}$	-
	0.10	$2.9 \pm 0.0 \cdot 10^{-8}$	$9.6 \pm 0.0 \cdot 10^{-6}$

At 52% RH, the addition of salt by exposure to 0.01 M $LiCF_3SO_3$ solution increases ionic conductivity approximately one order of magnitude, resulting in a higher-performance polymer electrolyte. Exposure to a higher concentration of salt fails to increase ionic conductivity significantly, and indeed seems responsible for a small decrease. It appears that although the films can be stably exposed to higher concentration salt solutions, the films do not solvate additional salt beyond a certain saturation limit. As a film dries, any salt present that is not soluble in the polymer matrix will form small crystallites within the film that can hinder ion motion and decrease overall ion dissociation due to equilibrium.

At higher levels of hydration, the benefits of adding salt to the LBL assembled film are lost. The ionic conductivity of the salt-invested film is comparable to the ionic conductivity of the unexposed film. This result suggests that the limitation to ion conductivity at low and intermediate humidity is the number of carriers, as determined by the degree of dissociation and ion solvation, while at high hydration levels, the limitation is mobility in the polymer matrix.

Based on these results, it is clear that further development of unplasticized LBL assembled polymer electrolytes should focus on maximization of ion count and dissociation, either by counterion inclusion or dissolution of different salts. For plasticized systems, the focus should be minimizing crosslink density or replacing electrostatic crosslinks with less rigid interactions such as hydrogen bonds. To this end, our ongoing studies have concentrated on systems employing completely hydrogen-bonded LBL assembled films with high polyether content to provide the next generation of high-performance LBL assembled polymer electrolytes.

5.2.4 Conclusions from electrostatically LBL assembled polymer electrolyte studies

The applications of LBL assembled films have been extended to polymer electrolytes with the development of LBL assembled composites with ionic conductivity levels appropriate for many electrochemical applications. The LPEI/Nafion system has limited ion conductivity, as the LBL process crosslinks sulfonic acid sites, preventing rearrangement to the nanoporous morphology required for fast ion conduction in Nafion. The LPEI/PAMPS system exhibits ionic conductivity greater than 10^{-5} S/cm, which is two orders of magnitude greater than any LBL assembled polymer electrolyte studied thus far. LPEI/PAMPS was discovered to assemble through two different types of interactions, which can be selectively screened to create films with different ion conduction properties, including a film assembled from weak interactions that displays ion conductivity of 10^{-5} S/cm at intermediate hydration (52% RH). The LPEI/PAA system exhibited very high ionic conductivity similar to LPEI/PAMPS at high hydration (100% RH), and also possessed excellent mechanical properties, being stable to flowing water and high ionic strength solutions. The addition of salt to LBL assembled films was shown to enhance ion conduction at intermediate hydration. For each system studied, assembly conditions were shown to affect the ion conduction of the composite, in some cases dramatically. For LBL assembled polymer electrolytes, the ion conduction limitation with low plasticizer levels is the dissociation-moderated number of free ions to act as charge carriers. At high levels of plasticizer, the limitation is ion mobility in the LBL matrix. Ion mobility is directly related to the segmental motion of the polymers, so less ionically crosslinked systems exhibit superior performance. Future work will explore LBL assembled films assembled by hydrogen bonding and LBL assembled films containing polyions with domains of uncomplexed polyether matrices to facilitate ion mobility. These developments can lead to exciting new uses for LBL assembled films in micropower and other power storage applications such as lightweight lithium batteries and portable fuel cells, and in other electrochemical devices such as electrochromic displays and chemical/biological sensors.

5.3 Hydrogen bonded LBL assembled polymer electrolytes

5.3.1 Introduction to hydrogen bonded LBL assembled polymer electrolytes

Although the electrostatically LBL assembled polymer electrolytes show a great deal of promise as ion conduction media, they still suffer from the inherent problems introduced by the presence of a high density of ionic crosslinking. Even though the use of partially charged LPEI as a polycation enhanced the ionic conductivity in LBL assembled films, that conductivity remains one or two orders of magnitude too small for application in demanding applications such as batteries and fuel cells. The presumably conductivity-inhibiting effects of ionic crosslinking in LBL films can be alleviated to some extent by the introduction of other forces for LBL assembly such as hydrogen bonding.

The use of hydrogen bonding as an assembly force to create LBL assembled films was first described by Rubner and co-workers.[38] In this work, LBL assembled films were assembled using the strong hydrogen bonding capabilities of protonated PANI. PANI was combined with many nonionic polymers such as poly(ethylene oxide) (PEO), poly(acrylic acid) (PAA, nonionic at low pH), and poly(acrylamide) (PAAm). Reproducible, robust film formation of electronically conductive films was attributed to the unparalleled hydrogen bonding capabilities of PANI.

More recently, Granick and colleagues have described more delicate LBL assembled films that have been assembled using hydrogen bonding forces between poly(carboxylic acids), such as PAA, and nonionic polymers such as PEO at pH conditions sufficiently low to promote carboxylic acid protonation.[25,39] Granick's work has paralleled our own efforts to create polymer electrolyte systems from LBL assembled films of these same component species. The reason that these films have remained elusive is that at pH conditions sufficiently basic to ionize the component polyacids, the film will decompose and dissolve due to the high concentration of unbalanced polyanionic ionization.

Perhaps fortuitously, hydrogen bonded LBL assembled films can be assembled quite straightforwardly by exploiting hydrogen-bonding forces between protonated PAA and PEO. This film formation allows us the opportunity to explore the ionic conduction in LBL assembled films containing the most widely studied and widely applied solid electrolyte matrix polymer: PEO. PEO is so widely used because its chemical structure can dissolve small alkali cation salts (most notably lithium salts) directly within a glassy or crystalline PEO solid polymer matrix. Facile ion conduction is facilitated in glassy PEO matrices by an activated process wherein the lithium cations "hop" between PEO cradle coordination sites.[1] If PEO is below its melting temperature of 65°C, then the 85% crystalline PEO matrix that forms does not allow for facile

activated site hopping and the resultant ionic conduction is quite low; the whole of the ionic conduction is expected to take place in the remaining 15% amorphous phase.

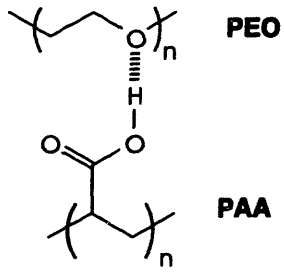

Figure 5.8. LBL assembly mechanism for PEO/PAA films.

Because of this typically poor ion conduction at room temperature, PEO is often used in tandem with an organic liquid plasticizer that dispels crystallinity within the PEO matrix and allows for fast ion motion. The addition of plasticizer also leads to non-activated and more diffusive ion motion in the solid electrolyte, which now must be considered a "gel electrolyte." Plasticized PEO gels possess poor mechanical properties and invariably deform and flow slowly over time. Chemical processes initiated by the plasticizer are often responsible for the corruption of electrochemical cells employing PEO-type polymer electrolytes, especially in lithium batteries at the interface between the graphitic lithium anode and the electrolyte.[1]

LBL assembly of PEO with PAA may provide a method to circumvent plasticizer use or modify plasticization requirements for PEO while also adding to the mechanical stability of the solid electrolyte film. The proposed means for this stabilization is based on the LBL assembly mechanism. Ether oxygens on the PEO main chain are directly coordinated to PAA carboxyl groups during assembly. As these oxygens are somewhat strongly bound, the presence of PAA in the matrix effectively inhibits crystallinity. No crystallinity can be observed in PEO/PAA LBL assembled films, and in fact even films several microns thick do not scatter light and do not exhibit birefringence when examined under crossed polarizers using optical microscopy.

This section explores the possibilities of the fabrication of polymer electrolytes using the PEO/PAA system. In keeping with the previous section of this chapter, the effects of water plasticization on the ionic conductivity of the films were explored. The authors are fully aware that the presence of water effectively bars application of these films directly in lithium battery applications. Furthermore we are aware that poly(ethers) such as PEO are not suitable for a fuel cell environment and we do not propose to use these films directly for application in either of these areas. However, ionic conductivity in electrostatically LBL assembled films has been shown to be similar when either water or an organic solvent is employed as plasticizer. Thus, we employ

water as a model plasticizer for PEO/PAA because the concentration of plasticizer in the measurement environment is easily controllable by virtue of water's well-characterized liquid-vapor equilibrium. With the use of anhydrous plasticizers, the PEO/PAA system might be developed for use in lithium battery applications.

Results from this exploration are encouraging as they demonstrate that PEO/PAA can handily outperform all electrostatically assembled systems studied to date as polymer electrolytes. However, due to issues of measurement platform stability (which are related to the high hydrophilicity of PEO/PAA), the maximum conductivity for this system could not be fully ascertained. Further studies by future investigators will be required to fully elucidate the full potential of this very promising electrolyte system.

5.3.2 Experimental details for hydrogen bonded LBL assembled polymer electrolytes

5.3.2.1 Materials.

The nonionic polymer PEO (4,000,000 M_w, Polysciences, Inc.) was used as-received as were polyanions PAA (90,000 M_w, Polysciences), and poly(methacrylic acid) (PMAA, 100,000 M_w, Polysciences). The polymers were dissolved in MilliQ-filtered deionized water and then pH adjusted with dilute HCl or NaOH solutions. All solutions were 0.020 M (polyelectrolyte concentrations are with respect to repeat unit). Some assembly conditions required the dissolution of $LiCF_3SO_3$ salt (Aldrich), which was added directly to the polymer solutions. Substrates were 1"×2" indium-tin oxide (ITO) coated glass purchased from Donelly Applied Films and patterned by DCI, Inc to form multiple 3 mm ITO stripes. ITO film resistance was measured to be 28 Ω/square after patterning. The ITO substrates were cleaned by ultrasonication in a series of solvents including detergent, deionized MilliQ-filtered water, acetone, methanol, and 1,1,1-trichloroethane, for 15 minutes each. Immediately before use, the ITO glass substrates were plasma etched in a Harrick PCD 32G plasma cleaner with oxygen bleed for 5 minutes. Following plasma etch, the substrates were immediately immersed in a pH 4 solution of LPEI (25,000 M_w, Polysciences, Inc.) for 10 minutes to prepare the surface for PEO/PAA deposition.

5.3.2.2 Assembly.

Films were constructed using a modified Carl Ziess DS50 programmable slide stainer. Substrates were exposed first to PEO solution for 15 minutes, followed by 4 minutes of rinsing in three MilliQ water baths that had also been pH-adjusted, then exposed to polyanion solution for 15 minutes, rinsed, and then the cycle was repeated for the required number of layer pairs. Some LBL assembled films were invested with salt by soaking the films in aqueous solutions of

$LiCF_3SO_3$ overnight and then drying without rinsing. This soaking was performed before test bed fabrication.

Thickness and roughness measurements were performed with a Tencor P10 profilometer using a 2 μm stylus and 5 mg stylus force. Following analysis of film assembly, films for ionic conductivity evaluation were fabricated.

5.3.2.3 Test bed fabrication.

After assembly, films for ionic conductivity evaluation were dried at 110°C for 24 hours, which has been shown to effectively remove water from LBL assembled films.[18] The drying was followed by thermal evaporation through a custom designed shadow mask of 2mm wide, 1000 Å thick gold electrodes perpendicular to the 3mm wide patterned ITO stripes. This technique creates 2-electrode test beds of 6 mm^2 area in which the LBL assembled film is sandwiched between ITO and gold electrodes. The dimensions allowed 8 such cells per substrate. The cells were profiled to verify the absence of significant gold penetration into the LBL assembled film.

5.3.2.4 Testing.

Following fabrication, the cells were exposed to a controlled humidity environment. First the cells were exposed to a chamber that contained anhydrous $CaSO_4$ (Drierite) the solid-vapor equilibrium of which controls humidity to approximately 17% relative humidity (RH), as measured by a VWR pen thermometer/hygrometer (all RH measurements ±2%) at a room temperature of 25°C. The chamber was approximately 0.05 m^3 and contained a fan recirculating at 0.15 m^3/min; equilibrium RH at any humidity level was reached within approximately 5 minutes with this configuration. The cells were exposed to this relatively dry environment for 7 days. After this equilibration period, ionic conductivity was evaluated within the chamber by impedance spectroscopy. Substrates were accessed by means of electrodes built into the chamber wall.

Impedance spectroscopy was performed using a Solartron 1260 scanning from 1 MHz to 1 Hz. Due to noise at low frequency and high impedance, the lowest frequency included in analysis was variable and typically greater than 1 Hz; the lowest frequency was chosen so that the measurement would be within the <2% error region of impedance measurement for the instrument. The initial signal amplitude was 10 mV with no bias; amplitude was increased to 100 mV for each sample to reduce noise and increase the effective measurement range. Results at 100 mV amplitude were compared with the earlier 10 mV measurement to ensure no artifacts from increasing amplitude above kT (or approximately 25 mV at 25°C), which in some cases can cause nonlinearity in the impedance response, especially in the interfacial component.[19] Fitting of the

impedance results is described in the Results and discussion section of this publication. The absence of any cell shorting, even for rough samples, further substantiated that evaporation-deposited gold did not penetrate the LBL assembled film.

Following impedance spectroscopy, the anhydrous calcium sulfate was replaced with a saturated solution of $Mg(NO_2)_2 \cdot 6H_2O$ (Aldrich) in MilliQ water, the vapor-liquid equilibrium of which controls relative humidity to 52% RH at 25°C.[20] After 7 days the ionic conductivity was again evaluated by impedance spectroscopy. Finally, the $Mg(NO_2)_2 \cdot 6H_2O$ solution was replaced with pure MilliQ water for 100% RH at 25°C, with 7-day equilibration and subsequent ionic conductivity evaluation.

5.3.3 Results and discussion

5.3.3.1 Assembly behavior.

Effect of pH

Hydrogen bonding crosslinking that drives the LBL assembly of PEO/PAA can only be expected at assembly pH conditions sufficiently low to suppress PAA ionization. There are two reasons that ionization must be suppressed. The first, most obvious reason is that protonation of the poly(carboxylic acid) groups is required in order to actually assemble the film by the mechanism shown in Figure 5.8. The second, somewhat less obvious reason is that excessive uncompensated negative ionization within the film should be sufficient to cause repulsion of adjacent PAA chains and thus lead to film dissolution. Therefore, even a small lack of complete PAA protonation may be sufficient to inhibit PEO/PAA film formation. The pH of assembly controls the level of PAA ionization and an understanding of the effects of pH is critical to the examination of the assembly of these LBL systems.

The effect of pH was characterized for the PEO/PAA system and the closely similar PEO/PMAA system as shown in Figure 5.9. For both systems, it is clear that assembly proceeds to a much greater extent under lower pH conditions. LBL deposition of the PEO/PAA system begins to falter at pH greater than 2.75, and deposition is completely inhibited at pH greater than 3. Deposition of the PEO/PMAA system begins to fail at pH greater than 3, and is inhibited at pH greater than 3.5, though there appears to be some remaining deposition even at higher pH conditions. The pH conditions that inhibit deposition are consistent with the onset of polyacid ionization in solution that would be expected based on potentiometric titration.[40,41] According to these ionization figures, PAA would be 1% ionized at a pH 3; apparently this small amount of

uncompensated negative charge is sufficient to suppress deposition thickness. Ionization of ~5% at pH 3.5 is apparently sufficient to completely inhibit film formation. These "critical" pH values for film formation are consistent with those determined by Sukhishvili and Granick, though somewhat more acidic; those investigators determined that PEO/PAA dissolved at pH 3.6 while PEO/PMAA films dissolved at pH 4.6.[25] Importantly, Sukhishvili and Granick measured *dissolution* pH conditions of films that were previously assembled at lower pH conditions, while the study presented in Figure 5.9 indicates actual *assembly* pH conditions. Although the onset of assembly suppression occurs at more acidic pH conditions (pH 2.8 and pH 3.5) than those determined for dissolution, pH conditions required for complete assembly inhibition (pH 3.5 and pH 4.5) are fully consistent with those determined for dissolution (pH 3.6 and pH 4.6)[25]. This comparison indicates that there could be some hysteresis in the pH response; that is, once the films are assembled, they may be stable to pH conditions that would normally suppress (but not completely inhibit) assembly.

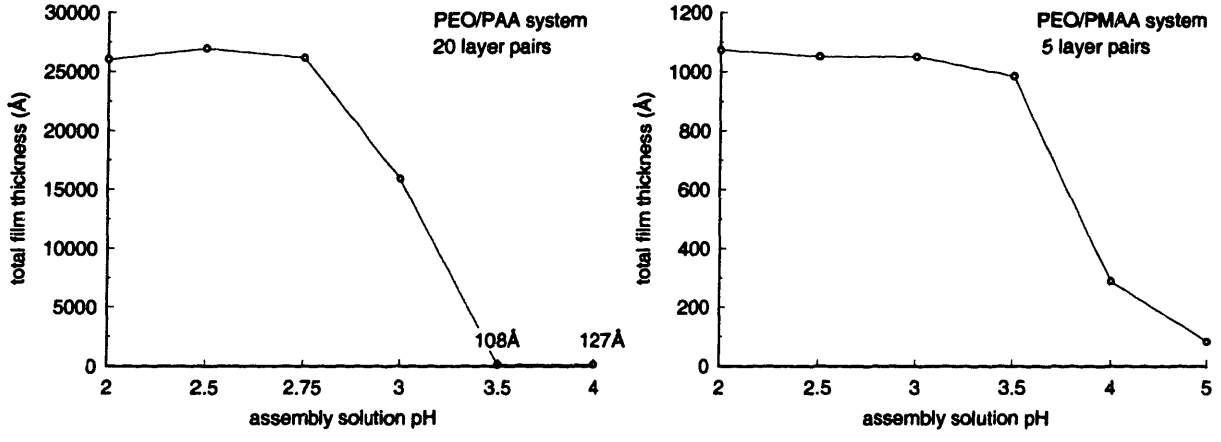

Figure 5.9. Correlation of film thickness to assembly pH for the PEO/PAA and PEO/PMAA systems.

Effect of PEO molecular weight

Based on the results of the pH study, a standard assembly pH of 2.5 was chosen for subsequent investigations of the PEO/PAA system. The next step in examining assembly was to characterize the effects of polymer molecular weight on the quality of the LBL assembled films. For this purpose, 10-layer pair films incorporating PEO polymers of several different polymer molecular weights were assembled using PAA of a single molecular weight (90 kDa). The film thickness and roughness for each 10-layer pair film were recorded as shown in Figure 5.10. As the PEO molecular weight increases, the per-layer thickness increases, and roughness decreases. At very low molecular weights such as 1,500 Da (36 EO repeats), the films exhibit roughness greater than the total film thickness, indicating essentially no controlled deposition but rather the

adhesion of globular agglomerates. With increasing molecular weight, the films eventually become smoother and thicker, asymptotically approaching a limiting thickness. This strong dependency on polymer molecular weight even beyond 20 kDa (almost 500 repeats) is due to the inherently low crosslink density of hydrogen-bonded LBL assembled films. Using FTIR methods, Sukhishvili and Granick have estimated that 10% of the carboxylic groups in PMAA/PEO participate in hydrogen bonding with ether oxygens.[25] Thus as compared to electrostatically assembled LBL films, hydrogen-bond LBL assembled films would be expected to show a greater degree of dependence on component polymer molecular weight because the conditions for total surface reversal and thermodynamic limitation should be reached at a greater number of polymer repeats. Put differently, in the PEO/PAA system we could describe 10 repeats as a nominal "macro repeat" for the calculation of the density of interacting sites on the chain. Thus the molecular weight dependency for hydrogen bonding LBL would be expected to be 10 times greater than that for electrostatic LBL assembly, wherein every repeat is crosslinked.

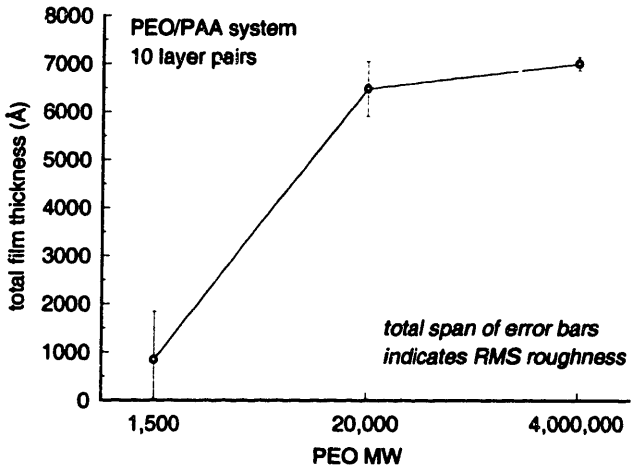

Figure 5.10. Correlation of PEO/PAA film thickness to PEO molecular weight.

5.3.3.2 Explorations of PEO/PAA ionic conduction

Kinetic study

Following the above studies, it was determined that the most favorable assembly conditions for the creation of robust, thick, and smooth PEO/PAA films would be an assembly pH of 2.5 and a PEO molecular weight of 4,000,000 Da. All films subsequently evaluated employed these optimal assembly conditions. The next step in the evaluation of these films was a direct measurement of the ionic conductivity of a PEO/PAA film to determine the rate of atmospheric water uptake. This study was designed to determine the time required for the

equilibration of films for ionic conductivity measurement in humid environments. A PEO/PAA film was assembled and allowed to equilibrate at 52% RH for 1 week. The film was then removed to a 100% RH environment, and the increase in ionic conductivity was evaluated as a function of time. The result of this study is shown in Figure 5.11.

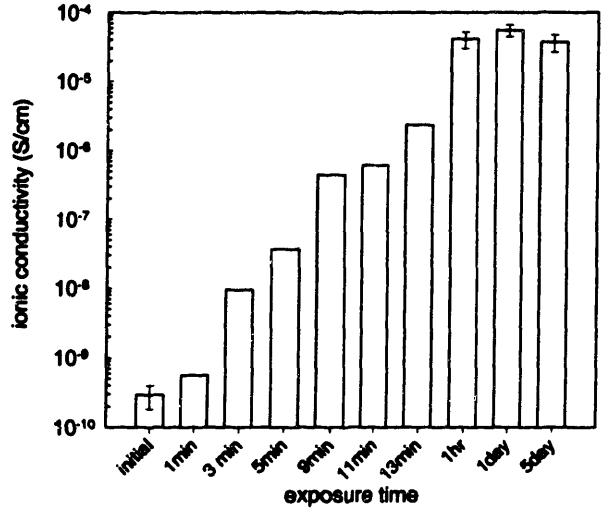

Figure 5.11. Ionic conduction of PEO/PAA in response to a step change from 52 to 100% RH.

As the film is exposed to the higher-humidity environment, the ionic conductivity increases precipitously, and the film appears saturated with water after approximately one hour of exposure. This behavior is distinctly different than that of LPEI/Nafion films that were evaluated in the previous section of this chapter, which required a full week of exposure to reach an equilibrium ionic conductivity level. Fast water uptake in PEO/PAA is due to the intrinsic hydrophilicity that would be expected of a film containing a polyacid and substantial ethylene oxide content. The film thickness at high humidity levels could not be ascertained due to its softness, but we would expect a great deal of film swelling with hydration. As the calculation of film ionic conductivity is based on the thinner dry film thickness, it is actually a more conservative, lower estimate. Any increase in film thickness due to swelling would increase the conductivity calculation proportionately.

From this first study it is clear that the PEO/PAA system can outperform the LPEI-based systems at high relative humidity (and thus high plasticizer loading). With full hydration, the ionic conductivity exceeds 10^{-5} S/cm, coming close to the level required for commercial consideration in batteries, and easily sufficient for application in electrochromic devices or sensors. Based on these promising initial results, the possibilities of this hydrogen bonding system were pursued further.

Effect of heat crosslinking

The next level of study undertaken for the PEO/PAA system was to investigate the effects of heat-induced crosslinking on the system stability and ionic conductivity. Heat-induced crosslinking in systems based on the hydrogen bonding of poly(acryl amide) (PAAm) and PAA has been shown to create both imide and anhydride crosslinks, the former formed between PAAm and PAA, and the latter formed between adjacent PAA units.[42] These crosslinks were employed to enhance the stability of PAAm/PAA films in neutral pH water. Because PEO does not contain any reaction-capable groups, the only heat-induced stabilization reaction available in PEO/PAA films is anhydride formation. Because some 90% of the PAA units are expected to be uninvolved in hydrogen bonding interactions with PEO, it can be assumed that many of these units are instead involved in the strong PAA:PAA dimerization; these dimers are susceptible to the formation of anhydride crosslinks between adjacent PAA moieties, as shown in Figure 5.12.

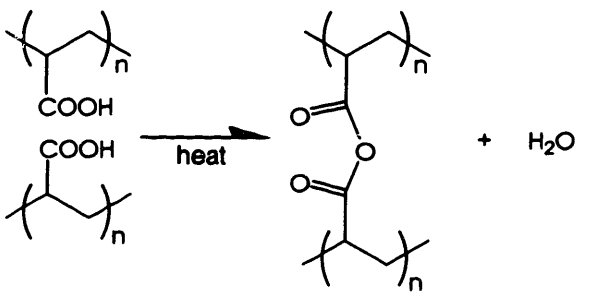

Figure 5.12. Formation of PAA:PAA anhydride crosslinks.

Several PEO/PAA films were exposed to varying levels of heat for varying durations to fully explore the possibilities of heat-induced anhydride crosslinking. This heat exposure caused marked shrinkage as shown in Figure 5.13. This shrinkage is due to water removal, either as the evaporation of associated water, or the water product of anhydride formation. Because treatment at 100°C for 16 hours should be sufficient to remove water from most LBL assembled films (thought this has not been verified for these extremely hydrophilic systems),[18] it might be assumed that any greater shrinkage at higher heat levels could be due exclusively to anhydride formation.

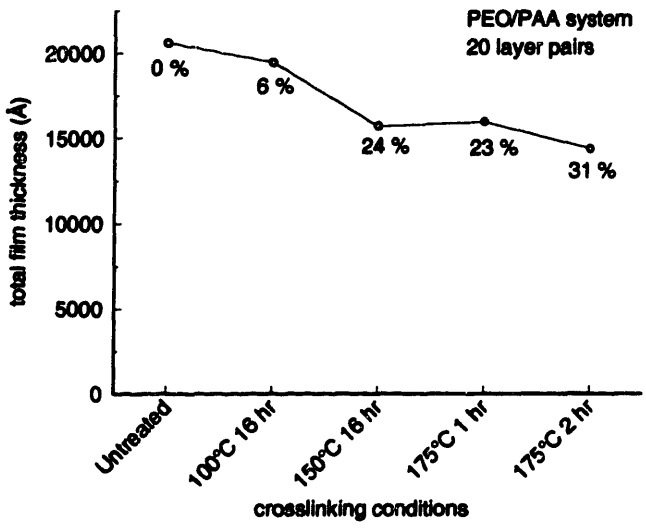

Figure 5.13. Thickness and shrinkage at different crosslinking conditions.

The stability of these crosslinked films was then assessed by exposing the films to aqueous electrolyte solutions at neutral pH. The crosslinked films were exposed to solutions for 24 hours and the remaining film thickness was measured. The electrolyte ionic strength was continually increased to challenge film stability. For all films, there was no gradual or partial dissolution observed; the films remained at post-assembly thickness until they suddenly dissolved above a critical ionic strength. The results of this stability study are depicted in Figure 5.14, which shows the range of ionic strength over which the films did not dissolve.

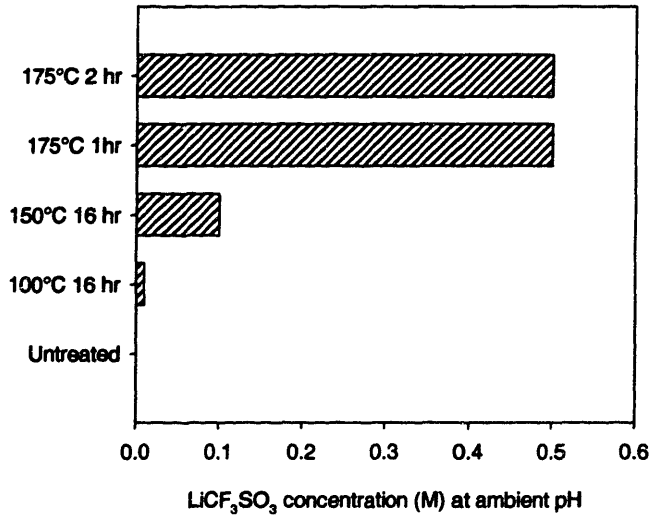

Figure 5.14. Stability regimes for anhydride crosslinked PEO/PAA.

As expected, the untreated film dissolved immediately in neutral pH water. However, all of the treated films were stable in neutral pH water for the 24-hour exposure time with no observed

film dissolution or roughening. The film with the weakest crosslinking could be stably exposed to 0.01 M, while films with the strongest crosslinks were stable to 0.5M, finally destabilizing in 1 M $LiCF_3SO_3$ solutions. These results indicate that there is some short-term stability to be gained from anhydride crosslinking of PEO/PAA. However, later results from ionic conductivity evaluation demonstrated that the anhydride crosslinks might eventually be severed.

The next step in the evaluation of the crosslinked PEO/PAA was to evaluate ionic conductivity. Films assembled at 10 layer pairs and exposed to the crosslinking conditions described above were subjected to impedance spectroscopy at several different levels of humidity. Films were equilibrated for one week at each condition, and the ionic conductivity was then evaluated with the results shown in Figure 5.15. In general, the ionic conductivity under very dry conditions is extremely low, just as that observed for LPEI-based electrostatically LBL assembled films. Upon increasing the humidity to intermediate levels, the conductivity increases somewhat, though the increase varies depending on the film. Finally, at high humidity, all of the films display a uniformly high ionic conductivity on par with the uncrosslinked PEO/PAA film evaluated in Figure 5.11.

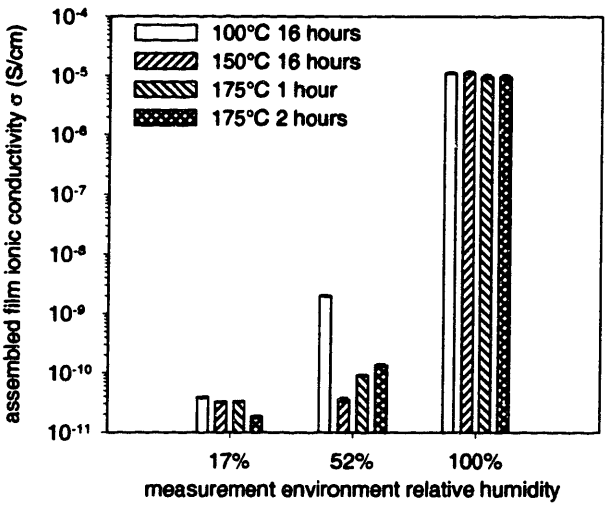

Figure 5.15. Effect of heat crosslinking on ionic conductivity.

At 17% RH, the conductivities shown in Figure 5.15 trend as would be expected; films with greater crosslinking exhibit lower conductivity. In fact, the trend exactly parallels that of shrinkage observations in Figure 5.13. Ionic conduction is limited by the dissociation-moderated number of charge carrying PAA protons within the film, which would be expected to be quite low at this humidity level.

At 52% RH, the trend changes dramatically. The least crosslinked film shows a strongly increased ionic conductivity, while the other three films show an inverted trend; increasing ionic conductivity with increasing heat exposure. The reason for this inversion may be related to the volatility of HCl. Each of these films was assembled at pH 2.5, which was achieved using dilute HCl. Deposition solutions and rinse baths were maintained at this pH, so solid films post-assembly can also be expected to contain sufficient HCl to maintain this pH. The presence of HCl within the films may suppress the ionization of PAA within the film, and thus decrease the number of charge carriers present within the films, which from the conclusions of the previous section of this chapter is the most critical factor controlling ionic conduction at this level of plasticizer loading. Increasing heat treatment may abate this acid effect to some extent by vaporizing HCl remaining in the film, thus increasing the number of protons that can dissociate from PAA. Hence the trend at 52% RH may indicate competition between the conductivity-decreasing effect of increased crosslinking and the conductivity-increasing effect of lower acid content.

At 100% RH, all of the films described in Figure 5.15 have almost identical levels of ionic conductivity. At this level of plasticizer loading, similar conductivities indicate similar ionic mobilities in the films, as humidity levels are sufficient for complete PAA dissociation. Because mobility is directly correlated to polymer segmental motion, similar mobilities suggest similar crosslink densities. At this condition, all of the films appeared glistening and highly wetted, comparable to the appearance of a polymer gel. Because of swelling, small wrinkle deformations in the conductivity cell (that do not appear to influence the ionic conductivity measurement significantly) were observed across all of the films. All of these similarities together suggest but do not confirm that the effects of anhydride crosslinking are lost over long exposure times to high humidity conditions. Although the highly crosslinked films were stable to neutral pH conditions for 24-hour periods, prolonged exposure to various humidity levels over 2 weeks may have been sufficient to break the anhydride bonds.

Anhydride crosslinking may provide some processing advantages in terms of enhancing short-term stability of PEO/PAA films to electrolyte solutions at neutral pH. This enhanced stability may be sufficient to invest the films with salt much in the manner of the electrostatically LBL assembled films investigated in the previous section of this chapter. Beyond short-term enhanced stability, anhydride crosslinking does not provide significant processing advantages, and appears to be degraded over long-term use in environments containing high-donicity small molecules. It is likely that the use of other protic plasticizers besides water may lead to anhydride breaking as well, with the possible formation of small molecule byproducts. Given these

considerations, the subject of anhydride crosslinking was set aside in favor of more lucrative explorations into the possibilities of PEO/PAA polymer electrolytes.

Salt exposure post-assembly

The PEO/PAA anhydride stability tests suggested that these films could be stably exposed to electrolyte solutions of considerable ionic strength before dissolution. To avoid the requirement of anhydride crosslinking to render the films stable to such exposure, the simpler tactic of adjusting the electrolyte solution pH can be employed. If the electrolyte solution pH is adjusted to the same level as the PEO/PAA assembly pH, then even untreated films can be stably exposed to very high levels of ionic strength. This stability is shown in Figure 5.16, which depicts the film thickness remaining after exposing 10-layer pair PEO/PAA films to the specified $LiCF_3SO_3$ concentration (at pH 2.5) for 24 hours. As can be seen, the first evidence of film dissolution is at 2.0 M salt concentration, far higher than even crosslinked films could tolerate at a neutral pH.

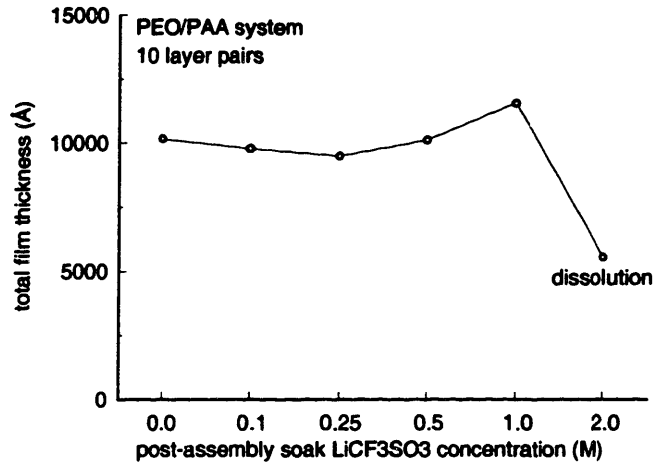

Figure 5.16. Thickness effect of soaking assembled PEO/PAA in salt solutions post assembly.

The thickness of the salt-exposed PEO/PAA films increases slightly with increasing salt concentration up to 1.0 M. This increase may be due to the partitioning of salt from the exposure solution into the PEO/PAA film. When the film is dried before measurement, salt within the film may form crystallites or otherwise contribute to the film bulk, increasing the overall film thickness. In fact, the roughness of the underlying films could not be evaluated due to the appearance of salt crystals on the film surface that could not be removed using a high velocity nitrogen stream. Once a critical electrolyte concentration is reached – for these films between 1.0 and 2.0 M $LiCF_3SO_3$ - the films do dissolve, but they do so in a gradual manner

different from the abrupt dissolution observed for anhydride crosslinked films in neutral pH electrolyte.

The high stability of these hydrogen-bonded LBL assembled films in electrolyte solutions at appropriate pH is propitious from the standpoint of adding additional charge carriers into the film by partitioning of salt into the film from the exposure solution. In the previous section of this chapter, such exposure was shown to increase the level of ionic conductivity in electrostatically LBL assembled films by one order of magnitude at intermediate humidity levels, though the films appeared to become saturated with salt at fairly low ionic strengths. A similar study was performed for PEO/PAA films by exposing three films to 0.1, 0.5 , and 1.0 M $LiCF_3SO_3$ solutions for 24 hours, drying the films without rinsing, and fabricating test beds from those films to measure ionic conductivity. As expected, exposure to salt dramatically influenced the ionic conductivity, as exhibited in Table 5-3. Although conductivity at 17% RH remained similar to that of an unexposed film, the PEO/PAA ionic conductivity at intermediate humidity levels was increased by a factor of 10,000 after exposure to a 1.0 M $LiCF_3SO_3$ solution. Again it should be stressed that film thickness increases due to swelling could not be measured; these ionic conductivity calculations are conservative lower estimates.

In fact, the conductivity of these salt-exposed films could not be evaluated at 100% RH due to radical cell deformation (wrinkling/buckling of the evaporated metal foil) from film swelling, which was much greater for salt-exposed PEO/PAA than for unexposed PEO/PAA. The PEO/PAA cell that was exposed to 0.1 M $LiCF_3SO_3$ deformed the least, allowing a tentative ionic conductivity evaluation of $\sim 10^{-4}$ S/cm at 100% RH– approximately 10,000 times greater than its conductivity at 52% RH. This result would suggest that the other salt-exposed films might benefit similarly from increased humidity and plasticizer loading. A more robust cell design will be required to fully capture and evaluate this benefit.

Table 5-3. Room temperature (25°C) ionic conductivity of $LiCF_3SO_3$ invested PEO/PAA films. Uncertainty indicates 95% confidence intervals

measurement	17% RH	52% RH
$LiCF_3SO_3$ soak (M)	ionic conductivity (S/cm)	
none	$3.9 \pm 0.2 \cdot 10^{-11}$	$2.0 \pm 0.0 \cdot 10^{-9}$
0.1	$3.8 \pm 0.4 \cdot 10^{-12}$	$8.5 \pm 0.6 \cdot 10^{-8}$
0.5	$1.7 \pm 0.2 \cdot 10^{-11}$	$4.3 \pm 0.4 \cdot 10^{-6}$
1.0	$8.9 \pm 0.8 \cdot 10^{-12}$	$1.3 \pm 0.1 \cdot 10^{-5}$

The results of the salt-investment of PEO/PAA indicate that a much greater amount of $LiCF_3SO_3$ salt can dissolve into PEO/PAA films than can dissolve into LPEI-based LBL assembled films. This difference is due in no small part to the nonionicity of PEO; LPEI possesses a positive

charge that could discourage hard acid / hard base interactions with lithium cations whilst PEO has no such limitation. This consideration is the primary reason that PEO is employed overwhelmingly more often over LPEI in the creation of polymer electrolytes (aside from cost), even though both possess similar primary chemical structures and donicities. At intermediate humidity levels, the PEO/PAA system exposed to 1.0 M $LiCF_3SO_3$ displays the greatest ionic conductivity observed so far in LBL assembled films. Carrier investment by salt exposure is thus a very successful practice for enhancing the performance of PEO-based LBL assembled polymer electrolyte films. Even higher levels of conductivity may be measured using anhydrous plasticizers in more robust cell configurations; this technology could lead to a direct application of LBL assembled films in lithium polymer batteries or other types of electrochemical power storage devices.

Salt exposure during assembly

The stability of PEO/PAA films to electrolytes of high ionic strength suggests that these films might also be assembled at high ionic strengths. This would be an alternative strategy whereby the films would be invested with salt throughout the assembly process by the consistent presence of a specified level of salt in both the deposition solutions and rinse baths, which would also be maintained at appropriate pH. This strategy was successfully employed to make several films, with the thickness characteristics shown in Figure 5.17.

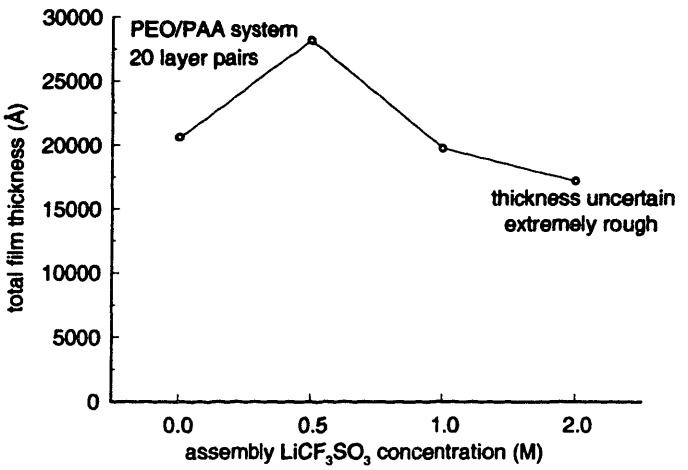

Figure 5.17. Correlation of deposition solution salt addition to PEO/PAA final film thickness.

This analysis of salt addition to PEO and PAA assembly solutions is a novel study – this influence has not been previously examined for hydrogen-bonded systems. Interestingly, the thickness behavior parallels that of electrostatically LBL assembled films; there is an initial increase in film thickness analogous to shielding-enhanced adsorption, followed by a decrease in film thickness

with the creation of rougher and uneven films at high electrolyte concentrations that is analogous to screening-reduced adsorption. In electrostatic LBL systems, screening enhanced adsorption is attributed to a change in the morphology of polyelectrolytes; with additional small ions present, polyions assume a more globular morphology as repulsion forces between adjacent charged repeats are abated. The enhancement of thickness in PEO/PAA may be attributed to a similar argument in that it is most likely a change in the solution morphology to a more globular state that is causing the thickness increase. For PEO, the reasons for this shift in conformation are based on the interactions between PEO and the lithium cations. PEO in pure water is extremely hydrated due to its high polarity and hydrogen bonding interactions. When salt is added to this water, alkali cations disrupt this hydration layer by engaging in Lewis acid / base interactions with PEO ether oxygens. Disruption of hydration leads to a decrease in PEO solvation. Ethylene oxide sites that are strongly complexed with salt will become hydrophobic and will be internalized into a more globular structure with surface hydration and interior dehydration. This well-understood PEO dehydration phenomenon is thus primarily responsible for the increase in LBL assembled film thickness. A second, interrelated contribution is the reduction in the chain density of interacting sites due to the sequestration of hydrogen bonding ether oxygen electron density by these dehydrating ionic interactions. At higher ionic strengths, PEO dehydration and binding competition become too severe, resulting in a complete disruption of the interactions responsible for the LBL assembly, and proper film formation is no longer evident.

Given the differences in film thickness, PEO/PAA films assembled at several different levels of ionic strength might be expected to display different film morphologies just as has been observed in electrostatic LBL assembly. In addition, each of these assembly conditions should result in a different level of lithium salt investment because the salt concentration level was maintained in deposition solutions and rinsing solutions. Both of these factors can profoundly influence ionic conductivity. Films assembled at the conditions shown in Figure 5.17 were therefore incorporated into measurement cells and the ionic conductivity was evaluated at several levels of relative humidity, with results shown in Table 5-4.

Unlike the films that were simply salt-exposed, PEO/PAA films that were salt-assembled display a definite increase in ionic conduction at 17% RH with increasing salt content. This might suggest that assembly in the presence of salt results in a greater amount of salt dissolved into the film, or that the morphology that is assumed from dehydrated PEO is somewhat more advantageous to dry ion conduction. This advantage disappears at 52% RH; at this level of humidity, ionic conductivities of films exposed to salt or assembled with salt are approximately equivalent for the same salt concentration (comparing values in Table 5-3 and Table 5-4 for 0.5

and 1.0 M $LiCF_3SO_3$ concentrations). Again, the ionic conductivities of these films could not be properly measured at 100% RH due to exaggerated swelling.

Table 5-4. Room temperature (25°C) ionic conductivity of $LiCF_3SO_3$ assembled PEO/PAA films. Uncertainty indicates 95% confidence intervals

measurement	17% RH	52% RH
$LiCF_3SO_3$ assy (M)	ionic conductivity (S/cm)	
none	$3.9 \pm 0.2 \cdot 10^{-11}$	$2.0 \pm 0.0 \cdot 10^{-9}$
0.5	$9.4 \pm 0.8 \cdot 10^{-11}$	$2.5 \pm 0.2 \cdot 10^{-6}$
1.0	$3.6 \pm 0.4 \cdot 10^{-10}$	$2.3 \pm 0.4 \cdot 10^{-5}$
2.0	$1.3 \pm 0.4 \cdot 10^{-10}$ *	$1.7 \pm 0.0 \cdot 10^{-5}$ *

* Questionable data point –cell deformation due to rough film and swelling.

Thus the manipulation of PEO/PAA film morphology is possible by adjusting the ionic strength of the deposition solutions. This adjustment leads to films that show clear differences in film thickness, and dry ionic conductivity is enhanced. Just as for salt-exposed films, measurable ionic conductivity may be further enhanced using anhydrous plasticizers or more robust cell configurations. The assembly of PEO/PAA with added electrolyte in the assembly solutions is an even more flexible addition to the PEO/PAA polymer electrolyte design toolkit because film thickness manipulation is also possible.

5.3.4 Conclusions from hydrogen bonded LBL assembled polymer electrolyte studies

An exploration into the ionic conduction properties of the hydrogen bonded LBL system PEO/PAA has revealed many details concerning this promising polymer electrolyte system, though there remains a great deal more to be studied. Assembly feasibility and behavior were first evaluated. Critical assembly pH conditions are consistent with PAA ionization onset, and film architecture benefits from increased PEO molecular weight with increased thickness and reduced roughness due to the intrinsically low PEO/PAA crosslink density. PEO/PAA LBL assembled films are far thicker than those assembled via electrostatic interactions; thickness results of ~100nm per layer pair are typical.

The ionic conductivity properties of PEO/PAA were explored with water plasticization. Initial ionic conductivity results for PEO/PAA were very promising, with conductivities greater than 10^{-5} S/cm achievable in these films even after a short exposure to 100 % RH. Increased stabilization of PEO/PAA using anhydride crosslinking was then explored. While short-term film stability to water and aqueous electrolytes at neutral pH were improved, long-term conductivity evaluations suggested that anhydrides were lost over 2 weeks of exposure to humid air. While heat crosslinking does stabilize films sufficiently for salt investment by electrolyte exposure, a simpler method was more promising.

This simpler method involved exposing already-assembled, non heat-treated PEO/PAA films to electrolyte solutions adjusted to the assembly pH of 2.5. Using this technique, PEO/PAA films were stable even when challenged by an electrolyte of 1.0 M ionic strength. Films thus exposed exhibited dramatically enhanced ionic conductivity, reaching levels of greater than 10^{-5} S/cm at 52% RH. The salt-invested films swelled to too great an extent for evaluation of conductivity at 100 % RH, but tentative results suggest levels of 10^{-4} S/cm or greater.

The stability of PEO/PAA films in electrolyte solutions led to an examination of PEO/PAA assembly in the presence of added salt. The modulation of LBL assembly behavior was analogous to that of electrostatic LBL assembly, although shielding resulted from dehydration and Lewis acid/base interactions rather than ionic screening. Stable films were assembled up to a salt concentration of 1.0 M with dramatically different film thicknesses, implying different film morphologies. Dry ionic conductivity was enhanced in these salt-assembled films as compared to the salt-exposed films. Conductivities in the humid state were similar for the two strategies. The manipulation of PEO/PAA LBL assembled films by added salt provides another tool to optimize these promising LBL assembled polymer electrolytes. Future work exploring the adjustment of film composition (the PEO:PAA ratio) by manipulating pH and ionic strength, as well as the incorporation of anhydrous plasticizers and alternative salts will result in the fabrication of LBL assembled polymer electrolytes suitable for high-performance lithium polymer batteries, supercapacitors, and other electrochemical power-storage applications.

5.4 Cited literature

(1) Gray, F. M. *Polymer Electrolytes*; The Royal Society of Chemistry: Cambridge, UK, 1997.
(2) Durstock, M. F.; Rubner, M. F. *Langmuir* **2001**, *17*, 7865-7872.
(3) Toyota, S.; Nogami, T.; Mikawa, H. *Solid State Ion.* **1984**, *13*, 243-247.
(4) Michaels, A. S. *Ind. Eng. Chem.* **1965**, *57*, 32-40.
(5) Farhat, T. R.; Schlenoff, J. B. *Langmuir* **2001**, *17*, 1184-1192.
(6) LeNest, J. F.; Gandini, A. In *Second International Symposium on Polymer Electrolytes*; Scrosati, B., Ed.; Elsevier Science Publishing Co., Inc.: New York, 1990, pp 129-141.
(7) Berthier, C.; Gorecki, W.; Minier, M.; Armand, M. B.; Chabagno, J. M.; Rigaud, P. *Solid State Ion.* **1983**, *11*, 91-95.
(8) Chiang, C. K.; Davis, G. T.; Harding, C. A.; Takahashi, T. *Solid State Ion.* **1986**, *18-9*, 300-305.
(9) Takahashi, T.; Davis, G. T.; Chiang, C. K.; Harding, C. A. *Solid State Ion.* **1986**, *18-9*, 321-325.
(10) Yoo, D.; Shiratori, S. S.; Rubner, M. F. *Macromolecules* **1998**, *31*, 4309-4318.
(11) Shiratori, S. S.; Rubner, M. F. *Macromolecules* **2000**, *33*, 4213-4219.
(12) Decher, G.; Hong, J. D. *Ber. Bunsen-Ges. Phys. Chem. Chem. Phys.* **1991**, *95*, 1430-1434.
(13) Vandesteeg, H. G. M.; Stuart, M. A. C.; Dekeizer, A.; Bijsterbosch, B. H. *Langmuir* **1992**, *8*, 2538-2546.
(14) Lvov, Y.; Decher, G.; Mohwald, H. *Langmuir* **1993**, *9*, 481-486.
(15) Clark, S. L.; Montague, M. F.; Hammond, P. T. *Macromolecules* **1997**, *30*, 7237-7244.
(16) Papke, B. L.; Ratner, M. A.; Shriver, D. F. *J. Electrochem. Soc.* **1982**, *129*, 1434-1438.
(17) Alamgir, M.; Abraham, K. M. *Ind. Chem. Libr.* **1994**, *5*, 93-136.
(18) Farhat, T.; Yassin, G.; Dubas, S. T.; Schlenoff, J. B. *Langmuir* **1999**, *15*, 6621-6623.
(19) MacDonald, J. R.; Johnson, W. B. In *Impedance Spectroscopy*; MacDonald, J. R., Ed.; John Wiley & Sons: New York, 1987, pp 1-20.
(20) Washburn, E. W.; West, C. J.; Hull, C., Eds. *International Critical Tables*; McGraw Hill Book Company and U.S. National Research Council, 1926; Vol. 1.
(21) Bloys van Treslong, C. J. *Recueil, J. Royal Neth. Chem. Soc.* **1978**, *97*, 13-21.
(22) Weyts, K. F.; Goethals, E. J. *Makromol. Chem., Rapid Commun.* **1989**, *10*, 299-302.
(23) Smits, R. G.; Koper, G. J. M.; Mandel, M. *Journal of Physical Chemistry* **1993**, *97*, 5745-5751.
(24) Clark, S. L.; Hammond, P. T. *Langmuir* **2000**, *16*, 10206-10214.
(25) Sukhishvili, S. A.; Granick, S. *Macromolecules* **2002**, *35*, 301-310.
(26) Gray, F. M. In *Polymer Electrolyte Reviews*; MacCallum, J. R., Vincent, C. A., Eds.; Elsevier Applied Science Publishers, Ltd.: London, 1987; Vol. 1, pp 139-172.
(27) Mellander, B. E.; Albinsson, I. *Solid State Ionics, [Proc. Asian Conf.], 5th* **1996**, 83-95.
(28) Bruce, P. G. In *Polymer Electrolyte Reviews*; MacCallum, J. R., Vincent, C. A., Eds.; Elsevier Applied Science Publishers, Ltd.: London, 1987; Vol. 1, pp 237-274.
(29) Jiang, S. P.; Love, J. G.; Badwal, S. P. S. *Key Eng. Mater.* **1997**, *125-126*, 81-132.
(30) Mount, A. R.; Robertson, M. T. *Compr. Chem. Kinet.* **1999**, 439-459.
(31) Randin, J. P. *J. Electrochem. Soc.* **1982**, *129*, 1215-1220.
(32) Selman, J. R.; Lin, Y. P. *Electrochim. Acta* **1993**, *38*, 2063-2073.
(33) Nagai, J.; Mizuhashi, M.; Kamimori, T. In *Large Area Chromogenics: Materials and Devices for Transmittance Control*; Lampert, C. M., Granqvist, C. G., Eds.; SPIE Optical Engineering Press: Bellingham, Washington, 1988, pp 378-385.
(34) Cappadonia, M.; Erning, J. W.; Niaki, S. M. S.; Stimming, U. *Solid State Ion.* **1995**, *77*, 65-69.
(35) Wintersgill, M. C.; Fontanella, J. J. *Electrochim. Acta* **1998**, *43*, 1533-1538.
(36) Zaluski, C.; Xu, G. *Macromolecules* **1994**, *27*, 6750-6754.

(37) Goff, A. H.-L.; Bernard, M.-C.; Zang, W. *Electrochim. Acta* **1998**, *44*, 781-796.
(38) Stockton, W. B.; Rubner, M. F. *Macromolecules* **1997**, *30*, 2717-2725.
(39) Sukhishvili, S. A.; Granick, S. *J. Am. Chem. Soc.* **2000**, *122*, 9550-9551.
(40) Katchalsky, A.; Spitnik, P. *J. Polym. Sci.* **1947**, *2*, 432-446.
(41) Mandel, M. *Eur. Polym. J.* **1970**, *6*, 807-822.
(42) Yang, S. Y.; Rubner, M. F. *J. Am. Chem. Soc.* **2002**, *124*, 2100-2101.

Chapter 6. Conclusions and recommendations

This thesis has presented the application of the LBL assembly technique to the directed engineering of two related electrochemical elements: electrochromic electrode films and ionically conductive polymer electrolyte films. The development of these elements led to many systems and phenomena that have been studied herein for the first time, and therefore this thesis contains many system-specific details. However, several general conclusions can be drawn from the individual results when considered as a whole work. These conclusions address electrochromism and ion conduction separately, and then some general statements regarding the engineering of electrochemical phenomena in LBL assembled films can be declared.

Electrochromism conclusions

Electrochromic films can be very successfully fabricated using the LBL technique. The electrochromophores for these films can be appropriated from all corners of the materials spectrum, including discrete electrochromic polymers, conjugated polymers, soft colloidal suspensions, and inorganic particle dispersions. Electrochromic performance of single electrochrome LBL assembled films as compared by contrast and switching speed typically equals or exceeds the performance of films containing the same electrochromophores yet fabricated by more traditional methods. A strong advantage of LBL assembled single-electrochrome films is the precise control exercised over film thickness, allowing straightforward design of an electrochromic electrode to provide optimum thickness for maximum contrast, as was demonstrated for systems such as LPEI/PEDOT:SPS. The large-area uniformity of LBL assembled films reduces scattering in electrochromic windows, leading to higher-than-typical contrasts for LBL PANI films. These advantages also enhance the performance of LPEI/PB, which contains the PB dispersion. This truly nano-sized PB dispersion was created using a simple yet powerful synthesis that was generalized to PB analogues, leading to assembly of several inorganic/polymer LBL assembled composites with electrochromic colorations suitable for the fabrication of a full-color CMYK display. This thesis is the first and only work in which these benefits have been fully established and exploited for the creation of a broad library of electrochromic LBL assembled films with performance suitable for commercial application.

In addition to these general advantages, some striking and unique effects were observed. Employing a counterpolyion known for fast ionic conduction dramatically enhanced the switching speed of PXV. Furthermore, the dimerization of PXV radical cations could be controlled in LBL assembled films by counterpolyanion hydrophobicity. Changing counterpolymer identity modulated the extinction of PANI coloration by influencing the acidity-

dependent equilibrium between two PANI forms within the film. The morphology of LPEI/PEDOT:SPS moderated its electrochemical resistivity, and that morphology changed with increasing film thickness, leading to a non-monotonic switching variation. Surprisingly, the LPEI/PB system proved to be one of the best-behaved LBL systems, exhibiting reproducible and highly linear variation in thickness, electrochemistry, and optical absorbance. Together, these novel results display the power of LBL assembly to modulate the properties of individual electrochromophores with subtle influences on electrochemical kinetics and coloration brought about by changes to the polymer matrix acidity/bascicity, hydrophilicity and plasticity, and morphology.

The power of the LBL technique is especially apparent with the successful fabrication of dual electrochrome electrodes. The concept of combining two electrochromophores into a single electrode led to two strategies: enhanced contrast and multihued coloration. Both of these strategies proved to be quite viable. The design of the PXV/PEDOT:SPS system resulted in contrast superior to all but one polymer electrochrome reported in literature to date. This high contrast spanned a large range of the visible spectrum owing to the additive electrochromism of the two polymers. The design of the PANI/PB system resulted in highly tunable multihued coloration, with a color switching reversibly between clear, green, and blue. These two dual electrochromes exhibited very different operation. In the PXV/PEDOT:SPS system, the two electroactive polymers featured widely separated redox potentials; the resultant film exhibited strong interactions between the two polymers, displaying unusual electrochemistry resulting from a suspected charge-trapping mechanism. In the PANI/PB system, the two electroactive materials featured almost exactly superimposed redox potentials; the resultant film exhibited no observable interactions, displaying instead a clear superposition of two separate and distinct electrochemistries and absorbance spectra. The excellent performance of both these dual electrochrome design strategies is clear evidence that LBL assembly is a vitally important addition to the field of electrochromic film fabrication; because of issues of phase separation and the insolubility of polyion complexes in all common solvents, dual electrochrome composites are essentially *impossible* to make by other means, aside from crude co-electropolymerization attempts that do not feature the level of control or uniformity of LBL assembly.

Electrochromism recommendations

Despite the advantages uncovered in this thesis work, there do remain some areas in which further LBL engineering could benefit the field of electrochromic films. While enhanced contrast and multi-hued coloration have now been demonstrated in LBL assembled films, one

key remaining factor that is yet to be enhanced is the switching speed. Even the most evolved dual electrochrome films exhibit switching speeds on the order of several seconds for high contrast coloration and bleaching, which is too slow for dynamic displays, but suitable for windows or electrochromic print media. As was revealed in single-electrochrome studies, the hydrophilicity and plasticity of the counterpolyion can dramatically influence switching speed. This confirms the widely recognized fact that redox reaction kinetics in thin polymer films are often limited by resistance ion migration rather than resistance to electron transfer. Therefore the challenges of slow switching and ion conductivity are coupled, and more recommendations will stem from conclusions of the LBL ionic conductivity studies.

There are some ways in which electrochromic electrodes may uniquely be engineered to switch faster. One critical strategy would be to profoundly alter the electrode architecture. An example of this strategy can be found in modern electrochromic devices with contrasts and switching speeds that are competitive with liquid crystal display (LCD) devices that have recently received commercial attention. The high contrast and fast switching of these devices are not based on novel electrochromic materials (they employ viologens), but instead result because cell electrodes are nanostructured or nanoroughened, typically by adsorbed titania particles, with a single monolayer of electrochrome then grafted to the electrode. When the monolayer is electrochemically colored, light absorbance is dramatically enhanced because of the large monolayer-covered surface area and because specular reflectance results in multiple reflections of incident light between adjacent (colored) surfaces on the electrode before light is reflected back toward the viewer. The switching time of these devices is very fast (20-100 ms) because ionic transfer occurs at a monolayer instead of through a thick polymer film. The conformal coating capabilities of LBL assembly potentially allow this type of electrode architecture to be exploited to enhance the contrast of the LBL assembled electrochromes engineered in this thesis. By applying these LBL assembled films to a nanostructured electrode, the number of required layer pairs could be greatly reduced while contrast and switching speed could be greatly enhanced. An alternative strategy would be to engineer a nano- or even micro-porous morphology within the LBL assembled electrochromic film itself, as has been done by Rubner and co-workers for more inert polyion pairs. With proper pore size and connectivity, electrolyte could fill the pores so that ion migration during switching would occur though pore walls rather than through the entire film bulk (an operational concept similar to supercapacitor operation). Changes to the electrolyte itself could also enhance switching speed; because ion migration is coupled to ion diffusion, the concentration of ions in the electrolyte directly influences switching speed. The highest ionic concentration that can be attained is that of an ionic liquid, which might be

employed as an electrolyte in LBL assembled electrochromic devices, though it remains to be seen whether electrostatically crosslinked LBL assembled films would be stable when challenged by such a high concentration of ions.

Aside from switching speed, the coloration of LBL assembled electrochromes can certainly be extended by incorporating other electrochromic materials. Some that have not been explored in this thesis are the transition metal oxides, the related poly(oxometallates), and all small-molecule electrochromes. The work with hexacyanoferrate particles in this thesis provides some guidelines for the incorporation of transition metal oxide particles, and poly(oxometallates) have previously been employed by other researchers. The possibility of including a small-molecule species such as methyl viologen into a previously LBL fabricated film is intriguing but thus far no examples of electrodes of this type are extant, possibly due to ionic binding competition within the film and also the prevention of small molecule diffusion out of the film and into the electrolyte. Such a strategy would almost certainly require covalent fixation of some sort. Finally, it is important to point out that poor water solubility and the lack of interaction capability of many electrochromic materials prohibits their incorporation into LBL assembled films. This difficulty is particularly acute for conjugated polymers that have been specially designed for high contrast or specific colors such as the "rainbow" of electrochromic PEDOT derivatives synthesized by Reynolds and co-workers. While these materials might be incorporated into LBL assembled films using a colloidal strategy like that for PEDOT, even the synthetic procedures for general colloid formation remain undeveloped. Thus, further synthetic work to create a wider variety water-soluble and polyionic electrochromic polymers is sorely needed and will greatly broaden the available library of electrochromic LBL assembled films. The strategies described in this thesis for enhancing the performance of single- and dual electrochrome LBL assembled electrodes can be applied to any newly introduced electrochromic species. In this way, LBL assembly can provide definitive contributions to the evolution of electrochromic films toward advanced display applications.

Ionic conduction conclusions

With the appropriate choice of component polymers, the ionic conductivity of LBL assembled films can approach that required for use in electrochromic devices and sensors. The electrostatic systems LPEI/PAMPS and LPEI/PAA can achieve levels exceeding 10^{-5} S/cm while the hydrogen bonded PEO/PAA system can reach levels close to 10^{-4} S/cm. To achieve these levels of conductivity requires substantial plasticization, which was introduced in this thesis by increasing the film water content. With plasticization, these high-performance LBL assembled electrolyte

systems should be considered gel electrolytes rather than true solid electrolytes. Even so, these systems appear more mechanically stable than most gel electrolytes because they maintain shape and do not flow even when a large amount of plasticizer is present at high humidity. Thus the optimal LBL assembled polymer electrolytes described in this thesis are superior to most gel electrolytes. The commercial potential of these novel systems is not diminished considering that all polymer electrolytes currently employed commercially are gels.

The engineering of ion conduction in LBL assembled films reveals many fundamental observations of considerable value. One of the most important observations is that the ionic conductivity of LBL assembled films can be greatly influenced by polycation and polyanion choice. The ionic conductivity of LPEI-containing LBL assembled films is approximately two orders of magnitude greater than that previously observed in LBL assembled films, which was recorded by Durstock and Rubner for poly(allylamine hydrochloride) (PAH)/PAA films. In fact it appears that the substitution of PAH with its near-isomer LPEI results in a general increase in ionic conduction. This increase must be due to the primary chemical structure of LPEI - in particular its heteronuclear backbone - that provides increased hydrophilicity and therefore greater ion solvation and mobility. The chemical structure of PAH – in particular its pure hydrocarbon backbone –may create hydrophobic regions within the film that hinder ion solvation and mobility. This theme continues as LPEI/PAMPS far outperforms LPEI/Nafion even though both PAMPS and Nafion are both strong polysulfonic acids. The hydrogen bonding capability and high polarity of PAMPS provide an environment within LBL assembled films that is much more conducive to ion migration than the highly fluorinated Nafion. Because of the vast differences in conductivity that can be observed amongst electrostatic LBL assembled films, it is very important that researchers not generalize when describing LBL assembled film properties or even when comparing LBL assembled films of weak polyacids/polybases vs. films of strong polyacids/polybases. Such generalizations, especially with regard to film transport properties or mechanisms of ion penetration and mobility, are either completely invalid or only valid for a select group of model polyelectrolytes with similar chemical properties. It must be recognized that each LBL assembled film possesses unique transport properties based on the component materials and the interactions between them.

The ionic conductivity of electrostatic LBL assembled films can be significantly altered by changes in deposition conditions. This was particularly true for the LPEI/PAMPS system, which appears to assemble with contributions from two different adsorption mechanisms. When contributions from the weaker mechanism are screened, ionic conductivity is greatly lowered. LPEI/PAMPS films assembled with both weak and strong contributions achieved the highest

levels of ionic conductivity ever measured in electrostatic LBL assembled films. The influence of deposition conditions was studied further in the weak polybase/polyacid system LPEI/PAA. The ionic conductivity of LPEI/PAA assembled at two different pH conditions was demonstrably different; higher levels of ionic conductivity were achieved in LPEI/PAA composites assembled at higher pH conditions where LPEI/PAA composites presumably contain a greater amount of unpaired LPEI.

It is important to note that these LPEI-based LBL systems have never before been so extensively studied, and they revealed very unusual assembly behavior, being extremely sensitive to assembly ionic strength and pH. The thickness of LPEI-based LBL assembled films, especially those assembled with PAA, can achieve extremely high levels that are at least one order of magnitude thicker than typical electrostatic LBL assembled films and are more similar to film thicknesses resulting from hydrogen-bonding LBL. Despite this unusually large thickness, the roughness of these films is very low - on par with the more typical ultrathin LBL assembled films. Because of these unusual characteristics, these novel films may have other applications where ultrasmooth polymer films with thickness on the order of microns are required.

The hydrogen-bonded PEO/PAA system was also explored in this thesis. This system was developed during the course of this thesis work independently from the efforts of Granick and Sukhishvili that were first published in the year 2000. Therefore, this thesis is amongst the first published works on the PEO/PAA system, and it is certainly the first work to recognize the potential of this system to act as a polymer electrolyte. The PEO/PAA system behaved similarly to the LPEI/PAA system during initial investigations, although it displayed a higher ionic conductivity at high humidity conditions. The true advantages of this system were realized during salt-exposure experiments, where the ionic conductivity of these systems was enhanced 10,000-fold by exposure to $LiCF_3SO_3$ solutions of up to 1 M concentration. The PEO/PAA films displayed a fundamentally greater capacity than LPEI-containing films to dissolve $LiCF_3SO_3$, and this greater carrier population resulted in higher conductivity.

A significant conclusion was reached by extending the study of PEO/PAA films to evaluate the influence of ionic strength on the hydrogen-bonding LBL assembly as a means to influence internal morphology and also to invest the films with salt during assembly. It was discovered that the addition of salt influences the deposition of PEO/PAA films in a manner completely analogous to the well-known ionic screening mechanisms of electrostatic LBL assembly. In the case of PEO/PAA the solution morphology is changed with salt addition by dehydrating Lewis acid/base interactions that cause PEO to assume a more globular morphology and sequester electron density resulting in lower hydrogen bonding interaction potential. This is

a surprising result that demonstrates that hydrogen bond LBL assembled films can be modulated using the same flexible set of variables commonly associated with LBL assembly, namely pH and ionic strength. Importantly, the dry state ionic conductivity of the screened PEO/PAA complexes was greater than that of simple salt-exposed, unscreened PEO/PAA films, suggesting a different internal morphology more conducive to PEO plasticity even when dry. Using both of these variables, future studies of hydrogen bond LBL assembled films have a vast parameter space to explore; this thesis has only revealed some initial possibilities.

Ionic conduction recommendations

Although the ionic conductivity of the LBL systems engineered in this thesis achieved levels far beyond those measured previously, even higher levels are required for consideration in power storage and delivery applications such as lithium polymer batteries and fuel cells. Furthermore, the *dry* ionic conductivities of LPEI and PEO were not enhanced using LBL assembly; even salt-exposed PEO/PAA systems exhibited very low dry ionic conductivity. This result indicates that the simple presence of a LBL partner polymer cannot replace the effect of adding a small molecule plasticizer. Although crystallization is inhibited in PEO, this inhibition is not sufficient to provide large, contiguous domains of amorphous PEO for ionic conduction, and indeed the dry ionic conduction of PEO/PAA more resembles what would be expected from dry PAA. The ultimate goal of anhydrous polymer electrolyte design is a high performance polymer electrolyte that can operate completely unplasticized. To reach this goal will require substantial further improvements in the properties of LBL assembled polymer electrolytes.

The first step in improving the performance of LBL assembled polymer electrolytes is to select a target application. Now that this thesis has surveyed the ion conduction properties of many different LBL systems, the selection of a system to meet the needs of a target application should be straightforward. For example, a lithium polymer battery application requires a completely anhydrous polymer electrolyte that can facilitate lithium ion conductivity. The system most appropriate for this battery application would be PEO/PAA. By contrast, a target application such as the fuel cell proton exchange membrane (PEM) requires a very different system. In most modes of operation, this film would be fully hydrated, so it must work with water as a constantly present plasticizer. In addition, the film must be stable to extremely low pH conditions and high temperatures. The PEO/PAA system is a poor choice for such an application, as it would be quickly degraded.

To meet a lithium battery application, tools such as FTIR should be used to advance understanding of the composition ratio in the PEO/PAA system. Ionic conductivity will be

enhanced if the ratio of PEO to PAA can be increased; this increase would be analogous to the increase of LPEI in LPEI/PAA films at higher pH that led to greater conductivity. The reason that this is important is because PEO/PAA films likely include a much larger amount of PAA relative to PEO due to PAA:PAA dimerization that would effectively sequester proton donating PAA groups from participating in hydrogen bonding interactions. The single most effective method to adjust this ratio would be to set the assembly pH to a condition where the PAA is partially ionized yet PEO/PAA hydrogen bonding is still supported. Coulombic repulsion between PAA repeats should lead to a lesser PAA content and thinner films. From the PEO/PAA assembly results, the pH range for modulation of this nature is very narrow, and the pH must be controlled extremely precisely to achieve control over the composition ratio without dissolving the films. Modulation of PEO/PAA thickness and morphology by adjusting ionic strength could also be employed at pH conditions that include partial PAA ionization. Using these strategies, a reduction in PAA content due to ionization and an enhancement in PEO content due to dehydration at high ionic strengths may result in a much greater amount of amorphous and lithium cation-containing PEO in these films. Ideally this film would operate without the addition of plasticizer, but in early stages of development, the use of an anhydrous plasticizer such as ethylene carbonate or a small oligo(ethylene glycol) may satisfy performance demands.

To meet a fuel cell application, more exotic materials not investigated in this thesis are required. The cation LPEI and the nonionic polymer PEO would not be chemically stable in a fuel cell environment. This new LBL system must be highly tolerant to acid and heat. A general strategy for creating such a LBL assembled film would be to focus on the engineering of controlled porosity. A film with controlled porosity in which the chemical identity of pore interior surfaces could be controlled would be most ideal. In this hypothetical system, proton conduction could take place in a similar mode to pure Nafion membranes, with proton hopping between adjacent acid sites on the interior surfaces of water-filled pores. From work performed by Rubner and co-workers, it is clear that controlled porosity can be achieved in some LBL systems. For fuel cells, possible candidate polymers would include perfluorinated ionomers such as DuPont's Nafion or its carboxylic acid analog FLEMION (manufactured by Asahi). Covalent modification of the sulfonyl chloride Nafion precursor can result in cationic, amine functionalized varieties of the polymer that could be combined with acid types to create a fully perfluorinated LBL matrix. An alternative polyanion could be a poly(amic acid), which can be heated to form poly(imides) that are renowned for heat stability (but not for ionic conductivity). From the poor ionic conductivity results gathered in this thesis for LPEI/Nafion, it is clear that much work must be performed before the LBL combination of *two* highly hydrophobic polyions

could result in any LBL assembled film with ionic conductivity appropriate for fuel cell applications.

Overall summary

It was the original intention of this thesis to create an electrochromic device from the bottom up using LBL assembly to create the anode, electrolyte and cathode sequentially. Although these individual elements for the electrochromic cell could be engineered quite successfully, their combination into a cell has not been presented in this thesis because this combination presents some very unique challenges that have yet to be resolved. The challenge to creating an entire electrochemical cell using LBL assembly is that the inclusion of LBL elements that are highly ion-permeable such as the LPEI/PAA or PEO/PAA electrolyte systems results in a film that can *also* be permeated by polyions. Because of this permeation, prototype devices exhibit two types of defects. The first type of defect resulted when the electrolyte became contaminated with cathode or anode electrochromic polymers. Because these contaminants were typically conducting polymers PANI or PEDOT, electronic conduction shorted these cells, and they behaved as linear resistors. The second type of defect resulted when the deposition of an upper layer of the cell disrupted the adhesion of a lower layer, resulting in delamination of the entire cell from its substrate support. Deposition of the LPEI/PEDOT:SPS system seemed in particular to be a culprit in causing this type of defect. It is interesting to note that the LPEI/PEDOT:SPS system exhibited a substantial superlinear growth regime, and recent explanations of superlinear growth (put forth by Picart and Lavalle) focus on interdiffusion and exchange of polymer chains deep within the film interior. This interdiffusion and chain exchange may be responsible for adhesion disruption and delamination. Other researchers have shown that discrete layer "blocks" or elements with little cross-contamination can be created and even single-layer resolution can be achieved in LBL assembled films, so one cannot conclude that these effects are general. However, these effects do appear with far greater prevalence when LBL systems are employed that display high hydrophilicity and water plasticization, giving rise to an internal film environment that can facilitate rapid diffusion. The implication of this conclusion is that creating better-performing LBL assembled electrochromic electrodes and electrolytes actually exacerbates the challenge of combining them into a device. Very recently, some positive cell fabrication results have been achieved using a variant of the LBL technique that employs spin coating to deposit the individual cationic and anionic layers. It is believed that these successes could be achieved because the spin variant is inherently "drier" and water is removed from the

film by centripetal force before interdiffusion can give rise to cross-contamination or adhesion interference.

Overall, the results gained in this thesis present a consistent picture of general electrochemical behavior in LBL assembled films. The subject of LBL assembled electrochemical materials has proven to be both a fruitful and rich topic area for investigation, with a diverse range of phenomena to be observed and a host of variables that can be manipulated to create an ever-expanding library of electroactive materials. Electrochromism and ion conduction are only two fundamental examples of the many applications of electrochemical materials. Extension of these systems could be used in the creation of all-polymer batteries, electrochemical sensors, or photovoltaic devices, to name but a few possibilities. Engineers considering any of these subject areas should consider the LBL process as an alternative to traditional fabrications methods. This thesis provides some foundations for this extension, and it is my fervent hope that continued research along this vein will strike a mother lode of high-performance commercial applications in the years to come.

THESIS PROCESSING SLIP

FIXED FIELD: ill. _____ name _____

index _____ biblio _____

► **COPIES:** (Archives) Aero Dewey Barker Hum

[illegible] Music Rotch (Science) Sche-Plough

TITLE VARIES: ► ☐ _____

NAME VARIES: ► ☑ Michael

IMPRINT: (COPYRIGHT) _____

► **COLLATION:** _____

► **ADD: DEGREE:** _____ ► **DEPT.:** _____

► **ADD: DEGREE:** _____ ► **DEPT.:** _____

SUPERVISORS: _____

NOTES:

cat'r: date:

page: 540

► **DEPT:** Chem. Eng

► **YEAR:** 2003 ► **DEGREE:** Ph.D.

► **NAME:** DELONGCHAMP, Dean M.